

This electronic thesis or dissertation has been downloaded from the King's Research Portal at <https://kclpure.kcl.ac.uk/portal/>



Bifunctional chelators containing dibromomaleimides for the preparation of radioimmunoconjugates for PET imaging

Farleigh, Matt

Awarding institution:
King's College London

The copyright of this thesis rests with the author and no quotation from it or information derived from it may be published without proper acknowledgement.

END USER LICENCE AGREEMENT



Unless another licence is stated on the immediately following page this work is licensed

under a Creative Commons Attribution-NonCommercial-NoDerivatives 4.0 International

licence. <https://creativecommons.org/licenses/by-nc-nd/4.0/>

You are free to copy, distribute and transmit the work

Under the following conditions:

- Attribution: You must attribute the work in the manner specified by the author (but not in any way that suggests that they endorse you or your use of the work).
- Non Commercial: You may not use this work for commercial purposes.
- No Derivative Works - You may not alter, transform, or build upon this work.

Any of these conditions can be waived if you receive permission from the author. Your fair dealings and other rights are in no way affected by the above.

Take down policy

If you believe that this document breaches copyright please contact librarypure@kcl.ac.uk providing details, and we will remove access to the work immediately and investigate your claim.

Bifunctional chelators containing
dibromomaleimides for the preparation
of radioimmunoconjugates for PET
imaging

By

Matthew Farleigh

This thesis is submitted in partial fulfilment of the
requirements for the degree of

Doctor of Philosophy

2021

Department of Imaging Chemistry and Biology, School of Biomedical
Engineering and Imaging Sciences, Faculty of Life Sciences and Medicine

King's College London

Declaration

I Matthew Farleigh confirm that no part of this thesis has been submitted in support of any other application for a degree or qualification of King's College London, or any other university or institute of learning. I confirm that this work is my own. Where information has been derived from other sources it has been indicated in this thesis. The copyright of this thesis rests with the author and no quotation from it or information derived from it may be published without proper acknowledgement.

Publications

Directly resulting from this work:

M. Farleigh, T. T. Pham, Z. Yu, J. Kim, K. Sunassee, G. Firth, N. Forte, V. Chudasama, J. R. Baker, N. J. Long, C. Rivas and M. T. Ma, New Bifunctional Chelators Incorporating Dibromomaleimide Groups for Radiolabeling of Antibodies with Positron Emission Tomography Imaging Radioisotopes, *Bioconjug. Chem.*, 2021, **32**, 1214–1222.

Additional publication:

J. E. Blower, J. K. Bordoloi, A. Rigby, M. Farleigh, J. Kim, H. O'Brien, J. Jackson, C. Poyiatzis, J. Bezer, K. Sunassee, P. J. Blower and L. Livieratos, Protocols for Dual Tracer PET/SPECT Preclinical Imaging, *Front. Phys.*, 2020, **8**, 1–8.

Acknowledgements

Firstly, I would like to thank Dr Michelle Ma, for her constant support and careful supervision. Over the last 4 years, Michelle has supported my academic development, gently directing my efforts towards the completion of this thesis. Michelle also nurtured my personal development and was always happy to chat about life and the future. I am indebted to Michelle for suggesting a career in consulting even though she still didn't really know what a consultant was (and probably still doesn't!).

I am also grateful to my second supervisor Prof. Nick Long who first directed me towards the Medical Imaging Centre for Doctoral Training 4 years ago. This journey would have never started if it wasn't for him. Nick has shown me a great deal of support during my studentship and has always made me feel welcome in his research group.

The 4th Floor of the Lambeth Wing at St. Thomas' Hospital requires constant maintenance and a degree of creativity, love, and care to keep it running. The quality and quantity of research making its way out of our small institution is a testament to the lab management team to whom I am most grateful. In particular, I wish to thank Mr David Thakor and Dr Matt Hutchings who have supported my research from the start. I reckon that I could complete an additional PhD in the time I have spent gossiping with Matt Hutchings. I also want to thank Dr Jana Kim and Dr Kavitha Sunassee for their assistance planning and conducting *in vivo* studies.

Thank you to all my friends and peers for providing emotional and scientific support over the course of my PhD, my door is always open to you. Though each of you have improved my experience immeasurably, I want to thank some people in particular: Jess and IB, I consider you to be the other members of the 1st generation Ma group. The experience we have shared will remain with me for life; George, for our experiment planning sessions, and long Teams chats over lockdown; Alex, for your humour and lab-based pyrotechnics; Aiden for your scientific passion and loyal friendship; Chris, for your biological prowess; Truc, for your help planning and executing experiments; and Charlotte, I am grateful for your guidance and friendship - I hope we continue to laugh in inappropriate settings together for years to come.

Lastly, I want to thank my family and friends for supporting me in everything that I do. To my parents, thank you for always being supportive, and for guiding me towards my own happiness. A special thanks goes to Jo who has always shared my curiosity and passion for science. Lastly to Danielle, I am so grateful for the support and patience you have shown me, especially over these last few years, which have been more challenging than anyone could have expected.

Thank you everyone.

Table of contents

Declaration.....	2
Publications.....	2
Acknowledgements.....	3
Abstract.....	8
List of Abbreviations	10
1 Introduction	13
1.1 Molecular Imaging	13
1.2 Positron Emission Tomography	13
1.2.1 Basic Principles of Positron Emission Tomography.....	13
1.2.2 PET Radiometals.....	14
1.3 Receptor targeted PET contrast agents based on peptides and proteins labelled with radiometals	15
1.3.1 Receptor targeted radiopharmaceuticals	15
1.3.2 Chelator selection	21
1.3.3 Chelators for Cu radioisotopes	23
1.4 Sarcophagine.....	31
1.4.1 Introduction to sarcophagines.....	31
1.4.2 Amine-reactive sarcophagine bifunctional chelators	34
1.4.3 Sarcophagine peptide conjugates.....	38
1.4.4 Sarcophagine protein conjugates	46
1.5 DFO.....	56
1.5.1 Introduction to desferrioxamine.....	56
1.5.2 ⁸⁹ Zr-DFO antibody conjugates.....	58
1.6 Maleimide Antibody Bioconjugations.....	65
1.6.1 The limitations of stochastic antibody conjugations	65
1.6.2 Maleimide antibody bioconjugations	66
1.7 Next generation maleimides and other thiol-reactive reagents	73
1.7.1 Monobromomaleimides	73
1.7.2 Disulfide rebridging.....	77
1.8 Thesis aims.....	86
1.9 Chapter 1 references	86
2 Sarcophagine-based dibromomaleimides for the preparation of ⁶⁴ Cu- radioimmunoconjugates for PET imaging.....	113

2.1 Introduction	113
2.2 Aims.....	113
2.3 Synthesis of a sarcophagine-based dibromomaleimide bifunctional chelator	114
2.3.1 Synthesis of [Mg(NH ₂) ₂ sar](CF ₃ SO ₂) ₂ (12)	114
2.3.2 Synthesis of 3,4-dibromomaleimide-N-hexanoic acid (14).....	115
2.3.3 Synthesis of sar-DBM (18).....	116
2.3.4 Optimising the synthesis of sar-DBM.....	121
2.4 Synthesis of sar-DBM-trastuzumab	132
2.4.1 Conjugation of sar-DBM to trastuzumab monitored by SDS-PAGE	132
2.4.2 The effect of varying hydrolysis periods on the bioconjugation reaction between sar-DBM and trastuzumab.....	136
2.4.3 The effect of varying the number of sar-DBM equivalents on the bioconjugation reaction between sar-DBM and trastuzumab	138
2.4.4 Mass spectrometry of sar-DTM-trastuzumab.....	140
2.4.5 Comparison of sar-DTM-trastuzumab with reported alkyne-DTM-trastuzumab conjugates (27 -trastuzumab)	143
2.5 ⁶⁴ Cu radiolabelling of sar-DTM-trastuzumab	145
2.6 Serum stability of ⁶⁴ Cu-sar-DTM-trastuzumab.....	149
2.7 <i>In vitro</i> specificity of ⁶⁴ Cu-sar-DTM-trastuzumab for the HER2 receptor ...	150
2.8 Evaluation of ⁶⁴ Cu-sar-DTM-trastuzumab in healthy mice	152
2.8.1 <i>Ex vivo</i> biodistribution of ⁶⁴ Cu-sar-DTM-trastuzumab in healthy mice	153
2.8.2 PET imaging of ⁶⁴ Cu-sar-DTM-trastuzumab in healthy mice.....	154
2.8.3 SDS-PAGE analysis of <i>ex vivo</i> serum samples from mice administered ⁶⁴ Cu-sar-DTM-trastuzumab.....	156
2.9 Chapter 2 summary.....	157
2.10 Chapter 2 experimental	158
2.11 Chapter 2 references	165
3 Comparison of a dibromomaleimide-based bifunctional chelator to a commercially available maleimide-based bifunctional chelator	171
3.1 Chapter 3 introduction.....	171
3.2 Chapter 3 aims	171
3.3 Synthesis of DFO-DBM (28).....	171
3.4 Synthesis and characterisation of DFO-DTM-trastuzumab	177
3.5 Synthesis and characterisation of DFO-mal-trastuzumab	183
3.6 Comparing the bioconjugations DFO-DBM and DFO-maleimide with trastuzumab.....	186

3.7 Radiolabelling DFO-DTM-trastuzumab and DFO-mal-trastuzumab with $^{89}\text{Zr}^{4+}$	187
3.8 Stability of ^{89}Zr -DFO-DTM-trastuzumab and ^{89}Zr -DFO-mal-trastuzumab in glutathione solution and human serum over 8 days	193
3.9 Specificity of ^{89}Zr -DFO-DTM-trastuzumab and ^{89}Zr -DFO-mal-trastuzumab for HER2	200
3.10 Evaluation of immunoreactive fraction for ^{89}Zr -DFO-DTM-trastuzumab and ^{89}Zr -DFO-mal-trastuzumab.....	201
3.11 Bioorthogonal DFO conjugation strategy using SPAAC	206
3.12 Chapter 3 summary.....	213
3.13 Chapter 3 experimental	215
3.14 Chapter 3 references	220
4 Conclusions and future work	224
4.1 Conclusions	224
4.1.1 Summary	224
4.1.2 Comparison of sar-DBM and DFO-DBM.....	224
4.1.3 Advantages of dibromomaleimide-based BFCs compared to existing site-specific conjugation methods	228
4.1.4 Bioorthogonal conjugation reactions involving dibromomaleimide ...	230
4.2 Future work.....	231
4.2.1 Improving DBM-conjugate homogeneity	231
4.2.2 Improving the specific activities of ^{64}Cu -sar-DTM-trastuzumab and ^{89}Zr -DFO-DTM-trastuzumab.....	233
4.2.3 <i>In vivo</i> assessment of ^{89}Zr -DFO-DTM-trastuzumab with comparison to ^{89}Zr -DFO-mal-trastuzumab and an isothiocyanate analogue.	233
4.2.4 ^{89}Zr -radiolabelling of DFO-BCN-trastuzumab, and serum stability of ^{89}Zr -DFO-BCN-trastuzumab.....	234
4.2.5 Dibromopyridazinedione-based bifunctional chelators	235
4.2.6 Closing remarks.....	236
4.3 Chapter 4 references	237
5 Appendix	241

Abstract

Bifunctional chelators (BFCs) can be conjugated to antibodies, and then radiolabelled with metallic radioisotopes, to produce radioimmunoconjugates capable of imaging disease, predicting patient response to therapy, and informing pharmacokinetics of antibody biodistribution. Non-site-specific bioconjugations are simple and reliable but generate heterogeneous conjugates that can show compromised target receptor affinity and stability *in vivo*. Site-specific bioconjugation techniques are more complex but generate homogeneous bioconjugates, often with high target receptor affinity and stability *in vivo*. Dibromomaleimides (DBM) enable simple and reliable site-specific conjugation to antibodies *via* rebridging of reduced disulfide bonds to first give dithiomaleimide conjugates, that rapidly undergo hydrolysis to yield stable dithiomaleamic acid (DTM) conjugates. Here, new DBM-based BFCs have been synthesised and conjugated to the HER2-targeting antibody, trastuzumab, which is used in breast cancer treatment. These new immunoconjugates have been radiolabelled, and then studied in serum, *in vitro* and *in vivo*, to assess their stabilities and targeting properties.

Sarcophagine (sar) is a macrobicyclic chelator which has been extensively radiolabelled with $^{64}\text{Cu}^{2+}$ ($t_{1/2}$ 12.7 h). This chelator-radiometal pair were used to develop a proof-of-concept platform for DBM-based BFCs. Sarcophagine-dibromomaleimide (sar-DBM) was synthesised in 8 % yield following optimisation, and subsequently reacted with trastuzumab, to give sar-DTM-trastuzumab. Near-quantitative radiolabelling of the immunoconjugate with $^{64}\text{Cu}^{2+}$ was achieved in 5 min at pH 7. The ^{64}Cu -sar-DTM-trastuzumab radioimmunoconjugate was stable in human serum over 40 h. Cell uptake SKOV3 cells (HER2 +ve) demonstrated retained radioimmunoconjugate specificity for the HER2 receptor. Lastly, the stability and HER2 affinity of ^{64}Cu -sar-DTM-trastuzumab were assessed *in vivo* in healthy female mice using PET imaging and *ex vivo* biodistribution studies over 48 h. Size-exclusion HPLC and SDS-PAGE analysis of blood serum showed no evidence of bioconjugate degradation or transchelation of radiometallic ions to serum proteins over 48 h. Additionally, low initial uptake and gradual clearance of radioactivity in the liver, indicated high radioimmunoconjugate stability whilst uptake and retention in HER2-expressing healthy tissues (skin, ovaries, uterine horn) demonstrated HER2 affinity.

To facilitate radiolabelling with the longer-lived PET isotope $^{89}\text{Zr}^{4+}$ ($t_{1/2}$ 3.3 d), desferrioxamine-DBM (DFO-DBM) was prepared. This enabled comparison between a dibromomaleimide-based BFC and the commercially available maleimide derivative of DFO, which is commonly used to radiolabel antibodies with $^{89}\text{Zr}^{4+}$. DFO-DBM was synthesised in 22 % yield whilst DFO-maleimide was obtained commercially. The bifunctional chelators were conjugated to trastuzumab to give DFO-DTM-trastuzumab and DFO-mal-trastuzumab. Radiolabelling with $^{89}\text{Zr}^{4+}$, near-quantitative radiochemical yields were achieved for both species in just 10 min at pH 7, although higher specific activities were achieved with the maleimide conjugate (40 MBq mg^{-1}) than with the DTM conjugate (5 MBq mg^{-1}). Radioimmunoconjugate stability was compared in glutathione solution (10 mM) at pH 5.5 and pH 7, as well as in human serum over 8 days. Both species exhibited high stability in serum and in glutathione solution at pH 7. However, ^{89}Zr -DFO-DTM-trastuzumab was significantly less stable than ^{89}Zr -DFO-mal-trastuzumab in glutathione solution at pH 5.5. Uptake studies in SKOV3 cells showed that HER2 specificity, and the fraction of radioimmunoconjugate with retained affinity for the target receptor (immunoreactive fraction) was similar for both conjugates.

New dibromomaleimide-based BFCs have been developed to prepare site-specific radioimmunoconjugates with retained target receptor affinity and sufficiently high stability for preclinical *in vivo* use. The use of native unmodified antibodies, and interchain disulfide rebridging in dibromomaleimide conjugations are advantages over existing site-specific and maleimide-based conjugation techniques respectively.

List of Abbreviations

ADC	antibody drug conjugate
ADCC	antibody-dependent cell-mediated cytotoxicity
BBS	borate buffered saline
BCN	bicyclo-[6.1.0]-nonyne
BFC	bifunctional chelator
BME	2-mercaptoethanol
Boc	tert-butyloxycarbonyl
BTG	bacterial transglutaminase
CH	constant heavy chain domain
CL	constant light chain domain
COSY	correlation spectroscopy
CT	computed tomography
DAR	drug to antibody ratio
DBM	dibromomaleimide
DFO	desferrioxamine
DFT	density functional theory
DIM	diiodomaleimide
DIPEA	<i>N,N</i> -diisopropylethylamine
DLL3	delta-like ligand 3
DMF	<i>N,N</i> -Dimethylformamide
DMSO	dimethylsulfoxide
DOTA	2,2',2'',2'''-(1,4,7,10-tetraazacyclododecane-1,4,7,10-tetrayl)tetraacetic acid
Dox	doxorubicin
DTM	dithiomaleamic acid
DTPA	diethylenetriaminepentaacetic acid
DTT	dithiothreitol
EDC	1-ethyl-3-(3-dimethylaminopropyl)-carbodiimide
EDTA	ethylenediaminetetraacetic acid
EEDQ	<i>N</i> -ethoxycarbonyl-2-ethoxy-1,2-dihydroquinoline
ELISA	enzyme-linked immunosorbent assay
EpCAM	epithelial cell adhesion molecule
ESI-MS	electrospray ionisation mass spectrometry
Fab	fragment antigen binding
Fc	fragment crystallisable
FcγR	Fc-gamma receptors
FDA	United States of America Food and Drug Administration
Fmoc	fluorenylmethyloxycarbonyl
Fv	fragment variable
GMP	good manufacturing practice
GSH	glutathione
HATU	2-(7-aza-1H-benzotriazole-1-yl)-1,1,3,3-tetramethyluronium hexafluoro-phosphate
HC	heavy chain
HCTU	(2-(6-chloro-1-H-benzotriazole-1-yl)-1,1,3,3-tetramethylaminium hexafluorophosphate
HEPES	4-(2-hydroxyethyl)-1-piperazineethanesulfonic acid

HER2	human epidermal growth factor receptor 2
HNSCC	head and neck squamous cell carcinoma
HPLC	high performance liquid chromatography
HSA	human serum albumin
HSQC	heteronuclear single quantum coherence
IEDDA	inverse electron demand Diels-Alder
Ig	immunoglobulin
ITLC	instant thin layer chromatography
ivDde	(Nε-1-(4,4-dimethyl-2,6-dioxocyclohexylidene)ethyl)
LC	light chain
LCMS	liquid chromatography-mass spectrometry
LIBS	ligand-induced binding sites
mal	maleimide
MALDI	matrix assisted laser desorption/ionisation
MeCN	acetonitrile
MMAE	monomethyl auristatin E
MMAF	monomethyl auristatin F
MRI	magnetic resonance imaging
MWCO	molecular weight cut-off
NGM	next generation maleimide
NHS	<i>N</i> -hydroxy succinimide
NMR	nuclear magnetic resonance
NODAGA	1,4,7-triazacyclononane,1-glutaric acid-4,7-acetic acid
NOTA	2,2',2''-(1,4,7-triazacyclononane-1,4,7-triyl)triacetic acid
NSG	NOD scid gamma
PD	pyridazinedione
PD-L1	programmed death ligand 1
PEG	polyethylene glycol
PET	positron emission tomography
PODS	phenyloxadiazolyl methylsulfones
PRRT	peptide receptor radionuclide therapy
PSMA	prostate specific membrane antigen
RNA	ribonucleic acid
Sar	sarcophagine
scFv	single chain variable fragment
SDS-	
PAGE	sodium dodecyl sulfate polyacrylamide gel electrophoresis
SE-HPLC	size exclusion high performance liquid chromatography
SPAAC	strain promoted azide-alkyne coupling
SPECT	single photon emission computed tomography
SrtA	sortase A
SSTR2	somatostatin receptor 2
TACN	1,4,7-triazacyclononane
TCEP	tris(2-carboxyethyl)phosphine
TCO	transcyclooctene
TETA	1,4,8,11-tetraazacyclododecane-1,4,8,11-tetraacetic acid

TFA	trifluoroacetic acid
TFP	tetrafluorophenyl
TIPS	triisopropylsilane
TLC	thin layer chromatography
Tz	tetrazine
US	ultrasound
UV	ultraviolet
VH	variable heavy chain domain
VL	variable light chain domain

1 Introduction

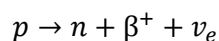
1.1 Molecular Imaging

Molecular imaging enables the visualisation of biochemical events occurring at the molecular and cellular level. This contrasts with conventional methods for obtaining molecular information from *ex vivo* tissue samples, such as histology. Many imaging modalities enable whole body molecular imaging including Magnetic Resonance Imaging (MRI), Computed Tomography (CT), Positron Emission Tomography (PET), Single Photon Emission Computed Tomography (SPECT), Ultrasound (US), and optical imaging. PET and SPECT are both used in nuclear medical imaging in combination with radioactively labelled compounds (radiotracers). Once administered to the patient, the radiotracer can be visualised using PET or SPECT, aiding in the diagnosis of disease. SPECT radionuclides are cheaper, and more widely available than PET radionuclides.¹ Additionally, there are a greater number of SPECT and γ -scintigraphy cameras than PET scanners.² However, clinical PET imaging provides superior spatial resolution and sensitivity compared to SPECT and γ -scintigraphy.

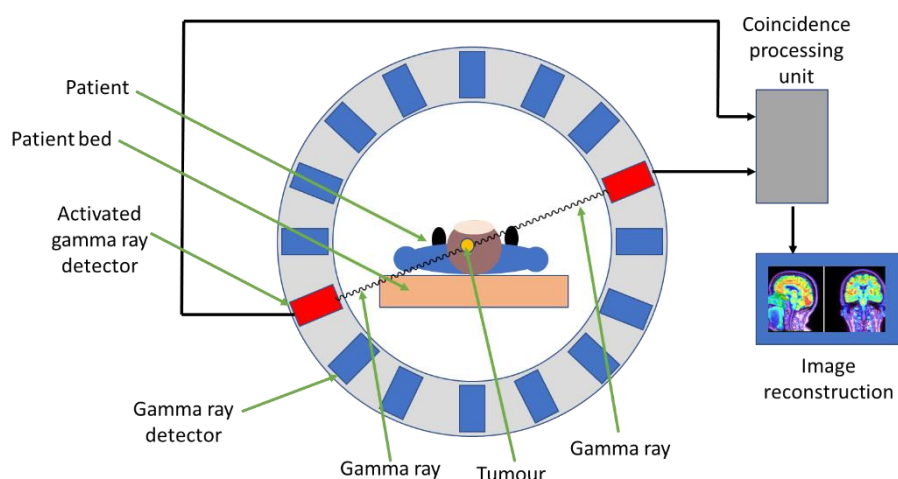
1.2 Positron Emission Tomography

1.2.1 Basic Principles of Positron Emission Tomography

The spontaneous conversion of a proton to a neutron can result in the emission of a positron and an electron neutrino (equation 1a). The positron is the antimatter counterpart of the electron, with the same spin and mass, but with the opposite charge. When a positron encounters an electron, two γ -photons (each 511 keV) are emitted at a trajectory of approximately 180° from each other (electron-positron annihilation). PET scanners detect these coincident 511 keV γ -photons *via* a circular array of detectors (equation 1b). The detection of these γ -photons enables the localisation of their source, in the body, with a resolution of ~ 5 mm (using a clinical PET scanner), with exact resolution depending on the energy of the positron emitted by the specific radionuclide.³



Equation 1a – The spontaneous conversion of a proton into to a neutron (n), releasing a positron (β^+) and an electron neutrino (ν_e).



Equation 1b – A schematic representation of a PET scanner being used to evaluate a patient with a suspected brain tumour.

1.2.2 PET Radiometals

Table 1 – A summary of radionuclides of importance to nuclear medicine⁴⁻⁷

Radionuclide	Use case	Half-life	E _{max} (keV)	Atomic radii (pm)	Common oxidation states
Ga-68	PET	68 min	1899	187	+3
Zr-89	PET	3.2 d	897	206	+4
Cu-64	PET	12.7 h	660	140	+2
Cu-67	therapy	2.6 d	577	140	+2
Tc-99m	SPECT	6.0 h	141	183	+1, +4, +5, +7
In-111	SPECT	2.8 d	245	193	+3
Lu-177	therapy	6.8 d	149	217	+3

The most accessible and radiochemically developed PET radiometals are ⁶⁸Ga, ⁶⁴Cu, and ⁸⁹Zr.

⁶⁸Ga ($t_{1/2}$ =68 min, β^+ E_{max}=1880 keV, 90%) has been used in clinical PET imaging where its short half-life makes it suitable for imaging with radiolabelled peptides. These species accumulate at target receptors and clear circulation quickly (within 30-60 min). ⁶⁸Ga can be produced either using a cyclotron *via* the ⁶⁸Zn(p,n)⁶⁸Ga nuclear reaction,⁸ or by using a benchtop ⁶⁸Ge/⁶⁸Ga generator system. The availability of these two production methods improves this radiometal's accessibility.

^{64}Cu ($t_{1/2}=12.7$ h, β^+ $E_{\text{max}}=656$ keV, 18%) has a longer half-life than ^{68}Ga , making it amenable to imaging with both peptides and proteins. This radionuclide is widely produced using a cyclotron, most often *via* the $^{64}\text{Ni}(p,n)^{64}\text{Cu}$ nuclear reaction.⁹ ^{64}Cu has been proposed for use in a theranostic (a portmanteau of the words diagnostic and therapeutic) pair with the therapeutic radionuclide ^{67}Cu ($t_{1/2}=61.9$ h, β^- =100%, $E_{\text{mean}\beta^-}=141$ keV).¹⁰ In this capacity, ^{64}Cu radiopharmaceuticals are used to image disease, predict patient response to targeted radiotherapy, and to inform pharmacokinetics of antibody biodistribution.¹⁰

Lastly, ^{89}Zr ($t_{1/2} = 3.2$ d, β^+ $E_{\text{max}} = 897$ keV, 23%) has the longest half-life of these radionuclides, making it well suited to PET imaging of IgG antibodies. It should be noted that a high energy γ -ray (909 keV) is emitted by ^{89}Zr with 99% efficiency. Whilst this emission does not complicate the detection of coincident 511 keV photons from positron annihilation, additional care must be taken with regards to transport, radiopharmaceutical manipulation, and patient dosimetry. Over the last decade, ^{89}Zr availability has increased from cyclotrons *via* the $^{89}\text{Y}(p,n)^{89}\text{Zr}$ transmutation reaction,¹¹ leading to the development of highly sensitive ^{89}Zr -labelled antibody-based PET imaging agents.

1.3 Receptor targeted PET contrast agents based on peptides and proteins labelled with radiometals

1.3.1 Receptor targeted radiopharmaceuticals

Accumulation of a PET radionuclide at the site of disease enables its spatial localisation by PET imaging.

The specific cell surface receptor binding exhibited by many peptides and proteins has resulted in their use as targeting vectors in radiopharmaceuticals. In many diseases, cellular changes lead to the overexpression of certain cell surface receptors. Peptides or proteins can be modified by reaction with a bifunctional chelator to yield bioconjugates.¹² These bioconjugates can then be radiolabelled *via* complexation of a radiometallic ion. Cell surface receptor binding is facilitated by the biomolecule, whilst the chelator effectively precludes release of the radiometallic ion *in vivo*. Bioconjugates can be designed to bind to specific target receptors, leading to radionuclide accumulation at diseased tissues where high concentrations of the target receptor exist. This in turn yields medical images representative of the distribution of diseased cells throughout the body, aiding clinicians in the diagnosis and staging of disease. Proteins and peptides have also

been radiolabelled with therapeutic radionuclides in order to deliver cytotoxic doses of ionising radiation to tumours in a targeted fashion.

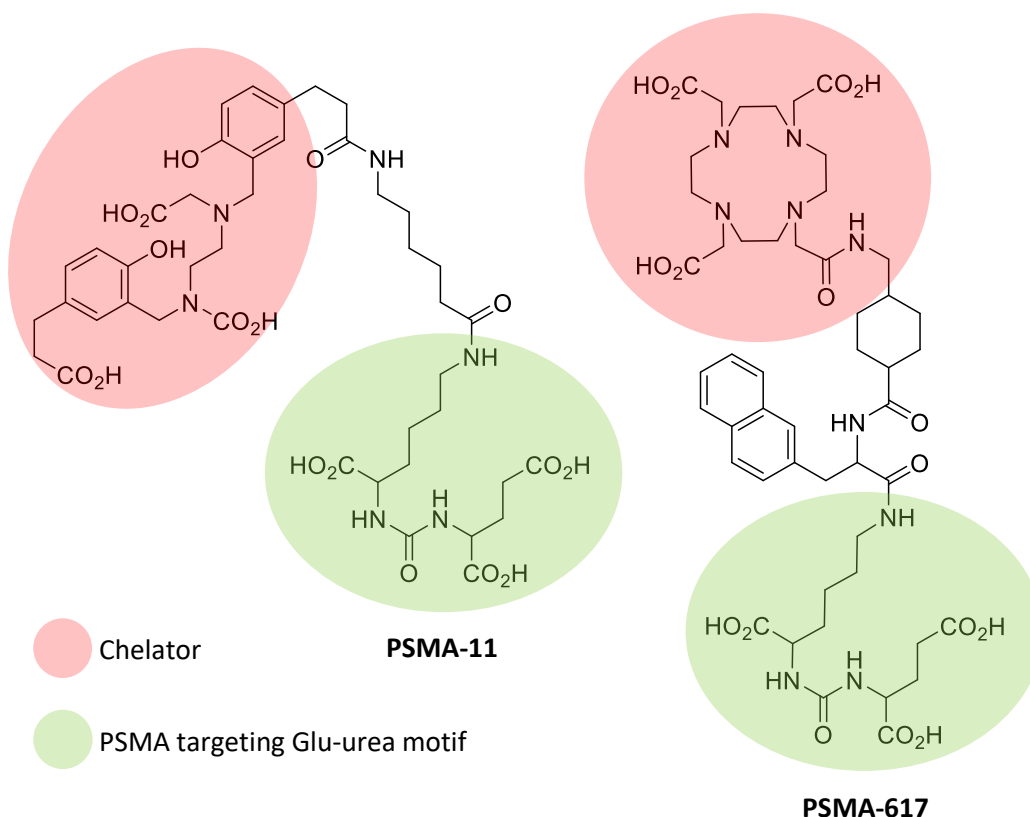


Figure 1 – The structures of PSMA-11 and PSMA-617 which have been radiolabelled with $^{68}\text{Ga}^{3+}$ and $^{177}\text{Lu}^{3+}$ for use in prostate cancer diagnosis and treatment respectively.

For example, the prostate-specific membrane antigen (PSMA) is a receptor is found in most prostate cancers.¹³ Peptides have been developed that possess affinity for PSMA (figure 1). When these ligands bind to the PSMA receptor they are internalised and retained within the target cell. Bioconjugates of these PSMA targeting peptides can be radiolabelled with short-lived PET radiometals such as ^{68}Ga . Administration of these radiopharmaceuticals enables diagnostic imaging of prostate cancers. The $^{68}\text{Ga}^{3+}$ complex of PSMA-11 (figure 1, left) has been approved for PET imaging of PSMA positive lesions in men with prostate cancer in select centres in the USA. This radiotracer is also a companion diagnostic for the therapeutic $^{177}\text{Lu}^{3+}$ (β^- , $t_{1/2} = 6.7$ d) complex of PSMA-617 (figure 1, right).¹³

Radiolabelled peptides have been used extensively in the field of nuclear imaging where they rapidly clear circulation and accumulate at diseased tissues, generating

high target tissue to non-target tissue contrast. Peptides are typically labelled using short-lived radionuclides such as ^{99m}Tc ($t_{1/2} = 6.01 \text{ h}$, γ) and ^{68}Ga ($t_{1/2} = 68 \text{ min}$, β^+). For certain peptides, ^{64}Cu with its intermediate half-life ($t_{1/2} = 12.7 \text{ h}$, β^+) has also been used. Matching the biological half-life of the targeting vector, with the physical half-life of the radionuclide is a common strategy used when designing radiopharmaceuticals.

Since radiopharmaceuticals continue to undergo physical decay after imaging, the total ionising radiation dose to the patient must be considered to ensure optimal compromise between patient dose and the clinical effectiveness of the imaging study in question. Ideally, once the imaging procedure is complete the patient's exposure to ionising radiation must be limited as much as possible. Therefore, from a radiochemical perspective, a good match between the radionuclide's physical half-life and the targeting vector's biological half-life is a major step towards limitation of unnecessary patient exposure to ionising radiation post-imaging. Peptides used in nuclear imaging have been designed for a range of targets:¹⁴ somatostatin receptors 2 and 5,^{15–18} melanocortin receptors (MC_1 , $\text{MC}_3\text{-MC}_5$),^{19,20} gastrin releasing peptide receptor,^{17,21–23} prostate specific membrane antigen,^{24–26} integrin receptors ($\alpha\beta 3$, $\alpha\beta 5$, $\alpha\beta 6$, $\alpha 5\beta 1$),^{27–31} and various chemokine receptors.^{32,33,42,34–41}

Generally, proteins undergo extravasation (the leakage through the walls of blood vessels into surrounding tissues) slower than peptides by virtue of their higher molecular weights and so are often radiolabelled with longer-lived radionuclides such as ^{111}In ($t_{1/2} = 2.8 \text{ d}$, γ) and ^{89}Zr ($t_{1/2} = 3.3 \text{ d}$, β^+). A radiolabelled protein-bioconjugate will slowly clear blood circulation and accumulate at the target receptor often over the course of several days.⁴³ Imaging can then take place, generating excellent target tissue to non-target tissue contrast. Proteins that have been radiolabelled for nuclear imaging include cytokines, serum proteins, antibodies, and antibody fragments.

Antibodies, also known as immunoglobulins (Ig), are glycoproteins produced by plasma cells. Collectively, antibodies form a critical component of the immune response. In humans there are five known classes of antibodies (IgG, IgM, IgE, IgA, and IgD) each with a different structure and function. The IgG class is the most common serum immunoglobulin accounting for 10-20% of all serum proteins.⁴⁴ This

class is further subdivided into four subclasses: IgG1, IgG2, IgG3, and IgG4. Although each IgG subclass varies in its structure and immunological function, all are capable of binding to specific biomolecules. IgG1 is the most abundant subclass and is largely responsible for binding to soluble protein antigens and cell surface receptors.⁴⁴ By virtue of their high biological abundance and their ability to bind cell surface receptors with high affinity and specificity, IgG1 antibodies are used in therapeutic applications. As such, research on radiolabelled antibodies for application to nuclear medicine has focussed on this subclass. From this point on IgG1 antibodies will be referred to simply as “IgGs”.

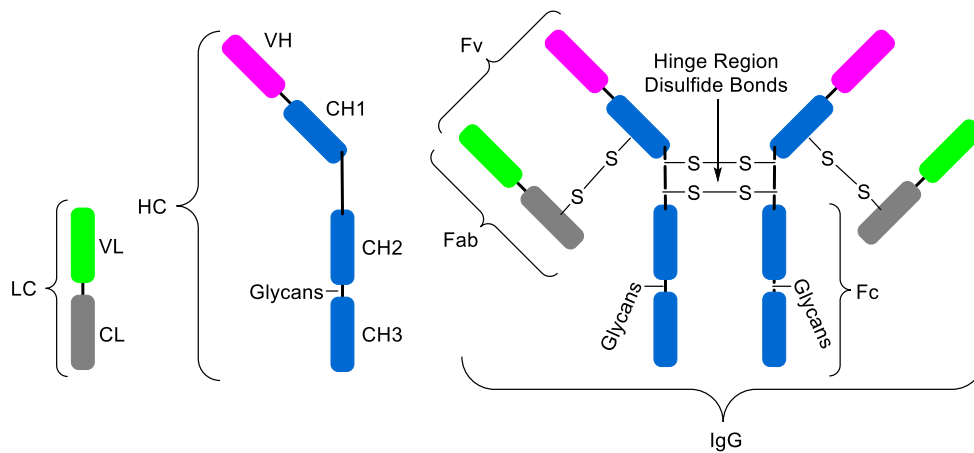


Figure 2 – The structure of an immunoglobulin G (IgG). LC = light chain, VL = variable light chain domain, CL = constant light chain domain, HC = heavy chain, VH = variable heavy chain domain, CH1-CH3 = constant heavy chain domains, Fv = fragment variable, Fab = fragment antigen binding, Fc = fragment crystallisable.

IgGs consist of four polypeptide chains, composed of two identical light chains (LC), and two identical heavy chains (HC) linked together by interchain disulfide bonds (figure 2). Each light chain consists of an N-terminal variable domain (VL), and a constant domain (CL). Similarly, each heavy chain consists of an N-terminal variable domain (VH) and three constant domains (CH1, CH2, and CH3), with a ‘hinge-region’ between CH1 and CH2. VL and CL associate with VH and CH1 respectively to form a Fab (fragment antigen binding) *via* a disulfide bond between CL and CH1. Collectively, the variable components of the IgG formed from each pair of VL-VH are known as Fv (fragment variable). The variability of this region is largely responsible for the diversity of IgG antibodies, and their highly specific interactions with antigens. Two HC-LC heterodimers associate to form a single IgG *via* disulfide

bonds in the hinge region, as well as non-covalent interactions between CH3 domains. The trunk formed by the lower part of the hinge region and CH2/CH3 domains is referred to as the fragment crystallisable (Fc). In contrast to the Fab region, the Fc region for all antibodies in a class (e.g. IgG) are the same for each species.⁴⁴ Rather than generating antigen specificity, the Fc region is responsible for effector functions. The Fc domain interacts with Fc-gamma receptors (FcγR) that are found on the surface of effector immune cells including natural killer cells, macrophages, and mast cells. Binding of an antibody's Fv region to its complementary antigen followed by binding of the Fc domain to an FcγR stimulates the destruction of the antigen by phagocytotic or cytotoxic cells, either by antibody-mediated phagocytosis or antibody-dependent cell-mediated cytotoxicity (ADCC) pathways. In the context of antibody-targeted cell surface receptor-based molecular imaging, interaction between antibody Fc domains and Fc receptors found in the blood - for example on effector cells - contributes to longer blood pool circulation times. A highly conserved N-linked glycosylation site is found between CH2 and CH3 at position 297. Glycosylation at this position induces subtle changes in the quaternary structure of the Fc region. This can aid in the formation of a more exposed FcγR docking-site, whilst the glycans can also directly engage in FcγR binding. Variation of the glycosylation pattern has an immunomodulatory effect by altering FcγR binding. Interestingly, another glycosylation site is observed in 10-15% of IgGs in the Fv region.⁴⁴

IgG are used therapeutically by virtue of their exceptional antigen affinity and selectivity for their target receptors, which themselves are often key drivers of disease progression. Binding of a therapeutic antibody to its target receptor on cancer cells leads to an inhibitory effect, thereby slowing, halting or even reversing disease progression. Antibodies have also been modified to bear drug molecules enabling delivery of cytotoxic drugs to target cells, leading to cell death after antibody internalisation. Before prescription of these therapies, it is important to understand whether the cancer cells, or target diseased cells express the complementary cell surface receptor to enable antibody-mediated targeting. This can be achieved by taking a biopsy and submitting the sample for histology where specific stains and dyes are used to enable visualisation of cancer cells that express the desired receptor *via* microscopy. However, the expression of antibody target receptors is often highly heterogeneous.⁴⁵⁻⁴⁷ PET imaging with radiolabelled

antibodies can be used to establish whether the patient has receptor positive cancer whilst simultaneously evaluating the degree of *inter-* and *intra-*tumoral heterogeneity, thus informing the therapeutic decision-making process.

For example, patients with tumours expressing programmed death ligand 1 (PD-L1) are more likely to respond to antibody therapy aiming to block the interaction between PD-L1 and its receptor (PD-1). Whilst biopsies are used to assess PD-L1 and PD-1 expression by immunohistochemistry and RNA (ribonucleic acid) sequencing, intra- and inter-tumoral heterogeneity limits their predictive value. Following pre-clinical investigations,^{48,49} a first-in-human study was carried out to show that PD-L1 and PD-1 expression could be quantified using PET in patients with non-small cell lung cancer.⁵⁰ Imaging with ⁸⁹Zr-labelled Nivolumab (anti PD-1) the study showed significant tumour tracer uptake heterogeneity both *inter-*tumorally and between patients. Another study assessed the feasibility of imaging with ⁸⁹Zr-atezolizumab (anti-PD-L1), to test its potential to predict patient response to PD-L1 blockade. Heterogeneous PD-L1 expression was observed *inter-* and *intra-*tumorally as well as between patients. Promisingly, clinical responses were better correlated with pre-treatment PET signal (imaging with ⁸⁹Zr-atezolizumab) than with immunohistochemistry, or RNA sequencing.

Different considerations exist for the modification of peptides versus proteins. Short chain peptides do not possess significant secondary or tertiary structure and are therefore less prone to denaturation and can withstand relatively harsh conditions (> 40°C, pH ≤ 6, pH ≥ 8), and non-physiologically compatible solvents and reagents. Therefore, radiolabelling reactions can take place under these harsh conditions without compromising peptide biological activity. In contrast, proteins rely on extensive non-covalent interactions to maintain their high-level structure (secondary, tertiary, and quaternary structure). These weak forces can be disrupted under harsh conditions or in the presence of non-physiologically compatible reagents and solvents. Compromised protein structure often results in decreased or even absent bioactivity. In the case of antibodies, this corresponds to a loss of antigen binding affinity. Therefore, when modifying proteins greater care must be taken to retain bioactivity by limiting denaturation. Additionally, care must be taken to ensure that modifications do not significantly alter the antibody's physical properties such as its thermal stability and propensity for aggregate formation. Additionally, where possible antibody modification should not impact effector

functions such as complement system activation, FcγR binding, and antibody dependent cellular cytotoxicity.

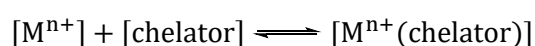
1.3.2 Chelator selection

To incorporate a radiometallic ion into a biomolecule, the radiometallic ion must be effectively complexed by a suitable ligand or chelator. A chelator is covalently bound to a peptide or protein to give a bioconjugate. This species is then added to a solution containing the radiometallic ion. The chelator reacts with the radiometallic ion to form a stable complex, ideally precluding the release of the radiometallic ion *in vivo*, to enable delivery to the target receptor. Within ligand design there are several radiochemical challenges that must be overcome:

- Radiometallic ions are present at very low concentrations, usually in the presence of adventitious trace metal ion contaminants. The chelator should be able to form the desired radiometal-complex under these conditions.
- The ligand concentration should preferably remain low in the radiolabelling reaction. Since in many cases excess, non-radioactive ligand is not separated from the radiolabelled ligand, the administered dose contains both radioactive and non-radioactive ligand. Administration of high amounts of non-radiolabelled ligand could result in adverse pharmacological reactions *in vivo*. Additionally, non-radiolabelled ligand can compete with the radiolabelled ligand for binding to the target receptor. This can lead to blocking of the target receptor, and hence impede delivery of the radiolabelled ligand to its biological target.
- Radiometal complexation kinetics should be fast. Due to the short half-life of many radionuclides (e.g. ^{68}Ga $t_{1/2}$ 68 min), fast complexation kinetics are essential. Whilst longer-lived radionuclides are compatible with longer radiolabelling protocols (sometimes lasting hours) should this time be required to achieve near quantitative radiochemical yields. Practically, in clinical settings rapid radiolabelling protocols are preferred no matter which radionuclide is used.
- The complexation reaction should generate near-quantitative yields whilst maintaining low ligand concentrations. This obviates the need for time-intensive purification processes such as chromatography. Experimentally, the equilibrium constant K (equations 2 and 3) can be used to determine

the position of equilibrium for a complexation reaction, and is a measure of thermodynamic stability.

- Ideally the radiolabelling reaction should generate a single metal complex, aiding in product characterisation, and simplifying or preventing the need for purification. If multiple metal complexes are formed in the reaction, it is possible that each species has different stability profiles, and behaviours *in vivo*. More reliable and informative results are gained when signal intensity can be directly correlated to the degree to which a *specific* biochemical process is taking place involving a single, well-characterised radioactive molecule.
- Radiolabelling should take place in aqueous, physiologically compatible solutions, under mild conditions. As previously discussed, (see 1.3.1), to prevent denaturation of sensitive proteins, radiolabelling should take place under mild conditions (<40 °C, near neutral pH), with physiologically compatible reagents, and in aqueous solutions. This means choosing complexation reactions with low kinetic barriers (low activation energy). From a practical perspective, using physiologically compatible reagents and aqueous conditions enables direct administration of the radiolabelling mixture without the need for additional steps to remove non-physiologically compatible reagents and solvents.
- Lastly, the radiopharmaceutical should possess high kinetic stability to preclude release of the radiometallic ion *in vivo*. Upon intravenous administration the radiopharmaceutical is exposed to highly diluting conditions (the average human body contains approx. 5 L of blood) and high concentrations of competing ligands such as serum albumin, transferrin, superoxide dismutase, and glutathione. Under these conditions, dissociation or transchelation of the radiometallic ion is thermodynamically favoured. Therefore, the radiopharmaceutical must have sufficiently high kinetic stability i) to preclude radiometallic ion dissociation *in vivo*, and ii) to prevent transchelation of the radiometallic ion to endogenous ligands.



Equation 2 – The equilibrium formed by the reaction between a metal ion and a chelator, to give a metal ion complex.

$$K = \frac{[M^{n+}(\text{chelator})]}{[M^{n+}][\text{chelator}]}$$

Equation 3 – The equilibrium constant K can be used to describe the position of equilibrium.

The following sections of this introduction will review: chelators for ^{64}Cu with a particular focus on the sarcophagine class of chelators; ^{89}Zr and its use in antibody radiolabelling specifically involving the chelator desferrioxamine (DFO); lastly, maleimide and disulfide bridging conjugation technologies. Later chapters of this thesis will describe new chemical platforms involving sarcophagine, DFO, maleimide and dibromomaleimide chemistry.

1.3.3 Chelators for Cu radioisotopes

Complexes of Cu^{2+} often form kinetically labile complexes due to the low ligand field stabilisation energy of d^9 complexes. Additionally, the Jahn-Teller effect causes many octahedral Cu^{2+} complexes to display a degree of tetragonal distortion (figure 3a).⁵¹ The Jahn Teller effect is a geometric distortion seen for non-linear molecules, which results in a reduction in symmetry and energy. In some cases, a square planar geometry predominates because of rapid ligand exchange at the axial positions. Complexes of Cu^{2+} can be kinetically stabilised by using multidentate ligands (chelators).

The phenomenon responsible for the increased stability of multidentate ligand complexes is called the chelate effect, which describes the entropically favoured complexation of a metal ion by a multidentate ligand (chelator).

Complexes of macrocyclic chelators are usually more stable than their acyclic counterparts, this is known as the macrocyclic effect. Compared to acyclic chelators, the conformational “pre-arrangement” of macrocycles results in a lower entropic barrier to complex formation relative to their acyclic homologues.

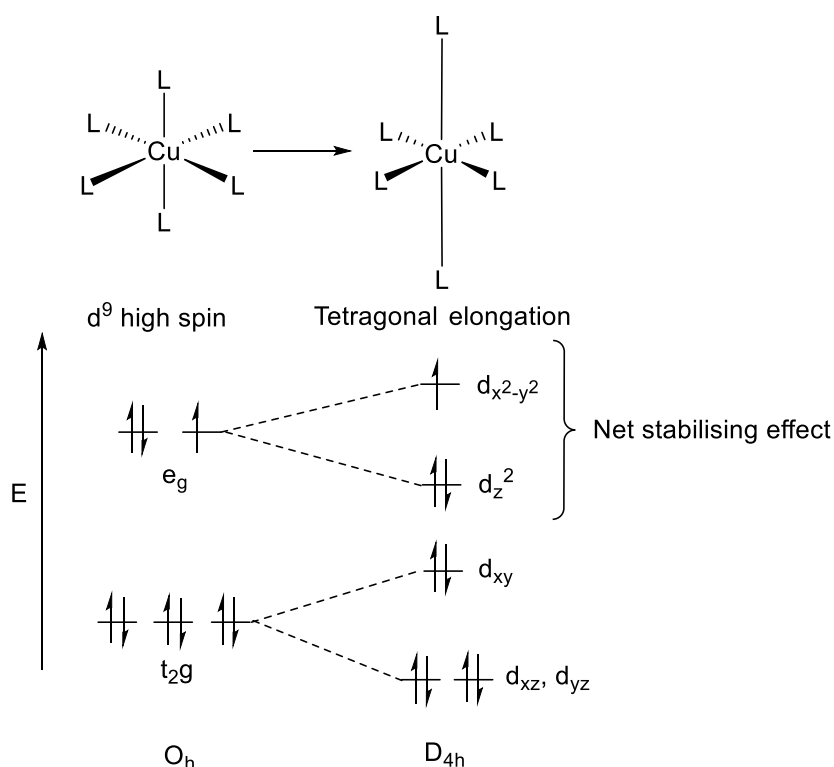


Figure 3a – A d^9 Cu^{2+} system undergoing Jahn Teller distortion resulting in a tetragonally elongated distorted octahedral geometry. Charges have been removed from the complexes for clarity.

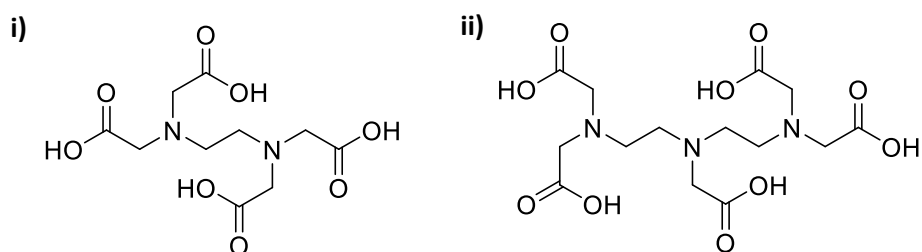


Figure 3b – Structures of i) EDTA and b) DTPA.

Radiochemists have exploited the chelate effect and the macrocyclic effect in developing stable complexes of Cu^{2+} radioisotopes. Early copper radiochemistry focussed on the complexation of ^{67}Cu – a therapeutic copper radioisotope (β^- , $t_{1/2} = 61.8$ h). Complexes of $^{67}\text{Cu}^{2+}$ were formed using the readily available chelators ethylenediaminetetraacetic acid (EDTA, figure 3i) and diethylenetriaminepentaacetic acid (DTPA, figure 3ii).

The Cu^{2+} complex of DTPA is more thermodynamically stable than the EDTA complex with $\text{Log } K$ values of 20 and 18 respectively.⁵² Despite their relatively high $\text{Log } K$ values, incubation of these complexes in serum led to almost complete radiometallic ion dissociation after just 24 hours.^{53,54} In contrast, in the same study,

it was found that the cyclam-derived macrocycle 1,4,8,11-tetraazacyclododecane-1,4,8,11-tetraacetic acid (TETA, figure 4) formed a more stable complex, undergoing minimal $^{67}\text{Cu}^{2+}$ dissociation in serum over 10 days (3 % dissociation). This observation is in agreement with the higher Log K of the Cu^{2+} complex of TETA with Log K values reported at 20.49 and 21.87.^{55,56} In TETA complexes of Cu^{2+} the metal ion is positioned in the plane of the macrocycle with the coordinating amines occupying the equatorial plane and the carboxylate groups trans with respect to one another in the axial positions.⁵⁷ In the solid state, X-ray crystal diffractometry data suggests that the Cu^{2+} complex of TETA possesses a Jahn-Teller distorted octahedral geometry. Macrocycles often display high kinetic stability, which along with the macrocyclic effect generate the improved stability observed for the TETA complex relative to that of EDTA or DTPA.

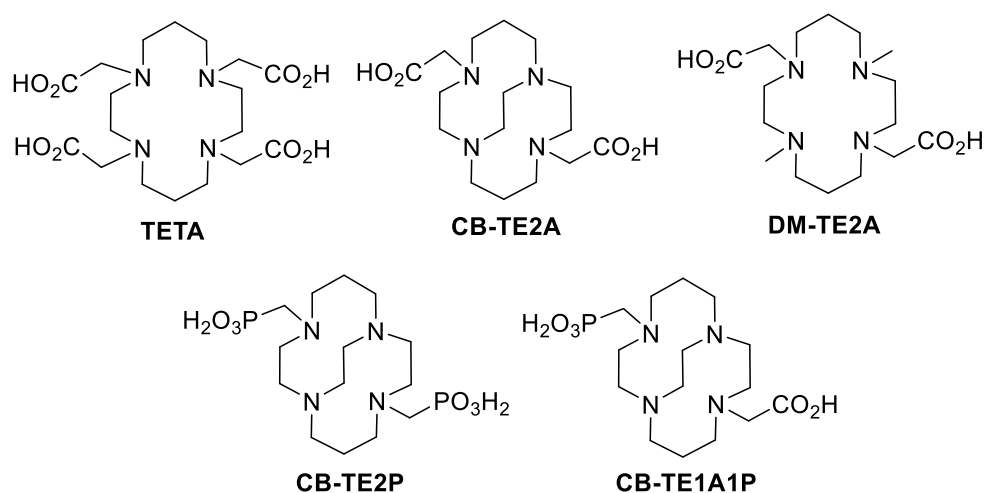


Figure 4 – Structures of TETA and other cyclam derivatives that have been investigated as chelators for $^{64}\text{Cu}^{2+}$.

Building on this work, an anti-colorectal carcinoma monoclonal antibody (1A3) was conjugated to a TETA-based bifunctional chelator.⁵⁸ This bioconjugate was then radiolabelled with $^{64}\text{Cu}^{2+}$ and $^{67}\text{Cu}^{2+}$ at pH 5.5, in a 0.1 M ammonium acetate solution. Radiolabelling efficiencies of between 60% and 75% were achieved in 15 minutes, indicative of suboptimal complexation kinetics. The radioimmunoconjugates were purified, and then administered to tumour bearing hamsters. Biodistribution studies were conducted and compared with those of ^{111}In - and ^{125}I - labelled analogues. The study found that tumour uptake at 24 h post injection was significantly better for the ^{64}Cu -labelled antibody (14.4 ± 4.80 % injected dose/g (% ID/g)) than both the ^{111}In -labelled antibody (8.6 ± 2.9 % ID/g)

and the ^{125}I -labelled antibody ($10.4 \pm 4.4\%$ ID/g). Immunoreactivity values observed for these three radioimmunoconjugates was routinely $>85\%$. Therefore, compromised antigen binding is unlikely to be the source of this observed difference. A more likely explanation is that ^{64}Cu -TETA-1A3 bioconjugate possesses superior *in vivo* stability with respect to radionuclide retention.

Despite this initial success, $^{64}\text{Cu}^{2+}$ complexes of TETA were eventually found to possess suboptimal properties for clinical PET applications. Further pre-clinical studies in rats using ^{64}Cu -TETA-octreotide have shown that the complex undergoes transchelation to superoxide dismutase, leading to radionuclide accumulation in the liver.⁵⁹ This finding suggests that the Cu^{2+} complex of TETA lacks sufficient kinetic inertness to preclude demetallation *in vivo*. Other cyclam derivatives including CB-TE2A,⁶⁰ DM-TE2A,⁶¹ and methylphosphonate derivatives^{62,63} have been synthesised and assessed as $^{64}\text{Cu}^{2+}$ chelators (figure 4). Some of these chelators have generated more kinetically stable Cu^{2+} complexes, but harsh labelling conditions are often required to generate high radiochemical yields. For example, quantitative radiolabelling of CB-TE2A-peptide conjugates with $^{64}\text{Cu}^{2+}$ has been achieved after incubation for 2 h at $95\text{ }^\circ\text{C}$.⁶⁰ These forcing conditions are indicative of high kinetic barriers to complexation.

Cyclen derivatives have also been used to form $^{64}\text{Cu}^{2+}$ complexes. The macrocycle 2,2',2'',2'''-(1,4,7,10-tetraazacyclododecane-1,4,7,10-tetrayl)tetraacetic acid (DOTA, figure 5) is the most widely used macrocycle in nuclear medicine.⁶⁴ As a result of the Jahn-Teller effect, DOTA forms a distorted octahedral complex with Cu^{2+} . In contrast to TETA, DOTA complexes of Cu^{2+} position the metal ion above the plane of the four tertiary amines, with two *trans*-annular carboxylates occupying the remaining positions in a *cis* configuration. Studies have shown that despite its high thermodynamic stability ($\text{Log } K = 22.7$)⁵⁵ this complex also possesses insufficient kinetic stability to prevent radiometallic ion dissociation *in vivo*.⁶⁵ In male Lewis rats, just 1 hour p.i. almost 90% of the radiometal undergoes transchelation to serum proteins, accumulating in the liver. Since $^{64}\text{Cu}^{2+}$ complexes of DOTA are highly susceptible to transchelation they are not generally considered appropriate for nuclear imaging applications. Many other cyclen derivatives have been proposed as chelators for $^{64}\text{Cu}^{2+}$ including CB-DO2A,^{65,66} and methanephosphonate functionalised macrocycles (figure 5).⁶⁷ However, in most cases these cyclen derivatives require high radiolabelling temperatures or long

radiolabelling times to achieve near-quantitative radiochemical yields, or alternatively, radiochemical yields of $^{64}\text{Cu}^{2+}$ complexes are low.

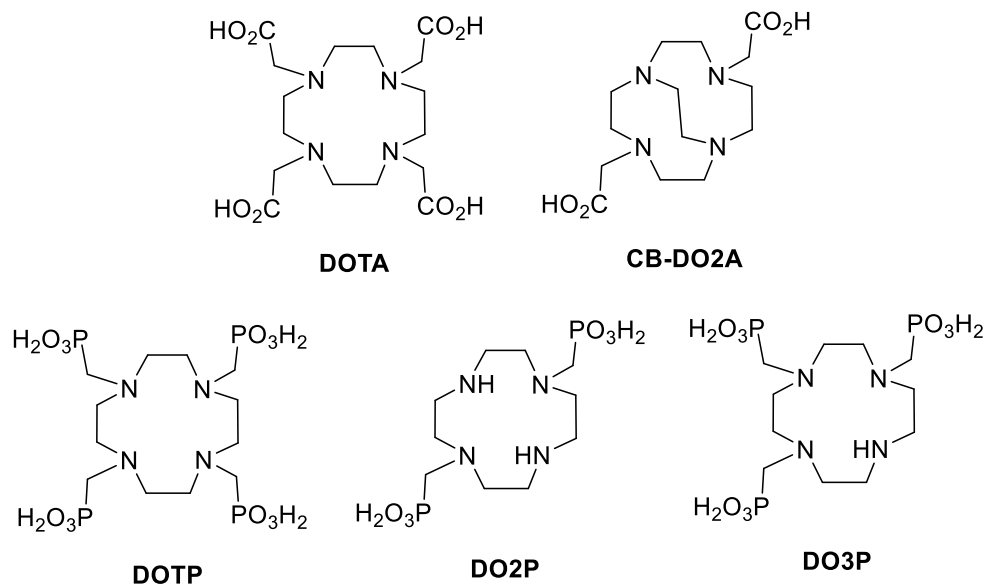


Figure 5 - Structures of DOTA, and other cyclen derivatives that have been investigated as chelators for $^{64}\text{Cu}^{2+}$.

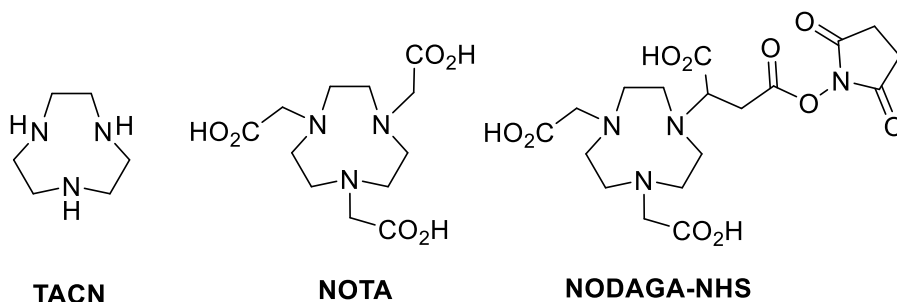


Figure 6 - Structures of TACN, NOTA, and NODAGA-NHS that have been investigated as chelators for $^{64}\text{Cu}^{2+}$.

The 1,4,7-triazacyclononane (TACN, figure 6) derivative 2,2',2''-(1,4,7-triazacyclononane-1,4,7-triyl)triacetic acid (NOTA, figure 6) has been successfully used for chelation of $^{64}\text{Cu}^{2+}$.^{68–70} This cyclononane possesses a smaller cavity size compared to the cyclam and cyclen derivatives mentioned previously. NOTA forms a hexadentate octahedral complex with Cu^{2+} , with the metal ion tightly enclosed by the ligand's six donor atoms in a 3 *fac*-N, 3 *fac*-O configuration. Whilst the Cu^{2+} complex of DOTA is more thermodynamically stable ($\text{Log } K = 22.7$)⁵⁵ than that of NOTA ($\text{Log } K = 21.6$),⁷¹ the latter possesses greater kinetic stability as demonstrated by its superior radionuclide retention *in vivo*.⁷² A recent ^{64}Cu study compared the labelling efficiency, specific activity (amount of radioactivity per unit mass,

compared to molar activity, which refers to the amount of radioactivity per mole) and *in vitro* / *in vivo* stability of eight radioummunoconjugates bearing different bifunctional chelators (figure 7).⁷³ Overall, NOTA was one of the highest performing chelators with radiolabelling

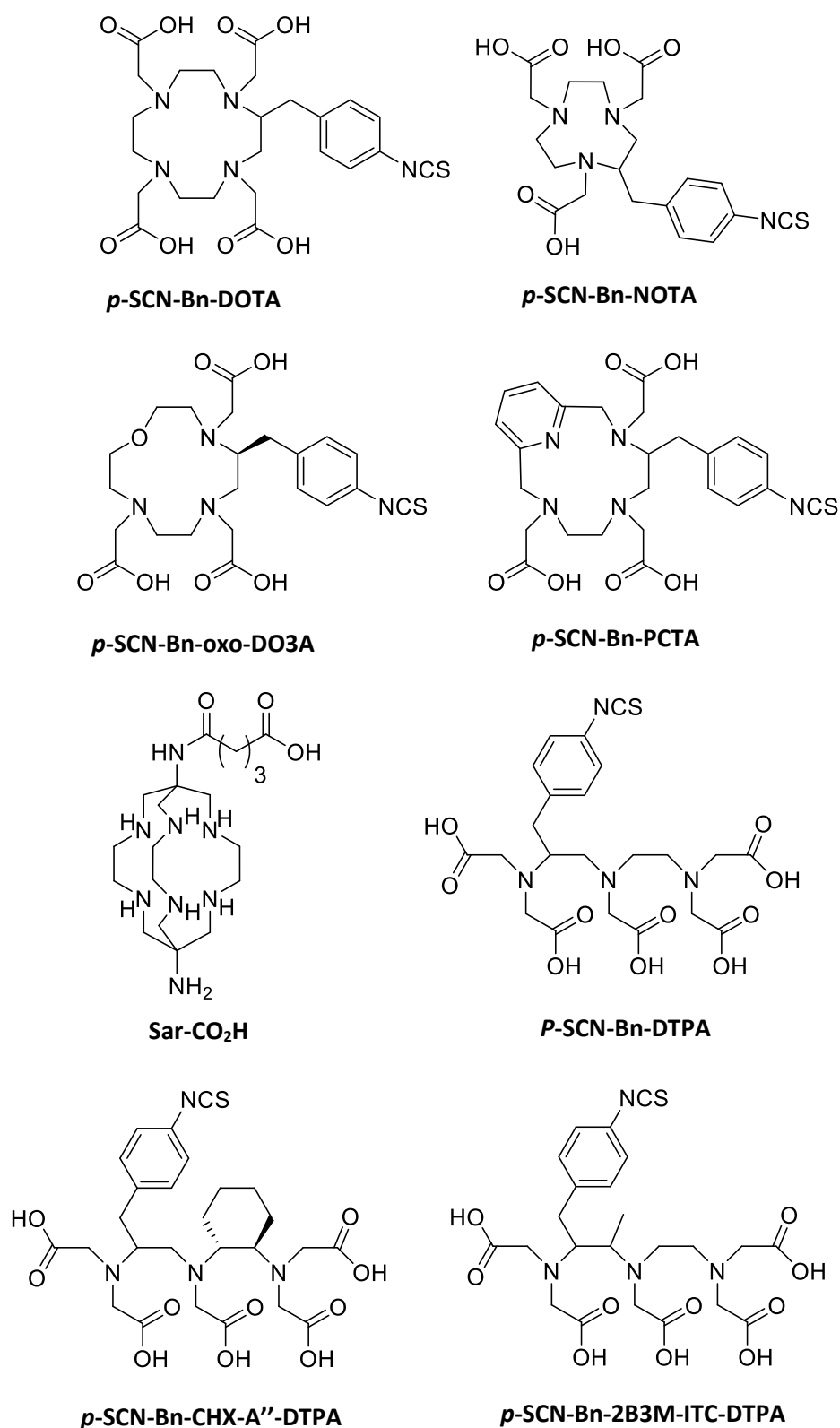


Figure 7 - Bifunctional chelators for $^{64}\text{Cu}^{2+}$, $^{73}\text{Ga}^{3+}$.

efficiency of 95.2%, in 20 min, at room temperature, at pH 6, with a low concentration of bifunctional chelator (31.3 nM). Under the same conditions the DOTA analogue, had a radiolabelling efficiency of just 1.4% highlighting the

significant kinetic barrier to complexation when labelling DOTA with $^{64}\text{Cu}^{2+}$. The concentration of the DOTA conjugate had to be increased to 250 nM before a radiolabelling efficiency of > 95 % was generated. As a result, higher specific activities are achievable using NOTA conjugates than those of DOTA, which is preferable from an imaging perspective (see 1.3.2). Impressive results were also obtained using the sarcophagine based chelator (sar-CO₂H), which generated comparable radiolabelling efficiencies compared to the NOTA conjugate at the same concentration of bifunctional chelator. Both the NOTA- and sarcophagine-based radioimmunoconjugates displayed high kinetic stability *in vivo*, with minimal liver uptake 48 h after administration.

In a direct comparison study DOTA-NHS and 1,4,7-triazacyclononane,1-glutaric acid-4,7-acetic acid (NODAGA-NHS, figure 8) were conjugated to mAb7, which targets epithelial cell adhesion molecule (EpCAM). The immunoconjugates were radiolabelled with $^{64}\text{Cu}^{2+}$ and directly compared for their ability to detect EpCAM in a prostate cancer model in mice.⁷⁴ The DOTA conjugate yielded an average of 3.3 chelators per antibody, compared to 2.5 for the NODAGA conjugate. Radiolabelling was carried out by mixing 100 µg of immunoconjugate with 37 MBq of $^{64}\text{Cu}^{2+}$ in 0.1 M ammonium acetate solution (pH 6). The DOTA conjugate was heated to 40 °C, whilst the NODAGA conjugate was kept at room temperature. This temperature difference is likely reflective of the slower complexation kinetics seen for DOTA compared to NODAGA, and were deemed to be necessary to improve radiochemical yields. Radiochemical yields were 71.9 ± 9.0 % and 59.3 ± 2.1 % respectively, necessitating post-radiolabelling purification using Zeba desalting spin columns to give both conjugates in > 99% radiochemical purity. The stabilities of the two radioimmunoconjugates was assessed over 48 h in mouse serum at 37 °C. The DOTA conjugate possessed good serum stability, with 88.7 ± 0.9 % intact after 48 h. The NODAGA conjugate possessed similar stability with 84.5 ± 0.2 % intact after 48 h. *In vivo* biodistribution studies highlighted a statistically significant ($p < 0.05$) difference in liver uptake for the DOTA (6.21 ± 0.96 %ID/g) and NODAGA (4.65 ± 0.44 % ID/g) conjugates at 48 h p.i. The lower liver uptake of the NODAGA conjugate compared to the DOTA conjugate is evidence of better radiocomplex stability. Additional evidence for the superior *in vivo* stability of the NODAGA conjugate is represented by its higher blood retention of 10.10 ± 0.66 %ID/g

compared to 4.51 ± 2.23 %ID/g for the DOTA conjugate, conferring increased bioavailability.

Overall, studies have shown that: i) macrocyclic chelators often form more stable complexes with $^{64}\text{Cu}^{2+}$ than acyclic ones; ii) macrocyclic cyclam and cyclen derived $^{64}\text{Cu}^{2+}$ radiocomplexes possess relatively low *in vivo* stability; iii) the TACN derivative NOTA, and the macrobicyclic sarcophagine ligand appear to possess excellent characteristics as chelators for $^{64}\text{Cu}^{2+}$.

1.4 Sarcophagine

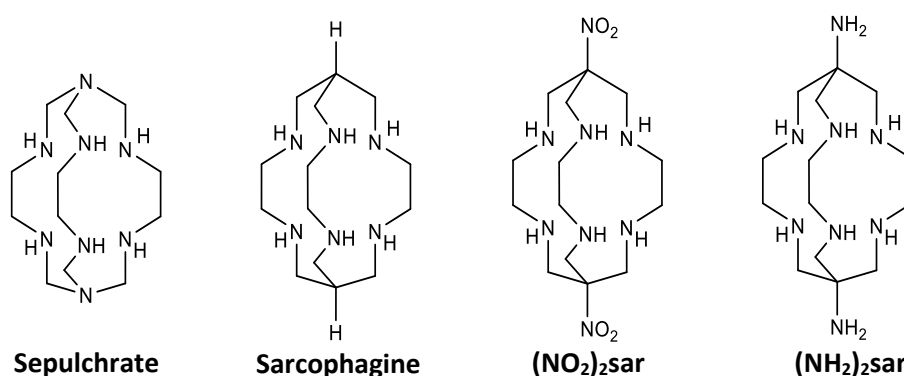


Figure 8 – The chemical structures of sepulchrates, $(\text{NO}_2)_2\text{sar}$, and $(\text{NH}_2)_2\text{sar}$.

1.4.1 Introduction to sarcophagines

Following their work on sepulchrates (figure 8), Sargeson and co-workers were the first to prepare “sarcophagine” ligands during the 1980’s.^{75–79} Sarcophagines are macrobicyclic molecules with a cage-like structure based upon 3,6,10,13,16,19-hexaazabicyclo[6.6.6]icosane (sarcophagine, figure 8).

Sarcophagines are synthesised using a templated method where a metal ion provides a “scaffold”, around which the ligand can be constructed (figure 9). Diaminosarcophagine ($(\text{NH}_2)_2\text{sar}$, figure 8) is commonly used as a synthon: its two nucleophilic amines facilitate further derivatisation. To synthesise $(\text{NH}_2)_2\text{sar}$, $[\text{Co}(\text{en})_3]^{3+}$ is reacted with formaldehyde and nitromethane under basic aqueous conditions (pH 10) to yield $[\text{Co}((\text{NO}_2)_2\text{sar})]^{3+}$. The nitro groups are then reduced using Zn/HCl, followed by reoxidation of Co^{2+} with hydrogen peroxide to give $[\text{Co}((\text{NH}_3)_2\text{sar})]^{5+}$. The cobalt ion is usually removed from the cage to enable complexation of another metal ion at a later stage. This can be achieved in two ways. The first involves addition of zinc dust to reduce Co^{3+} to Co^{2+} , followed by refluxing in concentrated HBr solution. Under these conditions the now kinetically labile Co^{2+} is extruded from the sarcophagine ligand to yield $[(\text{NH}_3)_2\text{sar}]^{2+}$. This can

be performed using HCl instead of HBr, but in order to generate comparatively efficient metal ion extrusion, the reaction must be carried out in a Carius tube placed inside a pressurised container and heated to 130 °C.⁸⁰ The second method involves addition of $[\text{Co}(\text{NH}_3)_2\text{sar}]^{5+}$ to a basic solution ($> \text{pH } 10$) containing excess sodium cyanide and CoCl_2 . $[\text{Co}(\text{CN})_4]^{2-}$ is formed *in situ*, which then reduces Co^{3+} to Co^{2+} in the sarcophagine complex. Co^{2+} then reacts with excess CN^- to form $[\text{Co}(\text{CN})_4]^{2-}$. The free base can then be extracted by dissolving in hot acetonitrile, filtering and cooling the filtrate to yield white crystals of $(\text{NH}_2)_2\text{sar}$.

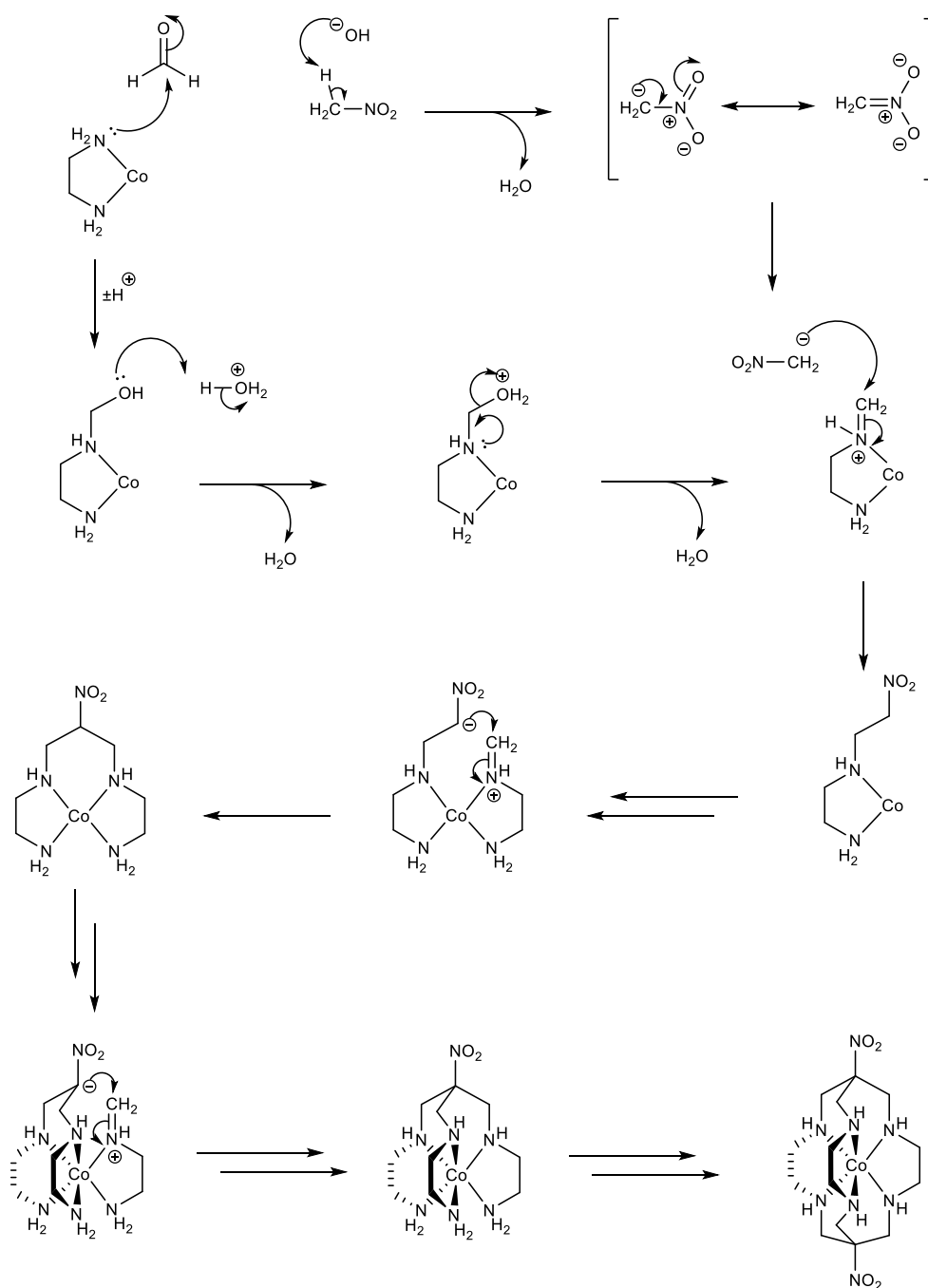
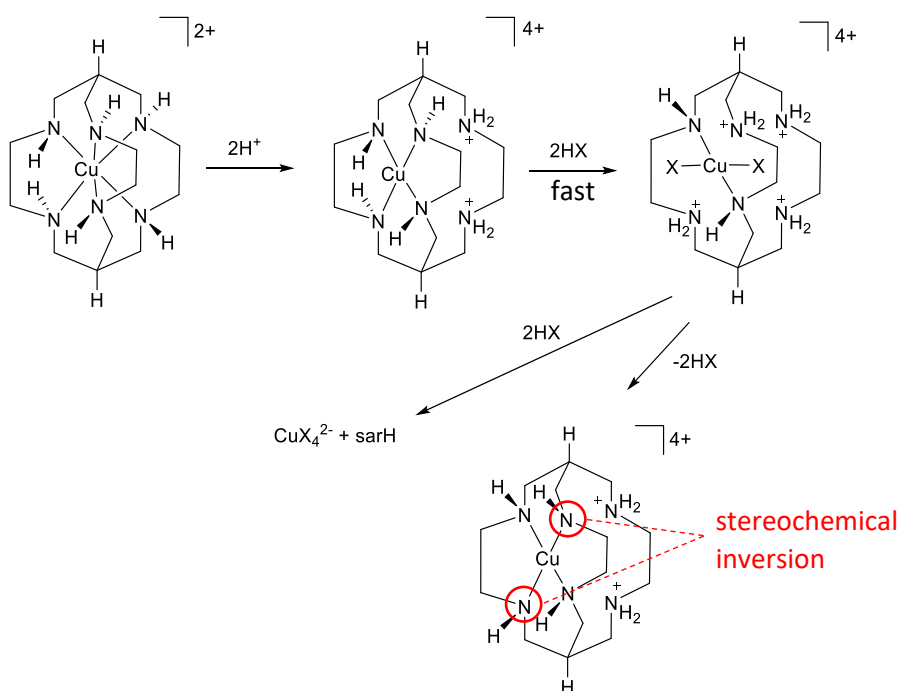


Figure 9 – The templated synthesis of $[\text{Co}(\text{NO}_2)_2\text{sar}]^{3+}$.⁷⁵

Sarcophagines rapidly form highly thermodynamically and kinetically stable complexes with a variety of metal ions including Cu^{2+} under mild conditions (25 °C, pH 6-8).⁸¹ The complex $[\text{Cu}(\text{NH}_2)_2\text{sar}]^{2+}$ is resistant to Cu^{2+} dissociation in 4 M hydrochloric acid solutions for prolonged periods of time (>7 months), indicative of the complex's high kinetic stability.⁸² In comparison the Cu^{2+} complex of DO2A, undergoes dissociation with a half-life of 3.3 h under significantly milder conditions (1.0 M KNO_3 , 0.1 M HNO_3 , 25 °C). The behaviour of Cu^{2+} sarcophagine complexes



under acidic conditions (5 M HCl) has been studied; a proposed scheme for metal ion dissociation is shown in figure 10.⁷⁵ The stability of Cu^{2+} sarcophagine complexes in concentrated acid is an extreme demonstration of their high kinetic stability.

Figure 10 – Route for the extraction of Cu^{2+} from $[\text{Cu}(\text{sar})]^{2+}$ under acidic conditions.⁷⁵

A dissociation constant (Log K) for $[\text{Cu}((\text{NH}_2)_2\text{sar})]^{2+}$ has never been determined since the complex is highly inert to dissociation.^{52,77} However, dissociation constants have been acquired for more labile Hg^{2+} sarcophagine complexes. Comparing the dissociation constant of $[\text{Hg}((\text{NH}_2)_2\text{sar})]^{2+}$ (Log $K = 26.3$) with that of $[\text{Hg}(\text{cyclam})]^{2+}$ (Log $K = 23.0$) shows that the former is roughly three orders of magnitude more thermodynamically stable than the latter.^{52,83} Therefore, it is likely

that $[\text{Cu}((\text{NH}_2)_2\text{sar})]^{2+}$ has a higher stability constant than $[\text{Cu}(\text{cyclam})]^{2+}$ ($\text{Log } K = 28.1$).⁸⁴

Sarcophagines display a preference for Cu^{2+} complexation in the presence of competing metal ions. In one study, $(\text{NH}_2)_2\text{sar}$ was mixed in equimolar quantities with Cu^{2+} and various divalent transition metal ions.⁷⁷ A marked preference for the formation of $[\text{Cu}((\text{NH}_2)_2\text{sar})]^{2+}$ was observed relative to $[\text{M}((\text{NH}_2)_2\text{sar})]^{2+}$ (where $\text{M} = \text{Mg}, \text{Mn}, \text{Ni}, \text{Zn}, \text{Cd}, \text{Hg}$). Sarcophagine's selectivity and ability to form kinetically inert complexes with Cu^{2+} , make this class of ligand well suited to overcome many challenges associated with radiolabelling biomolecules with $^{64}\text{Cu}^{2+}$.

1.4.2 Amine-reactive sarcophagine bifunctional chelators

Early sarcophagine bioconjugation work suggested that direct couplings between $(\text{NH}_2)_2\text{sar}$ and electrophilic amino acids (such as glutamic acid) were not efficient, possibly due to the steric bulk of the macrobicyclic hexamine rings. This led to the development of SarAr (figure 11) where diaminosarcophagine was functionalised with a para-substituted aniline enabling attachment to proteins *via* coupling reactions with carboxylic acids located on the side chains of glutamic acid and aspartic acid, or at the C-terminus.⁸¹

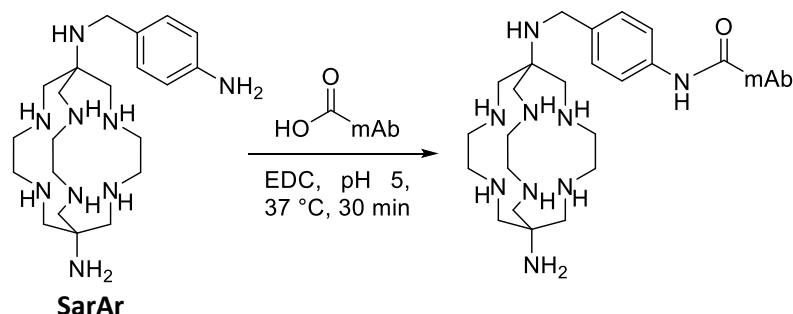


Figure 11 – The reaction used to synthesise an immunoconjugate between the aromatic primary amine group on SarAr and a carboxylic acid on the cd19.18 antibody (mAb).

Since SarAr many different sarcophagine BFCs and their accompanying bioconjugates have been prepared. Most modern bioconjugations make use of bifunctional chelators bearing electrophiles. These derivatives enable conjugation to peptides and proteins *via* the nucleophilic amine on lysine side chains and at the N-terminus. Carboxylic acid-bearing sarcophagines have been synthesised by reacting the Cu^{2+} complex of diaminosarcophagine with glutaric anhydride (figure 12).^{17,23}

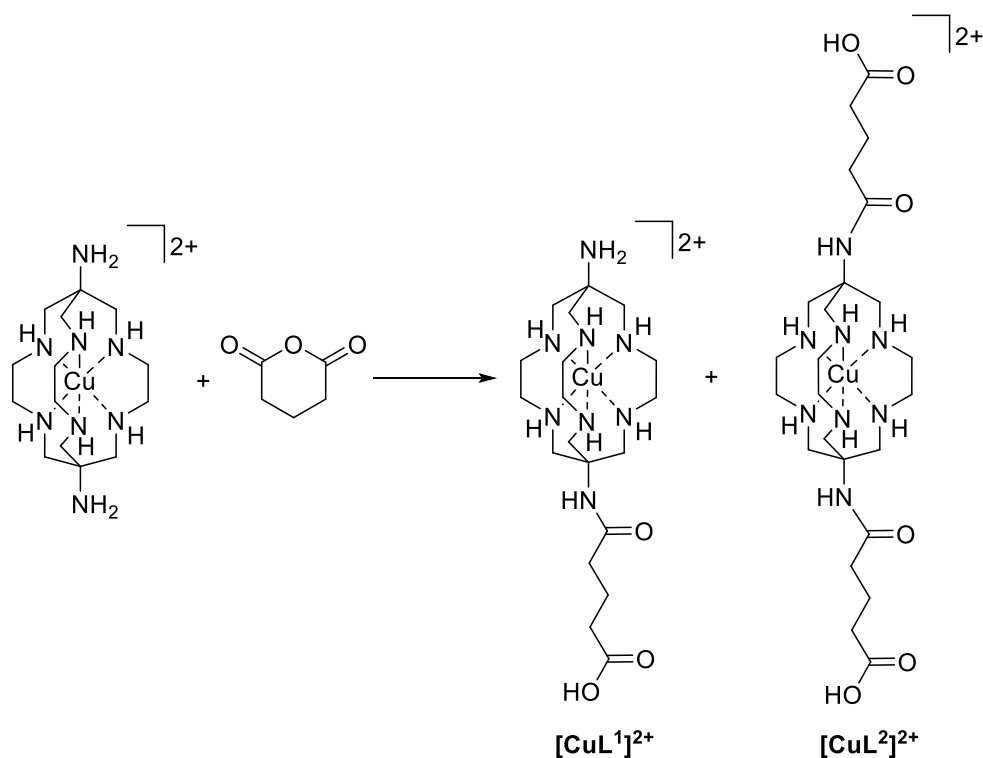


Figure 12 - The synthesis of carboxylate bearing sarcophagines using a Cu^{2+} protection strategy.¹⁷

The Cu^{2+} complex of $(CH_3)(NH_2)sar$ (figure 13) has also been used to synthesise the mono-carboxylic acid functionalised sarcophagine MeCOsar (figure 13). In these reactions, protecting strategies involving use of a coordinating metal ion were used to prevent unwanted reactions between secondary amines and anhydrides, as these species contain one or two primary amines and six secondary amines all of which are nucleophilic.⁸⁵ To selectively functionalise at one or both apical positions, the secondary amines can be ‘protected’ through metal ion complexation. Cu^{2+} has been used for this purpose and can be removed when desired by reducing Cu^{2+} to Cu^+ . This change in oxidation state causes the metal ion to be ejected from the ligand, presumably because the ligand is unable to accommodate the larger ionic radii of Cu^+ .⁸⁶ This hypothesis is supported by the observation that larger cage amines with expanded cavities are able to form more stable complexes with Cu^+ .⁸⁷ Reduction of Cu^{2+} can be performed by electrochemical means,⁸⁶ with Na_2S ,¹⁷ or using sodium borohydride in the presence of Pd/C.⁸⁸ These

deprotection/demetallation conditions are not tolerated by many biomolecules, including some peptides and most proteins. Therefore, Cu^{2+} must be removed from the sarcophagine chelator *prior* to attachment to biomolecules.

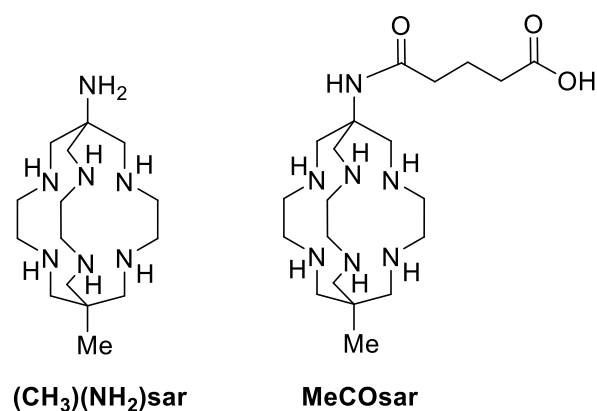


Figure 13 - The structures of $(\text{CH}_3)(\text{NH}_2)\text{sar}$ and MeCOsar.

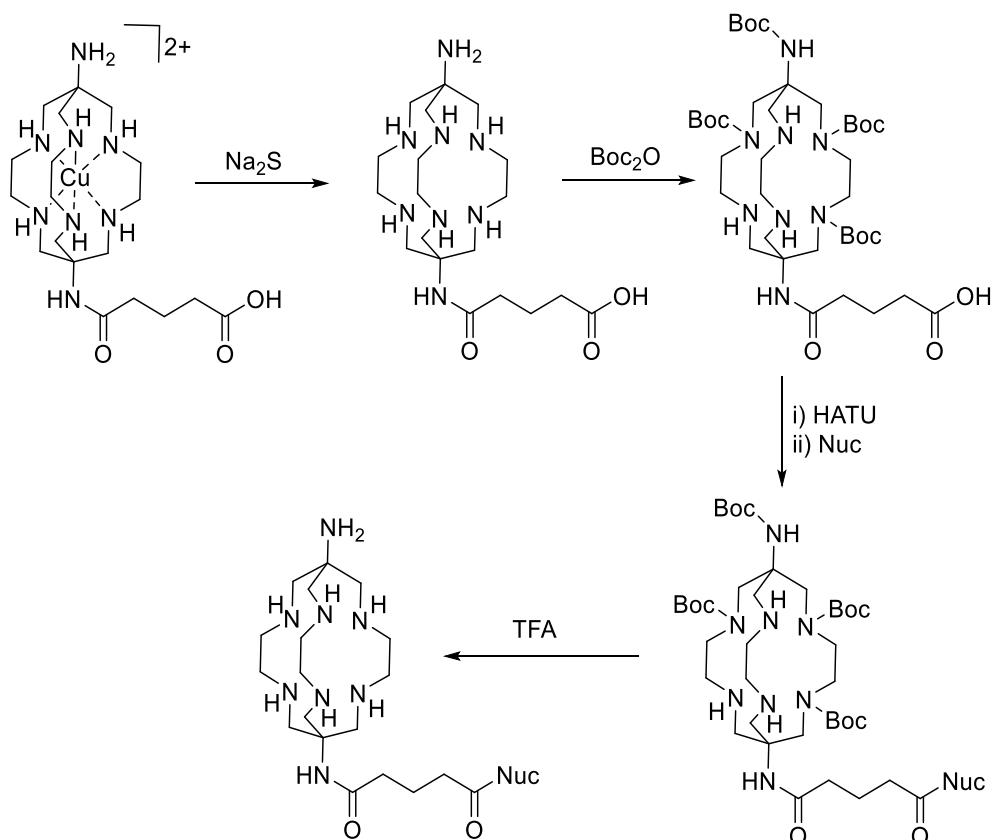


Figure 14 - Removal of Cu^{2+} from a carboxylate functionalised sarcophagine, followed by protection of the primary and secondary amines using Boc anhydride (Boc_2O). Then the carboxylic acid is activated using a coupling agent such as HATU before adding the nucleophile. Lastly, the Boc groups are removed using TFA to give the final deprotected conjugate.

Coupling carboxylic acid bearing sarcophagines to nucleophiles leads to a similar problem. Upon activation of the apical carboxylic acid (e.g. with peptide coupling agents such as HATU), the secondary cage amines can act as nucleophiles leading to undesired by-product formation. Protection using Cu^{2+} is not an option since the biomolecule attached may not withstand the harsh deprotection conditions. Instead, organic protection strategies have been employed. The primary and secondary amines can be protected using di-*t*-butyl dicarbonate (Boc anhydride), yielding a mixture of sarcophagine products bearing between three and five *t*-Boc substituents.^{17,22,89} Once the conjugation reaction is complete, deprotection of sarcophagine amines can be achieved by the addition of an acid such as trifluoroacetic acid. Peptides can withstand this acidic deprotection step - trifluoroacetic acid is commonly used in peptide synthesis to cleave peptides from the solid phase support. In contrast, proteins often undergo denaturation under highly acidic conditions.

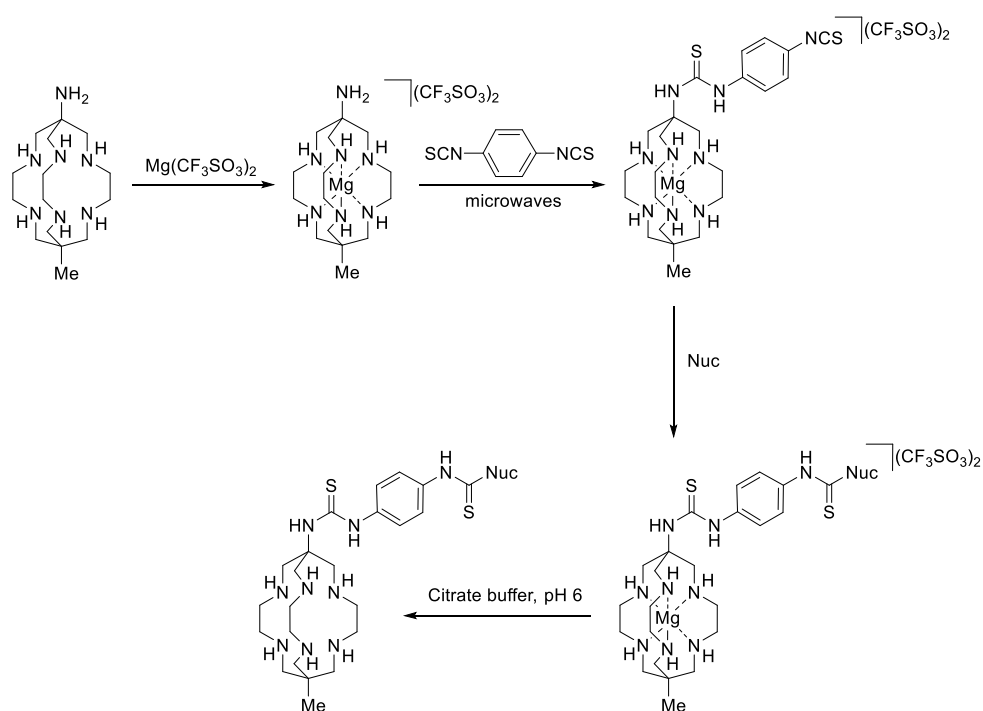


Figure 15 - The protection of sarcophagine secondary amines with Mg^{2+} enabling selective functionalisation of the primary amine with an amine reactive isothiocyanate group. Post conjugation, the Mg^{2+} can be removed from the chelator under mild conditions using citrate buffer (pH 6).⁹⁰

Mg^{2+} complexation has been used as a milder sarcophagine protection strategy during coupling reactions involving sensitive species such as proteins.⁹⁰ This approach was used to form a sarcophagine-antibody bioconjugate (figure 15).⁹⁰

[Mg(CF₃SO₃)₂] was added to (CH₃)(NH₂)sar to give [Mg(CH₃)(NH₂)sar](CF₃SO₃)₂ where the secondary amines are protected by complexation to Mg²⁺. This species was then reacted with a bis-isothiocyanate, to yield [Mg(CH₃)(*p*-NCS-Ph)sar](CF₃SO₃)₂. This species was then added to trastuzumab under mild basic conditions (pH 8.6, HEPES) to give a sarcophagine-trastuzumab bioconjugate. Since only one reactive primary amine exists in (CH₃)(NH₂)sar, formation of the unwanted bis-isothiocyanate side product is prevented. Additionally, the lack of another reactive primary amine in the product, mitigates concerns over self-reactivity. Reaction with amines of lysine residues in the antibody trastuzumab formed stable thiourea bonds. Post-conjugation, Mg²⁺ extrusion was achieved by exchanging the buffer to a citrate buffer at pH 6. At approximately pH 6, citrate is present in its trianionic form, where it displays its highest affinity for Mg²⁺, and in these reactions, competes with the sarcophagine chelator for coordination of Mg²⁺, efficiently removing it from the new sarcophagine-trastuzumab immunoconjugate. This approach facilitates direct conjugation reactions between sensitive proteins and sarcophagine derivatives bearing amine-reactive electrophilic motifs.

1.4.3 Sarcophagine peptide conjugates

Compared to proteins, peptides are much less complex, containing fewer amino acids and displaying no (or very limited) high order (secondary, tertiary, and quaternary) structure. Solid-phase synthetic methods can be used to synthesise peptides. Here, by using orthogonally protected amino acids, a great deal of control can be leveraged from a bioconjugation perspective since specific reactive groups can be deprotected selectively. Electrophile-bearing bifunctional chelators are often conjugated to reactive amines on peptides, either at their deprotected N-termini, or to deprotected side chain amines on lysine residues. The chosen nucleophile should be situated such that receptor binding is minimally compromised after conjugation. From a practical standpoint, since peptides are less prone to degradation and denaturation than proteins, harsher conjugation conditions, and the use of non-physiologically compatible reagents is possible. In the context of sarcophagine-peptide conjugations both Mg²⁺ and Boc protection strategies are viable. In the case of the latter, sarcophagine deprotection can be achieved simultaneously with peptide cleavage from the solid phase using neat trifluoroacetic acid.

In the first example of a sarcophagine-peptide conjugate, a carboxylic acid functionalised sarcophagine was conjugated to the SSTR2 (somatostatin receptor 2) targeting peptide Tyr³-octreotate (H–dPhe-Cys-Tyr-dTrp-Lys-Thr-Cys-Thr–OH) (figure 16).¹⁷ Tyr³-octreotate contains two primary amines: one at the N-terminus (Fmoc-protected), and another in the side chain of a lysine residue (Boc-protected). Peptide synthesis was achieved using standard Fmoc (fluorenylmethyloxycarbonyl) solid-phase peptide synthesis procedures enabling selective functionalisation of the N-terminal amine. Boc-protected carboxylate-functionalised sarcophagine was added to the resin-bound peptide along with diisopropylethylamine (DIPEA) and the coupling agent HCTU (2-(6-Chloro-1-H-benzotriazole-1-yl)-1,1,3,3-tetramethylammonium hexafluorophosphate). The Tyr³-octreotate-conjugate was then simultaneously cleaved from the resin and Boc-deprotected using TFA in the presence of triisopropylsilane (TIPS).

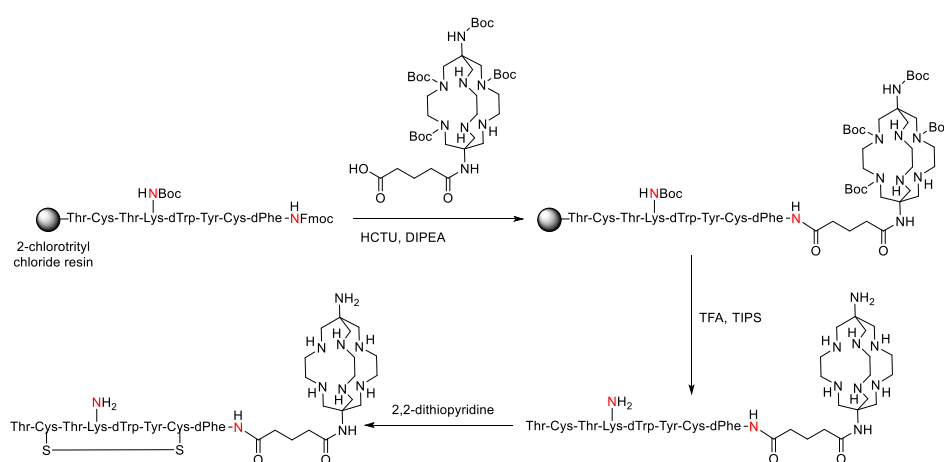


Figure 16 - A solid-phase route to form a Tyr³-octreotate sarcophagine conjugate.¹⁷

In the same paper, to show the versatility of the bifunctional chelator, the GRP receptor targeting peptide Lys³-bombesin (Pyr-Gln-Lys-Leu-Gly-Asn-Gln-Trp-Ala-Val-Gly-His-Leu-Met–NH₂) was conjugated to a carboxylate-functionalised sarcophagine (figure 17). The peptide was synthesised using standard Fmoc solid phase peptide synthesis procedures and the side chain of the Lys-3 residue was protected with an ivDde (N_ε-1-(4,4-dimethyl-2,6-dioxocyclohexylidene)ethyl) group. This was selectively deprotected with 5% hydrazine in DMF. Boc-protected carboxylate-functionalised sarcophagine was then coupled to the deprotected amine using HATU (2-(7-aza-1H-benzotriazole-1-yl)-1,1,3,3-tetramethyluronium

hexafluoro-phosphate). The Lys³-bombesin-conjugate was then simultaneously cleaved from the resin and deprotected using TFA in the presence of TIPS.

A subsequent paper conjugated a Boc-protected sarcophagine bearing two NHS-esters to Lys³-bombesin to give a single sarcophagine containing two peptides (figure 18).²³ Such multivalent constructs often display enhanced receptor binding since they are able to bind simultaneously to more than one cell surface receptor.²⁸ The Boc-protected sarcophagine bearing two NHS-esters was added to Lys³-bombesin in DMF in the presence of DIPEA. Solution phase conjugation was used to enable the attachment of two peptides to the bivalent cage amine since this conjugation is much less efficient when the peptide is bound to the resin.

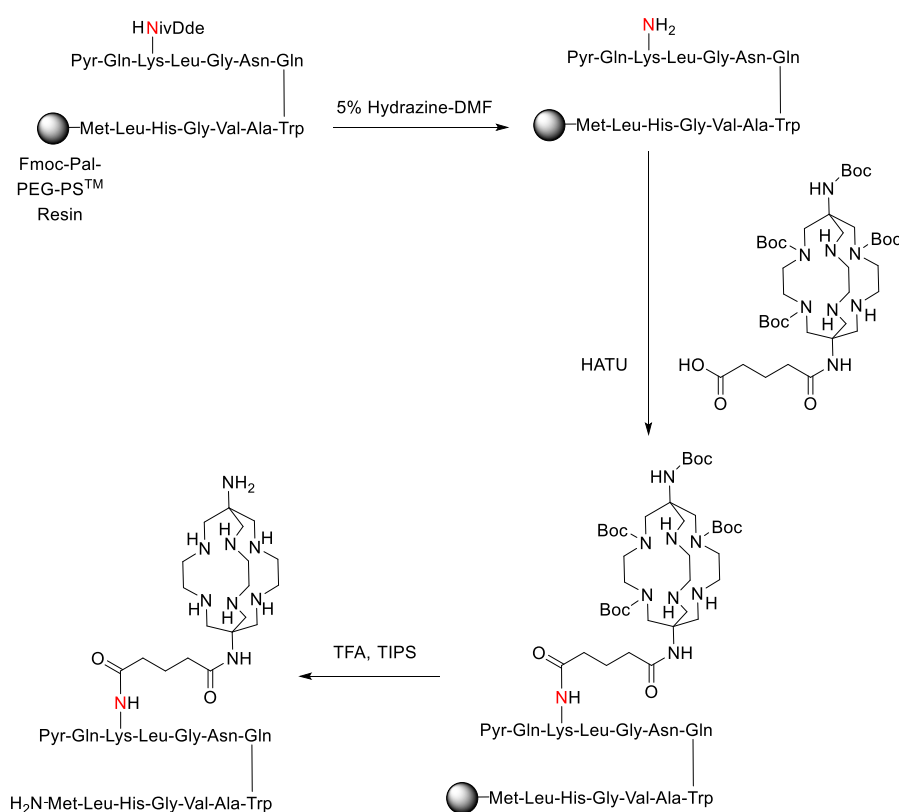


Figure 17 - A solid-phase route to form a Lys³-bombesin sarcophagine conjugate.¹⁷

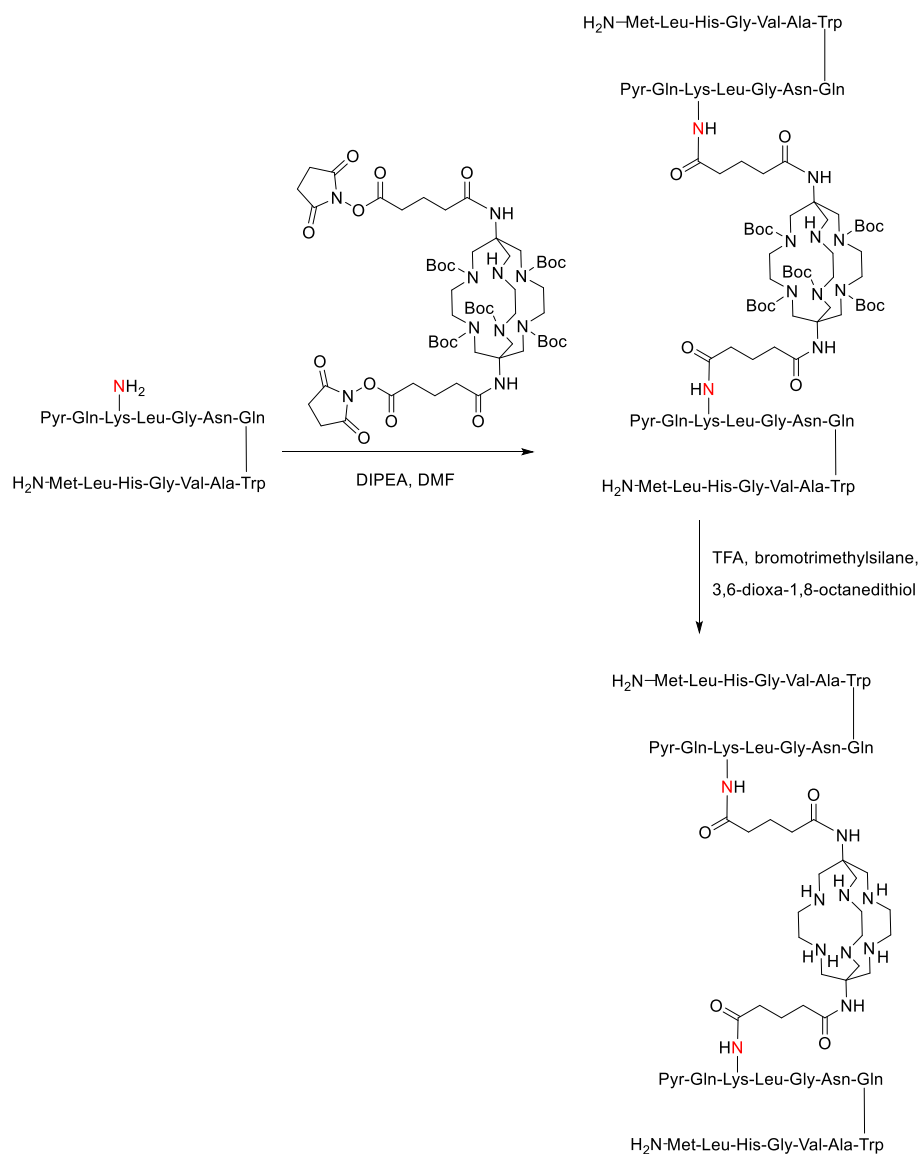


Figure 18 - A solution-phase route to form a sarcophagine bearing two bombesin peptides.²³

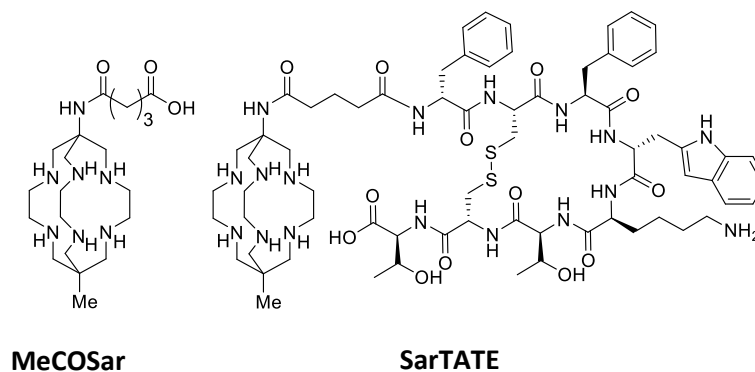


Figure 19 – Structures of MeCOSar and SarTATE.

In the synthesis of a mono-carboxylic acid diaminosarcophagine, even with careful control of stoichiometries, formation of the corresponding dicarboxylate is unavoidable, negatively impacting chemical yields and necessitating separation of products. Additionally, mono-valent diaminosarcophagine derivatives possess an obsolete apical primary amine, which is usually protonated at physiological pH. This gives the conjugate an additional positive charge, which can adversely affect biological clearance.^{91–94} This led to the development of the methyl-capped bifunctional sarcophagine ligand MeCOSar.¹⁸ The derivative (tBoc)₄₋₅MeCOSar was added to resin-bound Tyr³-octreotate in the presence of HATU and DIPEA to form the conjugate. This product was then simultaneously deprotected and cleaved from the resin using TFA, TIPS and 3,6-dioxo-1,8-octanedithiol to give SarTATE (figure 19). This conjugate was then radiolabelled with ⁶⁴Cu²⁺ and evaluated *in vitro* where it displayed high selectivity for tumour cells expressing SSTR2. Compared to the previously reported DOTA analogue (⁶⁴Cu-DOTATATE),¹⁵ ⁶⁴Cu-SarTATE displayed less accumulation in non-target organs, liver, and lungs. Additionally, ⁶⁴Cu-SarTATE displayed greater retention at target tissues, leading to improved image contrast at later time points. These observed improvements can be attributed to the significantly greater kinetic stability of the sarcophagine complex relative to that of DOTA.

⁶⁸Ga-DOTATATE and related ⁶⁸Ga-labelled somatostatin analogues, are quickly becoming the gold-standard for the diagnosis and staging of neuroendocrine neoplasia.⁹⁵ ⁶⁸Ga-DOTATATE can be used to determine the suitability of patients for peptide receptor radionuclide therapy (PRRT) with therapeutic analogues such as ¹⁷⁷Lu-DOTATATE.^{16,47,96} Additionally, these radiotracers can be used to perform patient-specific dose estimation, maximising PRRT treatment efficacy and

minimising damage to non-target tissues. With its longer half-life, ^{64}Cu has been proposed as a replacement for ^{68}Ga , enabling dosimetry studies at more distant time-points post-injection. Recently, a first-in-man clinical study compared ^{64}Cu -SarTATE and ^{68}Ga -DOTATATE for their ability to localise disease at early and late imaging time-points.¹⁶ Overall the study found that ^{64}Cu -SarTATE possessed high uptake and retention in tumours, generating high-contrast diagnostic images up to 24 h post injection. Compared to ^{68}Ga -DOTATATE, which was imaged 1-hour post injection, ^{64}Cu -SarTATE increases the flexibility of the imaging procedure with regards to timing of diagnostic imaging, and the potential for multiple time-point dosimetry estimation.

Recently, sarcophagines bearing either one or two PSMA targeting peptides have been developed.⁹⁷ The bioconjugates were readily labelled with $^{64}\text{Cu}^{2+}$ at room temperature. In LNCaP-tumour bearing mice, excellent tumour uptake was observed, with prolonged tumour retention even 24 h p.i. The monomeric agent had a tumour uptake of 9 ± 1 %ID/g 1 hour post-injection, which was higher than the clinically used ^{68}Ga -PSMA-11, which had a tumour uptake of 5 ± 1 %ID/g at 1 hour post-injection. The bivalent agent in which two PSMA targeting peptides are tethered to the sarcophagine, dramatically outperformed its monovalent analogue with a tumour uptake of 22 ± 1 % ID/g. This high uptake persists for the bivalent species, which has a tumour uptake of 4 ± 1 % ID/g at 24 hours post-injection, compared to the monovalent species, which has a tumour uptake of 1 ± 0.1 % ID/g at 24 hours post-injection. The longer physical half-life of ^{64}Cu ($t_{1/2} = 12.7$ h) compared to ^{68}Ga ($t_{1/2} = 68$ min) permits the acquisition of PET images at later time points where clearance of non-bound tracer can lead to better image quality. This is of particular importance in imaging prostate cancers in the lower abdomen since accumulation of radioactivity in the bladder *via* renal clearance can obscure small prostate cancer metastases.⁹⁷

Whilst sarcophagine radiochemistry is dominated by $^{64}\text{Cu}^{2+}$, other metal ions are known to be stably complexed by this ligand. $^{68}\text{Ga}^{3+}$ (β^+ , $t_{1/2} = 68$ min) has been investigated for use diagnostic PET imaging with sarcophagine-based peptide conjugates.²⁷ Diaminosarcophagine was functionalised with two carboxylic acids in the apical positions. These were transformed into N-hydroxysuccinimide (NHS) esters to facilitate conjugation to two RGD ($\alpha_v\beta_3$ integrin receptor targeting) peptides *via* amide coupling to lysine residues. The bioconjugate was dissolved in a

sodium acetate/ethanol solution (0.1 M) containing $^{68}\text{Ga}^{3+}$. This solution was heated at 85 °C for 30-35 min achieving high radiochemical yields (> 98%). These forcing radiolabelling conditions are indicative of a high kinetic barrier to complexation of Ga^{3+} by the sarcophagine derivative. This radiolabelled peptide conjugate was then assessed in mice bearing tumours that overexpressed integrin $\alpha_v\beta_3$ receptor. Tumours were easily delineated from normal tissue, and low skeletal uptake suggested that the $^{68}\text{Ga}^{3+}$ sarcophagine complex possessed high kinetic stability *in vivo*. It is important to note that whilst this study demonstrated the feasibility of $^{68}\text{Ga}^{3+}$ sarcophagine complexes, many other chelators such as tris(hydroxypyridinone), desferrioxamine, and NOTA are able to complex ^{68}Ga under milder conditions.^{26,98-100} Whilst many of these $^{68}\text{Ga}^{3+}$ complexes have high kinetic stability, the short-lived nature of this radionuclide obviates the need for long term stability comparisons between them.

Another carboxylate-bearing sarcophagine (AmBaSar, figure 20) has been synthesised.^{88,101} Diaminosarcophagine was treated with CuCl_2 to protect the secondary amines, then methyl 4-formylbenzoate was added in the presence of NaBH_3CN : a reductive amination reaction yielded the benzoate derivative of diaminosarcophagine. Cu^{2+} was then removed using NaBH_4 and Pd/C , and lastly the ester was hydrolysed to give the benzoic acid sarcophagine derivative, AmBaSar. The coupling between RGD peptide and AmBaSar was accomplished in a single reaction. First the carboxylic acid was transformed to a sulfo-NHS ester *in situ*, then the side chain amine on lysine reacted with this to form the peptide conjugate. The authors found that without protection, the primary and secondary amines of the sarcophagine did not interfere with the coupling reaction. The conjugate was then labelled with $^{64}\text{Cu}^{2+}$ with more than 80% radiochemical yield. More recently AmBaSar has been conjugated to a neurotensin analogue as a potential imaging agent for pancreatic ductal adenocarcinoma, and prostate cancer.^{69,102} These neurotensin bioconjugates have been radiolabelled with $^{64}\text{Cu}^{2+}$ in high radiochemical yield (>90 %). The dicarboxylate analogue of AmBaSar has also been

synthesised, where both primary amines are derivatised with benzoic acid moieties.²⁹

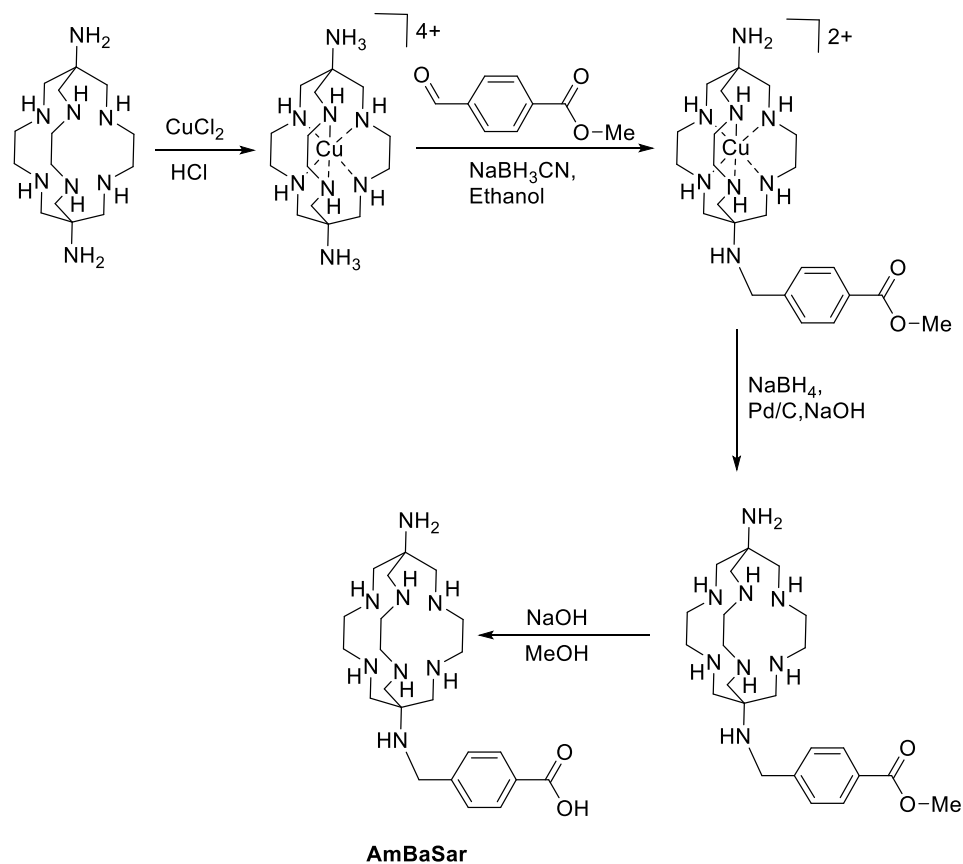


Figure 20 - Synthesis of AmBaSar utilising initial protection of secondary amines with Cu^{2+} .

An interesting bimodal PET-fluorescent imaging probe has been developed based upon sarcophagine (figure 21).¹⁰³ One apical position has been derivatised using a fluorophore enabling optical imaging. This fluorescence signal can be used to guide surgeons during intraoperative procedures and can provide sub-cellular resolution for *ex vivo* imaging of biopsy samples. The other apical position was functionalised with an azide group. Radiolabelling with $^{64}\text{Cu}^{2+}$ was carried out followed by attachment to an alkyne-bearing targeting peptide *via* a copper-catalysed Huisgen cycloaddition, facilitating biotargeting.¹⁰⁴

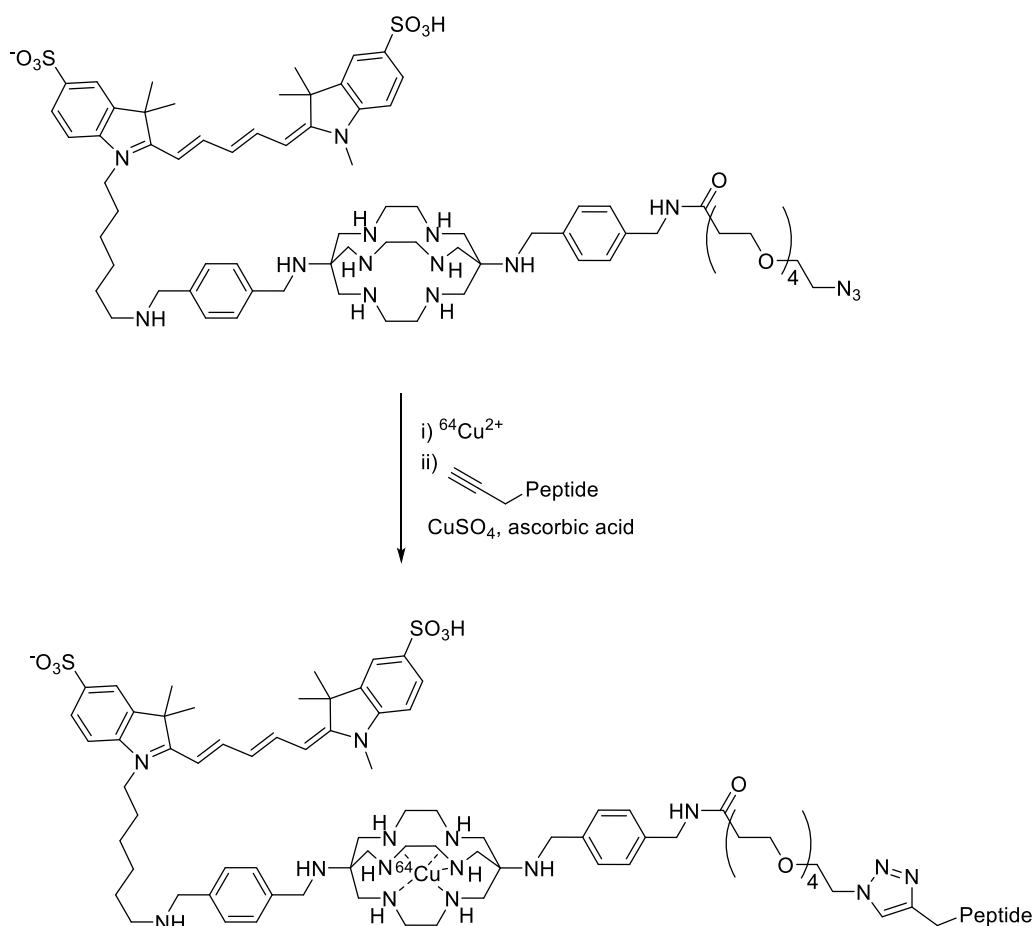


Figure 21 - Azide-alkyne Huisgen cycloaddition yielding a bimodal PET-fluorescent imaging probe.

1.4.4 Sarcophagine protein conjugates

The first ^{64}Cu -labelled sarcophagine-immunoconjugate was based on SarAr, and was used for PET imaging of neuroblastoma and melanoma.¹⁰⁵ Conjugation took place between the primary aromatic amino group on SarAr and carboxyl groups on aspartate and glutamate residues. This reaction was mediated by 1-ethyl-3-(3-dimethylaminopropyl)-carbodiimide (EDC) and took place rapidly (30 min) under mild conditions (pH 5, 37 °C), and importantly did not adversely affect immunoreactivity. The immunoconjugate was radiolabelled using $^{64}\text{Cu}^{2+}$ in 0.1 M sodium acetate solution, pH 5, for 30 min, at 37 °C. Under these conditions, near quantitative radiolabelling yields were achieved (>99 %). This seminal paper demonstrated the feasibility of using sarcophagines to produce stable immunoconjugates that could be readily labelled with $^{64}\text{Cu}^{2+}$ for PET imaging of tumours *in vivo*. Biodistribution data from this paper showed significant kidney retention, consistent with biodistribution data from a subsequent report where

high kidney uptake was observed when using a ^{64}Cu -labelled SarAr conjugate of an antibody fragment $(\text{F(ab}')_2)$.^{82,105} It was hypothesised that the high net positive charge of Cu-SarAr interacted strongly with the negatively charged basal cells of the glomerulus.¹⁰⁶ This hypothesis has since been tested by examining the biodistributions of a range of sarcophagine conjugates, and polyaza polycarboxylate conjugates with varying degrees of net positive charge.¹⁰⁶ This study showed that kidney uptake decreased with decreasing radiocomplex positive charge, supporting this hypothesis.

As discussed (see 1.4.2), the syntheses of sarcophagine-based bifunctional chelators and conjugates often require the use of secondary amine protection strategies. During conjugation, proteins are more susceptible to degradation than peptides. Therefore, Cu^{2+} and Boc protection strategies cannot be employed in the synthesis of sarcophagine-protein conjugates because their deprotection conditions would likely denature the protein. The mild conditions (citrate buffer, pH 6) used to extrude Mg^{2+} from sarcophagine means that this protection method can be used to synthesise sarcophagine-protein conjugates. This approach was exemplified using a Mg^{2+} protected bis-isothiocyanate sarcophagine derivative (see 1.4.2), which was conjugated to trastuzumab (anti-HER2) *via* amines on lysine side chains achieving 1.3 ± 0.3 chelators per antibody.¹⁰⁷ After removal of Mg^{2+} using a citrate buffer solution (pH 6), this bioconjugate was radiolabelled with $^{64}\text{Cu}^{2+}$ at pH 7.4 within 5 min. *In vivo* studies showed that antigen binding was not adversely affected during conjugation and radiolabelling as demonstrated by high tumour uptake and retention.

Proteins often contain many lysine residues in addition to an N-terminus. Therefore, conjugation using amine reactive bifunctional chelators leads to a wide distribution of products. A great degree of variability is observed in these stochastic protein bioconjugates, both in terms of the absolute number, and position of chelators attached. Excessive conjugation of chelators or other cargo to proteins can result in reduced affinity of proteins for their intended target receptors. Additionally, excessive protein bioconjugation can lead to aggregation, reduced thermal stability, and impaired effector functionality (e.g. Fc receptor binding and ADCC activity).

Several papers have utilised a sarcophagine conjugate of scFv_{anti-LIBS}, an antibody fragment targeted to the ligand-induced binding sites (LIBS) on GPIIb/IIIa.^{89,108,109} This glycoprotein receptor is an integrin complex found in platelets where it is required for normal platelet aggregation and endothelial adherence. The scFv_{anti-LIBS} agent is selective for activated platelets, which contain higher abundance of GPIIb/IIIa than circulating platelets. Radiolabelled scFv_{anti-LIBS} has the potential to be used as an imaging agent for the diagnosis of thrombosis and inflammation, both of which involve activated platelets.

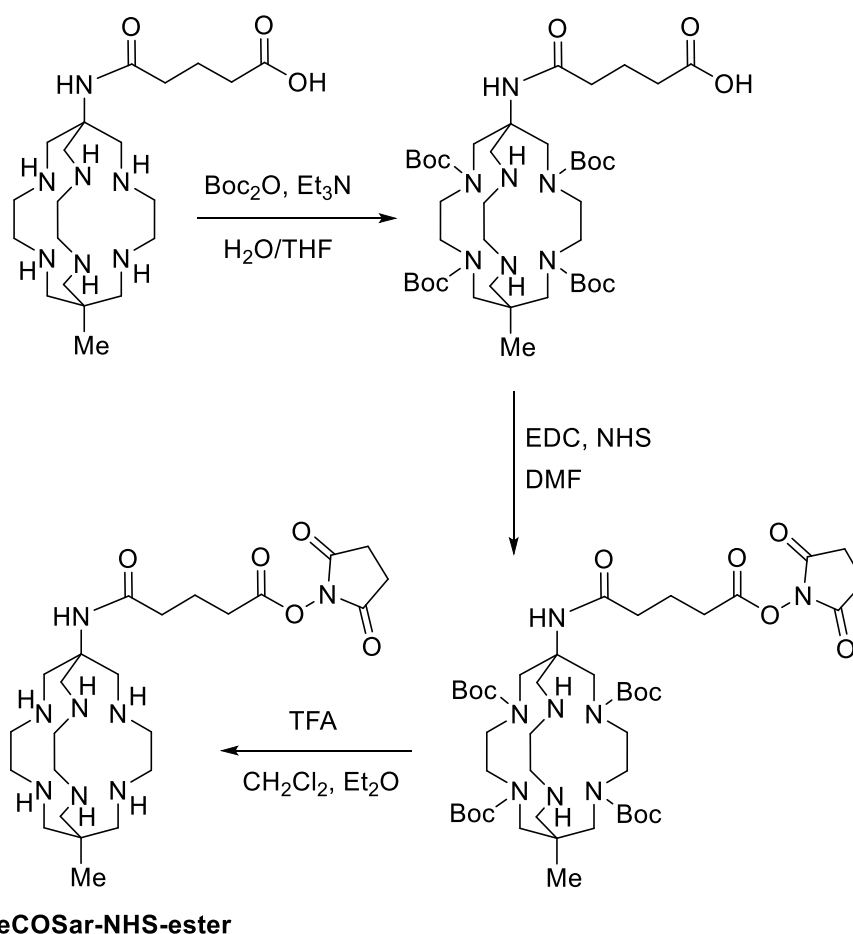


Figure 22 - Synthesis of MeCOSar-NHS-ester.

The bifunctional derivative, MeCOSar-NHS-ester (figure 22) has been conjugated scFv_{anti-LIBS} *via* primary amines on lysine side chains and the N-terminus.¹⁰⁹ Derivatisation of a protein or peptide with an NHS-ester results in the modification of primary amines. The conjugation took place in borate buffer (pH 8.4) for 3 hours at room temperature. Under these alkaline conditions, conjugation should ideally take place rapidly because NHS-ester hydrolysis competes with conjugation reactions, leading to inefficient conjugation. The conjugate was labelled with $^{64}\text{Cu}^{2+}$.

The authors investigated the effect of chelator to scFv_{anti-LIBS} ratio on the maximum specific activity achieved. Using 5×, 15×, and 30× equivalents of MeCOSar-NHS-ester over the scFv_{anti-LIBS}, the study found that specific activity increased as the ratio of of chelator to scFv_{anti-LIBS} increased. However, compared to the non-modified scFv_{anti-LIBS}, antigen binding fell by 7%, 20%, and 86% when using conjugates derived using 5×, 15×, and 30× excess of MeCOSar-NHS-ester. These results demonstrate that excessive stochastic conjugation can result in decreased antigen binding. Several recent and elegant sarcophagine papers have used enzyme-mediated and/or click chemistry to more reliably conjugate to proteins with a reduced impact on bioactivity.^{89, 108, 110}

One major class of enzymatic bioconjugation involves the bacterial transpeptidase sortase A (SrtA). In bacteria, the enzyme catalyses a cell wall sorting reaction, covalently attaching proteins to the bacterial cell wall. In the presence of SrtA an amide bond is cleaved between Thr and Gly in the peptidic recognition motif Leu-Pro-X-Thr-Gly (where X=any amino acid). The enzyme also catalyses the reverse reaction, forming an amide bond between Thr and a Gly containing species. This enzymatic bond cleavage and formation reaction has been used to attach sarcophagine to proteins (figure 23).¹⁰⁸ A Leu-Pro-Glu-Thr-Gly-Gly-FLAG motif was engineered at the C-terminus of scFv_{anti-LIBS} using recombinant techniques. (FLAG is a polypeptide sequence, which is included to facilitate separation of the bioconjugate using a FLAG affinity column to remove Gly-Gly-FLAG post-conjugation.) SrtA and a glycine-bearing sarcophagine derivative were added to form a new amide bond between Thr and the Gly residue of the sarcophagine derivative. The reaction took 5 hours at 37 °C, forming conjugate in 90 % yield. Since the new peptide sequence of the conjugate also contained the peptidic recognition motif, it was also a substrate for SrtA enzyme cleavage – i.e. the reaction is reversible. To obtain good yields, a high molar excess of the glycine-sarcophagine derivative and the SrtA enzyme were required – a potential drawback of this approach.

The site-specifically modified sar-scFv_{anti-LIBS} bioconjugate was then radiolabelled with ⁶⁴Cu²⁺ at pH 7, at room temperature within 30 minutes. The potential of this radiolabelled bioconjugate was then demonstrated in an *in vivo* model of carotid artery thrombosis using PET.

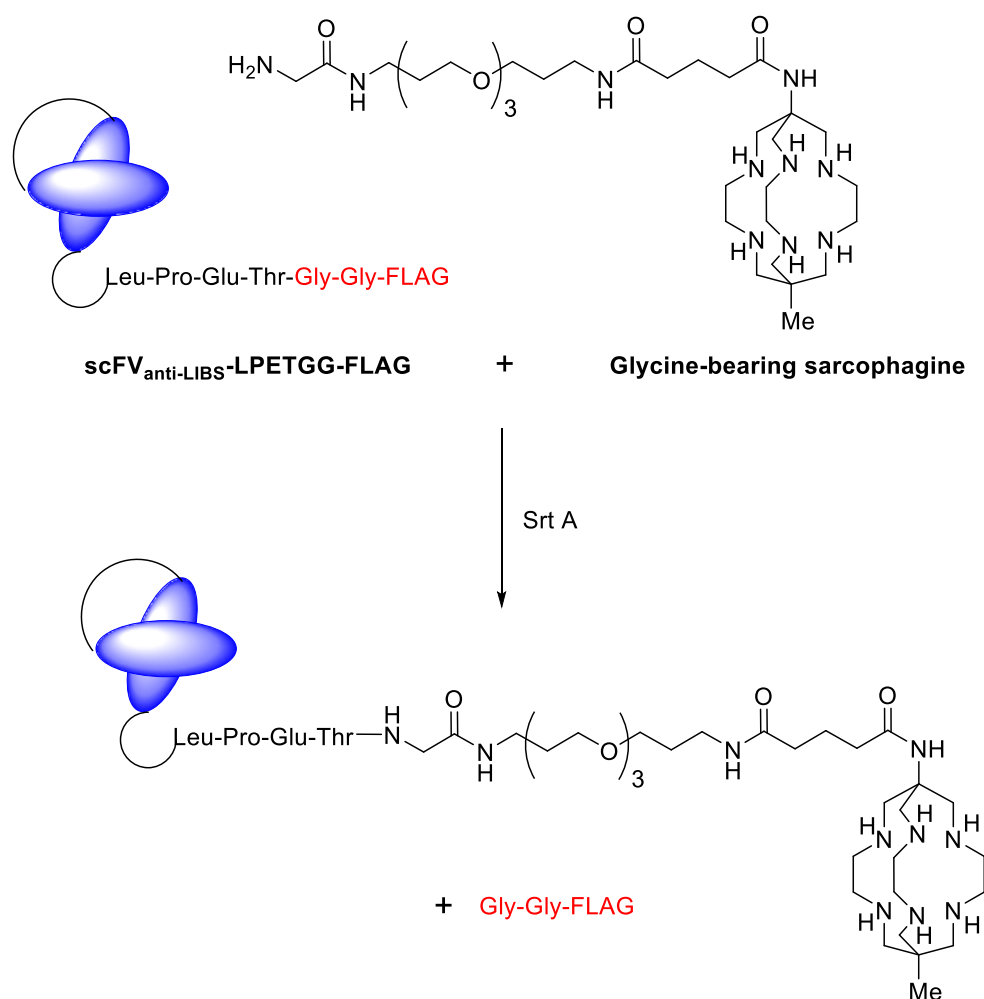


Figure 23 - Sortase A mediated conjugation of a glycine-bearing sarcophagine to scFV_{anti-LIBS}-LPETGG-FLAG.

SrtA coupling has also been combined with click chemistry to conjugate sarcophagine to scFV_{anti-LIBS} (figure 24).⁸⁹ First, a glycine-bearing bicyclo-[6.1.0]-nonyne (BCN) was attached to scFV_{anti-LIBS} using the SrtA coupling. Then an azide bearing sarcophagine was conjugated by triazole formation *via* the strain promoted azide-alkyne coupling (SPAAC) reaction. This bioorthogonal conjugation makes use of a strained alkyne avoiding the need for a Cu⁺ catalyst mitigating concerns over complexation of Cu²⁺ during conjugation. The conjugate was then radiolabelled with ⁶⁴Cu²⁺ at pH 7 and room temperature in < 30 min. A high level of specific binding to the target receptor was retained post-conjugation.

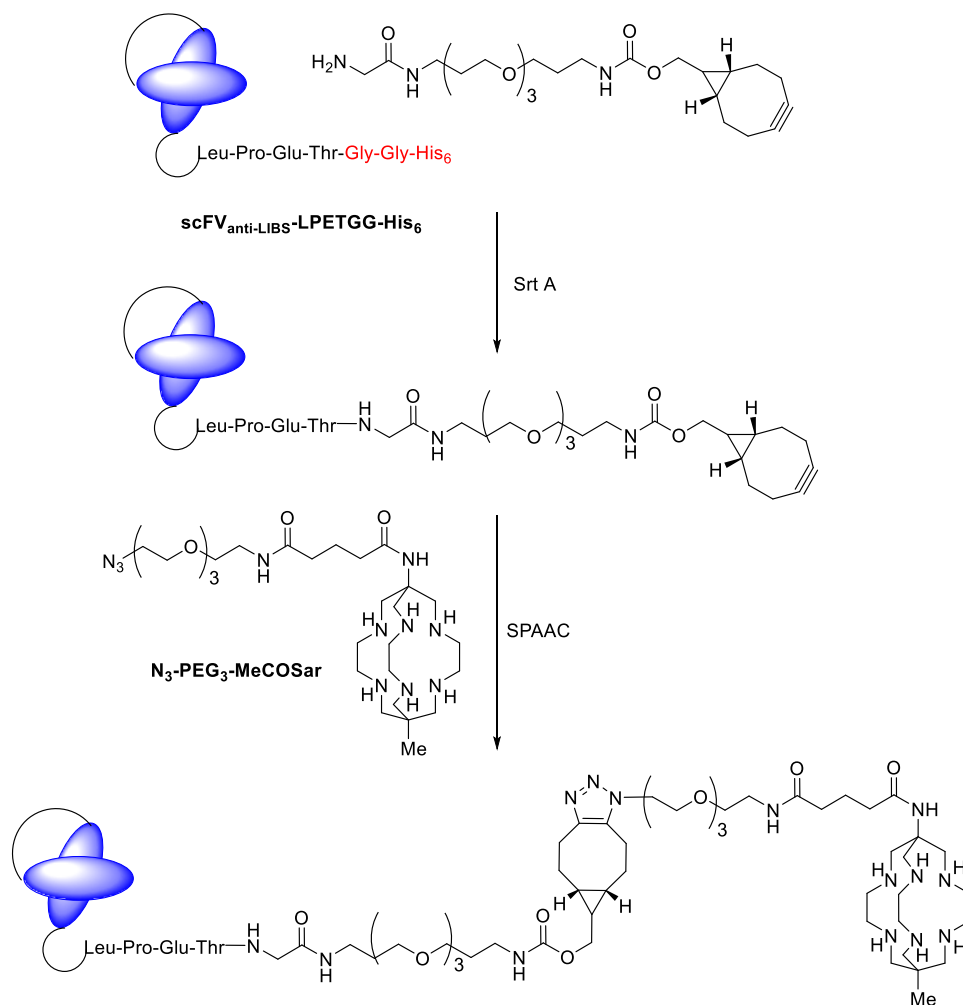


Figure 24 - The two-step bioorthogonal site-specific modification of scFv_{anti-LIBS-LPETGG-His₆} with Gly-PEG₃-BCN, followed by N₃-PEG₃-MeCOSar.

Whilst antibodies are promising targeting vectors for use in radiopharmaceuticals, their long pharmacologic half-lives sometimes requires the use of long-lived radioisotopes such as ¹¹¹In (γ , 2.8 d), and more recently ⁸⁹Zr (β^+ , 78 h). This leads to high radiation dose for patients. Pretargeting enables imaging of antibody distribution with prolonged intervals between the administration of non-radioactive antibody, and a subsequent injection of a radiotracer at a later stage (figure 25). Firstly, a bivalent antibody is administered, which is capable of binding to both the antigen and a radioligand. The antibody then slowly accumulates at its target, usually over the course of a few days. Next the radioligand is injected

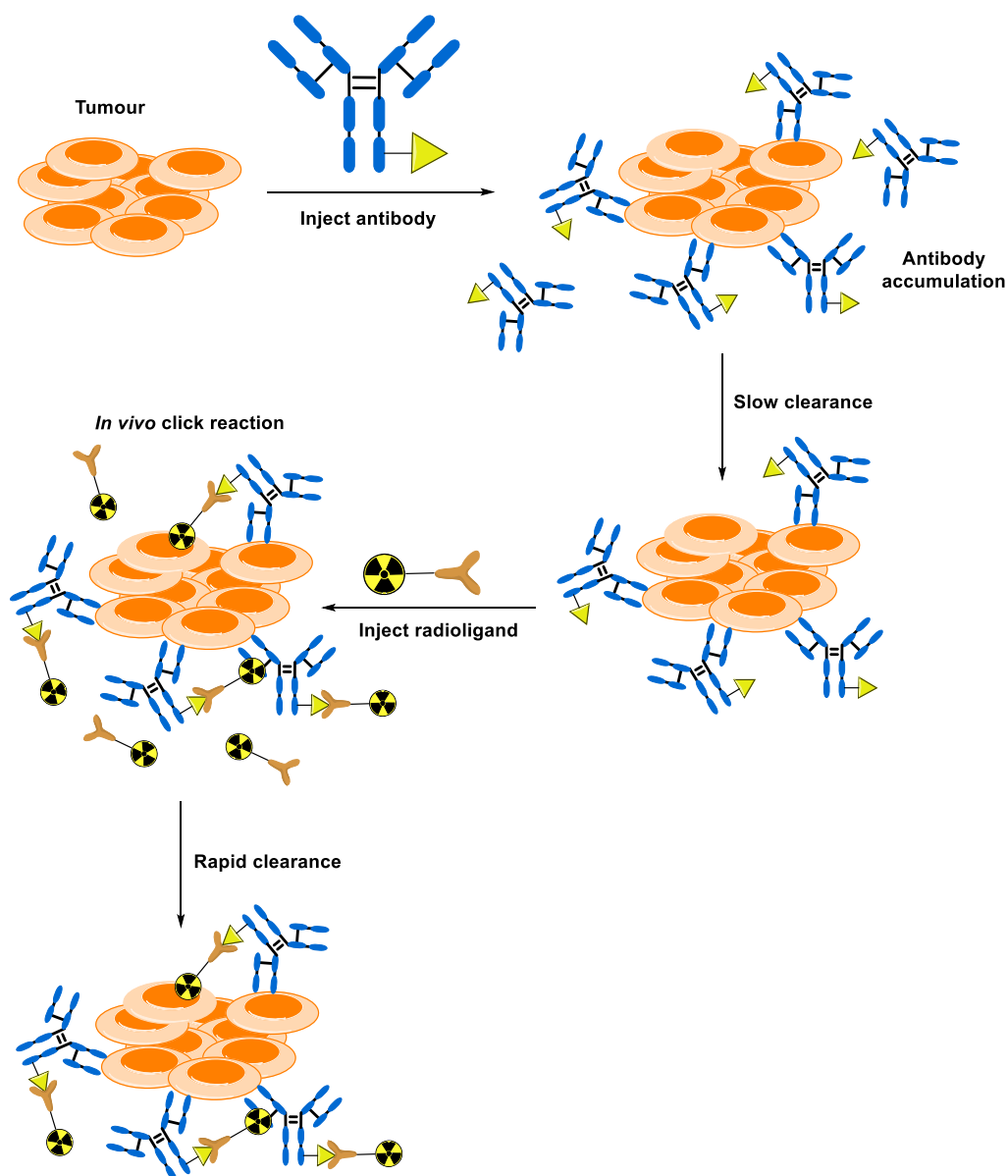


Figure 25 - Illustration of the steps involved in click chemistry-based pretargeting system.

intravenously and binds to the antibody *via* a bioorthogonal reaction at the target tissue, whilst excess radioligand undergoes rapid clearance. Since small molecule radioligands possess much more favourable pharmacokinetics than radioimmunoconjugates, the unnecessary radiation dose to the patient is greatly reduced. This approach also facilitates the use of shorter-lived radionuclides such as ^{68}Ga (β^+ , 68 min) and ^{64}Cu (β^+ , 12.7 h) since the time between radioligand administration and imaging is significantly reduced.

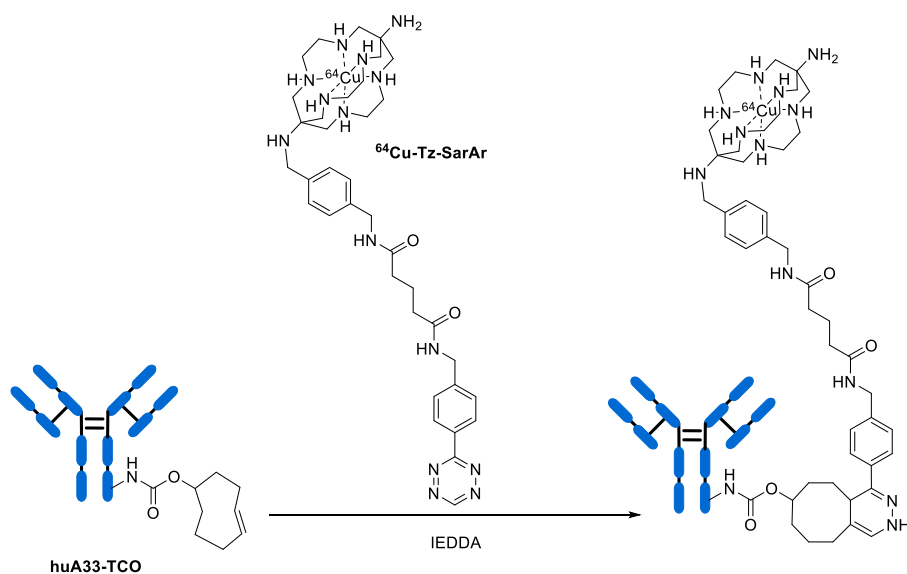


Figure 26 - The inverse electron demand Diels-Alder reaction between huA33-TCO and $^{64}\text{Cu-Tz-SarAr}$.

Building on earlier work,¹¹¹ a pretargeted strategy for the PET imaging using bioorthogonal ^{64}Cu -sarcophagine-antibody conjugates was developed (figure 26).¹¹⁰ The anti-colorectal carcinoma huA33 antibody was covalently modified using an amine reactive trans-cyclooctene (TCO-NHS). This immunoconjugate was then injected into mice bearing SW1222 (cells overexpressing A33 antigen) xenografts. After 24 h, 48 h, or 120 h, the same mice were then injected with a ^{64}Cu -labelled tetrazine functionalised sarcophagine ($^{64}\text{Cu-Tz-SarAr}$), and imaged at various time points p.i. The conjugation between the sarcophagine and the antibody then took place *in vivo* via the bioorthogonal inverse electron demand Diels-Alder (IEDDA) click reaction. Comparing different antibody accumulation intervals, an optimised pretargeting protocol was developed. In an optimised pretargeting protocol, 24 h was given between administration of the antibody, and the administration of $^{64}\text{Cu-Tz-SarAr}$. Longer antibody accumulation intervals (48 h and 120 h) yielded slight decreases in tumour uptake, but also slightly increased tumour-to-blood activity concentration ratios. This pretargeted approach harnesses the advantages of antibody-based radiopharmaceuticals whilst skirting their pharmacokinetic limitations.¹¹¹ Compared to conventional antibody imaging approaches, high tumour to background contrast is achieved at earlier time points, limiting uptake (and thus the ionising radiation dose) in non-target tissues. This is especially relevant when compared to antibodies bearing long-lived diagnostic

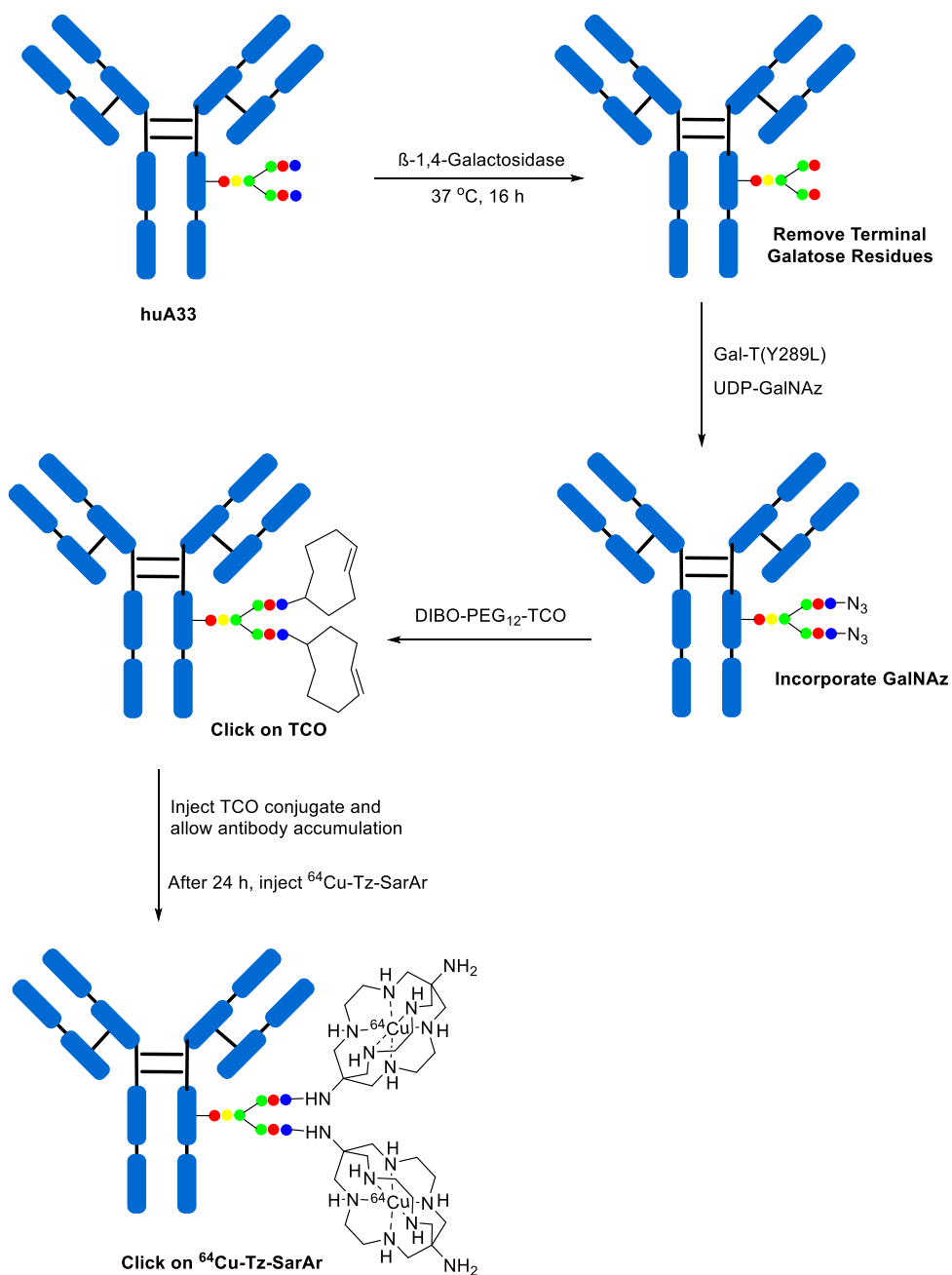
radionuclides such as ^{111}In and ^{89}Zr , or long-lived therapeutic radionuclides such as ^{177}Lu and ^{90}Y .¹¹¹

In the same study, two NOTA analogues were assessed, but it was found that the sarcophagine species possessed superior pharmacokinetic behaviour. The NOTA derivatives cleared largely through the intestines – a suboptimal trait for a colorectal cancer imaging agent. This behaviour was attributed to the overall 1-charge of the NOTA complexes. In contrast, the sarcophagine derivative with its overall 2+ charge cleared through the kidneys, possessing the most promising elimination pharmacokinetics for the author's pretargeted approach. PET imaging and biodistribution studies revealed that ^{64}Cu -Tz-SarAr provided better tumour uptake and a better tumour to background ratio than the NOTA analogues.

Whilst this pretargeted approach circumvents the need for long-lived radionuclides, it relies upon an initial non-site-specific conjugation between TCO-NHS esters and amine groups of the antibody to give amine bonds. Inherently, heterogeneous bioconjugates are generated in the process. Therefore, a chemoenzymatic approach was taken to improve the homogeneity of the TCO-bioconjugate: a site specifically modified antibody conjugate was produced *via* modification of the heavy chain glycans (figure 27).^{112,113} First, terminal galactose residues were removed by incubation with β -1,4-galactosidase. Then a β -1,4-galactosyltransferase mutant (Gal-T(Y289L)) was used to attach azide-containing glycan units (GalNAz) to the newly exposed termini, resulting in the attachment of 3.4 ± 0.3 azides per antibody. Then, a dibenzocyclooctyne-bearing variant of TCO (DIBO-PEG₁₂-TCO) was reacted with the modified antibody in a Strain Promoted Azide Alkyne Cycloaddition (SPAAC) reaction, to yield an immunoconjugate with 2.4 ± 0.5 TCO groups per antibody. This site-specifically modified conjugate was then administered to mice bearing SW1222 xenografts. After a 24 h accumulation period, ^{64}Cu -Tz-SarAr was injected followed by PET imaging at 4 h, 12 h, and 24 h after radiotracer injection. Tumour uptake increased over time, reaching a maximum (11.2 ± 2.4 %ID/g) 24 hours after radiotracer injection. Whilst this work demonstrates the possibility of pretargeted PET imaging with a site-specific bioconjugation approach, it should be noted that *in vivo* performance was comparable to pretargeted PET imaging using a stochastically labelled analogue.

However, the well-defined nature of this homogeneous bioconjugate may help to expedite the clinical translation of future pretargeting strategies.¹¹²

Figure 27 - A schematic to show how enzymatic modification of heavy chain glycans was used to incorporate GalNAz for the bioorthogonal attachment of



DIBO-PEG₁₂-TCO. This TCO-bearing antibody conjugate was injected and accumulated at the target tissue over the course of 24 hours. ⁶⁴Cu-Tz-SarAr was then injected, conjugating *in vivo* by means of the IEDDA reaction. PET imaging took place after 24 h.¹¹²

1.5 DFO

1.5.1 Introduction to desferrioxamine

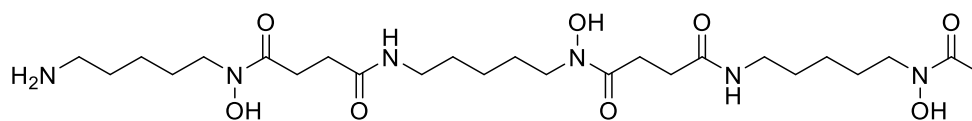


Figure 28 - The structure of desferrioxamine-B.

The group IV transition metal Zr exists predominantly as a 4+ ion in aqueous solutions. This ion can accommodate up to eight donor atoms and is usually classified as a 'hard' cation with a preference displayed for oxygen donor atoms. Desferrioxamine-B (DFO, figure 28) is a siderophore-derived acyclic chelator, which has been used clinically as a sequestration agent in the treatment of patients with iron overload disorders such as β -thalassemia.¹¹⁴ Additionally, DFO is used as a chelator for radiopharmaceuticals labelled with $^{89}\text{Zr}^{4+}$. Electrospray mass spectrometry (ESI-MS), nuclear magnetic resonance (NMR),¹¹⁵ and density functional theory (DFT) studies indicate that DFO forms a monomeric 1:1 metal:ligand complex with Zr^{4+} .¹¹⁶ However, more recent potentiometric studies have suggested that although the complexation reaction between Zr^{4+} and DFO gives rise to a very stable 2:1 metal:ligand complex, other complexes with metal:ligand ratios of 2:2 and 2:3 are also formed in solution.¹¹⁷ These findings were corroborated by small-angle X-ray scattering and MALDI mass spectrometry analyses of the complex solutions. Notably in all studies, the primary amine of DFO shows no evidence of participating in Zr^{4+} coordination. Since DFO binds to Zr^{4+} with six hydroxamic oxygen donor atoms, two coordination sites on the metal ion are not occupied by the chelator. DFT calculations have suggested that two water molecules can coordinate to the metal ion, satisfying its octadentate coordination sphere.

Complexation of $^{89}\text{Zr}^{4+}$ by DFO is typically complete within an hour,^{118,119} at room temperature and at physiological pH.¹¹⁹ The resulting complex mostly demonstrates high kinetic stability, undergoing minimal dissociation over the course of several days in serum stability studies.¹²⁰ In its unchelated form, $^{89}\text{Zr}^{4+}$ is known to have a high affinity for bone tissues in mice.¹²¹ *In vivo* studies in mice have found that the ^{89}Zr -DFO complex is excreted within 20 minutes *via* a renal pathway - little to no bone uptake was observed due to rapid clearance.¹¹⁶ However, some studies with ^{89}Zr -DFO-labelled antibodies have shown increasing accumulation of

radioactivity in the bones of mice from at least 24 hours post-injection. In one such study approximately 10 % ID/g bone uptake was observed 6 days post-injection.^{116,122,123} ⁸⁹Zr bone uptake has not been observed to the same extent in clinical trials with ⁸⁹Zr-DFO-labelled antibodies.¹²⁴ An early study examined the biodistribution of ⁸⁹Zr in humans and found that muscle uptake (7.6 % ID/kg) was greater than bone uptake (0.9 % ID/kg) 3 h p.i.¹¹⁹ It has been suggested that the faster metabolism of mice, paired with their less specific peptidases lead to more rapid degradation of ⁸⁹Zr-DFO leading to release of the radiometal into circulation where it can accumulate in bone mineral.¹²¹

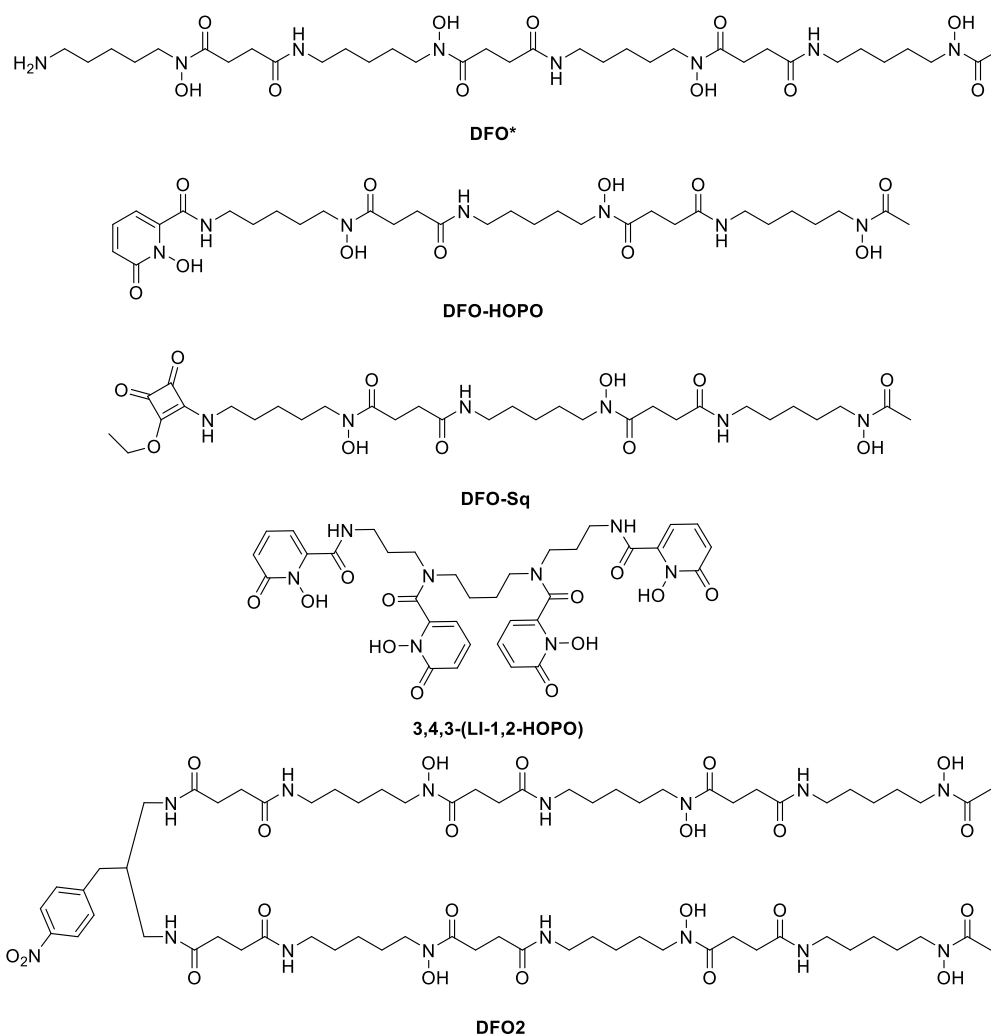


Figure 29 - Structures of some novel chelators that have been developed as alternatives to DFO.

Although DFO is suitable for Zr^{4+} chelation ($\log K = 36.14$),¹¹⁷ several novel Zr^{4+} chelators have been developed recently (figure 29). Most of these incorporate two additional donor atoms to saturate the metal ion's octadentate coordination

sphere. Examples of this strategy include the functionalisation of the primary amine group of DFO with another hydroxamate motif (DFO*),^{125,126} a hydroxypyridinone group (DFO-HOPO),¹²⁷ and a squaramide ester group (DFO-squarate).¹²⁸ Alternative approaches have involved synthesising an octadentate chelator incorporating four hydroxypyridinone groups (3,4,3-(LI-1,2-HOPO)),¹²⁹ tethering two DFO chains together (DFO2),¹³⁰ and using the tetraazamacrocycle DOTA.¹³¹ A literature review has been conducted examining novel DFO derivatives that have been developed for $^{89}\text{Zr}^{4+}$ chelation performed.¹¹⁴ Compared with $^{89}\text{Zr}(\text{DFO})^+$, many of these novel ligands exhibit improved stability in the presence of competing ligands. However, DFO is used more frequently due to its commercial availability, sufficiently high complex stability with $^{89}\text{Zr}^{4+}$, and literature precedence for clinical use.

1.5.2 ^{89}Zr -DFO antibody conjugates

DFO was first conjugated to an antibody using N-(S-acetyl)thioacetyl-DFO (DFO-SATA), which was reacted with antibodies bearing maleimide groups attached to the ϵ -amino group of lysine side chains (figure 30).^{132,133} Stability studies showed that this radioimmunoconjugate was unstable in human serum over 24 h at 37 °C, where transfer of the ^{89}Zr -chelator complex to serum proteins was observed.¹³⁴

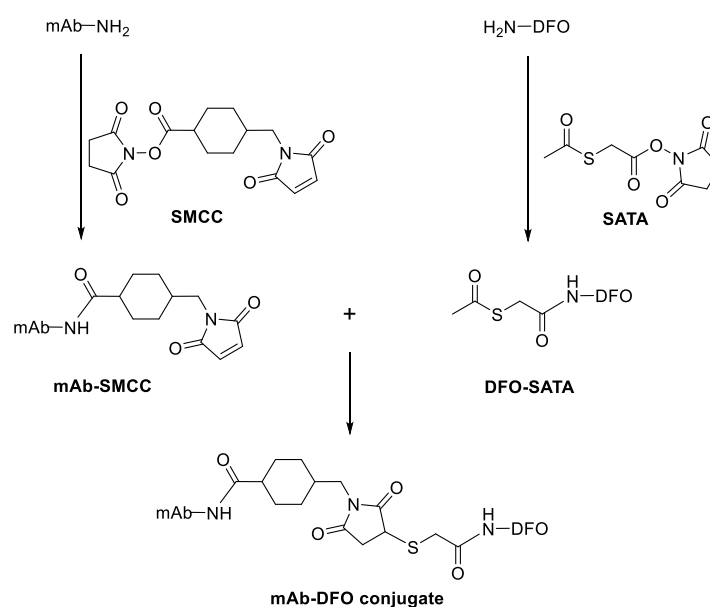


Figure 30 - Antibody-DFO conjugate synthesis *via* thioether bond formation.^{132,133}

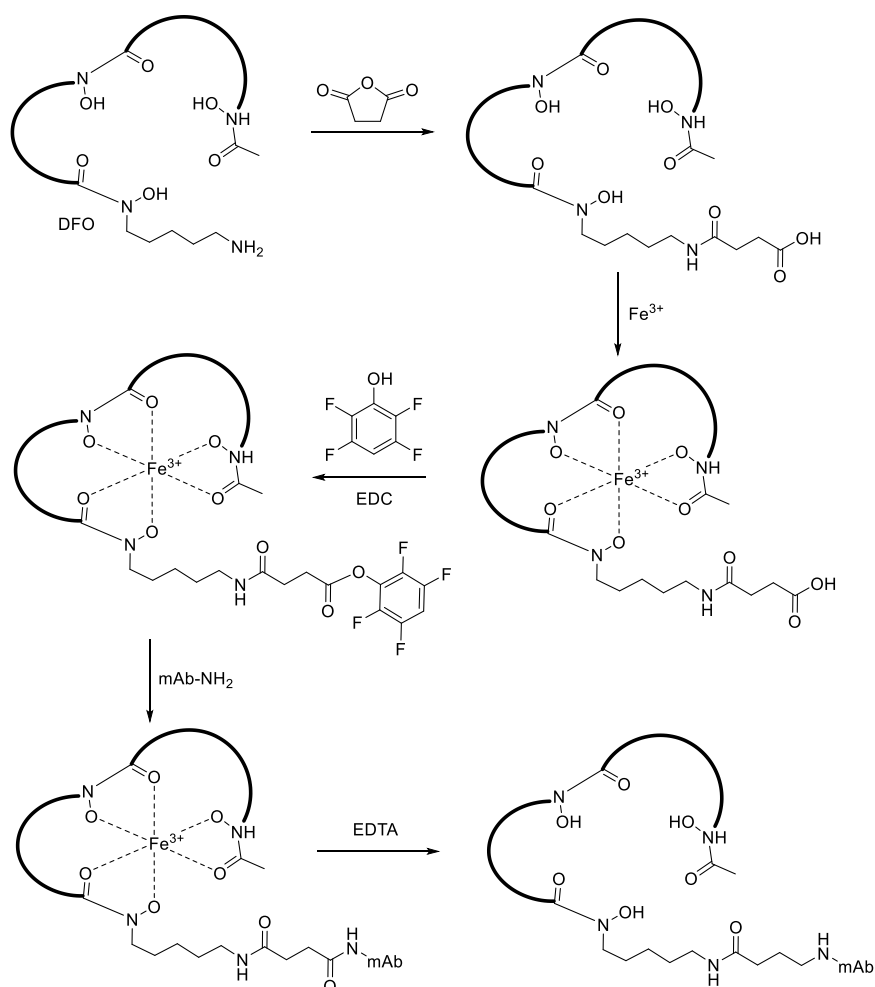


Figure 31 - DFO-antibody conjugation *via* coupling to a tetrafluorophenyl ester intermediate.¹³⁴

A new conjugation protocol was developed that did not rely on thioether bond formation (figure 31).¹³⁴ This method involved reaction of DFO with succinic anhydride to give a carboxylate functionalised DFO derivative. This species was then converted to a tetrafluorophenyl (TFP) ester by reaction with tetrafluorophenol mediated by 1-ethyl-3-(3-dimethylaminopropyl)carbodiimide (EDC). Addition of antibody led to conjugation *via* the antibody's primary amines on lysine side chains or at the N-terminus. Fe³⁺ was added before the conversion to a TFP-ester to prevent reaction of unprotected hydroxamate groups with EDC. Post-conjugation Fe³⁺ was removed by the addition of EDTA, to yield the metal-free immunoconjugate. This conjugation methodology was implemented in the first clinical ⁸⁹Zr-immuno PET study examining a ⁸⁹Zr-labelled antibody (U36) for the detection of lymph node metastases in patients with head and neck squamous cell carcinoma (HNSCC).¹³⁵ ⁸⁹Zr-immuno PET performed at least as well as CT/MRI for the detection of HNSCC metastases. Other significant clinical studies have since

used ^{89}Zr -labelled DFO-antibody immunoconjugates. In one study, ^{89}Zr -DFO-trastuzumab was synthesised using the TFP-ester method described above and used to determine the optimal radioimmunoconjugate dosage and administration time to enable PET visualisation and quantification of tumour lesions in 14 patients with HER2-positive metastatic breast cancer.¹²⁴ Patients receiving trastuzumab immunotherapy were given a 10 mg dose consisting of 1.5 mg ^{89}Zr -DFO-trastuzumab (37 MBq) replenished with non-radioactive trastuzumab. The best timing for PET imaging to evaluate tumour uptake was 4-5 days post-injection. Later time points (6-7 days) resulted in decreased image quality due to the lower amount of radioactivity remaining in the patients due to radioactive decay and excretion (intestinal). Interestingly, patients who had not received trastuzumab previously (trastuzumab naïve patients) required a 50 mg dose consisting of 1.5 mg of ^{89}Zr -DFO-trastuzumab (37 MBq) with additional non-radioactive trastuzumab to give a good tumour-to-non-tumour ratio. At the lower dose of 10 mg, relatively high liver uptake was observed in these trastuzumab naïve patients, with evidence of intestinal excretion. This observation was probably due to complex formation between ^{89}Zr -DFO-trastuzumab and extracellular HER2 domains that were present in blood plasma.¹³⁶ Many ^{89}Zr -labelled radioimmunoconjugates have been produced using this conjugation method.^{116,124,137-142} However, this protocol is complicated and time consuming, and therefore challenging with respect to Good Manufacturing Practice (GMP) compliancy.

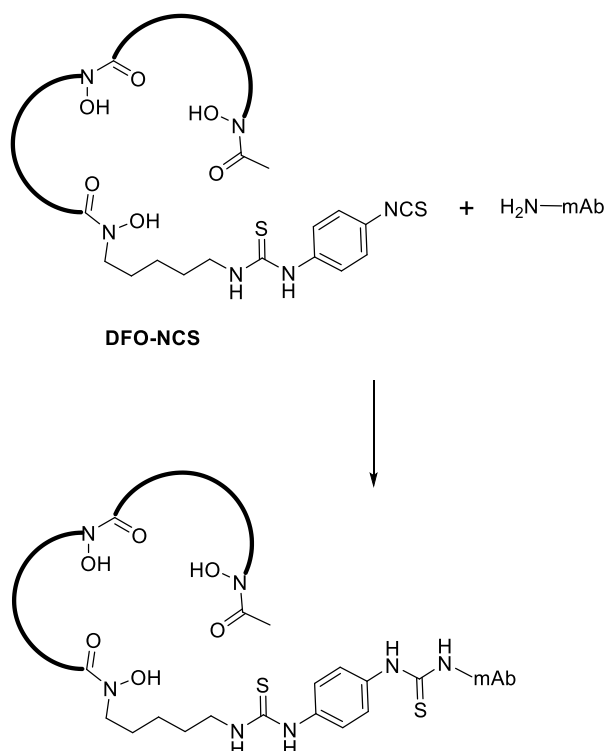


Figure 32 - Conjugation taking place between DFO-NCS and an amine on mAb.

A more simple, and rapid conjugation protocol has been developed using *p*-isothiocyanatobenzyl-desferrioxamine (DFO-NCS, figure 32).¹⁴³ Under basic conditions (pH 8.5-9) conjugation takes place *via* thiourea formation between amines (lysine side chains and N-terminus) on the antibody and the isothiocyanate group on the bifunctional chelator. Conjugation is typically complete within 30 min at 37 °C, and non-conjugated BFC can be removed by size exclusion chromatography. This has become the standard protocol for ⁸⁹Zr-DFO labelling of antibodies, and has been used to form a range of DFO-antibody conjugates.^{136,144-}

148

The DFO-antibody conjugations discussed so far have been non-site-specific, relying on direct addition to amines on lysine residues or N-termini. Since there are often multiple potential conjugation sites, heterogeneous bioconjugates are formed. As previously discussed (see 1.4.4) highly heterogeneous bioconjugates can display reduced antigen affinity and compromised effector functionality.¹⁰⁹ More recently, several site-specific methodologies have been developed and applied to DFO-antibody conjugations.

An enzymatic approach to generating site-specifically modified antibodies has been developed, where bacterial transglutaminase (BTG) was used to mediate

conjugation reactions between DFO and the CE7 antibody (anti-L1-CAM) (figure 33).¹⁴⁹ Transglutaminases catalyze acyl-transfer reactions between the γ -carboxamide group of glutamine residues, and the primary ϵ -amino group on lysine (figure 33a). To be recognized by BTG, the glutamine residue should be located in a flexible region of the protein, and flanked by specific amino acids.¹⁵⁰ It was hypothesized that BTG could mediate the conjugation between the primary amine of DFO and glutamine residues on the chimeric antibody CE7. However, antibody modification did not occur despite the abundance of glutamine residues on CE7 (figure 33b). Conjugation was also assessed using a mutant of CE7 in which asparagine-297 (N297) had been replaced by glutamine (Q297) preventing N-glycosylation at this position. This change resulted in increased flexibility of a specific region of the heavy chain between amino acid residues Q295 and T299 (C/E loop), whilst simultaneously incorporating two additional glutamine residues for BTG to act upon. In the presence of BTG and DFO, each heavy chain was modified with two DFO units - one at Q295, and the other at Q297 (figure 33d). Using this method, a highly homogeneous immunoconjugate was formed with a chelator to antibody ratio of 4:1. The conjugation was attempted again using wild-type (non-mutant) CE7 antibody but with the inclusion of a PNGase F mediated deglycosylation step prior to conjugation (figure 33c). This structural change enabled the BTG mediated conjugation between DFO and Q295, giving a homogeneous bioconjugate bearing two DFO moieties.

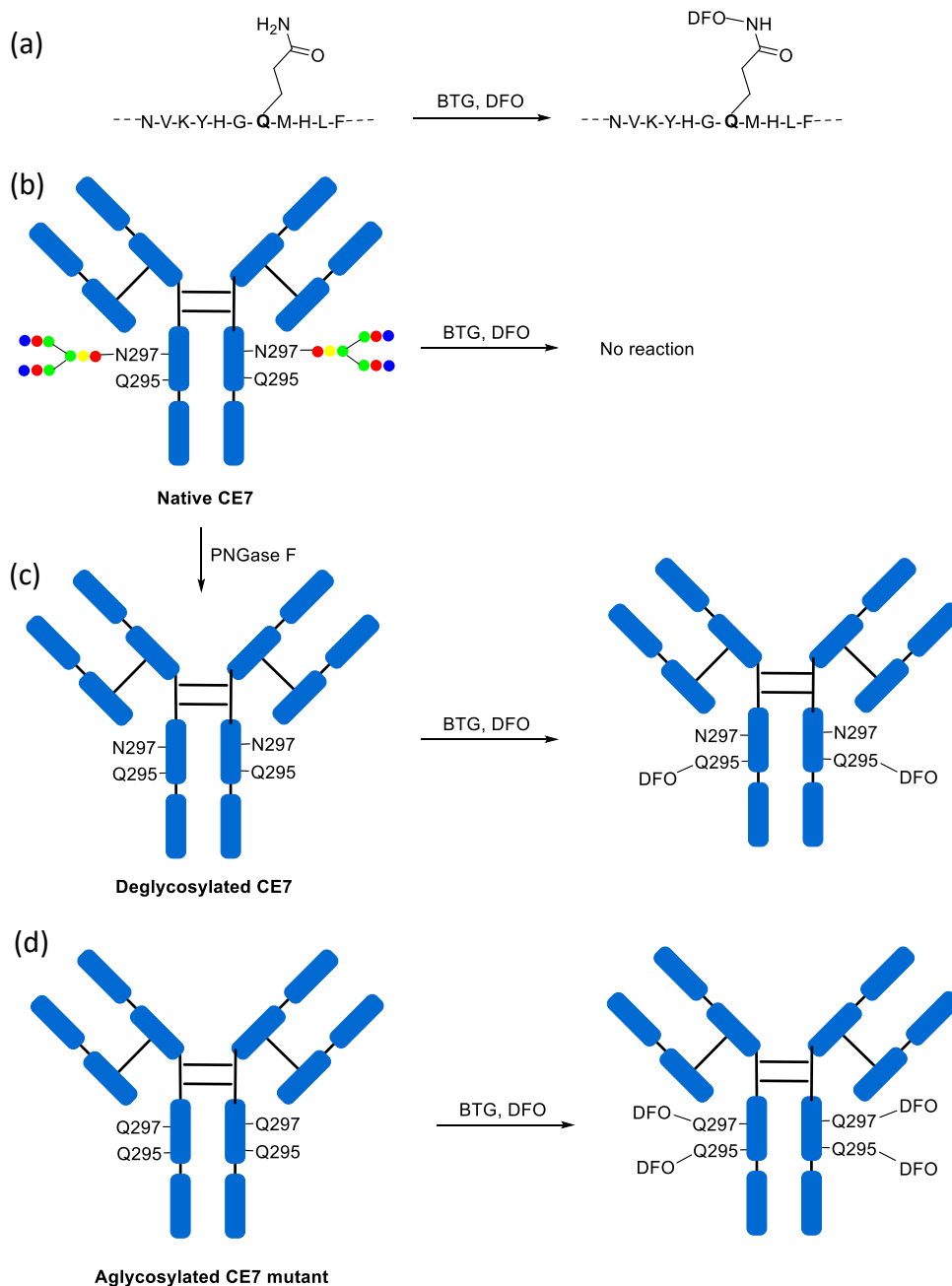


Figure 33 - a) Bacterial transglutaminase (BTG) mediates the conjugate reaction between DFO and glutamine residues (Q). b) No reaction occurs between native CE7 and DFO in the presence of BTG. c) Deglycosylation using PNGase F facilitates conjugation between DFO and Q residues mediated by BTG to give a bioconjugate bearing two DFO moieties. d) Using a mutant aglycosylated CE7 antibody yields a bioconjugate bearing four DFO moieties.

This conjugate was then labelled with $^{67}\text{Ga}^{3+}$ ($t_{1/2} = 78.3 \text{ h}$, γ) and administered to mice bearing SKOV3ip human ovarian cancer xenografts. Tumour uptake reached a mean maximum of $58.7 \pm 21.00 \text{ \% ID/g}$ after 72 hours post-injection. Non-specific uptake at off-target organs was considerably lower with the highest uptake in the

lungs and spleen at 6.22 ± 0.17 % ID and 5.96 ± 1.70 % ID/g respectively 72 hours post-injection. A non-site specific DFO-modified CE7 conjugate was also prepared, using DFO-NCS, with a calculated average of four chelators per antibody. Compared to the site-specific analogue, this conjugate generated a lower tumour uptake (14.70 ± 10.42 % ID/g). The conjugates were also labelled with ^{89}Zr , enabling PET scanning, which correlated well with ^{67}Ga biodistribution data.

DFO has been site-specifically conjugated to glycan residues of pertuzumab (anti-HER2) using the same heavy chain glycan modification technology discussed previously (see 1.4.4).^{118,151} To briefly summarise, bioconjugation was achieved in four steps: β -1,4-galactosidase catalysed the cleavage of heavy chain glycan terminal galactose residues; a β -1,4-galactosyltransferase mutant (GalT(Y289L)) catalysed the attachment of an azide-functionalised galactose sugar; dibenzocyclooctyne-bearing DFO was added conjugating to the antibody *via* the Inverse Electron Demand Diels-Alder (IEDDA) reaction. The resulting immunoconjugate can then be radiolabelled with $^{89}\text{Zr}^{4+}$. This glycan conjugate has been compared *in vitro* and *in vivo* to a ^{89}Zr -labelled stochastic conjugate of pertuzumab produced using the DFO-NCS platform (see 1.5.2).¹⁵² An enzyme-linked immunosorbent assay (ELISA) demonstrated that heavy chain glycan modification resulted in highly attenuated Fc γ R binding. *In vivo* this reduced Fc γ R binding led to improved tumour uptake in an immunocompromised mouse model relative to the stochastically conjugated analogue. Whilst in certain scenarios better image quality may be achieved using glycan modified antibodies, this same modification also prevents accurate determination of the biodistribution and pharmacokinetics of a native antibody.

The non-natural amino acid *p*-azidomethylphenylalanine has been site-specifically incorporated into aglycosylated trastuzumab using cell free protein synthesis.¹⁵³ This click-handle enables orthogonal and site-selective conjugation of chelators derivatized with transcyclooctyne derivatives *via* SPAAC in one step. This approach has been used to make DFO-antibody conjugates that have been labelled with $^{89}\text{Zr}^{4+}$. For comparison, a DFO-trastuzumab conjugate was also prepared using a non-site-specific DFO-NCS precursor and native trastuzumab. Additionally, a third immunoconjugate was prepared using DFO-NCS and aglycosylated trastuzumab. These stochastic conjugates were then radiolabelled with $^{89}\text{Zr}^{4+}$ and compared with the site-specifically labelled conjugate *in vitro* and *in vivo*. Stability studies were

carried out in rat plasma for 24 h at 37 °C where no immunoconjugate degradation or decomplexation was observed for the conjugates. The radioimmunoconjugates were compared in female NCr mice bearing SKOV3 (HER2 overexpressing) tumour xenografts. No statistical difference in target affinity was observed between the site-specific and the stochastic conjugates. However, the stochastic and site-specific aglycosylated antibody-conjugates demonstrated improved hepatic clearance compared to the stochastically conjugated native trastuzumab. Much like the glycan modified antibody conjugates described above, image quality was improved by structural modifications, but doing so precludes the use of native unmodified antibodies.

Lastly, DFO has also been functionalised with a terminal maleimide group enabling conjugation to thiol side chains on cysteine residues *via* Michael addition reactions.^{122,154,155} Since solvent accessible cysteine residues are relatively uncommon in antibodies, the conjugates formed by Michael addition are usually more homogeneous than those formed by direct addition to amine side chains on lysine residues. Interchain disulfide bonds can be reduced to yield up to eight reactive thiols, enabling conjugation with DFO-maleimide.¹⁵⁴ However, permanent cleavage of disulfide bonds can result in both reduced thermal stability and effector functionality.¹⁵⁶ Whilst maleimides can react with both amines and thiols, a marked preference is observed for the latter at neutral pH where most amines are protonated. In many antibodies there are no solvent accessible cysteine residues precluding the use of DFO-maleimide derivatives.

1.6 Maleimide Antibody Bioconjugations

1.6.1 The limitations of stochastic antibody conjugations

Most conventional conjugation strategies modify antibodies using electrophilic groups such as isothiocyanates and *N*-hydroxysuccinimides that react with solvent accessible primary amines on lysine residues and the N-terminus.^{43,120,157} These bioconjugation methods are simple, but are non-site-specific leading to heterogeneous product mixtures. The resulting stochastic conjugates often demonstrate reduced affinity for target receptors, particularly at high chelator to antibody conjugation ratios.^{158–160}

1.6.2 Maleimide antibody bioconjugations

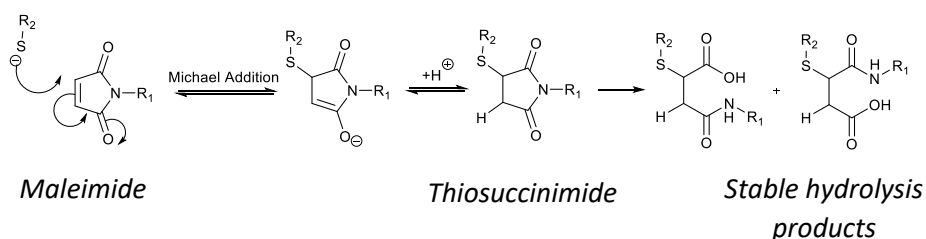


Figure 34 – Maleimide conjugation via Michael addition, followed by thiosuccinimide hydrolysis to give stable products.

Chemotherapeutic drugs have been used effectively to increase survival rates in cancer patients, but unfortunately, these compounds are often highly cytotoxic leading to severe side effects, and damage to non-target tissues. Chemotherapeutic drugs can be conjugated to antibodies, directing them to the cancer tissue, to diminish off-target toxicity. Currently, eight antibody drug conjugates (ADCs) have gained FDA approval, all of which are oncotherapies. Many ADC candidates fail in the development and testing stages, largely due to off target toxicity concerns.¹⁶¹

Ideally, the ADC would bind to all cells expressing the target antigen, and that cell population would mostly comprise of diseased cells. However, many target antigens are also expressed in healthy cells leading to off-target toxicity. If an ADC platform were developed using a combination of antibody and antigen that prevents ADC binding to non-target tissues, off target toxicity is still possible due to immunoconjugate instability. If the drug is released from the antibody it can accumulate at non-target tissues leading to off-target toxicity and reduced clinical efficacy.

In recent years, maleimides have emerged as a popular choice for selective conjugation to cysteine residues (figure 34). The selectivity of maleimide bioconjugation is generated not only by the low natural abundance of cysteine (< 2% of amino acid residues),¹⁶² but also by the ligation through Michael (1,4-) addition being highly specific for thiols. Maleimides react 1000 times faster with thiols than amines at pH 7.¹⁶³ The pKa of the cysteine thiol group (pKa ≈ 8.3) is significantly lower than that of the lysine amine group (pKa ≈ 10.5).

Maleimide derivatives have been used across many disciplines to modify proteins. One such use is in the development of ADCs for cancer therapy. The inherent site-specificity of maleimide bioconjugations results in a controlled conjugation reaction

that generates more homogenous ADCs. Five out of eight FDA approved ADCs (Adcetris™, Polivy™, Padcev™, Enhertu™, and Trodelvy™) use maleimides highlighting the importance of this method of conjugation.

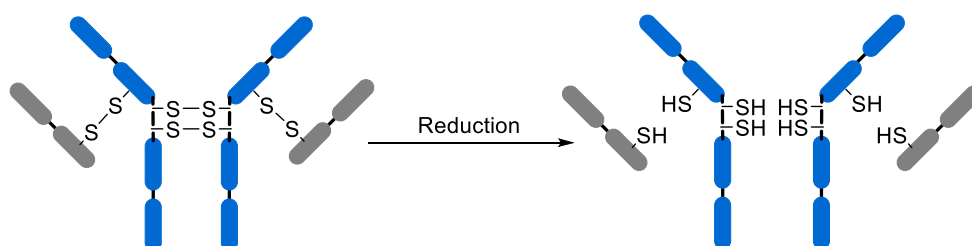


Figure 35 – The reduction of an IgG to give eight reactive thiols.

In the context of maleimide derived ADCs, at least one cysteine residue must be present on the antibody to enable drug conjugation. These free thiols are rarely found in antibodies and so are usually generated artificially for the purpose of maleimide conjugation. This can be done by genetically engineering the expression of a cysteine residue and this modification is usually carried out at the C-terminus of the protein to minimise its impact on protein folding, stability, and biological activity. Maleimide conjugation to a biomolecule possessing a single cysteine residue is site specific, so the resulting bioconjugates are often homogeneous and display good biological activity. However, engineering thiol expression is both time and cost intensive, requiring significant optimisation for each new antibody or protein. Alternatively, free cysteine thiol residues can be generated by reduction of disulfide bonds. In the case of an IgG, two hinge region disulfide bonds and two Fab disulfide bonds can be reduced to give eight reactive thiols (figure 35). These thiols can then react with maleimides to form a bioconjugate with up to 8 bioconjugate linkages. Unless a DAR of 8 is achieved, maleimide conjugates usually display some degree of heterogeneity. Maleimide conjugations result in permanent loss of disulfide bonds, which can negatively impact stability *in vivo*.^{158,164} Additionally, by inducing changes in protein quaternary structure, disruption of disulfide bonds can negatively impact effector functionalities such as FcγR binding, and result in reduced thermal stability.¹⁵⁶

Despite their widespread usage, it has been shown that maleimide bioconjugates exhibit some instability under biological conditions. This instability gives rise to off target effects and reduced clinical efficacy.^{165–167} The serum stability of alkyl-maleimide linked ADCs has been evaluated using antibody-conjugates bearing the potent antimimotic drug monomethyl auristatin F (MMAF).¹⁶⁶ In plasma, MMAF

was lost from the bioconjugate with a half-life of 7-days,¹⁶⁸ in agreement with previously reported values.¹⁶⁵ A retro-Michael reaction was proposed as the mechanism for drug release from the maleimide adduct. Kinetic studies have since confirmed that retro-Michael processes are responsible for the observed thiosuccinimide instability in maleimide bioconjugates.^{167,169}

The effects of thiol pKa, and electron withdrawing ability of the N-substituted group on the rate of the retro-Michael reaction have been evaluated using a range of different thiol and maleimide derivatives.¹⁶⁹ Lower thiol pKa values resulted in faster rates of retro-Michael addition, in agreement with earlier studies.¹⁶⁷ Additionally, increasing electron withdrawing ability of the N-substituted group was associated with reduced loss of thiol by retro-Michael processes. This was attributed to this effect being associated with an increased rate of maleimide hydrolysis to give a stable thiomaleamic acid (figure 34).

Hydrolysis increases the stability of thiol-maleimide conjugates.¹⁶⁴ Under near-physiological conditions (pH 8, 37 °C) thiosuccinimide hydrolysis occurs slowly over 5 days, with competing retro-Michael reactions resulting in a significant loss of thiol observed in this period.¹⁶⁷ Hydrolysis can be accelerated by increasing temperature and pH, but these harsh conditions are incompatible with most biomolecules, including antibodies (see 1.3.1).

Antibodies with cysteine residues engineered at various positions have been used to show the influence of local protein microenvironment upon the stability of the bioconjugate formed.¹⁶⁴ Local positively charged residues promote rapid thiosuccinimide hydrolysis, thereby decreasing the extent of retro-Michael mediated payload loss. Preclinical safety studies demonstrated that these more stable ADCs led to decreased liver toxicity in rats. This led to the development of maleimide agents that rapidly hydrolyse post-conjugation, without the requirement for a specific protein microenvironment.

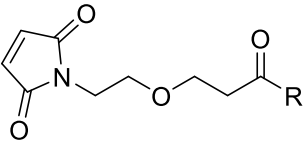
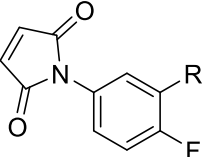
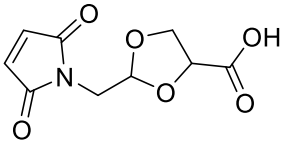
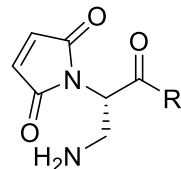
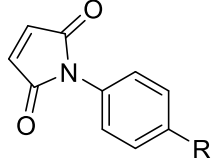
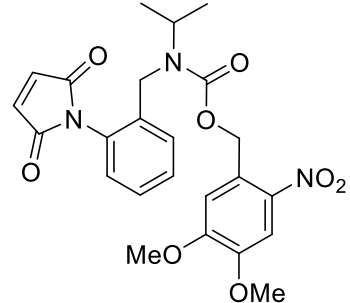
Maleimide structure	Hydrolysis rate of bioconjugate
	30 % hydrolysis over 16 h in PBS pH 7.4
	0.7 h half-life at pH 7.4, 37 °C
	100 % hydrolysis after 20 h in PBS, pH 7.4, 37 °C
	2-2.6 h half-life at pH 7.4
	1.5 h half-life at pH 7.4, 37 °C
	100 % hydrolysis after 50 min of UV irradiation at 0 °C

Figure 36 - Summary of self-hydrolysing maleimides.¹⁷⁰

Positioning a primary amine on the N-alkyl group of the maleimide leads to an increased rate of hydrolysis.¹⁷¹ This effect was initially explained by intramolecular base-catalysed hydrolysis by the amine. This hypothesis was later proven incorrect by demonstrating that even a protonated (and hence non-nucleophilic) amine greatly increases the rate of hydrolysis. The increased rate of hydrolysis was then attributed to the electron withdrawing inductive effect of the protonated amine.

The effect of uncharged electron withdrawing groups (amides, sulfones, ethers, thioethers, trifluoromethanes, polyethylene glycol chains, and alkynes)¹⁷² on the rate of hydrolysis has been studied: in all cases the rate of hydrolysis was increased relative to unmodified maleimides.¹⁷⁰

Despite their instability *in vivo*, maleimide derivatives are still widely used to incorporate radiolabelled chelators into peptides, IgG antibodies, and other proteins.^{29,115,122,173} Their continued usage is likely due to their simplicity, commercial availability, and reliability. The bioconjugation strategies described so far force the user to decide between either (i) simplicity and reliability at the expense of heterogeneity (non-site-specific bioconjugations), or (ii) high stability and immunoreactivity in exchange for high complexity (site-specific bioconjugations). The ideal antibody bioconjugation should be simple, site-specific, reliable, and generate bioconjugates that are both highly stable and preserve biological activity of the native, unmodified antibody.

Thiol-selective conjugation of fluorescein to an antibody has been achieved using various oxadiazolyl methyl sulfone-based reagents.¹⁷⁴ The resulting conjugate was more stable in serum than its maleimide analogue over time. Since then, more accessible synthetic routes to phenyloxadiazolyl methylsulfones (PODS, figure 37) have been developed.¹⁷⁵ The bifunctional chelator PODS-DFO (figure 37) was synthesised and successfully used for the thiol-selective modification (figure 37) and radiolabelling of trastuzumab. This conjugate was more stable *in vitro* than its maleimide analogue. PODS-DFO was also conjugated to huA33 (colorectal cancer targeting), radiolabelled with ⁸⁹Zr, and compared to its maleimide analogue *in vivo*. The PODS-based conjugate significantly outperformed the maleimide conjugate, particularly at later time points (>48 h p.i.). Clinically there is a preference to obtain ⁸⁹Zr-immuno PET images between 72 - 144 h p.i. The use of PODS-based immunoconjugates in these settings may lead to improved image quality.

PODS-DFO has been conjugated to an antibody (SC16-MB1) targeted to delta-like ligand 3 (DLL3).¹⁷⁶ DLL3 is a therapeutic target for the treatment of small cell lung cancer, neuroendocrine prostate cancer, and isocitrate dehydrogenase mutant glioma. SC16-MB1 contains two disulfide bonds in the *lower* hinge region bridging between the two heavy chains (figure 38). However, in the Fab region, the two cysteine residues, which normally form disulfide bonds with corresponding cysteine

residues on the light chain, were mutated leaving a pair of capped cysteine residues on the light chains. Selective reduction of the capped cysteines generates 'free thiols' enabling the attachment of thiol-reactive probes (figure 38).

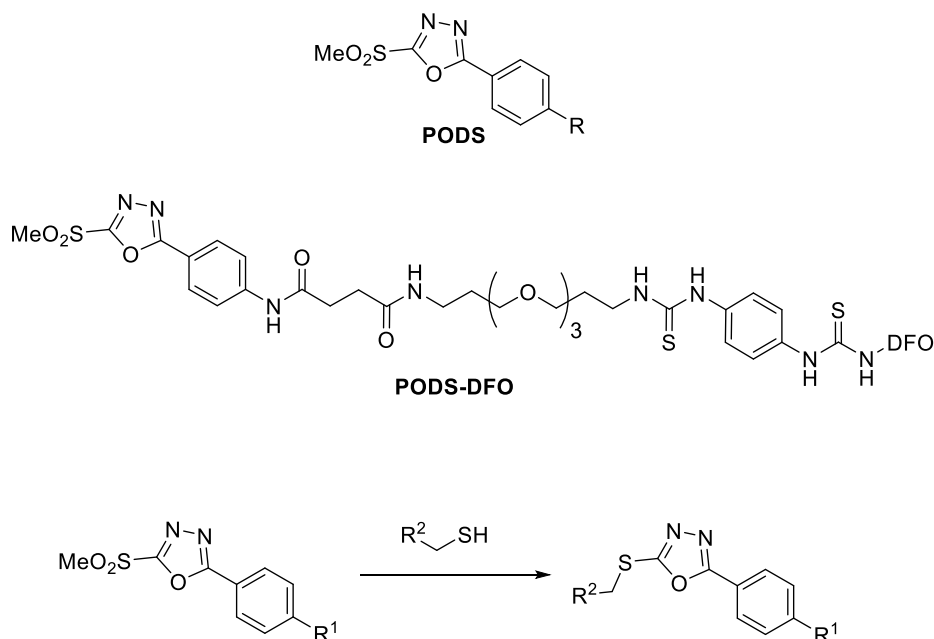


Figure 37 - Structures of PODS and PODS-DFO. The conjugation reaction between a thiol and PODS.

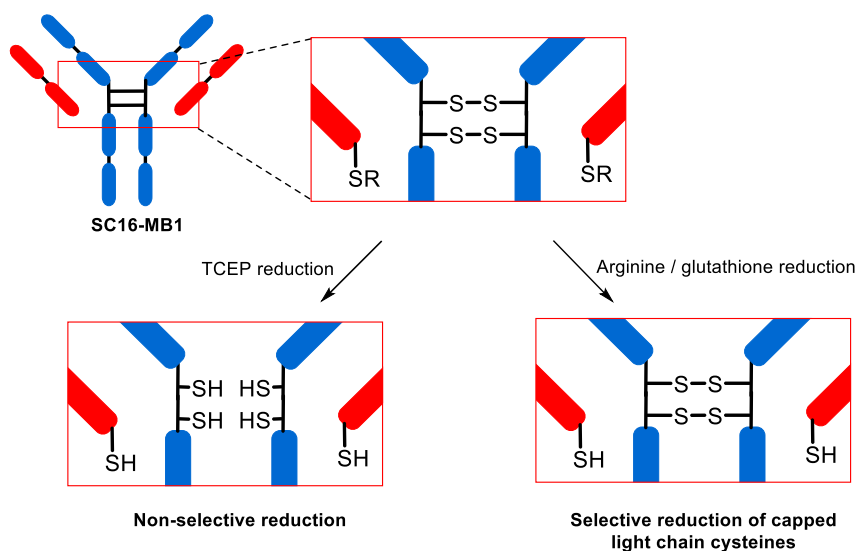


Figure 38 - Schematic of SC16-MB1 with expansion showing the intact hinge region disulfides and capped Fab cysteines on the light chains (red). Reduction with TCEP or arginine / glutathione solution results in non-selective or selective reduction respectively.

Ideally, the capped cysteines should be reduced to expose reactive thiols, whilst leaving the native interchain disulfide bonds untouched. DFO-maleimide was used

to assess the efficacy of two different thiol reduction methodologies. First, using 4 eq. of TCEP produced an immunoconjugate with an average DAR of 0.85, although mass spectrometry showed that 43 % of this immunoconjugate had a DAR ≥ 2 , and ~ 57 % remained unmodified. The presence of unmodified antibody suggested that some capped cysteines had been reduced labelled preferentially over the interchain disulfide thiols, but that a large proportion of capped thiol groups had not been reduced. Using 10 eq. of TCEP led to an immunoconjugate with an average DAR of 3.4. A wide distribution of species bearing 1-6 chelators was detected using mass spectrometry. These results indicate that using this greater number of TCEP eq. leads to the non-selective reduction of both the capped cysteines, and *lower* hinge region disulfides.

The second conjugation protocol used a two-step procedure employing a pair of buffers: one for reduction and another for bioconjugation. The reduction buffer contained GSH to act as a mild reducing agent, and arginine as a stabilising agent. This solution selectively reduced the capped cysteines. It has previously been shown that disulfides (and by extension the capped thiols) of the Fab region are more susceptible to reduction than those of the hinge region, which require more forcing reagents (such as TCEP).¹⁷⁷ The reduced antibody was then buffer exchanged into the conjugation buffer, and addition of DFO-maleimide yielded a bioconjugate where 76-78 % of constructs had a DAR of 2, with 15-17 % unmodified antibody. The rest of the immunoconjugates exhibited a DAR of 1 or >2 . Mass spectrometry of these conjugates confirmed that modification occurred predominantly at the light chains of the antibody, where the uncapped thiols were located.

With this optimised thiol reduction protocol in place, PODS-DFO-Fe was then attached to DLL3-targeted antibody. Fe³⁺ was removed post-conjugation by the addition of EDTA, and adjusting the pH to 4.5, before purifying *via* size exclusion chromatography using a PD-10 desalting column. The resulting immunoconjugate was then radiolabelled with ⁸⁹Zr and compared with its maleimide analogue *in vivo* using mice bearing H82 xenografts (DLL3 expressing). Tumour uptake was similar for the two immunoconjugates 120 h p.i., with the maleimide generating 19.2 ± 3.5 % ID/g compared with 23.3 ± 4.8 % ID/g for the PODS-based reagent. However, higher kidney uptake was observed for the maleimide conjugate (4.7 ± 0.5 % ID/g) compared to the PODS-based reagent (3.3 ± 0.5 % ID/g) at 120 h p.i. ($p = 0.002$).

Maleimide conjugate degradation by retro-Michael addition in the kidneys is one possible explanation for this observed difference in biodistribution. The kidneys are known to be a redox microenvironment conducive to retro-Michael reactions due to the presence of biological thiols such as GSH.^{176,178}

1.7 Next generation maleimides and other thiol-reactive reagents

“Next generation maleimides” (NGM, figure 39) have been developed where one or both vinylic positions are functionalised with a leaving group such as bromide, iodide or thiophenol.^{179–184} This modification allows bioconjugation to proceed *via* an addition-elimination pathway forming a thiomaleimide product, which is mechanistically unsusceptible to retro-Michael processes. However, the thiomaleimide is susceptible to thiol exchange reactions and must be hydrolysed to give thiomaleamic acid derivatives that are stable towards thiol mediated degradation.

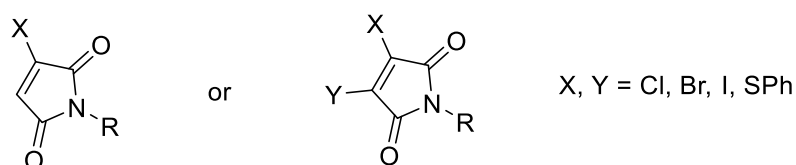


Figure 39 - Next generation maleimides where one or both vinylic positions are functionalised with leaving groups.

1.7.1 Monobromomaleimides

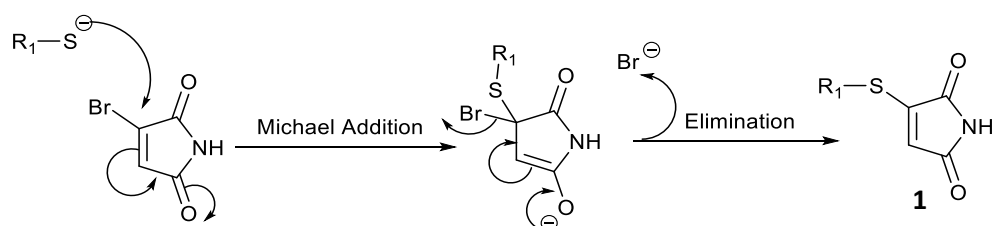


Figure 40 – A monobromomaleimide bioconjugation proceeding via an addition-elimination pathway

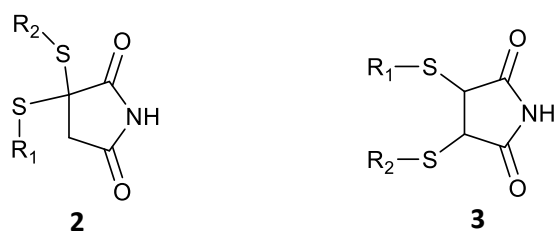


Figure 41 – The potential products of a second thiol addition to a thiomaleimide. Only the vicinal product 3 is observed since the reaction is under steric control.

In monobromomaleimide bioconjugations (figure 40) the thiomaleimide product (**1**, figure 40) can be formed by the addition of one equivalent of thiol. The addition of further equivalents results in a second Michael-addition to give a dithiosuccinimide (figure 41). The regioselectivity of the second thiol addition is under steric control: the geminal product (**2**, figure 41) is not observed, and only the vicinal dithiosuccinimide (**3**, figure 41) is isolated as a mixture of diastereomers. However, dithiosuccinimides are susceptible to thiol exchange processes, and so loss of the conjugate is observed in the presence of excess competing thiol.

Monobromomaleimides are therefore not suited to the generation of bis-thiol adducts. To prevent thiol exchange reactions, monobromomaleimide conjugations are carried out under stoichiometric control, followed by rapid post conjugation hydrolysis to yield stable thiomaleamic acid derivatives. This approach has been exemplified using an engineered Grb2 adapter protein (figure 42).¹⁸⁵ Treatment of this protein with one stoichiometric equivalent of N-phenyl monobromomaleimide (**4**, figure 42) at pH 8, 0 °C, for 1 hour yielded bioconjugate (**5**, figure 42). Upon heating to 37 °C for 4 h, quantitative hydrolysis of the maleimide occurred to give the thiomaleamic acid conjugate (**6**, figure 42). This species was stable towards treatment with excess 2-mercaptoethanol (BME), and GSH at 0 °C, 20 °C and 37 °C.

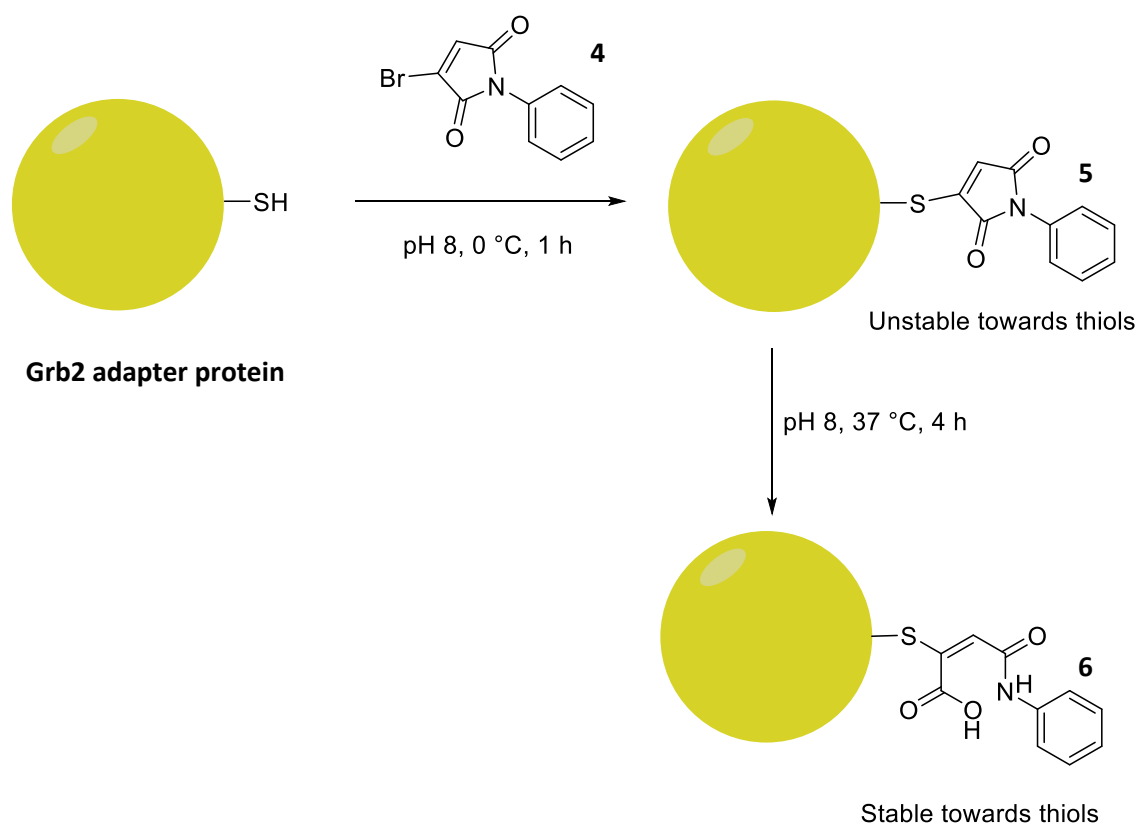


Figure 42 – Irreversible protein modification with N-phenyl monobromomaleimide.

Monobromomaleimides have been used to generate reagents for the selective and reversible modification of cysteine, as thiol cleavage from the thiomaleimide is possible.¹⁸⁶ For example, a monobromomaleimide-biotin compound has been used to reversibly biotinylate the Grb2 adapter protein enabling protein purification by application to neutravidin coated agarose beads. Pure samples of protein could then be generated by suspension of the beads in PBS containing 2-mercaptoethanol (25 mM) at 37 °C for 2 h, to cleave the unmodified Grb2 adapter protein.

Monobromomaleimides have been used effectively to conjugate fluorophore and drug payloads to single cysteine bearing biomolecules such as human serum albumin (HSA). Relative to unmodified HSA, some HSA conjugates display increased solubility and circulatory half-lives, as well as increased uptake and retention in tumours.^{187,188} Monobromomaleimide has been used as a platform to construct an HSA conjugate of paclitaxel (a chemotherapeutic) *via* the Cys-34 residue of HSA. Modification of this residue with maleimides proceeds rapidly, but since Cys-34 resides within a hydrophobic cleft, the rate of hydrolysis is slow, requiring overnight incubation at pH 9, 37 °C to achieve stabilising hydrolysis. Many sensitive drugs

including paclitaxel are known to degrade under these conditions.¹⁸⁹ Use of a paclitaxel-monobromomaleimide containing an electron withdrawing C2 linker (-CH₂-C(O)-), allows conjugation to HSA, as well as mild, rapid hydrolysis (pH 8.0-8.5, 1-2 h post conjugation) to achieve a stable conjugate.

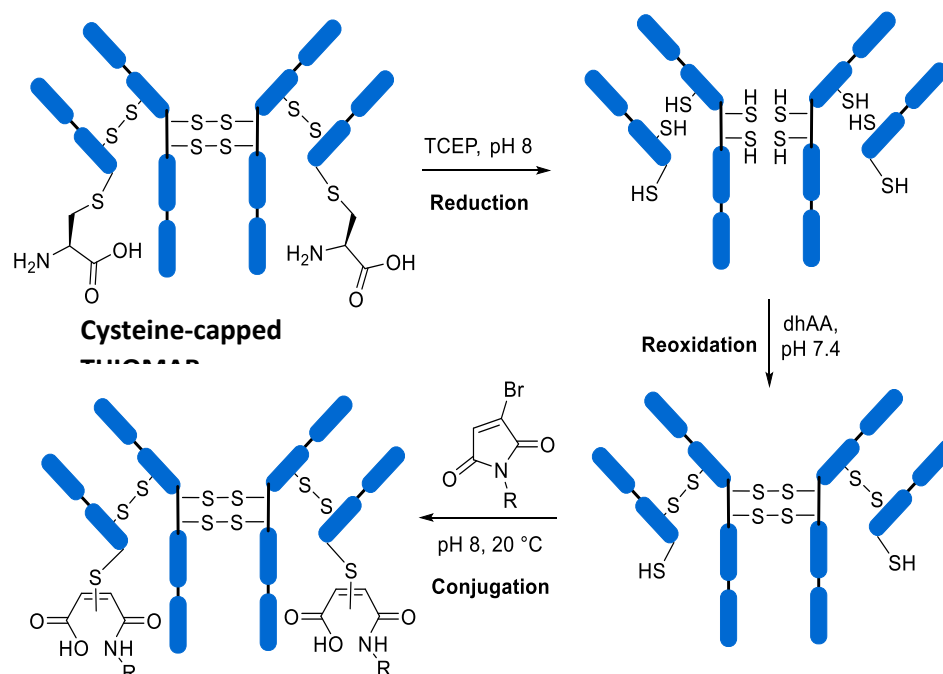


Figure 43 - Conjugation of a monobromomaleimide to a THIOMAB.

Stable, potent, and near homogeneous antibody-drug conjugates have been prepared with bromomaleimide derivatives using the THIOMAB platform (figure 43).¹⁹⁰ THIOMABs are generated using site-directed mutagenesis to incorporate non-native “capped” cysteine residues onto the antibody’s two light chains. Reduction of the engineered antibody with TCEP yields 10 sulfhydryls, with hinge region cysteines then selectively reoxidised with dehydroascorbic acid (dhAA) to reform interchain disulfide bonds. The non-native light chain cysteine residues remain available for conjugation to thiol reactive compounds such as bromomaleimides.

A bromomaleimide-bearing the antineoplastic agent monomethyl auristatin E (MMAE) was coupled to a trastuzumab-based THIOMAB using this technology. The conjugate was stabilised by hydrolysis in just 1 hour at pH 8, achieving a DAR of 1.8 (close to the theoretical maximum of 2). The potency of the MMAE conjugate was assessed in two cell lines expressing HER2 (SKBR-3 and HCC-1954), and also in MCF-7 cells that do not express HER2 as a negative control. All cell lines were observed to be sensitive to MMAE prior to conjugation, with IC₅₀ values of 0.19 nM and 0.21

nM, and 0.01 nM for SKBR-3, HCC-1954, and MCF-7 respectively. MMAE potency was retained for the conjugate when incubated with HER2 expressing cell lines where IC₅₀ values of 0.14 nM and 0.31 nM were generated for SKBR-3 and HCC-1954 respectively. In contrast when the conjugate was incubated with the HER2 negative MCF-7 cell line, where minimal potency was observed. These results demonstrated the MMAE conjugate's targeted cell-killing ability against HER2-expressing cell lines.

1.7.2 Disulfide rebridging

Several conjugation platforms have been developed that enable site specific attachment of cargo to reduced antibody dithiol groups. In doing so, disulfide bonds are effectively 'rebridged'. Whilst self-hydrolysing maleimides (figure 36) effectively mitigate retro-Michael stability concerns, permanent cleavage of antibody disulfides leads to compromised thermal stability.¹⁵⁶

The first example of disulfide rebridging was a sulfone-based conjugation motif, which was used to append polyethylene glycol groups to a range of biomolecules, including glutathione (GSH), somatostatin, L-asparaginase, and interferon α -2b (IFN), in an attempt to increase these molecules' biological half-lives (figure 44).¹⁹¹ After any disulfide bond reduction with tris(2-carboxyethyl)phosphine (TCEP) or dithiothreitol (DTT), the sulfone reagent was added to yield a rebridged species where 3 carbon (C3) atoms have been inserted between sulfide groups. In the case of IFN, although PEGylation increased the biomolecule's biological half-life, its biological activity was diminished.

This loss of bioactivity was independent of PEG chain length and was not caused by any steric encumbrance resulting from PEG inclusion. It is likely that insertion of a C3 linker altered the distance and rigidity between the thiol residues, causing subtle changes in the biomolecule's tertiary structure, resulting in decreased bioactivity. Bis-sulfones have also been used as reagents for disulfide bridging, including ADC synthesis.^{192,193}

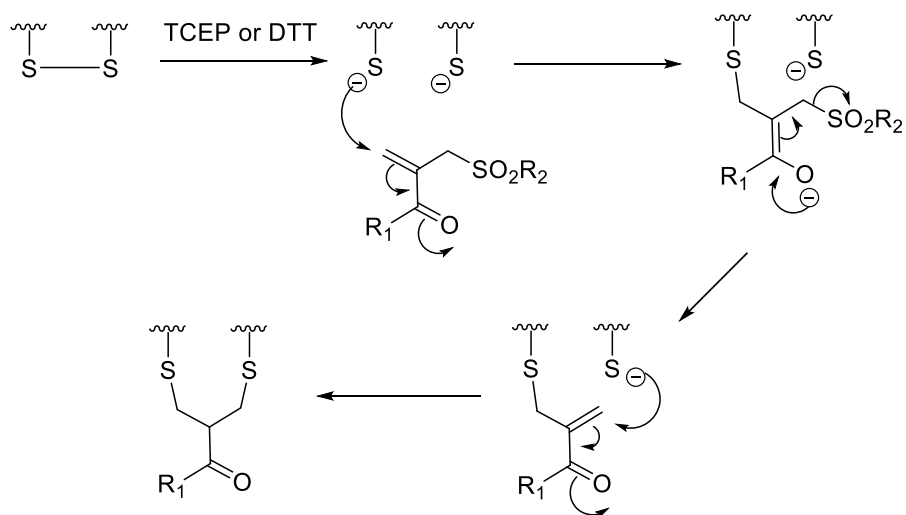


Figure 44 – A sulfone-based method for modification of a protein disulfide bond with rebridging.

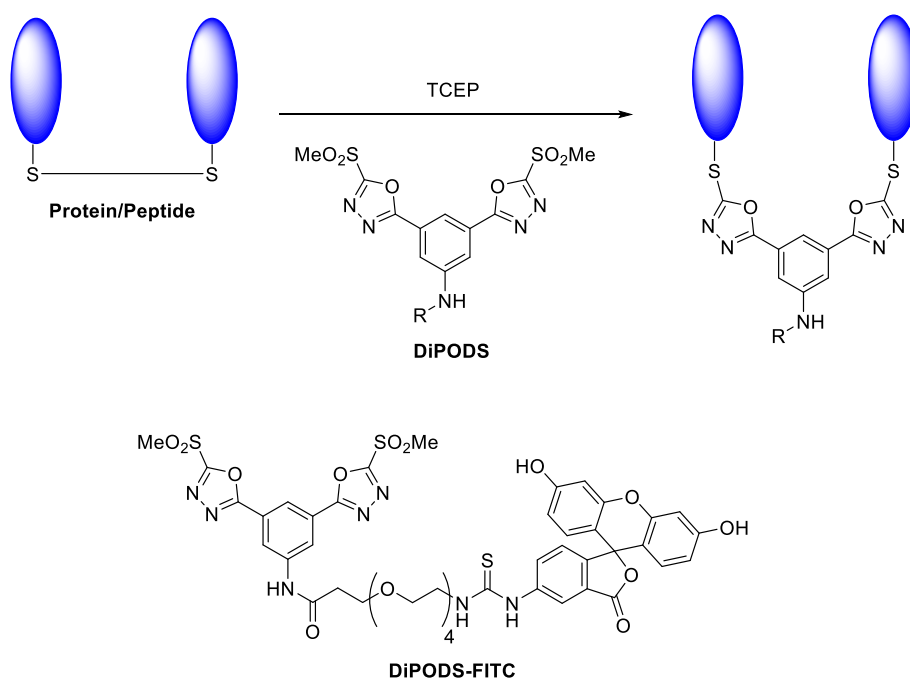


Figure 45 - The conjugation of a DiPODS reagent to a protein/peptide with a single disulfide bond. The structure of DiPODS-FITC is also shown.

Building upon previous work with PODS (see 1.6.2), bivalent PODS-based reagents (DiPODS, figure 45) have been developed for the irreversible rebridging of disulfide linkages.¹⁹⁴ Fab antibody fragments were used due to the presence of only one interchain disulfide bond, compared to the four found in full-length IgGs. The Fab disulfide bond was reduced with TCEP and subsequently treated with DiPODS bearing fluorescein (DiPODS-FITC, figure 45). A highly homogeneous bioconjugate was formed with a DAR of 0.95 ± 0.01 , indicating efficient rebridging of the cleaved disulfide bond. Flow cytometry was used to demonstrate that the DiPODS

conjugate exhibited superior antigen binding relative to a non-site-specific fluorescein-isothiocyanate lysine conjugate.

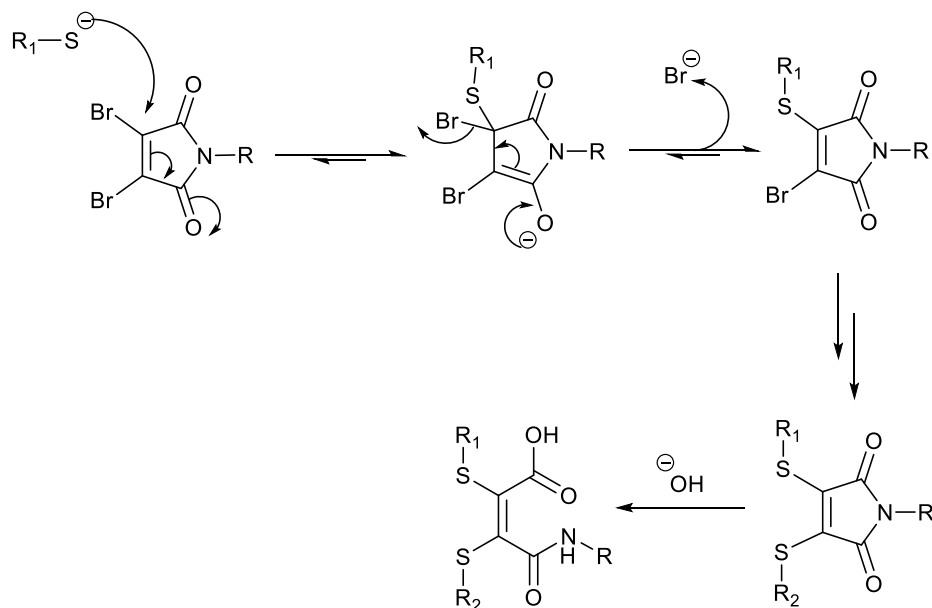


Figure 46 - Conjugation between a dibromomaleimide and two equivalents of thiol, followed by hydrolysis to yield a thiomaleamic acid derivative. 7

Dibromomaleimides can be used to rebridge disulfide bonds. Compared to monobromomaleimides (see 1.7.1), the presence of two leaving groups, one at each vinylic position, enables two sequential addition elimination reaction to take place (figure 46). The resulting dithiomaleimide (**7**, figure 46) is mechanistically unsusceptible to retro-Michael processes. However, this product is susceptible to thiol exchange by successive Michael additions with the elimination of a thiol – effectively thiol substitution. This dithiomaleimide can be hydrolysed to give a dithiomaleamic acid that is stable towards thiol exchange. Compared to the previously described sulfone-based reagents, conjugation to NGMs results in reduced distance between rebridged thiols (a C2 bridge) with increased rigidity by virtue of the conjugated maleamic acid system. In contrast to the site-specific conjugations described previously, NGM conjugations affect the overall structure of the antibody to a lesser extent – glycans remain unchanged, no new amino acid residues are introduced, and interchain covalent bonds are maintained. Hence, NGM bioconjugates usually have bioactivities and biological half-lives comparable to that of the unmodified antibody. This is especially important in the field of molecular imaging, where the radiolabelling technique employed should minimally alter the pharmacokinetic or pharmacodynamic properties of the targeting vector.

The rebridging of reduced disulfide bonds by NGMs was investigated using a dibromomaleimide derivative (figure 47).^{185,195} The cyclic peptide somatostatin was used as a model biomolecule since it possesses one intramolecular disulfide bond. Reduction of the disulfide bond was achieved using TCEP, then a dibromomaleimide functionalised with fluorescein was added to give a fluorescently labelled somatostatin bioconjugate. The pseudo-reversibility of the bioconjugation was demonstrated by the addition of 2-mercaptoethanol (BME, 100 eq.). Thiol exchange resulted in the elimination of the bioconjugate yielding somatostatin in its reduced form. The same bioconjugation was also carried out with an additional hydrolysis step to yield a bioconjugate that was stable towards serum thiols.

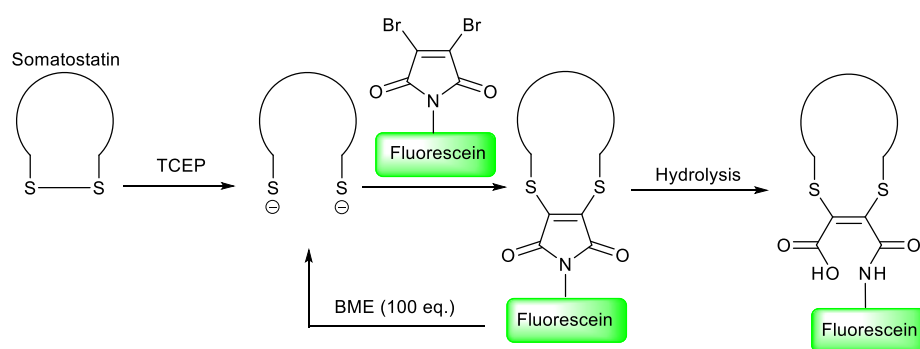


Figure 47 – Reduction of somatostatin disulfide bonds followed by bioconjugation with a fluorescein-labelled dibromomaleimide. The product can be cleaved to yield reduced somatostatin or hydrolysed to form a stable bioconjugate.

The rate of dithiomaleimide conjugate hydrolysis has been optimised, using three different dibromomaleimide bioconjugates with varying groups in the N-position (figure 48).¹⁸² After antibody disulfide reduction, the dibromomaleimide reagents were added and the subsequent bioconjugation and hydrolysis reactions were monitored by UV-vis spectroscopy. Thioether formation gives rise to an absorbance at ~400 nm. This signal is lost upon conversion of this species to the corresponding dithiomaleamic acid resulting from hydrolysis. Initial measurement (<1 min after DBM addition) revealed maximal dithiomaleimide absorbance, indicating rapid thioether formation for reactions of all three dibromomaleimide precursors.

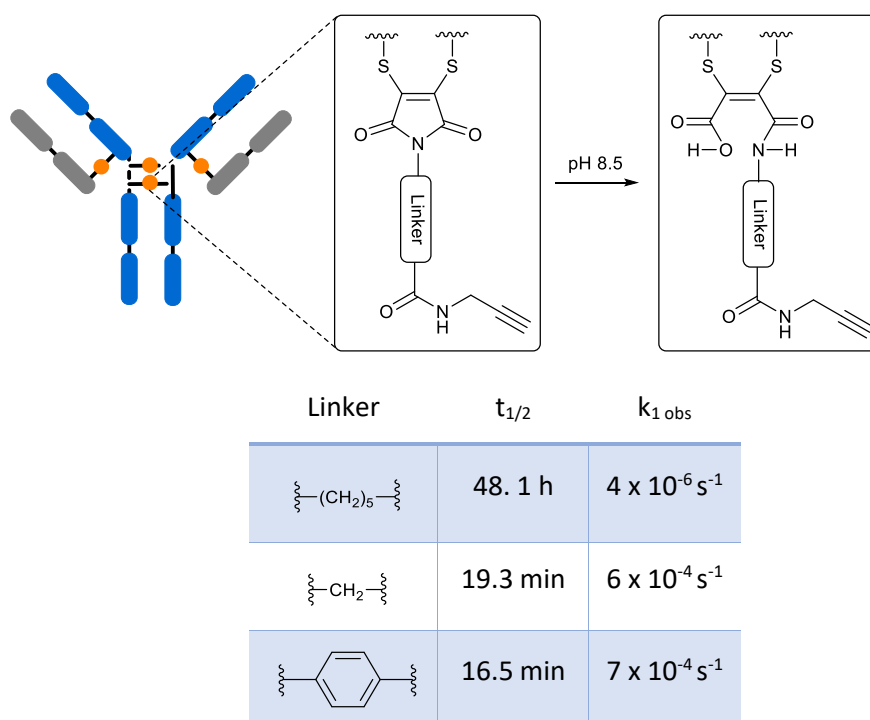


Figure 48 – Top - a scheme to show hydrolysis of a dibromomaleimide antibody conjugate. Bottom - the effect of linker electronic conductivity on the rate of dithiomaleimide hydrolysis at pH 8.5.¹⁸²

The bioconjugate with the pentyl linker resulted in the slowest rate of hydrolysis, with the rate of hydrolysis increased by approximately two orders of magnitude upon changing to the methyl linker. The phenyl linker resulted in an even faster rate of hydrolysis. These observations are consistent with prior data on maleimide hydrolysis, where the electron withdrawing ability of the N-substituent also increased the rate of hydrolysis.^{171,172,196} Here, the amide group attached to the linker functioned as the electron withdrawing group. As the linker length increased from methyl to pentyl linker, there was an increase in electronic insulation between the maleimide and the amide, resulting in a decrease in the rate of maleimide hydrolysis. The phenyl linker confers a slight increase in rate of hydrolysis compared to the methyl linker. This research led to the development of a dibromomaleimide conjugation protocol based on the variant with the methyl linker. Using this methodology, conjugation and hydrolytic bioconjugate stabilisation was achieved in just over one hour generating highly homogeneous antibodies with a DAR of 4, representing a significant improvement over previously described dibromomaleimide bioconjugation protocols, which typically required several days.

Antibody derivatives have been developed that can simultaneously bind two different antigens. These so-called bispecifics confer improved antitumour activity relative to their monospecific analogues. The first bispecific therapeutic to gain clinical approval was catumaxomab combining EpCAM targeting with T-cell recruitment for the treatment of malignant ascites.¹⁹⁷ In the past two decades, 45 different bispecific formats have been generated using recombinant technologies.¹⁹⁸ However, this synthetic approach cannot be applied to every protein pair. Fusion of proteins *via* their N or C termini can result in a decreased or complete loss of bioactivity, and variation in expression yields is observed due to complications in protein folding and processing.^{199–201}

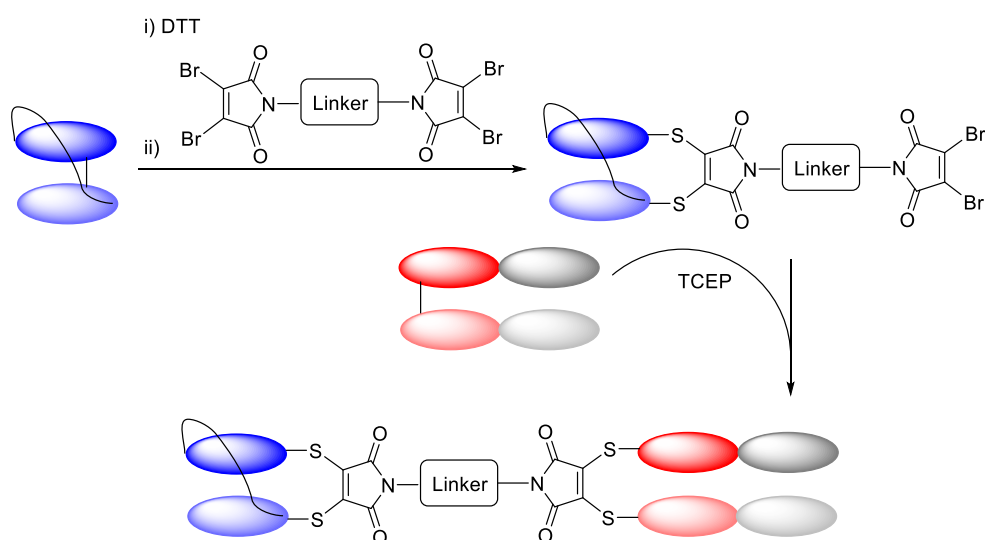


Figure 49 – Generation of an scFv-Fab bispecific using dibromomaleimide technology.

Dibromomaleimides have been used to generate homogeneous bispecifics (figure 49).²⁰² Here two dibromomaleimides have been attached *via* a polyethylene glycol linker. Thirty equivalents of this linker reagent were added to one equivalent of a reduced single chain variable fragment (scFv) to yield a dibromomaleimide functionalised scFv. Excess linker was then removed, and separately a Fab fragment was reduced and purified. The functionalised scFv was added to the reduced Fab in a 2:1 ratio, to give the bispecific in 52% yield with excellent homogeneity. An ELISA was used to demonstrate that the bispecific had retained its bioactivity.

The scope of these NGM linkers has been extended to enable bispecific formation with between scFv or Fab fragments and sterically hindered systems such as human serum albumin (HSA).¹⁸³ HSA was first reacted with a large excess of bis-

dibromomaleimide to give an HSA conjugate bearing a pendant dibromomaleimide group. However, upon addition of the scFv or Fab fragment to attempt bispecific formation, only a small amount of product was observed by sodium dodecyl sulfate polyacrylamide gel electrophoresis (SDS-PAGE). This result was attributed to inhibition of the reaction generated by the increased steric hindrance of HSA. Rapid hydrolysis of the pendant dibromomaleimide moiety was in competition with bioconjugation. Diiodomaleimide was shown to exhibit a slower rate of hydrolysis/degradation, and so this motif was incorporated into two homobifunctional crosslinkers DIM_{CL} and DIM_{CL-C6} (figure 50). These new compounds were used to synthesise HSA-scFv and HSA-Fab, achieving yields of 49% and 57% respectively. The synthesis of HSA-scFv required the use of the more hydrolytically stable DIM_{CL-C6} due to the more sterically hindered disulfide within the scFv compared to the Fab fragment.

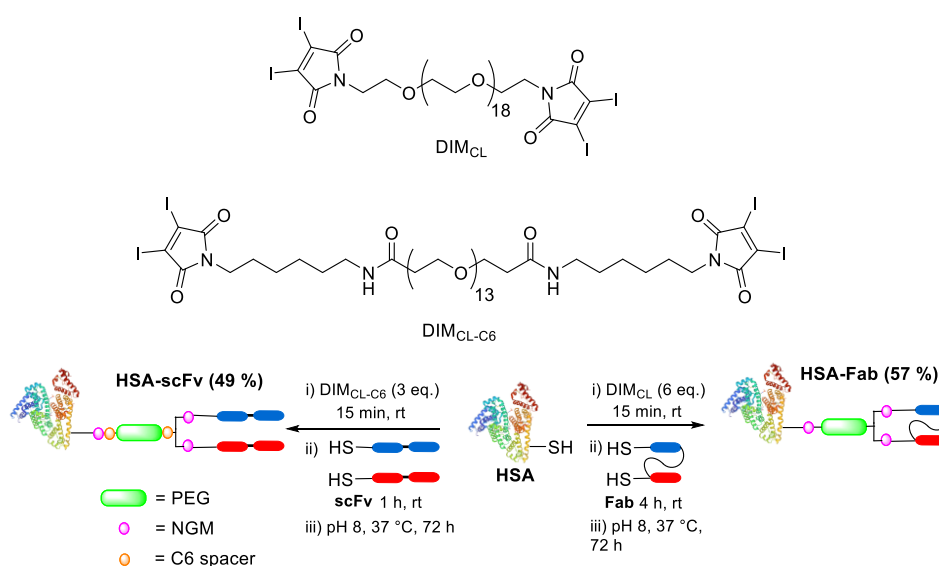


Figure 50 - The structures the homobifunctional crosslinking reagents DIM_{CL} and DIM_{CL-C6}. The synthesis of bispecifics HSA-scFv and HSA-Fab.

Recently a new method that enables attachment of both a thiol-containing molecule and an amine-containing molecule to a dibromomaleimide has been developed. In a proof of concept (figure 51), the authors synthesised a dibromomaleimide functionalised with biotin (widely used in affinity purification and biological assays). 1.5 eq. of this dibromomaleimide (**8**) were added to one equivalent of mutant HSA (mHSA) with a highly accessible free cysteine thiol group, followed by 20 eq. of a para-anisidine-based amine-azide (**9**) to yield an azide-bearing conjugate intermediate (**10**). Finally, the clickable fluorophore,

dibenzocyclooctyne-tetramethylrhodamine (DABCO-TAMRA), was reacted with the azide intermediate *via* SPAAC to give a trifunctional aminothiomaleimide product (**11**).

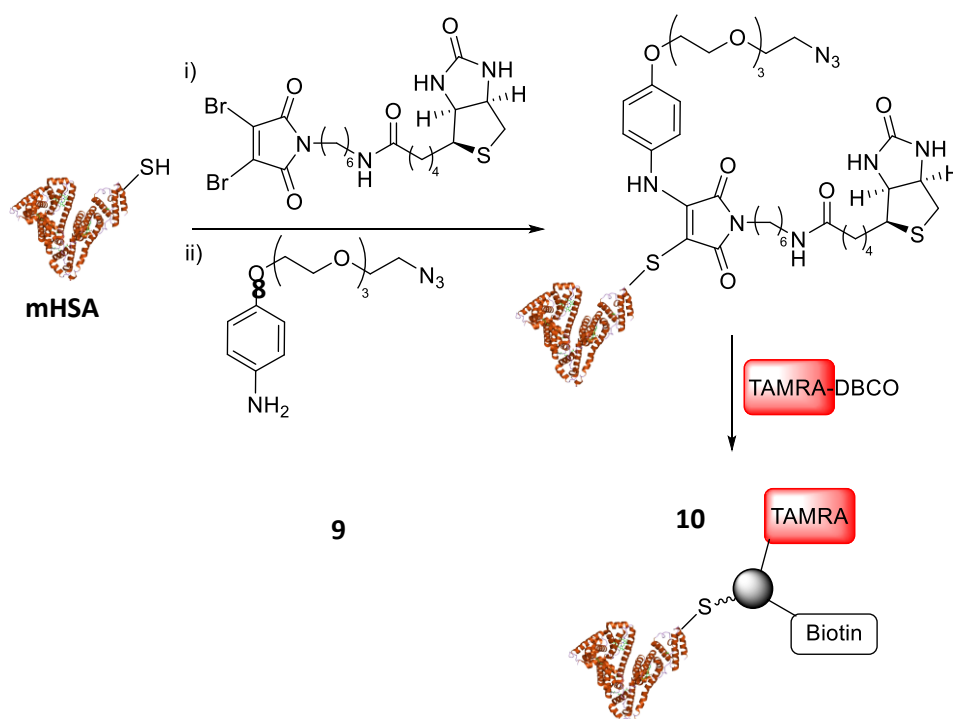


Figure 51 – Formation of a trifunctional aminothiomaleimide.²⁰³

Lastly, dibromopyridazinedione derivatives have also been used for conjugations to

11

reduced dithiols (figure 52).^{204–209} Compared to other dithiol conjugation strategies discussed, pyridazinedione (PD) conjugates are often the most homogeneous. In one study, a range of dibromopyridazinediones bearing MMAE were conjugated to an IgG.²⁰⁶ LCMS analysis of resulting ADCs showed that 90 % of conjugates had a DAR of 4. Compared to NGM conjugates, those of PDs are stable towards serum thiols without the need for an additional hydrolysis step, simplifying conjugation.¹⁷⁰ Additionally, the presence of an additional nitrogen in the pyridazinedione ring enables the inclusion of additional functionalities compared to NGMs. For example, a PD-trastuzumab conjugate bearing the chemotherapeutic doxorubicin (Dox), and the fluorophore Cy5 has been synthesised.²⁰⁹ This was achieved using a two-step, orthogonal click chemistry approach (figure 53). Antigen binding was uncompromised, and the conjugates were shown to be selectively cytotoxic towards cells expressing the HER2 target receptor.

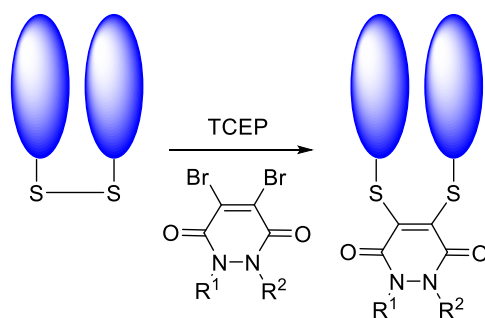


Figure 52 - The conjugation reaction between a disulfide bond and a dibromopyridazinedione.

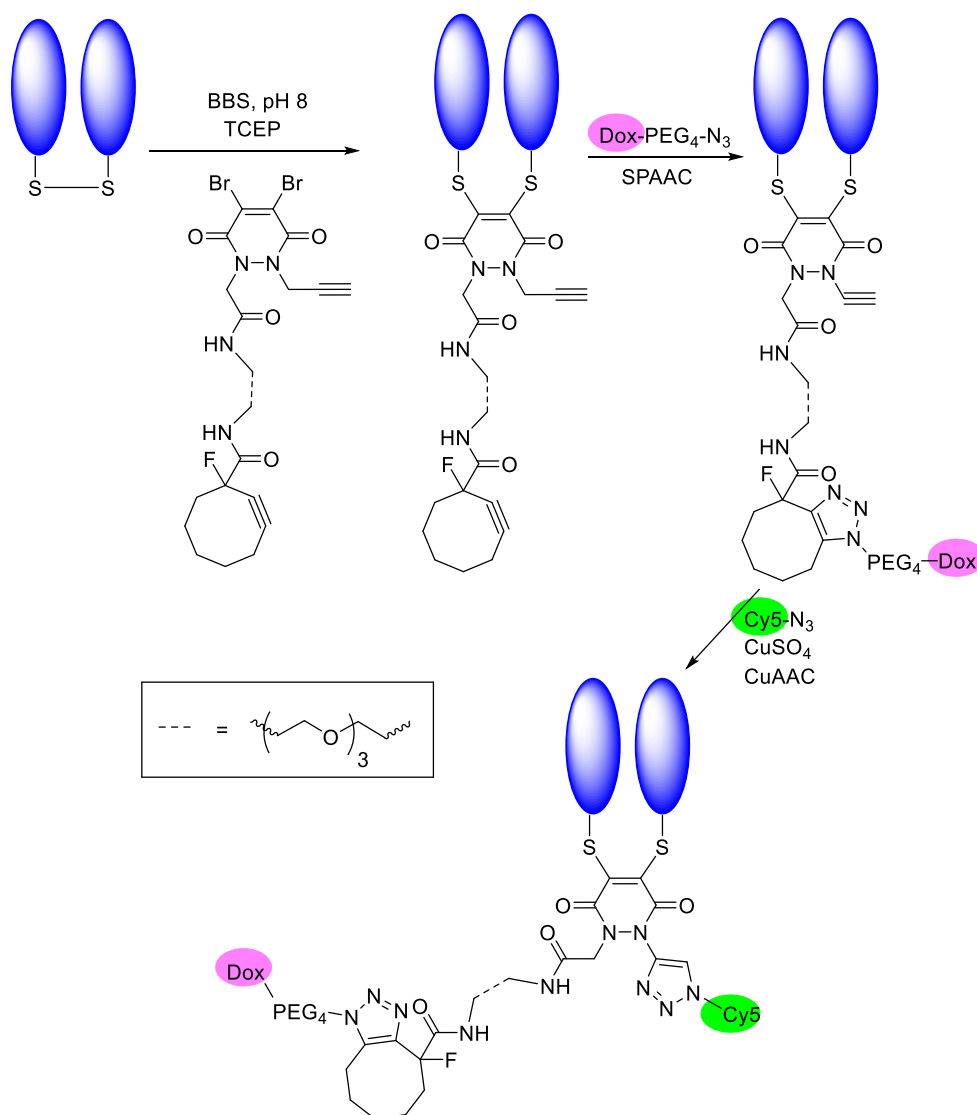


Figure 53 - Two-step orthogonal click chemistry synthesis of a PD conjugate bearing the chemotherapy drug doxorubicin (Dox), and the fluorophore Cy5.²⁰⁶

1.8 Thesis aims

The introduction above highlights state of the art radiometal chelation and bioconjugation methodologies. Currently, radiochemists must choose between non-site specific conjugations and site specific conjugations. Non-site specific conjugations afford simplicity and low cost, but at the expense of low bioconjugate homogeneity, and potentially disadvantageous impacts on the bioconjugate's biological behaviours (e.g. decreased target receptor affinity). In contrast, site specific conjugations product highly homogeneous bioconjugates, often with near-native biological behaviours, although this comes at the expense of increased complexity, higher costs. Next generation maleimide technologies, specifically dibromomaleimides share many of the benefits of non-site specific and site specific conjugations whilst largely avoiding the respective challenges posed by other bioconjugation technologies. However, this class of molecules has not yet been exploited for use in constructing bifunctional chelators for use in nuclear medicine. In this project we aimed to, for the first time, exploit the bioconjugation efficacy of dibromomaleimides pairing them with state-of-the-art radiometal chelators (sarcophagine and DFO) to form new bifunctional chelators, with subsequent attachment to antibodies (trastuzumab) as a proof of concept.

The overall aim of this thesis was to synthesise and assess new bifunctional chelators containing dibromomaleimides for the preparation of radioimmunoconjugates for PET imaging.

To achieve this aim, the following chapters of this thesis will discuss:

- The synthesis of dibromomaleimide-based bifunctional chelators containing either sarcophagine or desferrioxamine
- The conjugation of these bifunctional chelators to antibodies
- Radiolabelling of these immunoconjugates
- Assessing the properties and behaviours of these new radioimmunoconjugates

1.9 Chapter 1 references

- 1 Healthcare resource statistics - technical resources and medical technology, https://ec.europa.eu/eurostat/statistics-explained/index.php/Healthcare_resource_statistics_-_technical_resources_and_medical_technology#Availability_of_medical_t

- chnology, (accessed 21 January 2021).
- 2 Diagnostic Imaging Dataset Annual Statistic Release 2018-19, <https://www.england.nhs.uk/statistics/statistical-work-areas/diagnostic-imaging-dataset/diagnostic-imaging-dataset-2018-19-data/>, (accessed 21 January 2021).
 - 3 P. Zanzonico, Principles of Nuclear Medicine Imaging: Planar, SPECT, PET, Multi-modality, and Autoradiography Systems, *Radiat. Res.*, 2012, **177**, 349–364.
 - 4 D. Taïeb, P. Garrigue, M. Bardiès, A. E. Abdullah and K. Pacak, Application and dosimetric requirements for Gallium-68-labeled somatostatin analogues in targeted radionuclide therapy for gastroenteropancreatic neuroendocrine tumors, *PET Clin.*, 2015, **10**, 477–486.
 - 5 M. S. De Feo, M. Pontico, V. Frantellizzi, F. Corica, F. De Cristofaro and G. De Vincentis, ⁸⁹Zr-PET imaging in humans: a systematic review, *Clin. Transl. Imaging*, 2022, **10**, 23–36.
 - 6 N. E. Holden, in *Handbook of Chemistry and Physics*, ed. D. R. Lide, CRC Press, Boca Raton, 84th edn., 2004, pp. 50–213.
 - 7 A. Bondi, van der Waals Volumes and Radii, *J. Phys. Chem.*, 1964, **68**, 441–451.
 - 8 M. E. Rodnick, C. Sollert, D. Stark, M. Clark, A. Katsifis, B. G. Hockley, D. C. Parr, J. Frigell, B. D. Henderson, M. Abghari-Gerst, M. R. Piert, M. J. Fulham, S. Eberl, K. Gagnon and P. J. H. Scott, Cyclotron-based production of ⁶⁸Ga, [⁶⁸Ga]GaCl₃, and [⁶⁸Ga]Ga-PSMA-11 from a liquid target, *EJNMMI Radiopharm. Chem.*, , DOI:10.1186/s41181-020-00106-9.
 - 9 M. Jauregui-Osoro, S. De Robertis, P. Halsted, S. M. Gould, Z. Yu, R. L. Paul, P. K. Marsden, A. D. Gee, A. Fenwick and P. J. Blower, Production of copper-64 using a hospital cyclotron: Targetry, purification and quality analysis, *Nucl. Med. Commun.*, 2021, **42**, 1024–1038.
 - 10 B. M. Paterson and P. S. Donnelly, *Macrocyclic Bifunctional Chelators and Conjugation Strategies for Copper-64 Radiopharmaceuticals*, Elsevier Inc., 1st edn., 2016, vol. 68.

- 11 J. P. Holland, Y. Sheh and J. S. Lewis, Standardized methods for the production of high specific-activity zirconium-89, *Nucl. Med. Biol.*, 2009, **36**, 729–739.
- 12 B. M. Zeglis and J. S. Lewis, A practical guide to the construction of radiometallated bioconjugates for positron emission tomography, *Dalt. Trans.*, 2011, **40**, 6168.
- 13 C. Kratochwil, F. L. Giesel, M. Stefanova, M. Benesova, M. Bronzel, A. Afshar-Oromieh, W. Mier, M. Eder, K. Kopka and U. Haberkorn, PSMA-targeted radionuclide therapy of metastatic castration-resistant prostate cancer with ¹⁷⁷Lu-Labeled PSMA-617, *J. Nucl. Med.*, 2016, **57**, 1170–1176.
- 14 C. Rangger and R. Haubner, Radiolabelled Peptides for Positron Emission Tomography and Endoradiotherapy in Oncology, *Pharmaceuticals*, 2020, **13**, 22.
- 15 A. Pfeifer, U. Knigge, J. Mortensen, P. Oturai, A. K. Berthelsen, A. Loft, T. Binderup, P. Rasmussen, D. Elema, T. L. Klausen, S. Holm, E. von Benzon, L. Hojgaard and A. Kjaer, Clinical PET of Neuroendocrine Tumors Using ⁶⁴Cu-DOTATATE: First-in-Humans Study, *J. Nucl. Med.*, 2012, **53**, 1207–1215.
- 16 R. J. Hicks, P. Jackson, G. Kong, R. E. Ware, M. S. Hofman, D. A. Pattison, T. A. Akhurst, E. Drummond, P. Roselt, J. Callahan, R. Price, C. M. Jeffery, E. Hong, W. Noonan, A. Herschtal, L. J. Hicks, A. Hedt, M. Harris, B. M. Paterson and P. S. Donnelly, ⁶⁴Cu-SARTATE PET Imaging of Patients with Neuroendocrine Tumors Demonstrates High Tumor Uptake and Retention, Potentially Allowing Prospective Dosimetry for Peptide Receptor Radionuclide Therapy, *J. Nucl. Med.*, 2019, **60**, 777–785.
- 17 M. T. Ma, J. A. Karas, J. M. White, D. Scanlon and P. S. Donnelly, A new bifunctional chelator for copper radiopharmaceuticals: a cage amine ligand with a carboxylate functional group for conjugation to peptides, *Chem. Commun.*, 2009, 3237.
- 18 B. M. Paterson, P. Roselt, D. Denoyer, C. Cullinane, D. Binns, W. Noonan, C. M. Jeffery, R. I. Price, J. M. White, R. J. Hicks and P. S. Donnelly, PET imaging of tumours with a ⁶⁴Cu labeled macrobicyclic cage amine ligand tethered to Tyr 3 -octreotate, *Dalt. Trans.*, 2014, **43**, 1386–1396.

- 19 T. Quinn, X. Zhang and Y. Miao, Targeted melanoma imaging and therapy with radiolabeled alpha-melanocyte stimulating hormone peptide analogues, *G. Ital. di Dermatologia e Venereol.*, 2010, **145**, 245–258.
- 20 J. Q. Chen, Z. Cheng, T. J. Hoffman, S. S. Jurisson and T. P. Quinn, Melanoma-targeting properties of 99mtechnetium-labeled cyclic α -melanocyte-stimulating hormone peptide analogues, *Cancer Res.*, 2000, **60**, 5649–5658.
- 21 K. Zelenka, L. Borsig and R. Alberto, Trifunctional 99mTc based radiopharmaceuticals: metal-mediated conjugation of a peptide with a nucleus targeting intercalator., *Org. Biomol. Chem.*, 2011, **9**, 1071–1078.
- 22 E. Gourni, L. Del Pozzo, E. Kheirallah, C. Smerling, B. Waser, J. C. Reubi, B. M. Paterson, P. S. Donnelly, P. T. Meyer and H. R. Maecke, Copper-64 Labeled Macrobicyclic Sarcophagine Coupled to a GRP Receptor Antagonist Shows Great Promise for PET Imaging of Prostate Cancer, *Mol. Pharm.*, 2015, **12**, 2781–2790.
- 23 M. T. Ma, M. S. Cooper, R. L. Paul, K. P. Shaw, J. A. Karas, D. Scanlon, J. M. White, P. J. Blower and P. S. Donnelly, Macrobicyclic Cage Amine Ligands for Copper Radiopharmaceuticals: A Single Bivalent Cage Amine Containing Two Lys 3 -bombesin Targeting Peptides, *Inorg. Chem.*, 2011, **50**, 6701–6710.
- 24 J. Calais, A. U. Kishan, M. Cao, W. P. Fendler, M. Eiber, K. Herrmann, F. Ceci, R. E. Reiter, M. B. Rettig, J. V. Hegde, N. Shaverdian, C. R. King, M. L. Steinberg, J. Czernin and N. G. Nickols, Potential Impact of 68 Ga-PSMA-11 PET/CT on the Planning of Definitive Radiation Therapy for Prostate Cancer, *J. Nucl. Med.*, 2018, **59**, 1714–1721.
- 25 C. Kratochwil, F. Bruchertseifer, F. L. Giesel, M. Weis, F. A. Verburg, F. Mottaghy, K. Kopka, C. Apostolidis, U. Haberkorn and A. Morgenstern, 225Ac-PSMA-617 for PSMA-Targeted α -Radiation Therapy of Metastatic Castration-Resistant Prostate Cancer, *J. Nucl. Med.*, 2016, **57**, 1941–1944.
- 26 J. D. Young, V. Abbate, C. Imberti, L. K. Meszaros, M. T. Ma, S. Y. A. Terry, R. C. Hider, G. E. Mullen and P. J. Blower, 68Ga-THP-PSMA: A PET imaging agent for prostate cancer offering rapid, room-temperature, 1-step kit-

- based radiolabeling, *J. Nucl. Med.*, 2017, **58**, 1270–1277.
- 27 M. T. Ma, O. C. Neels, D. Denoyer, P. Roselt, J. A. Karas, D. B. Scanlon, J. M. White, R. J. Hicks and P. S. Donnelly, Gallium-68 complex of a macrobicyclic cage amine chelator tethered to two integrin-targeting peptides for diagnostic tumor imaging, *Bioconjug. Chem.*, 2011, **22**, 2093–2103.
- 28 C. Imberti, S. Y. A. Terry, C. Cullinane, F. Clarke, G. H. Cornish, N. K. Ramakrishnan, P. Roselt, A. P. Cope, R. J. Hicks, P. J. Blower and M. T. Ma, Enhancing PET Signal at Target Tissue in Vivo: Dendritic and Multimeric Tris(hydroxypyridinone) Conjugates for Molecular Imaging of $\alpha\beta_3$ Integrin Expression with Gallium-68, *Bioconjug. Chem.*, 2017, **28**, 481–495.
- 29 S. Liu, D. Li, C.-W. Huang, L.-P. Yap, R. Park, H. Shan, Z. Li and P. S. Conti, The Efficient Synthesis and Biological Evaluation of Novel Bi-Functionalized Sarcophagine for ^{64}Cu Radiopharmaceuticals, *Theranostics*, 2012, **2**, 589–596.
- 30 R. Haubner, S. Maschauer and O. Prante, PET Radiopharmaceuticals for Imaging Integrin Expression: Tracers in Clinical Studies and Recent Developments, *Biomed Res. Int.*, 2014, **2014**, 1–17.
- 31 M. Nieberler, U. Reuning, F. Reichart, J. Notni, H. J. Wester, M. Schwaiger, M. Weinmüller, A. Räder, K. Steiger and H. Kessler, Exploring the role of RGD-recognizing integrins in cancer, *Cancers (Basel)*, 2017, **9**, 1–33.
- 32 S. Habringer, C. Lapa, P. Herhaus, M. Schottelius, R. Istvanffy, K. Steiger, J. Slotta-Huspenina, A. Schirbel, H. Hänscheid, S. Kircher, A. K. Buck, K. Götze, B. Vick, I. Jeremias, M. Schwaiger, C. Peschel, R. Oostendorp, H. J. Wester, G. U. Grigoleit and U. Keller, Dual targeting of acute leukemia and supporting niche by CXCR4-directed theranostics, *Theranostics*, 2018, **8**, 369–383.
- 33 Z. Wang, M. Zhang, L. Wang, S. Wang, F. Kang, G. Li, O. Jacobson, G. Niu, W. Yang, J. Wang and X. Chen, Prospective study of ^{68}Ga -NOTA-NFB: Radiation dosimetry in healthy volunteers and first application in glioma patients, *Theranostics*, 2015, **5**, 882–889.
- 34 P. Herhaus, S. Habringer, K. Philipp-Abbrederis, T. Vag, C. Gerngross, M.

- Schottelius, J. Slotta-Huspenina, K. Steiger, T. Altmann, T. Weißer, S. Steidle, M. Schick, L. Jacobs, J. Slawska, C. Müller-Thomas, M. Verbeek, M. Subklewe, C. Peschel, H. J. Wester, M. Schwaiger, K. Götze and U. Keller, Targeted positron emission tomography imaging of CXCR4 expression in patients with acute myeloid leukemia, *Haematologica*, 2016, **101**, 932–940.
- 35 K. Philipp-Abbrederis, K. Herrmann, S. Knop, M. Schottelius, M. Eiber, K. Lückerrath, E. Pietschmann, S. Habringer, C. Gerngroß, K. Franke, M. Rudelius, A. Schirbel, C. Lapa, K. Schwamborn, S. Steidle, E. Hartmann, A. Rosenwald, S. Kropf, A. J. Beer, C. Peschel, H. Einsele, A. K. Buck, M. Schwaiger, K. Götze, H. Wester and U. Keller, In vivo molecular imaging of chemokine receptor CXCR 4 expression in patients with advanced multiple myeloma , *EMBO Mol. Med.*, 2015, **7**, 477–487.
- 36 C. Lapa, K. Herrmann, A. Schirbel, H. Hänscheid, K. Lückerrath, M. Schottelius, M. Kircher, R. A. Werner, M. Schreder, S. Samnick, S. Kropf, S. Knop, A. K. Buck, H. Einsele, H. J. Wester and K. Martin Kortüm, CXCR4-directed endoradiotherapy induces high response rates in extramedullary relapsed multiple myeloma, *Theranostics*, 2017, **7**, 1589–1597.
- 37 M. E. Mayerhoefer, U. Jaeger, P. Staber, M. Raderer, W. Wadsak, S. Pfaff, C. Kornauth, D. Senn, M. Weber, H. J. Wester, C. Skrabbs and A. Haug, Ga-Pentixafor PET/MRI for CXCR4 Imaging of Chronic Lymphocytic Leukemia: Preliminary Results, *Invest. Radiol.*, 2018, **53**, 403–408.
- 38 M. Schottelius, T. Osl, A. Poschenrieder, F. Hoffmann, S. Beykan, H. Hänscheid, A. Schirbel, A. K. Buck, S. Kropf, M. Schwaiger, U. Keller, M. Lassmann and H. J. Wester, [177Lu]pentixather: Comprehensive preclinical characterization of a first CXCR4-directed endoradiotherapeutic agent, *Theranostics*, 2017, **7**, 2350–2362.
- 39 C. Lapa, M. Schreder, A. Schirbel, S. Samnick, K. M. Kortüm, K. Herrmann, S. Kropf, H. Einsele, A. K. Buck, H. J. Wester, S. Knop and K. Lückerrath, [68Ga]Pentixafor-PET/CT for imaging of chemokine receptor CXCR4 expression in multiple myeloma - Comparison to [18F]FDG and laboratory values, *Theranostics*, 2017, **7**, 205–212.

- 40 C. Lapa, H. Hänscheid, M. Kircher, A. Schirbel, G. Wunderlich, R. A. Werner, S. Samnick, J. Kotzerke, H. Einsele, A. K. Buck, H. J. Wester and G. U. Grigoleit, Feasibility of CXCR4-directed radioligand therapy in advanced diffuse large B-cell lymphoma, *J. Nucl. Med.*, 2019, **60**, 60–64.
- 41 M. Kircher, P. Herhaus, M. Schottelius, A. K. Buck, R. A. Werner, H. J. Wester, U. Keller and C. Lapa, *Ann. Nucl. Med.*, 2018, **32**, 503–511.
- 42 T. Vag, C. Gerngross, P. Herhaus, M. Eiber, K. Philipp-Abbrederis, F. P. Graner, J. Ettl, U. Keller, H. J. Wester and M. Schwaiger, First experience with chemokine receptor CXCR4 Targeted PET imaging of patients with solid cancers, *J. Nucl. Med.*, 2016, **57**, 741–746.
- 43 M. Morais and M. T. Ma, Site-specific chelator-antibody conjugation for PET and SPECT imaging with radiometals, *Drug Discov. Today Technol.*, 2018, **30**, 91–104.
- 44 G. Vidarsson, G. Dekkers and T. Rispen, IgG subclasses and allotypes: From structure to effector functions, *Front. Immunol.*, 2014, **5**, 1–17.
- 45 R. Fisher, L. Pusztai and C. Swanton, Cancer heterogeneity: Implications for targeted therapeutics, *Br. J. Cancer*, 2013, **108**, 479–485.
- 46 G. Gebhart, L. E. Lamberts, Z. Wimana, C. Garcia, P. Emonts, L. Ameye, S. Stroobants, M. Huizing, P. Aftimos, J. Tol, W. J. G. Oyen, D. J. Vugts, O. S. Hoekstra, C. P. Schröder, C. W. Menke-van der Houven van Oordt, T. Guiot, A. H. Brouwers, A. Awada, E. G. E. de Vries and P. Flamen, Molecular imaging as a tool to investigate heterogeneity of advanced HER2-positive breast cancer and to predict patient outcome under trastuzumab emtansine (T-DM1): The ZEPHIR trial, *Ann. Oncol.*, 2016, **27**, 619–624.
- 47 R. J. Hicks, Use of molecular targeted agents for the diagnosis, staging and therapy of neuroendocrine malignancy, *Cancer Imaging*, 2010, **10**, 83–91.
- 48 S. Heskamp, W. Hobo, J. D. M. Molkenboer-Kuenen, D. Olive, W. J. G. Oyen, H. Dolstra and O. C. Boerman, Noninvasive imaging of tumor PD-L1 expression using radiolabeled Anti-PD-L1 antibodies, *Cancer Res.*, 2015, **75**, 2928–2936.
- 49 S. Chatterjee, W. G. Lesniak, M. Gabrielson, A. Lisok, B. Wharram, P. Sysa-

- Shah, B. B. Azad, M. G. Pomper and S. Nimmagadda, A humanized antibody for imaging immune checkpoint ligand PD-L1 expression in tumors, *Oncotarget*, 2016, **7**, 10215–10227.
- 50 A. N. Niemeijer, D. Leung, M. C. Huisman, I. Bahce, O. S. Hoekstra, G. A. M. S. van Dongen, R. Boellaard, S. Du, W. Hayes, R. Smith, A. D. Windhorst, N. H. Hendrikse, A. Poot, D. J. Vugts, E. Thunnissen, P. Morin, D. Lipovsek, D. J. Donnelly, S. J. Bonacorsi, L. M. Velasquez, T. D. de Gruijl, E. F. Smit and A. J. de Langen, Whole body PD-1 and PD-L1 positron emission tomography in patients with non-small-cell lung cancer, *Nat. Commun.*, 2018, **9**, 1–5.
- 51 C. Rivas, J. A. Jackson, I. N. Hungnes and M. T. Ma, in *Reference Module in Chemistry, Molecular Sciences and Chemical Engineering*, Elsevier, 3rd edn., 2020, pp. 1–35.
- 52 S. V. Smith, Molecular imaging with copper-64, *J. Inorg. Biochem.*, 2004, **98**, 1874–1901.
- 53 W. C. Cole, S. J. DeNardo, C. F. Meares, M. J. McCall, G. L. DeNardo, A. L. Epstein, H. A. O'Brien and M. K. Moi, Serum stability of ⁶⁷Cu chelates: Comparison with ¹¹¹In and ⁵⁷Co, *Int. J. Radiat. Appl. Instrumentation.*, 1986, **13**, 363–368.
- 54 W. C. Cole, S. J. DeNardo, C. F. Meares, M. J. McCall, A. L. Epstein, H. A. O'Brien and M. K. Moi, Comparative serum stability of radiochelates for antibody radiopharmaceuticals, *J. Nucl. Med.*, 1987, **28**, 83–90.
- 55 E. T. Clarke and A. E. Martell, Stabilities of the alkaline earth and divalent transition metal complexes of the tetraazamacrocyclic tetraacetic acid ligands, *Inorganica Chim. Acta*, 1991, **190**, 27–36.
- 56 S. Chaves, R. Delgado and J. J. R. F. Da Silva, The stability of the metal complexes of cyclic tetra-aza tetra-acetic acids, *Talanta*, 1992, **39**, 249–254.
- 57 J. D. Silversides, C. C. Allan and S. J. Archibald, Copper(II) cyclam-based complexes for radiopharmaceutical applications: Synthesis and structural analysis, *Dalt. Trans.*, 2007, 971–978.
- 58 C. J. Anderson, J. M. Connett, S. W. Schwarz, P. A. Rocque, L. W. Guo, G. W.

- Philpott, K. R. Zinn, C. F. Meares and M. J. Welch, Copper-64-labeled antibodies for PET imaging, *J. Nucl. Med.*, 1992, **33**, 1685–1691.
- 59 L. A. Bass, M. Wang, M. J. Welch and C. J. Anderson, In vivo transchelation of copper-64 from TETA-octreotide to superoxide dismutase in rat liver, *Bioconjug. Chem.*, 2000, **11**, 527–532.
- 60 T. J. Wadas and C. J. Anderson, Radiolabeling of TETA- and CB-TE2A-conjugated peptides with copper-64, *Nat. Protoc.*, 2006, **1**, 3062–3068.
- 61 A. V. Dale, D. N. Pandya, J. Y. Kim, H. Lee, Y. S. Ha, N. Bhatt, J. Kim, J. J. Seo, W. Lee, S. H. Kim, Y. R. Yoon, G. Il An and J. Yoo, Non-cross-bridged tetraazamacrocyclic chelator for stable ⁶⁴Cu-based radiopharmaceuticals, *ACS Med. Chem. Lett.*, 2013, **4**, 927–931.
- 62 R. Ferdani, D. J. Stigers, A. L. Fiamengo, L. Wei, B. T. Y. Li, J. A. Golen, A. L. Rheingold, G. R. Weisman, E. H. Wong and C. J. Anderson, Synthesis, Cu(ii) complexation, ⁶⁴Cu-labeling and biological evaluation of cross-bridged cyclam chelators with phosphonate pendant arms, *Dalt. Trans.*, 2012, **41**, 1938–1950.
- 63 N. Bhatt, N. Soni, Y. S. Ha, W. Lee, D. N. Pandya, S. Sarkar, J. Y. Kim, H. Lee, S. H. Kim, G. Il An and J. Yoo, Phosphonate Pendant Armed Propylene Cross-Bridged Cyclam: Synthesis and Evaluation as a Chelator for Cu-64, *ACS Med. Chem. Lett.*, 2015, **6**, 1162–1166.
- 64 Z. Cai and C. J. Anderson, Chelators for copper radionuclides in positron emission tomography radiopharmaceuticals, *J. Label. Compd. Radiopharm.*, 2014, **57**, 224–230.
- 65 C. A. Boswell, X. Sun, W. Niu, G. R. Weisman, E. H. Wong, A. L. Rheingold and C. J. Anderson, Comparative in Vivo Stability of Copper-64-Labeled Cross-Bridged and Conventional Tetraazamacrocyclic Complexes, *J. Med. Chem.*, 2004, **47**, 1465–1474.
- 66 M. Shokeen and C. J. Anderson, Molecular Imaging of Cancer with Copper-64 Radiopharmaceuticals and Positron Emission Tomography (PET), *Acc. Chem. Res.*, 2009, **42**, 832–841.
- 67 X. Sun, M. Wuest, Z. Kovacs, A. D. Sherry, R. Motekaitis, Z. Wang, A. E.

- Martell, M. J. Welch and C. J. Anderson, In vivo behavior of copper-64-labeled methanephosphonate tetraaza macrocyclic ligands, *J. Biol. Inorg. Chem.*, 2003, **8**, 217–225.
- 68 M. S. Cooper, M. T. Ma, K. Sunassee, K. P. Shaw, J. D. Williams, R. L. Paul, P. S. Donnelly and P. J. Blower, Comparison of 64 Cu-Complexing Bifunctional Chelators for Radioimmunoconjugation: Labeling Efficiency, Specific Activity, and in Vitro / in Vivo Stability, *Bioconjug. Chem.*, 2012, **23**, 1029–1039.
- 69 H. Deng, H. Wang, H. Zhang, M. Wang, B. Giglio, X. Ma, G. Jiang, H. Yuan, Z. Wu and Z. Li, Imaging Neurotensin Receptor in Prostate Cancer With 64 Cu-Labeled Neurotensin Analogs, *Mol. Imaging*, 2017, **16**, 153601211771136.
- 70 L. Y. Kwon, D. A. Scollard and R. M. Reilly, 64 Cu-Labeled Trastuzumab Fab-PEG 24 -EGF Radioimmunoconjugates Bispecific for HER2 and EGFR: Pharmacokinetics, Biodistribution, and Tumor Imaging by PET in Comparison to Monospecific Agents, *Mol. Pharm.*, 2017, **14**, 492–501.
- 71 V. Maheshwari, J. L. J. Dearling, S. T. Treves and A. B. Packard, Measurement of the rate of copper(II) exchange for 64Cu complexes of bifunctional chelators, *Inorganica Chim. Acta*, 2012, **393**, 318–323.
- 72 Y. Zhang, H. Hong, J. W. Engle, J. Bean, Y. Yang, B. R. Leigh, T. E. Barnhart and W. Cai, Positron Emission Tomography Imaging of CD105 Expression with a 64Cu-Labeled Monoclonal Antibody: NOTA Is Superior to DOTA, *PLoS One*, 2011, **6**, e28005.
- 73 M. S. Cooper, M. T. Ma, K. Sunassee, K. P. Shaw, J. D. Williams, R. L. Paul, P. S. Donnelly and P. J. Blower, Comparison of 64 Cu-Complexing Bifunctional Chelators for Radioimmunoconjugation: Labeling Efficiency, Specific Activity, and in Vitro / in Vivo Stability, *Bioconjug. Chem.*, 2012, **23**, 1029–1039.
- 74 S. C. Ghosh, K. L. Pinkston, H. Robinson, B. R. Harvey, N. Wilganowski, K. Gore, E. M. Sevick-Muraca and A. Azhdarinia, Comparison of DOTA and NODAGA as chelators for 64Cu-labeled immunoconjugates, *Nucl. Med. Biol.*, 2015, **42**, 177–183.

- 75 A. M. Sargeson, Encapsulated metal ions, *Pure Appl. Chem.*, 1984, **56**, 1603–1619.
- 76 R. J. Geue, A. M. Sargeson, T. W. Hambley, M. R. Snow and J. M. Harrowfield, Metal Ion Encapsulation: Cobalt Cages Derived from Polyamines, Formaldehyde, and Nitromethane, *J. Am. Chem. Soc.*, 1984, **106**, 5478–5488.
- 77 A. M. Sargeson, The potential for the cage complexes in biology, *Coord. Chem. Rev.*, 1996, **151**, 89–114.
- 78 I. Creaser, J. M. B. Harrowfield, A. J. Herlt, A. M. Sargeson, J. Springborg, R. J. Geue and M. R. Snow, Sepulchrates: A Macrobicyclic Nitrogen Cage for Metal Ions, *J. Am. Chem. Soc.*, 1977, **99**, 3181–3182.
- 79 I. I. Creaser, R. J. Geue, J. M. Harrowfield, A. J. Herlt, A. M. Sargeson, M. R. Snow and J. Springborg, Synthesis and Reactivity of Aza-Capped Encapsulated Co(III) Ions, *J. Am. Chem. Soc.*, 1982, **104**, 6016–6025.
- 80 I. J. Clark, I. I. Creaser, R. J. Geue, K. S. Hagen, G. A. Lawrance, P. A. Lay, A. M. Sargeson and F. R. Wilne, The synthesis and structure of encapsulating ligands: Properties of bicyclic hexamines, *Aust. J. Chem.*, 1994, **47**, 143–179.
- 81 N. M. Di Bartolo, A. M. Sargeson, T. M. Donlevy and S. V. Smith, Synthesis of a new cage ligand, SarAr, and its complexation with selected transition metal ions for potential use in radioimaging[†], *J. Chem. Soc. Dalton Trans.*, 2001, 2303–2309.
- 82 N. Di Bartolo, A. M. Sargeson and S. V. Smith, New ⁶⁴Cu PET imaging agents for personalised medicine and drug development using the hexa-aza cage, SarAr, *Org. Biomol. Chem.*, 2006, **4**, 3350.
- 83 L. Grøndahl, A. Hammershøi, A. M. Sargeson and V. J. Thöm, Stability and Kinetics of Acid- and Anion-Assisted Dissociation Reactions of Hexamine Macrobicyclic Mercury(II) Complexes, *Inorg. Chem.*, 1997, **36**, 5396–5403.
- 84 R. J. Motekaitis, B. E. Rogers, D. E. Reichert, A. E. Martell and M. J. Welch, Stability and structure of activated macrocycles. Ligands with biological applications, *Inorg. Chem.*, 1996, **35**, 3821–3827.

- 85 P. S. Donnelly, J. M. Harrowfield, B. W. Skelton and A. H. White, Carboxymethylation of Cage Amines: Control of Alkylation by Metal Ion Coordination, *Inorg. Chem.*, 2000, **39**, 5817–5830.
- 86 I. I. Creaser, J. M. Harrowfield, G. A. Lawrance, W. Mulac, D. Sangster, A. M. Sargeson, K. Schmidt and J. C. Sullivan, Rapid Reduction of [CuII(Sarcophagine)]²⁺ Ion and Elimination of CuI From the Cage: A Pulse Radiolysis Study, *J. Coord. Chem.*, 1991, **23**, 389–395.
- 87 P. V. Bernhardt, R. Bramley, R. J. Geue, S. F. Ralph and A. M. Sargeson, An expanded cavity hexaamine cage for copper(ii), *Dalt. Trans.*, 2007, 1244.
- 88 H. Cai, J. Fissekis and P. S. Conti, Synthesis of a novel bifunctional chelator AmBaSar based on sarcophagine for peptide conjugation and ⁶⁴Cu radiolabelling, *Dalt. Trans.*, 2009, 5395.
- 89 K. Alt, B. M. Paterson, E. Westein, S. E. Rudd, S. S. Poniger, S. Jagdale, K. Ardipradja, T. U. Connell, G. Y. Krippner, A. K. N. Nair, X. Wang, H. J. Tochon-Danguy, P. S. Donnelly, K. Peter and C. E. Hagemeyer, A versatile approach for the site-specific modification of recombinant antibodies using a combination of enzyme-mediated bioconjugation and click chemistry, *Angew. Chemie - Int. Ed.*, 2015, **54**, 7515–7519.
- 90 B. M. Paterson, G. Buncic, L. E. McInnes, P. Roselt, C. Cullinane, D. S. Binns, C. M. Jeffery, R. I. Price, R. J. Hicks and P. S. Donnelly, Bifunctional⁶⁴Cu-labelled macrobicyclic cage amine isothiocyanates for immuno-positron emission tomography, *Dalt. Trans.*, 2015, **44**, 4901–4909.
- 91 H. Akizawa, Y. Arano, M. Mifune, A. Iwado, Y. Saito, T. Mukai, T. Uehara, M. Ono, Y. Fujioka, K. Ogawa, Y. Kiso and H. Saji, Effect of molecular charges on renal uptake of ¹¹¹In-DTPA-conjugated peptides, *Nucl. Med. Biol.*, 2001, **28**, 761–768.
- 92 X. Sun, J. Kim, A. E. Martell, M. J. Welch and C. J. Anderson, In vivo evaluation of copper-64-labeled monooxo-tetraazamacrocyclic ligands, *Nucl. Med. Biol.*, 2004, **31**, 1051–1059.
- 93 J. L. J. Dearling, S. D. Voss, P. Dunning, E. Snay, F. Fahey, S. V. Smith, J. S. Huston, C. F. Meares, S. T. Treves and A. B. Packard, Imaging cancer using

- PET - the effect of the bifunctional chelator on the biodistribution of a ⁶⁴Cu-labeled antibody, *Nucl. Med. Biol.*, 2011, **38**, 29–38.
- 94 T. M. Jones-Wilson, K. A. Deal, C. J. Anderson, D. W. McCarthy, Z. Kovacs, R. J. Motekaitis, A. D. Sherry, A. E. Martell and M. J. Welch, The in vivo behavior of copper-64-labeled azamacrocyclic complexes, *Nucl. Med. Biol.*, 1998, **25**, 523–530.
- 95 M. S. Hofman, W. F. Eddie Lau and R. J. Hicks, Somatostatin receptor imaging with ⁶⁸Ga DOTATATE PET/CT: Clinical utility, normal patterns, pearls, and pitfalls in interpretation, *Radiographics*, 2015, **35**, 500–516.
- 96 D. J. Kwekkeboom, W. W. de Herder, C. H. J. van Eijck, B. L. Kam, M. van Essen, J. J. M. Teunissen and E. P. Krenning, Peptide Receptor Radionuclide Therapy in Patients With Gastroenteropancreatic Neuroendocrine Tumors, *Semin. Nucl. Med.*, 2010, **40**, 78–88.
- 97 N. A. Zia, C. Cullinane, J. K. Van Zuylekom, K. Waldeck, L. E. McInnes, G. Buncic, M. B. Haskali, P. D. Roselt, R. J. Hicks and P. S. Donnelly, A Bivalent Inhibitor of Prostate Specific Membrane Antigen Radiolabeled with Copper-64 with High Tumor Uptake and Retention, *Angew. Chemie Int. Ed.*, 2019, 14991–14994.
- 98 Z. B. Li, K. Chen and X. Chen, ⁶⁸Ga-labeled multimeric RGD peptides for microPET imaging of integrin $\alpha\beta_3$ expression, *Eur. J. Nucl. Med. Mol. Imaging*, 2008, **35**, 1100–1108.
- 99 Z. Liu, G. Niu, F. Wang and X. Chen, ⁶⁸Ga-labeled NOTA-RGD-BBN peptide for dual integrin and GRPR-targeted tumor imaging, *Eur. J. Nucl. Med. Mol. Imaging*, 2009, **36**, 1483–1494.
- 100 P. M. Smith-Jones, B. Stolz, C. Bruns, R. Albert, H. W. Reist, R. Fridrich and H. R. Macke, Gallium-67/gallium-68-[DFO]-octreotide - A potential radiopharmaceutical for PET imaging of somatostatin receptor-positive tumors: Synthesis and radiolabeling in vitro and preliminary in vivo studies, *J. Nucl. Med.*, 1994, **35**, 317–325.
- 101 H. Cai, Z. Li, C.-W. Huang, R. Park, A. H. Shahinian and P. S. Conti, An improved synthesis and biological evaluation of a new cage-like

- bifunctional chelator, 4-((8-amino-3,6,10,13,16,19-hexaazabicyclo[6.6.6]icosane-1-ylamino)methyl)benzoic acid, for ^{64}Cu radiopharmaceuticals, *Nucl. Med. Biol.*, 2010, **37**, 57–65.
- 102 X. Yin, M. Wang, H. Wang, H. Deng, T. He, Y. Tan, Z. Zhu, Z. Wu, S. Hu and Z. Li, Evaluation of neurotensin receptor 1 as a potential imaging target in pancreatic ductal adenocarcinoma, *Amino Acids*, 2017, **49**, 1325–1335.
- 103 C. Brand, D. Abdel-Atti, Y. Zhang, S. Carlin, S. M. Clardy, E. J. Keliher, W. A. Weber, J. S. Lewis and T. Reiner, In Vivo Imaging of GLP-1R with a Targeted Bimodal PET/ Fluorescence Imaging Agent, *Bioconjugate Chem*, 2014, **25**, 1323–1330.
- 104 V. V. Rostovtsev, L. G. Green, V. V. Fokin and K. B. Sharpless, A Stepwise Huisgen Cycloaddition Process: Copper(I)-Catalyzed Regioselective ‘Ligation’ of Azides and Terminal Alkynes, *Angew. Chemie - Int. Ed.*, 2002, **41**, 2596–2599.
- 105 S. D. Voss, S. V Smith, N. DiBartolo, L. J. McIntosh, E. M. Cyr, A. A. Bonab, J. L. Dearling, E. A. Carter, A. J. Fischman, S. T. Treves, S. D. Gillies, A. M. Sargeson, J. S. Huston and A. B. Packard, Positron emission tomography (PET) imaging of neuroblastoma and melanoma with ^{64}Cu -SarAr immunoconjugates, *Proc Natl Acad Sci U S A*, 2007, **104**, 17489–17493.
- 106 J. L. J. Dearling, B. M. Paterson, V. Akurathi, S. Betanzos-Lara, S. T. Treves, S. D. Voss, J. M. White, J. S. Huston, S. V. Smith, P. S. Donnelly and A. B. Packard, The ionic charge of copper-64 complexes conjugated to an engineered antibody affects biodistribution, *Bioconjug. Chem.*, 2015, **26**, 707–717.
- 107 B. M. Paterson, G. Buncic, L. E. McInnes, P. Roselt, C. Cullinane, D. S. Binns, C. M. Jeffery, R. I. Price, R. J. Hicks and P. S. Donnelly, Bifunctional Cu-64-labelled macrobicyclic cage amine isothiocyanates for immuno-positron emission tomography, *Dalt. Trans.*, 2015, **44**, 4901–4909.
- 108 B. M. Paterson, K. Alt, C. M. Jeffery, R. I. Price, S. Jagdale, S. Rigby, C. C. Williams, K. Peter, C. E. Hagemeyer and P. S. Donnelly, Enzyme-mediated site-specific bioconjugation of metal complexes to proteins: Sortase-mediated coupling of copper-64 to a single-chain antibody, *Angew. Chemie*

- *Int. Ed.*, 2014, **53**, 6115–6119.

- 109 K. Alt, B. M. Paterson, K. Ardipradja, C. Schieber, G. Buncic, B. Lim, S. S. Poniger, B. Jakoby, X. Wang, G. J. Okeefe, H. J. Tochon-Danguy, A. M. Scott, U. Ackermann, K. Peter, P. S. Donnelly and C. E. Hagemeyer, Single-Chain antibody conjugated to a cage amine chelator and labeled with positron-emitting copper-64 for diagnostic imaging of activated platelets, *Mol. Pharm.*, 2014, **11**, 2855–2863.
- 110 B. M. Zeglis, C. Brand, D. Abdel-Atti, K. E. Carnazza, B. E. Cook, S. Carlin, T. Reiner and J. S. Lewis, Optimization of a Pretargeted Strategy for the PET Imaging of Colorectal Carcinoma via the Modulation of Radioligand Pharmacokinetics, *Mol. Pharm.*, 2015, **12**, 3575–3587.
- 111 B. M. Zeglis, K. K. Sevak, T. Reiner, P. Mohindra, S. D. Carlin, P. Zanzonico, R. Weissleder and J. S. Lewis, A pretargeted PET imaging strategy based on bioorthogonal diels-alder click chemistry, *J. Nucl. Med.*, 2013, **54**, 1389–1396.
- 112 B. E. Cook, P. Adumeau, R. Membreno, K. E. Carnazza, C. Brand, T. Reiner, B. J. Agnew, J. S. Lewis and B. M. Zeglis, Pretargeted PET Imaging Using a Site-Specifically Labeled Immunoconjugate, *Bioconjug. Chem.*, 2016, **27**, 1789–1795.
- 113 P. Adumeau, K. E. Carnazza, C. Brand, S. D. Carlin, T. Reiner, B. J. Agnew, J. S. Lewis and B. M. Zeglis, A pretargeted approach for the multimodal PET/NIRF imaging of colorectal cancer, *Theranostics*, 2016, **6**, 2267–2277.
- 114 S. Heskamp, R. Raavé, O. Boerman, M. Rijpkema, V. Goncalves and F. Denat, ⁸⁹Zr-Immuno-Positron Emission Tomography in Oncology: State-of-the-Art ⁸⁹Zr Radiochemistry, *Bioconjug. Chem.*, 2017, **28**, 2211–2223.
- 115 M. T. Ma, L. K. Meszaros, B. M. Paterson, D. J. Berry, M. S. Cooper, Y. Ma, R. C. Hider and P. J. Blower, Tripodal tris(hydroxypyridinone) ligands for immunoconjugate PET imaging with ⁸⁹Zr⁴⁺: Comparison with desferrioxamine-B, *Dalt. Trans.*, 2015, **44**, 4884–4900.
- 116 J. P. Holland, V. Divilov, N. H. Bander, P. M. Smith-Jones, S. M. Larson and J. S. Lewis, ⁸⁹Zr-DFO-J591 for ImmunoPET of Prostate-Specific Membrane

- Antigen Expression In Vivo, *J. Nucl. Med.*, 2010, **51**, 1293–1300.
- 117 M. Savastano, C. Bazzicalupi, G. Ferraro, E. Fratini, P. Gratteri and A. Bianchi, Tales of the unexpected: The case of zirconium(IV) complexes with desferrioxamine, *Molecules*, 2019, **24**, 2–9.
- 118 B. M. Zeglis, C. B. Davis, R. Aggeler, H. C. Kang, A. Chen, B. J. Agnew and J. S. Lewis, Enzyme-Mediated Methodology for the Site-Specific Radiolabeling of Antibodies Based on Catalyst-Free Click Chemistry, *Bioconjug. Chem.*, 2013, **24**, 1057–1067.
- 119 J. Mealey, Turn-over of Carrier-free Zirconium-89 in Man, *Nature*, 1957, **179**, 673–674.
- 120 M. J. W. D. Vosjan, L. R. Perk, G. W. M. Visser, M. Budde, P. Jurek, G. E. Kiefer and G. A. M. S. Van Dongen, Conjugation and radiolabeling of monoclonal antibodies with zirconium-89 for PET imaging using the bifunctional chelate p-isothiocyanatobenzyl-desferrioxamine, *Nat. Protoc.*, 2010, **5**, 739–743.
- 121 D. S. Abou, T. Ku and P. M. Smith-Jones, In vivo biodistribution and accumulation of ⁸⁹Zr in mice, *Nucl. Med. Biol.*, 2011, **38**, 675–681.
- 122 J. N. Tinianow, H. S. Gill, A. Ogasawara, J. E. Flores, A. N. Vanderbilt, E. Luis, R. Vandlen, M. Darwish, J. R. Junutula, S. P. Williams and J. Marik, Site-specifically ⁸⁹Zr-labeled monoclonal antibodies for ImmunoPET, *Nucl. Med. Biol.*, 2010, **37**, 289–297.
- 123 E. C. F. Dijkers, J. G. W. Kosterink, A. P. Rademaker, L. R. Perk, G. A. M. S. Van Dongen, J. Bart, J. R. De Jong, E. G. E. De Vries and M. N. Lub-de Hooge, Development and characterization of clinical-grade ⁸⁹Zr-trastuzumab for HER2/neu immunoPET imaging, *J. Nucl. Med.*, 2009, **50**, 974–981.
- 124 E. C. Dijkers, T. H. Oude Munnink, J. G. Kosterink, A. H. Brouwers, P. L. Jager, J. R. De Jong, G. A. Van Dongen, C. P. Schröder, M. N. Lub-De Hooge and E. G. De Vries, Biodistribution of ⁸⁹Zr-trastuzumab and PET Imaging of HER2-Positive Lesions in Patients with Metastatic Breast Cancer, *Clin. Pharmacol. Ther.*, 2010, **87**, 586–592.

- 125 D. J. Vugts, C. Klaver, C. Sewing, A. J. Poot, K. Adamzek, S. Huegli, C. Mari, G. W. M. Visser, I. E. Valverde, G. Gasser, T. L. Mindt and G. A. M. S. van Dongen, Comparison of the octadentate bifunctional chelator DFO*-pPhe-NCS and the clinically used hexadentate bifunctional chelator DFO-pPhe-NCS for ⁸⁹Zr-immuno-PET, *Eur. J. Nucl. Med. Mol. Imaging*, 2017, **44**, 286–295.
- 126 M. Patra, A. Bauman, C. Mari, C. A. Fischer, O. Blacque, D. Häussinger, G. Gasser and T. L. Mindt, An octadentate bifunctional chelating agent for the development of stable zirconium-89 based molecular imaging probes, *Chem. Commun.*, 2014, **50**, 11523–11525.
- 127 L. Allott, C. Da Pieve, J. Meyers, T. Spinks, D. M. Ciobota, G. Kramer-Marek and G. Smith, Evaluation of DFO-HOPO as an octadentate chelator for zirconium-89, *Chem. Commun.*, 2017, **53**, 8529–8532.
- 128 S. E. Rudd, P. Roselt, C. Cullinane, R. J. Hicks and P. S. Donnelly, A desferrioxamine B squaramide ester for the incorporation of zirconium-89 into antibodies, *Chem. Commun.*, 2016, **52**, 11889–11892.
- 129 M. A. Deri, S. Ponnala, B. M. Zeglis, G. Pohl, J. J. Dannenberg, J. S. Lewis and L. C. Francesconi, Alternative Chelator for ⁸⁹Zr Radiopharmaceuticals: Radiolabeling and Evaluation of 3,4,3-(LI-1,2-HOPO), *J. Med. Chem.*, 2014, **57**, 4849–4860.
- 130 E. K. Sarbisheh, A. K. Salih, S. J. Raheem, J. S. Lewis and E. W. Price, A High-Denticity Chelator Based on Desferrioxamine for Enhanced Coordination of Zirconium-89, *Inorg. Chem.*, 2020, **59**, 11715–11727.
- 131 D. N. Pandya, N. Bhatt, H. Yuan, C. S. Day, B. M. Ehrmann, M. Wright, U. Bierbach and T. J. Wadas, Zirconium tetraazamacrocyclic complexes display extraordinary stability and provide a new strategy for zirconium-89-based radiopharmaceutical development, *Chem. Sci.*, 2017, **8**, 2309–2314.
- 132 W. E. Meijs, H. J. Haisma, R. P. Klok, F. B. van Gog, E. Kievit, H. M. Pinedo and J. D. M. Herscheid, Zirconium-labeled monoclonal antibodies and their distribution in tumor-bearing nude mice., *J. Nucl. Med.*, 1997, **38**, 112–8.
- 133 W. E. Meijs, H. J. Haisma, R. Van Der Schors, R. Wijbrandts, K. D. Van Den

- Oever, R. P. Klok, H. M. Pinedo and J. D. M. Herscheid, A facile method for the labeling of proteins with zirconium isotopes, *Nucl. Med. Biol.*, 1996, **23**, 439–448.
- 134 I. Verel, G. W. M. Visser, R. Boellaard, M. Stigter-van Walsum, G. B. Snow and G. A. M. S. van Dongen, ⁸⁹Zr immuno-PET: comprehensive procedures for the production of ⁸⁹Zr-labeled monoclonal antibodies., *J. Nucl. Med.*, 2003, **44**, 1271–81.
- 135 P. K. E. Börjesson, Y. W. S. Jauw, R. Boellaard, R. De Bree, E. F. I. Comans, J. C. Roos, J. A. Castelijns, M. J. W. D. Vosjan, J. A. Kummer, C. R. Leemans, A. A. Lammertsma and G. A. M. S. Van Dongen, Performance of immuno - positron emission tomography with zirconium-89-labeled chimeric monoclonal antibody U36 in the detection of lymph node metastases in head and neck cancer patients, *Clin. Cancer Res.*, 2006, **12**, 2133–2140.
- 136 Y. W. S. Jauw, C. W. Menke-van der Houven van Oordt, O. S. Hoekstra, H. N. Hendrikse, D. J. Vugts, J. M. Zijlstra, M. C. Huisman and G. A. M. S. van Dongen, Immuno-positron emission tomography with zirconium-89-labeled monoclonal antibodies in oncology: What can we learn from initial clinical trials?, *Front. Pharmacol.*, 2016, **7**, 1–15.
- 137 I. Verel, G. W. M. Visser, R. Boellaard, O. C. Boerman, J. Van Eerd, G. B. Snow, A. A. Lammertsma and G. A. M. S. Van Dongen, Quantitative ⁸⁹Zr immuno-PET for in vivo scouting of ⁹⁰Y-labeled monoclonal antibodies in xenograft-bearing nude mice, *J. Nucl. Med.*, 2003, **44**, 1663–1670.
- 138 I. Verel, G. W. M. Visser and G. A. van Dongen, The promise of immuno-PET in radioimmunotherapy., *J. Nucl. Med.*, 2005, **46 Suppl 1**, 164S–71S.
- 139 L. R. Perk, O. J. Visser, M. Stigter-Van Walsum, M. J. W. D. Vosjan, G. W. M. Visser, J. M. Zijlstra, P. C. Huijgens and G. A. M. S. Van Dongen, Preparation and evaluation of ⁸⁹Zr-Zevalin for monitoring of ⁹⁰Y-Zevalin biodistribution with positron emission tomography, *Eur. J. Nucl. Med. Mol. Imaging*, 2006, **33**, 1337–1345.
- 140 W. B. Nagengast, M. A. de Korte, T. H. Oude Munnink, H. Timmer-Bosscha, W. F. den Dunnen, H. Hollema, J. R. de Jong, M. R. Jensen, C. Quadt, C. Garcia-Echeverria, G. A. M. S. van Dongen, M. N. Lub-de Hooge, C. P.

- Schröder and E. G. E. de Vries, 89Zr-bevacizumab PET of early antiangiogenic tumor response to treatment with HSP90 inhibitor NVP-AUY922., *J. Nucl. Med.*, 2010, **51**, 761–767.
- 141 J. P. Holland, E. Caldas-Lopes, V. Divilov, V. A. Longo, T. Taldone, D. Zatorska, G. Chiosis and J. S. Lewis, Measuring the pharmacodynamic effects of a novel Hsp90 inhibitor on HER2/ neu expression in mice using 89Zr-DFO-trastuzumab, *PLoS One*, , DOI:10.1371/journal.pone.0008859.
- 142 S. B. M. Gaykema, C. P. Schröder, J. Vitfell-Rasmussen, S. Chua, T. H. O. Munnink, A. H. Brouwers, A. H. H. Bongaerts, M. Akimov, C. Fernandez-Ibarra, M. N. Lub-De Hooge, E. G. E. De Vries, C. Swanton and U. Banerji, 89Zr-trastuzumab and 89Zr-bevacizumab PET to evaluate the effect of the HSP90 inhibitor NVP-AUY922 in metastatic breast cancer patients, *Clin. Cancer Res.*, 2014, **20**, 3945–3954.
- 143 L. R. Perk, M. J. W. D. Vosjan, G. W. M. Visser, M. Budde, P. Jurek, G. E. Kiefer and G. A. M. S. Van Dongen, P-Isothiocyanatobenzyl-desferrioxamine: A new bifunctional chelate for facile radiolabeling of monoclonal antibodies with zirconium-89 for immuno-PET imaging, *Eur. J. Nucl. Med. Mol. Imaging*, 2010, **37**, 250–259.
- 144 J. L. Houghton, D. Abdel-Atti, W. W. Scholz and J. S. Lewis, Preloading with Unlabeled CA19.9 Targeted Human Monoclonal Antibody Leads to Improved PET Imaging with 89Zr-5B1, *Mol. Pharm.*, 2017, **14**, 908–915.
- 145 J. C. Knight, S. J. Paisey, A. M. Dabkowski, C. Marculescu, A. S. Williams, C. Marshall and B. Cornelissen, Scaling-down antibody radiolabeling reactions with zirconium-89, *Dalt. Trans.*, 2016, **45**, 6343–6347.
- 146 S. K. Sharma, J. M. Glaser, K. J. Edwards, E. Khozeimeh Sarbisheh, A. K. Salih, J. S. Lewis and E. W. Price, A Systematic Evaluation of Antibody Modification and 89 Zr-Radiolabeling for Optimized Immuno-PET, *Bioconjug. Chem.*, 2021, **32**, 1177–1191.
- 147 A. Ghai, D. Maji, N. Cho, C. Chanswangphuwana, M. Rettig, D. Shen, J. DiPersio, W. Akers, F. Dehdashti, S. Achilefu, R. Vij and M. Shokeen, Preclinical Development of CD38-Targeted [89 Zr]Zr-DFO-Daratumumab for Imaging Multiple Myeloma, *J. Nucl. Med.*, 2018, **59**, 216–222.

- 148 B. M. Zeglis and J. S. Lewis, The Bioconjugation and Radiosynthesis of ^{89}Zr -DFO-labeled Antibodies, *J. Vis. Exp.*, , DOI:10.3791/52521.
- 149 S. Jeger, K. Zimmermann, A. Blanc, J. Grünberg, M. Honer, P. Hunziker, H. Struthers and R. Schibli, Site-Specific and Stoichiometric Modification of Antibodies by Bacterial Transglutaminase, *Angew. Chemie Int. Ed.*, 2010, **49**, 9995–9997.
- 150 A. Fontana, B. Spolaore, A. Mero and F. M. Veronese, Site-specific modification and PEGylation of pharmaceutical proteins mediated by transglutaminase, *Adv. Drug Deliv. Rev.*, 2008, **60**, 13–28.
- 151 B. M. Zeglis, C. B. Davis, D. Abdel-Atti, S. D. Carlin, A. Chen, R. Aggeler, B. J. Agnew and J. S. Lewis, Chemoenzymatic Strategy for the Synthesis of Site-Specifically Labeled Immunoconjugates for Multimodal PET and Optical Imaging, *Bioconjug. Chem.*, 2014, **25**, 2123–2128.
- 152 D. Vivier, K. Fung, C. Rodriguez, P. Adumeau, G. A. Ulaner, J. S. Lewis, S. K. Sharma and B. M. Zeglis, The influence of glycans-specific bioconjugation on the FcγRI binding and in vivo performance of ^{89}Zr -DFO-Pertuzumab, *Theranostics*, 2020, **10**, 1746–1757.
- 153 S. H. Ahn, B. A. Vaughn, W. A. Solis, M. L. Lupper, T. J. Hallam and E. Boros, Site-Specific ^{89}Zr - And ^{111}In -Radiolabeling and in Vivo Evaluation of Glycan-free Antibodies by Azide-Alkyne Cycloaddition with a Non-natural Amino Acid, *Bioconjug. Chem.*, 2020, **31**, 1177–1187.
- 154 M. T. Ma, L. K. Meszaros, B. M. Paterson, D. J. Berry, M. S. Cooper, Y. Ma, R. C. Hider and P. J. Blower, Tripodal tris(hydroxypyridinone) ligands for immunoconjugate PET imaging with $^{89}\text{Zr}^{4+}$: comparison with desferrioxamine-B, *Dalt. Trans.*, 2015, **44**, 4884–4900.
- 155 K. Li, R. Tavaré, K. A. Zettlitz, S. M. Mumenthaler, P. Mallick, Y. Zhou, J. D. Marks and A. M. Wu, Anti-MET immunoPET for non-small cell lung cancer using novel fully human antibody fragments, *Mol. Cancer Ther.*, 2014, **13**, 2607–2617.
- 156 C. Bahou, E. A. Love, S. Leonard, R. J. Spears, A. Maruani, K. Armour, J. R. Baker and V. Chudasama, Disulfide Modified IgG1: An Investigation of

- Biophysical Profile and Clinically Relevant Fc Interactions, *Bioconjug. Chem.*, 2019, **30**, 1048–1054.
- 157 M. S. Cooper, M. T. Ma, K. Sunassee, K. P. Shaw, J. D. Williams, R. L. Paul, P. S. Donnelly and P. J. Blower, Comparison of 64 Cu-Complexing Bifunctional Chelators for Radioimmunoconjugation: Labeling Efficiency, Specific Activity, and in Vitro / in Vivo Stability, *Bioconjug. Chem.*, 2012, **23**, 1029–1039.
- 158 C. A. Boswell, E. E. Mundo, C. Zhang, D. Bumbaca, N. R. Valle, K. R. Kozak, A. Fourie, J. Chuh, N. Koppada, O. Saad, H. Gill, B.-Q. Shen, B. Rubinfeld, J. Tibbitts, S. Kaur, F.-P. Theil, P. J. Fielder, L. A. Khawli and K. Lin, Impact of Drug Conjugation on Pharmacokinetics and Tissue Distribution of Anti-STEAP1 Antibody–Drug Conjugates in Rats, *Bioconjug. Chem.*, 2011, **22**, 1994–2004.
- 159 B. K. Giersing, M. T. Rae, M. CarballidoBrea, R. A. Williamson and P. J. Blower, Synthesis and Characterization of ¹¹¹In–DTPA–N–TIMP-2: A Radiopharmaceutical for Imaging Matrix Metalloproteinase Expression, *Bioconjug. Chem.*, 2001, **12**, 964–971.
- 160 J. R. Junutula, H. Raab, S. Clark, S. Bhakta, D. D. Leipold, S. Weir, Y. Chen, M. Simpson, S. P. Tsai, M. S. Dennis, Y. Lu, Y. G. Meng, C. Ng, J. Yang, C. C. Lee, E. Duenas, J. Gorrell, V. Katta, A. Kim, K. McDorman, K. Flagella, R. Venook, S. Ross, S. D. Spencer, W. Lee Wong, H. B. Lowman, R. Vandlen, M. X. Sliwkowski, R. H. Scheller, P. Polakis and W. Mallet, Site-specific conjugation of a cytotoxic drug to an antibody improves the therapeutic index, *Nat. Biotechnol.*, 2008, **26**, 925–932.
- 161 A. W. Tolcher, Antibody drug conjugates: lessons from 20 years of clinical experience, *Ann. Oncol.*, 2016, **27**, 2168–2172.
- 162 M. N. Fodje and S. Al-Karadaghi, Occurrence, conformational features and amino acid propensities for the π -helix, *Protein Eng.*, 2002, **15**, 353–358.
- 163 G. T. Hermanson, *Bioconjugate Techniques*, Academic Press, London, 2nd edn., 2008.
- 164 B. Q. Shen, K. Xu, L. Liu, H. Raab, S. Bhakta, M. Kenrick, K. L. Parsons-

- Reponte, J. Tien, S. F. Yu, E. Mai, D. Li, J. Tibbitts, J. Baudys, O. M. Saad, S. J. Scales, P. J. McDonald, P. E. Hass, C. Eigenbrot, T. Nguyen, W. A. Solis, R. N. Fuji, K. M. Flagella, D. Patel, S. D. Spencer, L. A. Khawli, A. Ebens, W. L. Wong, R. Vandlen, S. Kaur, M. X. Sliwkowski, R. H. Scheller, P. Polakis and J. R. Junutula, Conjugation site modulates the in vivo stability and therapeutic activity of antibody-drug conjugates, *Nat. Biotechnol.*, 2012, **30**, 184–189.
- 165 R. J. Sanderson, M. A. Hering, S. F. James, M. M. C. Sun, S. O. Doronina, A. W. Siadak, P. D. Senter and A. F. Wahl, In vivo drug-linker stability of an anti-CD30 dipeptide-linked auristatin immunoconjugate, *Clin. Cancer Res.*, 2005, **11**, 843–852.
- 166 S. C. Alley, D. R. Benjamin, S. C. Jeffrey, N. M. Okeley, D. L. Meyer, R. J. Sanderson and P. D. Senter, Contribution of linker stability to the activities of anticancer immunoconjugates, *Bioconjug. Chem.*, 2008, **19**, 759–765.
- 167 A. D. Baldwin and K. L. Kiick, Tunable Degradation of Maleimide–Thiol Adducts in Reducing Environments, *Bioconjug. Chem.*, 2011, **22**, 1946–1953.
- 168 D. A. T. Xiao, D. C. Gao and D. S. Zhang, Profile of Specific Antibodies to SARS-CoV-2: The First Report, *J. Infect.*, , DOI:10.1016/j.jinf.2020.03.012.
- 169 H. Wu, P. J. Levalley, T. Luo, A. M. Kloxin and K. L. Kiick, Manipulation of Glutathione-Mediated Degradation of Thiol-Maleimide Conjugates, *Bioconjug. Chem.*, 2018, **29**, 3595–3605.
- 170 P. A. Szijj, C. Bahou and V. Chudasama, Minireview: Addressing the retro-Michael instability of maleimide bioconjugates, *Drug Discov. Today Technol.*, 2018, **30**, 27–34.
- 171 R. P. Lyon, J. R. Setter, T. D. Bovee, S. O. Doronina, J. H. Hunter, M. E. Anderson, C. L. Balasubramanian, S. M. Duniho, C. I. Leiske, F. Li and P. D. Senter, Self-hydrolyzing maleimides improve the stability and pharmacological properties of antibody-drug conjugates, *Nat. Biotechnol.*, 2014, **32**, 1059–1062.
- 172 S. D. Fontaine, R. Reid, L. Robinson, G. W. Ashley and D. V. Santi, Long-term

- stabilization of maleimide-thiol conjugates, *Bioconjug. Chem.*, 2015, **26**, 145–152.
- 173 L. Li, T. Olafsen, A.-L. Anderson, A. Wu, A. A. Raubitschek and J. E. Shively, Reduction of Kidney Uptake in Radiometal Labeled Peptide Linkers Conjugated to Recombinant Antibody Fragments. Site-Specific Conjugation of DOTA-Peptides to a Cys-Diabody, *Bioconjug. Chem.*, 2002, **13**, 985–995.
- 174 N. Toda, S. Asano and C. F. Barbas, Rapid, Stable, Chemoselective Labeling of Thiols with Julia-Kocięński-like Reagents: A Serum-Stable Alternative to Maleimide-Based Protein Conjugation, *Angew. Chemie Int. Ed.*, 2013, **52**, 12592–12596.
- 175 P. Adumeau, M. Davydova and B. M. Zeglis, Thiol-Reactive Bifunctional Chelators for the Creation of Site-Selectively Modified Radioimmunoconjugates with Improved Stability, *Bioconjug. Chem.*, 2018, **29**, 1364–1372.
- 176 S. K. Sharma, P. Adumeau, O. Keinänen, V. Sisodiya, H. Sarvaiya, R. Tchelepi, J. A. Korsen, J. Pourat, K. J. Edwards, A. Ragupathi, O. Hamdy, L. R. Saunders, C. M. Rudin, J. T. Poirier, J. S. Lewis and B. M. Zeglis, Synthesis and Comparative In Vivo Evaluation of Site-Specifically Labeled Radioimmunoconjugates for DLL3-Targeted ImmunoPET, *Bioconjug. Chem.*, 2021, **32**, 1255–1262.
- 177 H. Liu, C. Chumsae, G. Gaza-Bulseco, K. Hurkmans and C. H. Radziejewski, Ranking the susceptibility of disulfide bonds in human IgG1 antibodies by reduction, differential alkylation, and LC-MS analysis, *Anal. Chem.*, 2010, **82**, 5219–5226.
- 178 L. H. Lash, Role of glutathione transport processes in kidney function, *Toxicol. Appl. Pharmacol.*, 2005, **204**, 329–342.
- 179 F. F. Schumacher, J. P. M. Nunes, A. Maruani, V. Chudasama, M. E. B. Smith, K. A. Chester, J. R. Baker and S. Caddick, Next generation maleimides enable the controlled assembly of antibody–drug conjugates via native disulfide bond bridging, *Org. Biomol. Chem.*, 2014, **12**, 7261–7269.

- 180 L. Castañeda, A. Maruani, F. F. Schumacher, E. Miranda, V. Chudasama, K. A. Chester, J. R. Baker, M. E. B. Smith and S. Caddick, Acid-cleavable thiomaleamic acid linker for homogeneous antibody-drug conjugation, *Chem. Commun.*, 2013, **49**, 8187–8189.
- 181 J. P. M. Nunes, M. Morais, V. Vassileva, E. Robinson, V. S. Rajkumar, M. E. B. Smith, R. B. Pedley, S. Caddick, J. R. Baker and V. Chudasama, Functional native disulfide bridging enables delivery of a potent, stable and targeted antibody–drug conjugate (ADC), *Chem. Commun.*, 2015, **51**, 10624–10627.
- 182 M. Morais, J. P. M. Nunes, K. Karu, N. Forte, I. Benni, M. E. B. Smith, S. Caddick, V. Chudasama and J. R. Baker, Optimisation of the dibromomaleimide (DBM) platform for native antibody conjugation by accelerated post-conjugation hydrolysis, *Org. Biomol. Chem.*, 2017, **15**, 2947–2952.
- 183 N. Forte, M. Livanos, E. Miranda, M. Morais, X. Yang, V. S. Rajkumar, K. A. Chester, V. Chudasama and J. R. Baker, Tuning the Hydrolytic Stability of Next Generation Maleimide Cross-Linkers Enables Access to Albumin-Antibody Fragment Conjugates and tri-scFvs, *Bioconjug. Chem.*, 2018, **29**, 486–492.
- 184 T. T. Pham, Z. Lu, C. Davis, C. Li, F. Sun, J. Maher and R. Yan, Iodine-124 Based Dual Positron Emission Tomography and Fluorescent Labeling Reagents for In Vivo Cell Tracking, *Bioconjug. Chem.*, 2020, **31**, 1107–1116.
- 185 M. E. B. Smith, F. F. Schumacher, C. P. Ryan, L. M. Tedaldi, D. Papaioannou, G. Waksman, S. Caddick and J. R. Baker, Protein modification, bioconjugation, and disulfide bridging using bromomaleimides, *J. Am. Chem. Soc.*, 2010, **132**, 1960–1965.
- 186 L. M. Tedaldi, M. E. B. Smith, R. I. Nathani and J. R. Baker, Bromomaleimides: new reagents for the selective and reversible modification of cysteine, *Chem. Commun.*, 2009, 6583.
- 187 D. Sleep, Albumin and its application in drug delivery, *Expert Opin. Drug Deliv.*, 2015, **12**, 793–812.
- 188 D. Sleep, J. Cameron and L. R. Evans, Albumin as a versatile platform for

- drug half-life extension, *Biochim. Biophys. Acta - Gen. Subj.*, 2013, **1830**, 5526–5534.
- 189 J. Tian and V. J. Stella, Degradation of Paclitaxel and Related Compounds in Aqueous Solutions II: Nonpimerization Degradation Under Neutral to Basic pH Conditions, *J. Pharm. Sci.*, 2008, **97**, 3100–3108.
- 190 J. P. M. Nunes, V. Vassileva, E. Robinson, M. Morais, M. E. B. Smith, R. B. Pedley, S. Caddick, J. R. Baker and V. Chudasama, Use of a next generation maleimide in combination with THIOMAB™ antibody technology delivers a highly stable, potent and near homogeneous THIOMAB™ antibody-drug conjugate (TDC), *RSC Adv.*, 2017, **7**, 24828–24832.
- 191 S. Balan, J. W. Choi, A. Godwin, I. Teo, C. M. Laborde, S. Heidelberger, M. Zloh, S. Shaunak and S. Brocchini, Site-specific PEGylation of protein disulfide bonds using a three-carbon bridge, *Bioconjug. Chem.*, 2007, **18**, 61–76.
- 192 G. Badescu, P. Bryant, M. Bird, K. Henseleit, J. Swierkosz, V. Parekh, R. Tommasi, E. Pawlisz, K. Jurlewicz, M. Farys, N. Camper, X. Sheng, M. Fisher, R. Grygorash, A. Kyle, A. Abhilash, M. Frigerio, J. Edwards and A. Godwin, Bridging disulfides for stable and defined antibody drug conjugates, *Bioconjug. Chem.*, 2014, **25**, 1124–1136.
- 193 P. Bryant, M. Pabst, G. Badescu, M. Bird, W. McDowell, E. Jamieson, J. Swierkosz, K. Jurlewicz, R. Tommasi, K. Henseleit, X. Sheng, N. Camper, A. Manin, K. Kozakowska, K. Peciak, E. Laurine, R. Grygorash, A. Kyle, D. Morris, V. Parekh, A. Abhilash, J. W. Choi, J. Edwards, M. Frigerio, M. P. Baker and A. Godwin, In vitro and in vivo evaluation of cysteine rebridged trastuzumab-MMAE antibody drug conjugates with defined drug-to-antibody ratios, *Mol. Pharm.*, 2015, **12**, 1872–1879.
- 194 E. Khozeimeh Sarbisheh, G. Dewaele-Le Roi, W. E. Shannon, S. Tan, Y. Xu, B. M. Zeglis and E. W. Price, DiPODS: A Reagent for Site-Specific Bioconjugation via the Irreversible Rebridging of Disulfide Linkages, *Bioconjug. Chem.*, 2020, **31**, 2789–2806.
- 195 C. P. Ryan, M. E. B. Smith, F. F. Schumacher, D. Grohmann, D. Papaioannou, G. Waksman, F. Werner, J. R. Baker and S. Caddick, Tunable

- reagents for multi-functional bioconjugation: reversible or permanent chemical modification of proteins and peptides by control of maleimide hydrolysis, *Chem. Commun.*, 2011, **47**, 5452.
- 196 H. Wu, P. J. LeValley, T. Luo, A. M. Kloxin and K. L. Kiick, Manipulation of Glutathione-Mediated Degradation of Thiol–Maleimide Conjugates, *Bioconjug. Chem.*, 2018, **29**, 3595–3605.
- 197 M. M. Heiss, P. Murawa, P. Koralewski, E. Kutarska, O. O. Kolesnik, V. V. Ivanchenko, A. S. Dudnichenko, B. Aleknaviciene, A. Razbadauskas, M. Gore, E. Ganea-Motan, T. Ciuleanu, P. Wimberger, A. Schmittel, B. Schmalfeldt, A. Burges, C. Bokemeyer, H. Lindhofer, A. Lahr and S. L. Parsons, The trifunctional antibody catumaxomab for the treatment of malignant ascites due to epithelial cancer: Results of a prospective randomized phase II/III trial, *Int. J. Cancer*, 2010, **127**, 2209–2221.
- 198 H. Byrne, P. J. Conroy, J. C. Whisstock and R. J. O’Kennedy, A tale of two specificities: Bispecific antibodies for therapeutic and diagnostic applications, *Trends Biotechnol.*, 2013, **31**, 621–632.
- 199 P. Chames and D. Baty, Bispecific antibodies for cancer therapy: The light at the end of the tunnel?, *MAbs*, 2009, **1**, 539–547.
- 200 L. Baggio, Q. Huang, T. Brown and D. Drucker, A recombinant human glucagon-like peptide (GLP)-1–albumin protein (albugon) mimics peptidergic activation of GLP-1 receptor–dependent pathways coupled with, *Diabetes*, 2004, **53**, 2492–2500.
- 201 S. Berger, P. Lowe and M. Tesar, Fusion Protein Technologies for Biopharmaceuticals, *Fusion Protein Technol. Biopharm.*, 2013, **7**, 456–460.
- 202 E. A. Hull, M. Livanos, E. Miranda, M. E. B. Smith, K. A. Chester and J. R. Baker, Homogeneous bispecifics by disulfide bridging, *Bioconjug. Chem.*, 2014, **25**, 1395–1401.
- 203 A. Wall, A. G. Wills, N. Forte, C. Bahou, L. Bonin, K. Nicholls, M. T. Ma, V. Chudasama and J. R. Baker, One-pot thiol–amine bioconjugation to maleimides: simultaneous stabilisation and dual functionalisation, *Chem. Sci.*, 2020, **11**, 11455–11460.

- 204 L. Castañeda, Z. V. F. Wright, C. Marculescu, T. M. Tran, V. Chudasama, A. Maruani, E. A. Hull, J. P. M. Nunes, R. J. Fitzmaurice, M. E. B. Smith, L. H. Jones, S. Caddick and J. R. Baker, A mild synthesis of N-functionalised bromomaleimides, thiomaleimides and bromopyridazinediones, *Tetrahedron Lett.*, 2013, **54**, 3493–3495.
- 205 M. K. Greene, T. Chen, E. Robinson, N. L. Straubinger, C. Minx, D. K. W. Chan, J. Wang, J. F. Burrows, S. Van Schaeybroeck, J. R. Baker, S. Caddick, D. B. Longley, D. E. Mager, R. M. Straubinger, V. Chudasama and C. J. Scott, Controlled coupling of an ultrapotent auristatin warhead to cetuximab yields a next-generation antibody-drug conjugate for EGFR-targeted therapy of KRAS mutant pancreatic cancer, *Br. J. Cancer*, 2020, **123**, 1502–1512.
- 206 E. Robinson, J. P. M. Nunes, V. Vassileva, A. Maruani, J. C. F. Nogueira, M. E. B. Smith, R. B. Pedley, S. Caddick, J. R. Baker and V. Chudasama, Pyridazinediones deliver potent, stable, targeted and efficacious antibody–drug conjugates (ADCs) with a controlled loading of 4 drugs per antibody, *RSC Adv.*, 2017, **7**, 9073–9077.
- 207 A. Maruani, P. A. Szijj, C. Bahou, J. C. F. Nogueira, S. Caddick, J. R. Baker and V. Chudasama, A Plug-and-Play Approach for the de Novo Generation of Dually Functionalized Bispecifics, *Bioconjug. Chem.*, 2020, **31**, 520–529.
- 208 C. Bahou, D. A. Richards, A. Maruani, E. A. Love, F. Javaid, S. Caddick, J. R. Baker and V. Chudasama, Highly homogeneous antibody modification through optimisation of the synthesis and conjugation of functionalised dibromopyridazinediones, *Org. Biomol. Chem.*, 2018, **16**, 1359–1366.
- 209 A. Maruani, M. E. B. Smith, E. Miranda, K. A. Chester, V. Chudasama and S. Caddick, A plug-and-play approach to antibody-based therapeutics via a chemoselective dual click strategy, *Nat. Commun.*, 2015, **6**, 2–10.

2 Sarcophagine-based dibromomaleimides for the preparation of ^{64}Cu -radioimmunoconjugates for PET imaging

2.1 Introduction

Dibromomaleimides have previously been used to produce antibody conjugates of drug and fluorophore molecules (see 1.7.2). These reagents produce conjugates that are more homogeneous than those generated by stochastic conjugations. Additionally, dibromomaleimide conjugations are less complex than existing site-specific conjugation technologies. This chapter discusses the development of a new class of thiol-reactive bifunctional chelators based on dibromomaleimides. This new class of compound has the potential to deliver site-specifically labelled radioimmunoconjugates more simply than current state of the art conjugation platforms.

2.2 Aims

The overall aim of this chapter was to demonstrate a proof of concept for dibromomaleimide-based bifunctional chelators. In this proof of concept, ^{64}Cu was chosen as the radionuclide since its half-life is 12.7 h - well matched to a study designed to take place over several days. The sarcophagine chelator was chosen since it has been shown capable of reliable and efficient complexation of $^{64}\text{Cu}^{2+}$.

This chapter discusses:

1. The optimised synthesis of a new sarcophagine-dibromomaleimide bifunctional chelator (sar-DBM)
2. The conjugation of sar-DBM to trastuzumab to give sar-DTM-trastuzumab
3. The radiolabelling of sar-DTM-trastuzumab with $^{64}\text{Cu}^{2+}$
4. The stability of ^{64}Cu -sar-DTM-trastuzumab in human serum
5. *In vitro* assessment of ^{64}Cu -sar-DTM-trastuzumab specificity for the HER2 receptor
6. The *in vivo* target receptor specificity and stability of ^{64}Cu -sar-DTM-trastuzumab in healthy mice

2.3 Synthesis of a sarcophagine-based dibromomaleimide bifunctional chelator

2.3.1 Synthesis of $[\text{Mg}(\text{NH}_2)_2\text{sar}](\text{CF}_3\text{SO}_2)_2$ (**12**)

Sarcophagine was chosen as a model chelator following from previous work within the Ma group,¹⁻³ thanks to the synthetic flexibility granted by two primary amines within diaminosarcophagine ($(\text{NH}_2)_2\text{sar}$) (**13**, figure 54), and its facile radiolabelling with $^{64}\text{Cu}^{2+}$. Bifunctional derivatives of $(\text{NH}_2)_2\text{sar}$ can be synthesised by reaction of one or both of its primary amines with nucleophilic amine-reactive species such as activated carboxylic acids. As discussed in section 1.4.2, during this reaction the secondary amine groups of $(\text{NH}_2)_2\text{sar}$ need to be protected to prevent their reaction with the nucleophilic amine-reactive species. The secondary amines on $(\text{NH}_2)_2\text{sar}$ can be protected by complexation of a metal ion, which accepts electron density from the coordinating amines, reducing their nucleophilicity. Here, Mg^{2+} complexation was chosen as the protection strategy, as it requires milder deprotection conditions after functionalisation, compared to other protection strategies, such as Cu^{2+} complexation or Boc protection of secondary amines (see 1.4.2). $\text{Mg}(\text{CF}_3\text{SO}_3)_2$ was added to $(\text{NH}_2)_2\text{sar}$ in acetonitrile and refluxed to give $[\text{Mg}(\text{NH}_2)_2\text{sar}](\text{CF}_3\text{SO}_2)_2$ (**12**, figure 54). The CF_3SO_3^- (triflate) counterion was chosen because it greatly improves the solubility of the $[\text{Mg}(\text{NH}_2)_2\text{sar}]^{2+}$ complex in organic solvents such as acetonitrile. The free ligand, $(\text{NH}_2)_2\text{sar}$, was only sparingly soluble in acetonitrile at ambient temperatures, however upon heating to reflux, the sarcophagine dissolved enabling complexation of the Mg^{2+} . Upon cooling, $[\text{Mg}(\text{NH}_2)_2\text{sar}]^{2+}$ remained in solution highlighting the complex's improved solubility relative to $(\text{NH}_2)_2\text{sar}$. The solvent was removed under vacuum to yield the product as a white powder. To confirm the complexation of Mg^{2+} by $(\text{NH}_2)_2\text{sar}$, ^1H NMR spectra of $(\text{NH}_2)_2\text{sar}$ and $[\text{Mg}(\text{NH}_2)_2\text{sar}]^{2+}$ were acquired and compared (figure 54).

The ^1H NMR spectrum of $(\text{NH}_2)_2\text{sar}$ (figure 54) shows two proton environments with equal integrals. In D_2O , the aminic protons readily exchange with deuterons from the solvent, and so are not observed. The ^1H NMR spectrum of $[\text{Mg}(\text{NH}_2)_2\text{sar}]^{2+}$ (figure 54) shows four peaks containing 5 signals corresponding to five different proton environments. Protons of the methylene and ethylene bridges of the sarcophagine ligand form diastereotopic pairs upon metal ion complexation. Two of these signals appear at the same chemical shift and so an integral of 12 protons is seen for the signals at 3.15 ppm. The other two signals at 2.68 ppm and 2.42 ppm

each have integrals of 6 protons as expected. Interestingly, secondary amine protons are visible in this spectrum at 3.61 ppm as a broad quintet integrating to 5.40 protons, likely due to a slower rate of deuterium exchange at the secondary amines on $[\text{Mg}(\text{NH}_2)_2\text{sar}]^{2+}$ relative to $(\text{NH}_2)_2\text{sar}$. Metal ion complexation by these secondary amines reduces their basicity, and so their rate of deuterium exchange is decreased relative to $(\text{NH}_2)_2\text{sar}$.

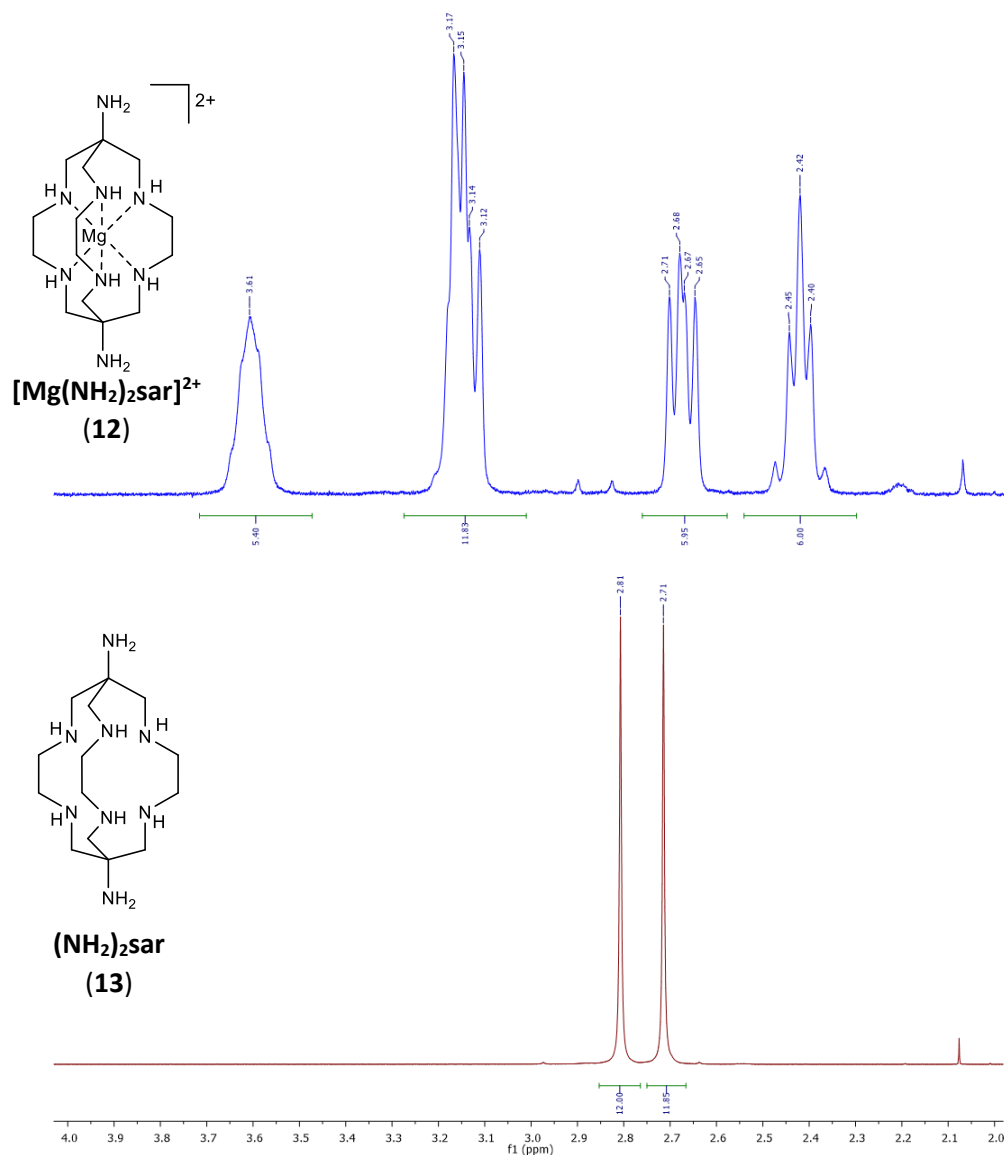
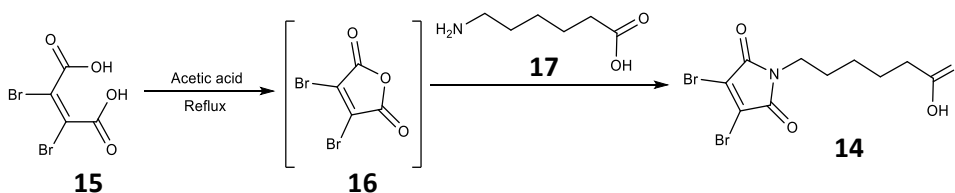


Figure 54 - ^1H NMR spectra and structures of $(\text{NH}_2)_2\text{sar}$ (12) and $[\text{Mg}(\text{NH}_2)_2\text{sar}](\text{CF}_3\text{SO}_2)_2$ (13). D_2O , 400 MHz).

2.3.2 Synthesis of 3,4-dibromomaleimide-N-hexanoic acid (14)

3,4-dibromomaleimide-N-hexanoic acid (**14**, scheme 1) was synthesised according to the literature.⁴ Dibromomaleic acid (**15**, scheme 1) was refluxed in acetic acid

forming dibromomaleic anhydride (**16**, scheme 1) *in situ*.⁵ Then aminocaproic acid (**17**, scheme 1) was added, to give 3,4-dibromomaleimide-*N*-hexanoic acid. This



product was characterised by ¹H NMR (see appendix, figure 115), and ¹³C NMR (see appendix, figure 116).

Scheme 1 - Synthesis of 3,4-dibromomaleimide-*N*-hexanoic acid (**14**).

2.3.3 Synthesis of sar-DBM (**18**)

Synthesis of sar-DBM (**18**, scheme 2) was achieved *via* an amide coupling reaction between $[\text{Mg}(\text{NH}_2)_2\text{sar}]^{2+}$ and 3,4-dibromomaleimide-*N*-hexanoic acid.⁶ This reaction used the coupling reagent *N*-ethoxycarbonyl-2-ethoxy-1,2-dihydroquinoline (EEDQ, **19**, scheme 2). This reagent is commonly employed for amide couplings between amines and dibromomaleimides bearing carboxylic acids.^{4,7,8} EEDQ was added to 3,4-dibromomaleimide-*N*-hexanoic acid and stirred to give a reactive anhydride intermediate (**20**, scheme 2). Quinoline and ethanol are generated as side products of the EEDQ activation and can be easily separated from the product by chromatography. $[\text{Mg}(\text{NH}_2)_2\text{sar}]^{2+}$ was then added, which reacted with **20** to give the Mg^{2+} complex of sar-DBM. The reaction was acidified with glacial acetic acid to quench unreacted EEDQ and prevent dibromomaleimide hydrolysis. Additionally, these acidic conditions promoted the extrusion of Mg^{2+} from sar-DBM (see 1.4.2). The mixture was evaporated to dryness and redissolved in water to give a colourless solution with a white precipitate. The precipitate (largely unreacted 3,4-dibromomaleimide-*N*-hexanoic acid) was removed, and the supernatant lyophilised to give the crude product, which was purified by C18 reverse phase preparative HPLC (see 2.10), to give the desired compound sar-DBM (20.7 mg, 8%).

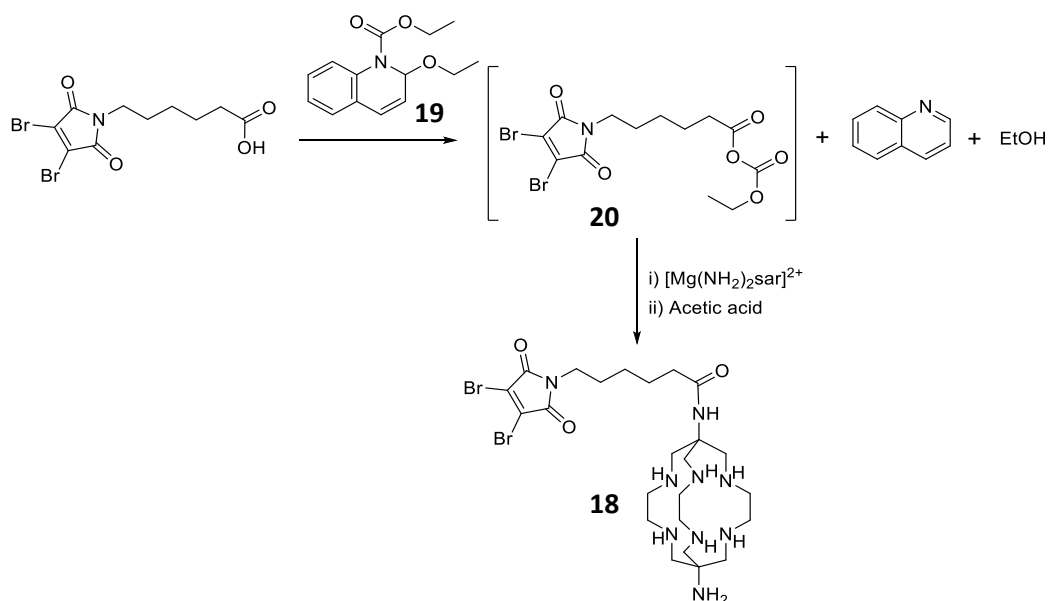
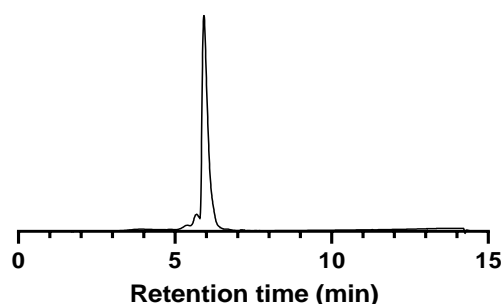


Figure 55 - Analytical C18 reverse-phase HPLC chromatogram with UV detection at λ_{254} of sar-DBM with a retention time of 5.92 min.



The analytical C18 reverse-phase HPLC chromatogram of sar-DBM (figure 55) shows the presence of a major peak with a retention time of 5.92 min, indicating high chemical purity. Full assignment of the ^1H NMR spectrum was made with the aid of ^1H - ^1H correlation spectroscopy (COSY, appendix, see figure 117). In the ^1H NMR spectrum (figure 56) of sar-DBM, signals at 3.45 ppm, 2.11 ppm, 1.43 ppm, and 1.12 ppm correspond to the five proton environments of the C_5 linker between the sarcophagine and the dibromomaleimide (figure 56, environments a-e). As expected, environments 'a' and 'e' are relatively deshielded due to their adjacent heteroatom (N) and carbonyl carbon respectively. The signals corresponding to environments 'b' and 'd' overlap on the ^1H NMR spectrum due to their similar chemical shifts whilst the electronically insulated protons in environment 'c' have the lowest chemical shift on this spectrum. Signals corresponding to sarcophagine CH_2 protons are observed from 3.6-2.7 ppm and do not possess splitting patterns

consistent with diastereotopic protons. This observation indicates successful Mg^{2+} removal during the acidic work up and purification. Some minor signals present in the region corresponding to sarcophagine cage protons do possess these splitting patterns, suggesting that a small proportion of sar-DBM was present as the Mg^{2+} complex. The ^{13}C NMR spectrum (figure 57) for sar-DBM contained 14 signals as expected and was assigned with the aid of a 1H - ^{13}C HSQC NMR spectrum (see appendix, figure 118). Three ^{13}C signals (a, b, and h) of sar-DBM were highly deshielded, corresponding vinylic and carbonylic carbon atoms. Carbon atoms of the sarcophagine cage are all deshielded slightly due to their adjacent nitrogen atoms and possess chemical shifts between 46.14 ppm and 55.91 ppm.

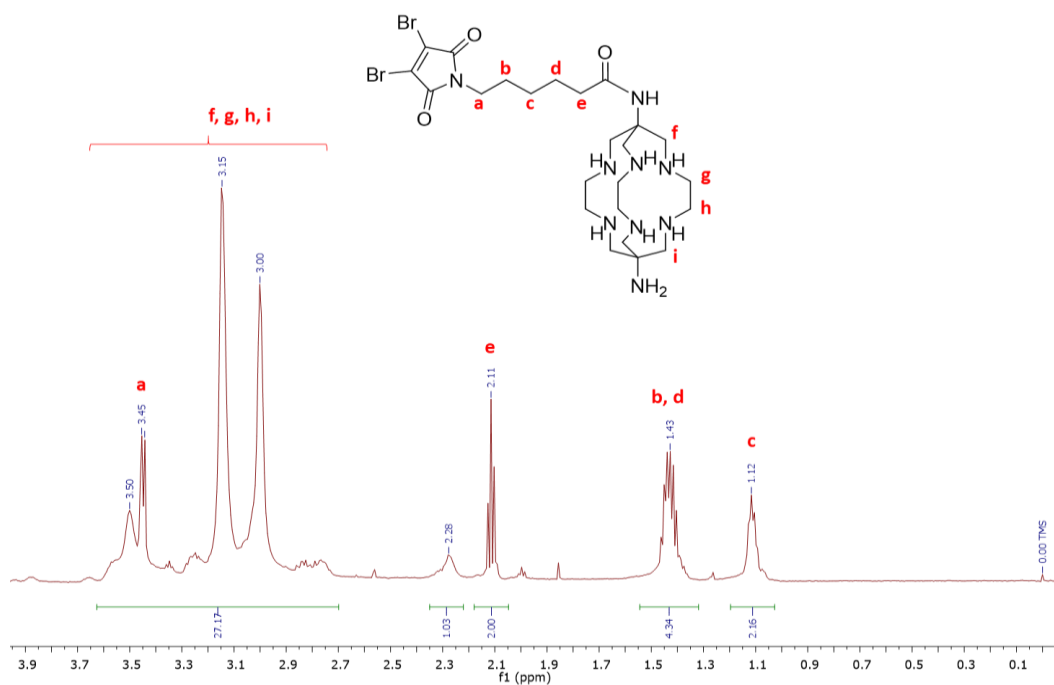


Figure 56 - Assigned structure and 1H NMR spectrum of sar-DBM (D_2O , 700 MHz).

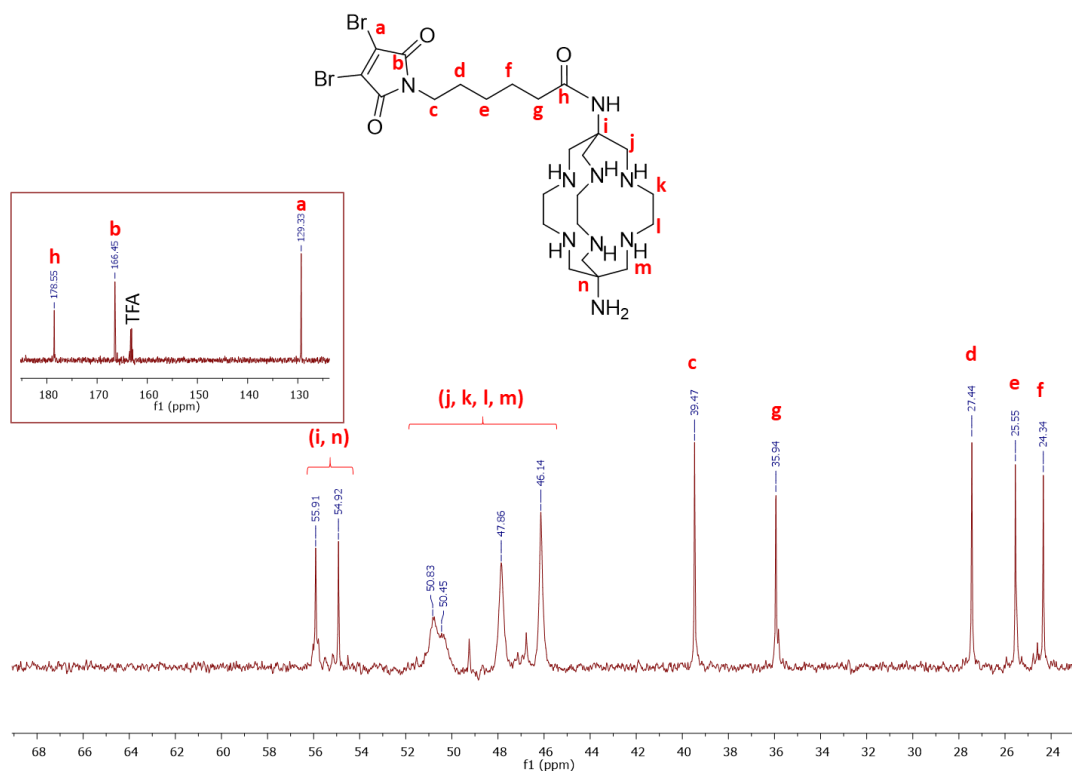


Figure 57 - Assigned structure and ^{13}C NMR spectrum of sar-DBM (D_2O , 176 MHz).

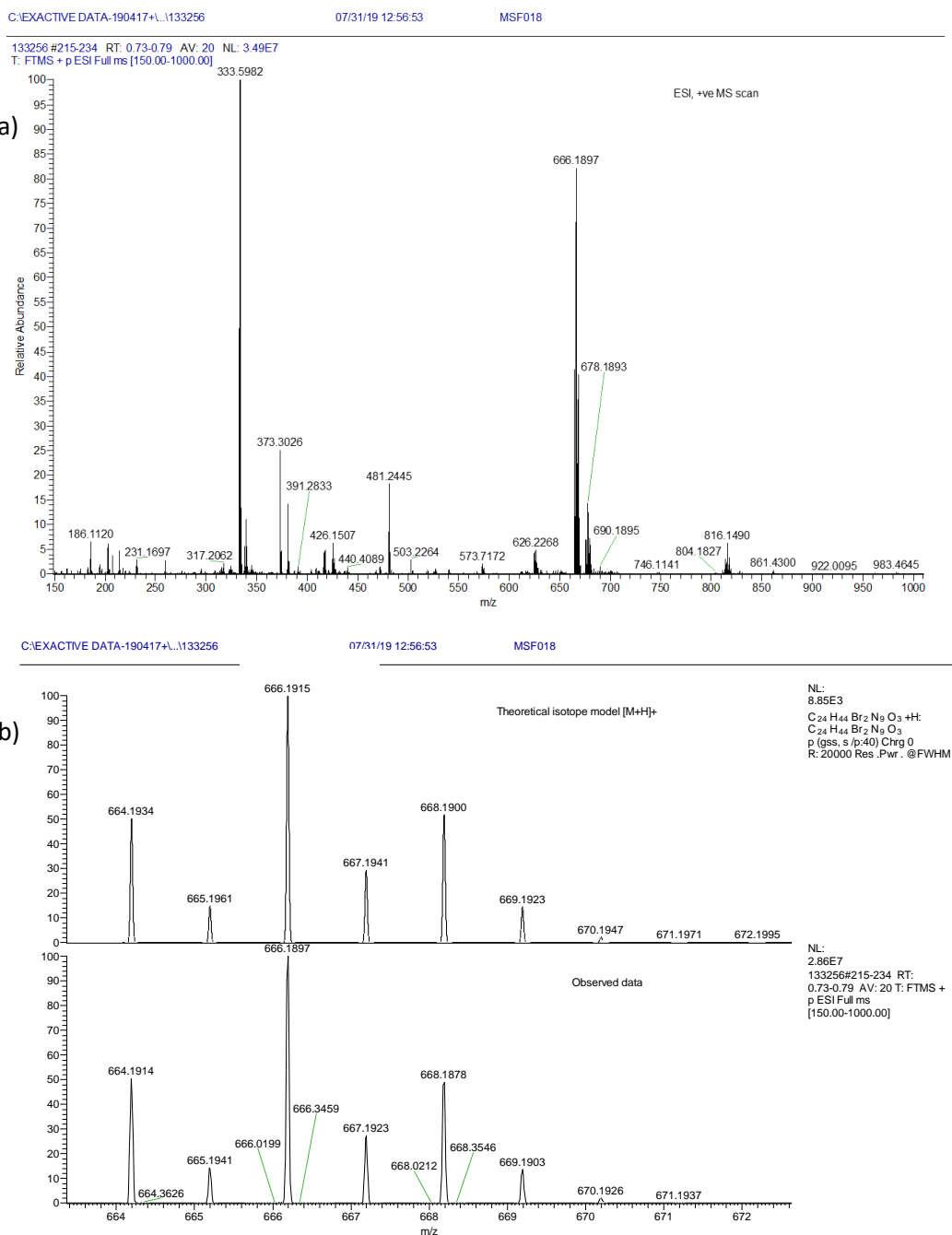


Figure 58 - High-resolution ESI-mass spectrum for sar-DBM: (a) full mass spectrum; (b) expanded view of the [MH]⁺ signal showing (top) calculated isotope pattern, and (bottom) observed data

The mass spectrum for sar-DBM (figure 58a) showed a [MH]⁺ peak at $m/z = 666.1897$ in good agreement with the calculated $m/z = 666.1915$. The peak corresponding to [MH₂]²⁺ was also observed at $m/z = 333.5982$. Bromine has two stable isotopes ⁷⁹Br and ⁸¹Br with 51% and 49% abundance respectively. Therefore, compounds containing bromine atoms give rise to characteristic isotope patterns in a mass spectrum. An expanded view of the [MH]⁺ peak (figure 58b) shows the

characteristic isotope fingerprint pattern for a species containing two bromine atoms, in good agreement with the calculated isotope pattern.

2.3.4 Optimising the synthesis of sar-DBM

The reported 8 % yield for sar-DBM was the result of an optimised synthesis where factors including the choice of solvent, the presence of base, the stoichiometry of reagents, the duration of the reaction and the temperature of the reaction were altered. The influence of each factor on the reaction was assessed by obtaining preparative HPLC chromatograms for each set of conditions (table 2, figures 59-63) (using the methods described in section 2.9). For each method tested, the same amount of crude product was loaded onto the HPLC column. Measuring absorbance at 254 nm, the relative size and resolution of the peak corresponding to sar-DBM (retention time 21.8 min, blue arrow), as well as the number and size of side product peaks were then used to compare the methods tested.

Table 2 – Summarised conditions used in the optimisation of sar-DBM synthesis. The optimised conditions are shown as serial 4.

Serial	Solvent	DIPEA eq.	Sar eq.	DBM eq.	EEDQ eq.	Temperature	Duration
1	DMF	0	1	1.6	1.6	r.t.	1 h
2	MeCN	0	1	1.6	1.6	r.t.	1 h
3	MeCN	5	1	1.6	1.6	r.t.	1 h
4	MeCN	0	1	3	3	r.t.	1 h
5	MeCN	0	1	3	3	40 °C	1 h
6	MeCN	0	1	3	3	r.t.	3 h

Initially, *N,N*-dimethylformamide (DMF) was used as the reaction solvent, and 1 eq. of $[\text{Mg}(\text{NH}_2)_2\text{sar}]^{2+}$ was added to 1.6 eq. of 3,4-dibromomaleimide-*N*-hexanoic acid activated with 1.6 eq. of EEDQ. The reaction was stirred for 1 h at ambient temperature. This reaction was repeated but DMF was replaced with acetonitrile as the solvent. HPLC chromatograms of the crude products from both these reaction conditions were obtained and compared (figure 59). The chromatographic yield of sar-DBM was higher when acetonitrile was used as the solvent and fewer side products were formed. Therefore, acetonitrile was adopted as the solvent of choice for this reaction.

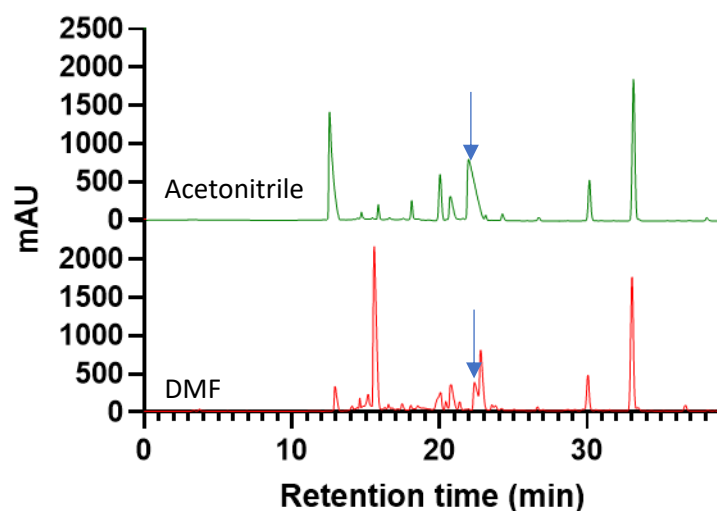


Figure 59 - HPLC chromatograms of the crude product obtained in the synthesis of sar-DBM, with either DMF (red) or acetonitrile (green) as the reaction solvent. The blue arrow indicates the peak corresponding to sar-DBM with a retention time of 21.8 min.

Next the influence of base on the reaction was assessed. Acetonitrile was used as the solvent, and 1 eq. of $[\text{Mg}(\text{NH}_2)_2\text{sar}]^{2+}$ was added to 1.6 eq. of 3,4-dibromomaleimide-*N*-hexanoic acid activated with 1.6 eq. of EEDQ. Then, 5 eq. of *N,N*-diisopropylethylamine (DIPEA) were added. The HPLC chromatogram of the crude product was obtained and compared (figure 60) with the previously acquired chromatogram for the reaction without base. These chromatograms showed that the addition of base resulted in a decrease in the relative amount of sar-DBM product and also generated unwanted side products. Therefore base was not used in further iterations of this reaction.

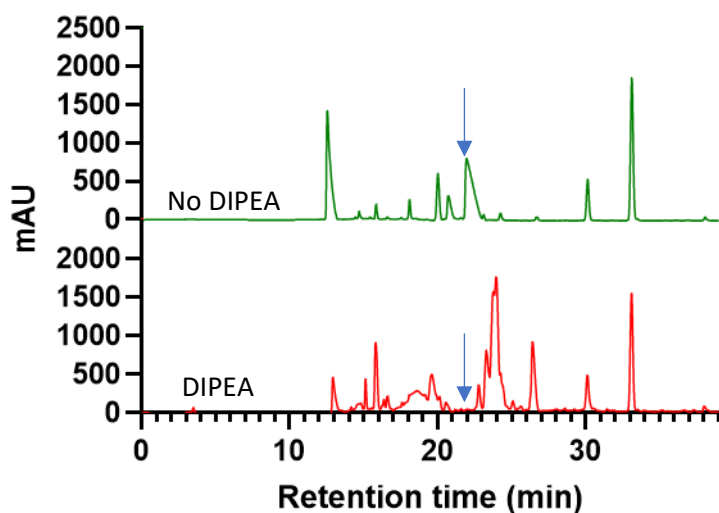


Figure 60 - HPLC chromatograms of the crude product obtained in the synthesis of sar-DBM, either with base (red) or without base (green). The blue arrow indicates the peak corresponding to sar-DBM with a retention time of 21.8 min.

The effect of increasing the number of equivalents of 3,4-dibromomaleimide-*N*-hexanoic acid and EEDQ relative to $[\text{Mg}(\text{NH}_2)_2\text{sar}]^{2+}$ was investigated. Acetonitrile was used as the solvent, and 1 eq. of $[\text{Mg}(\text{NH}_2)_2\text{sar}]^{2+}$ was added to 3 eq. of 3,4-dibromomaleimide-*N*-hexanoic acid activated with 3 eq. of EEDQ. A HPLC chromatogram was obtained for the crude product and compared (figure 61) to the previously acquired chromatogram for the reaction with 1.6 eq of 3,4-dibromomaleimide-*N*-hexanoic acid activated with 1.6 eq. of EEDQ. The relative size of the peak corresponding to sar-DBM was larger when 3 eq. of 3,4-dibromomaleimide-*N*-hexanoic acid and EEDQ are reacted with 1 eq. of $[\text{Mg}(\text{NH}_2)_2\text{sar}]^{2+}$, so this stoichiometry was chosen for optimised reaction conditions.

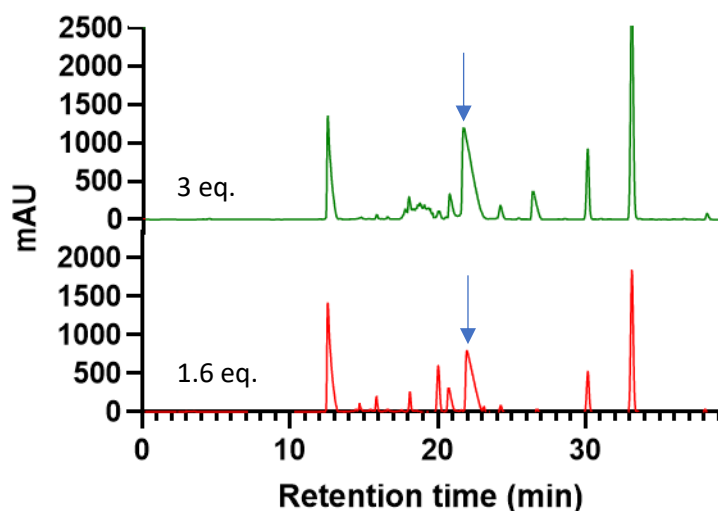


Figure 61 - HPLC chromatograms of the crude product obtained in the synthesis of sar-DBM, either with 1.6 eq. (red) or 3 eq. (green) of 3,4-dibromomaleimide-*N*-hexanoic acid and EEDQ. The blue arrow indicates the peak corresponding to sar-DBM with a retention time of 21.8 min.

Temperature was investigated as a factor: acetonitrile was used as the solvent, and 1 eq. of $[\text{Mg}(\text{NH}_2)_2\text{sar}]^{2+}$ was added to 3 eq. of 3,4-dibromomaleimide-*N*-hexanoic acid activated with 3 eq. of EEDQ, and the reaction was maintained at 40 °C for 1 h. A HPLC chromatogram was obtained for the crude product and compared (figure 62) to the previously acquired chromatogram for the reaction carried out at ambient temperature. Increasing the temperature to 40 °C led to increased side product formation, and poorer resolution of the desired product peak at 21.8 min. Therefore, the coupling reaction was carried out at ambient temperature.

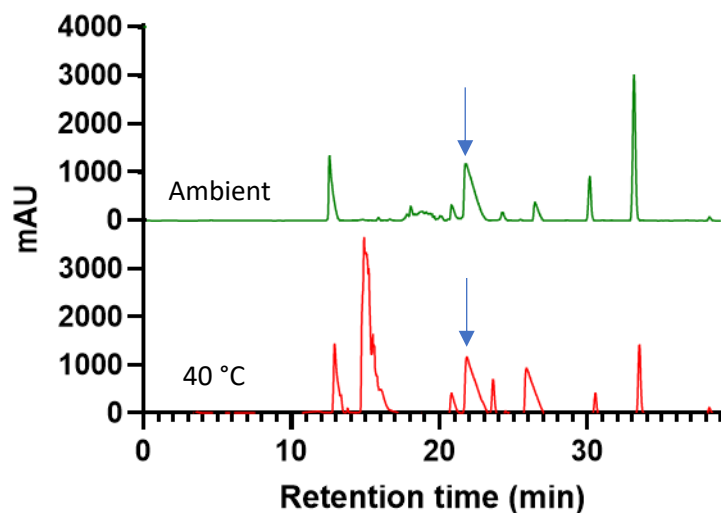


Figure 62 - HPLC chromatograms of the crude product obtained in the synthesis of sar-DBM, at 40 °C (red) or ambient temperature (green). The blue arrow indicates the peak corresponding to sar-DBM with a retention time of 21.8 min.

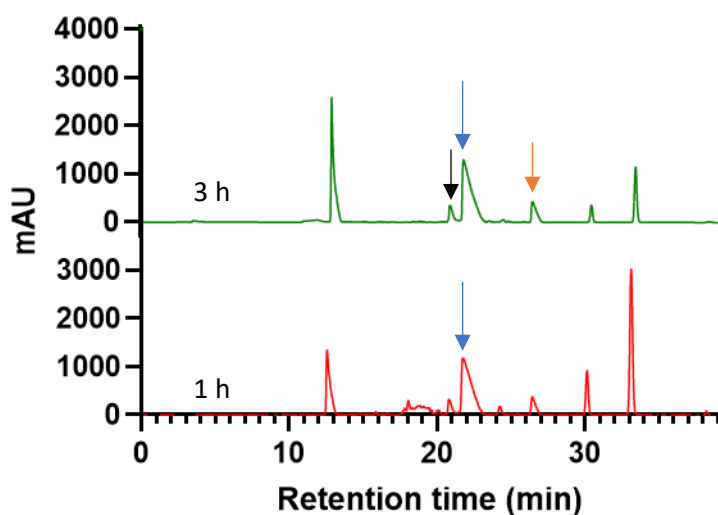


Figure 63 - HPLC chromatograms of the crude product obtained in the synthesis of sar-DBM with a duration of 1 h (red) or 3 h (green). The blue arrow indicates the peak corresponding to sar-DBM with a retention time of 21.8 min. The black arrow indicates the peak corresponding to $[\text{Mg}(\text{sar-DBM})]^{2+}$ with a retention time of 20.8 min. The orange arrow indicates the peak corresponding to sar-DBM₂ with a retention time of 26.4 min.

Lastly, the effect of reaction duration on the coupling reaction between $[\text{Mg}(\text{NH}_2)_2\text{sar}]^{2+}$ and 3,4-dibromomaleimide-*N*-hexanoic acid was investigated. Acetonitrile was used as the solvent, and 1 eq. of $[\text{Mg}(\text{NH}_2)_2\text{sar}]^{2+}$ was added to 3 eq. of 3,4-dibromomaleimide-*N*-hexanoic acid activated with 3 eq. of EEDQ, and the reaction was stirred for 3 h at ambient temperature. An HPLC chromatogram was

obtained for the crude product and compared (figure 63) to the previously acquired chromatogram for the reaction with 1 h duration. Increasing the reaction duration from 1 h to 3 h led to a decrease in the size of the side product peaks. Noticeably, the size of the side product peaks eluting at 18.6 min was greatly reduced.

Through this HPLC-guided optimisation process, isolated yields of sar-DBM increased from 0.8 % under the initial conditions (DMF, 1 eq. $[\text{Mg}(\text{NH}_2)_2\text{sar}]^{2+}$, 1.6 eq. 3,4-dibromomaleimide-*N*-hexanoic acid and EEDQ, 1 h, r.t) to 8 % under optimised conditions (acetonitrile, 1 eq. $[\text{Mg}(\text{NH}_2)_2\text{sar}]^{2+}$, 3 eq. 3,4-dibromomaleimide-*N*-hexanoic acid and EEDQ, 3 h, r.t.).

The optimised synthesis of sar-DBM was scaled up from 10 mg of $[\text{Mg}(\text{NH}_2)_2\text{sar}]^{2+}$ to 250 mg of $[\text{Mg}(\text{NH}_2)_2\text{sar}]^{2+}$. On this larger scale, two other compounds were isolated and characterised. The first compound was eluted from the HPLC column with a retention time of 20.8 min (figure 63, black arrow), and then lyophilised to give a white powder. ^1H NMR (figure 64, top), and low-resolution mass spectrometry were used to characterise this material as $[\text{Mg}(\text{sar-DBM})]^{2+}$ (1.9 %, **21**, figure 64). ESI-MS +ve mode ($\text{C}_{24}\text{H}_{43}\text{Br}_2\text{MgN}_9\text{O}_3^{2+}$): calculated $m/z = 344.5$, observed $m/z 344.5$). Many of the chromatograms above contain a peak corresponding to $[\text{Mg}(\text{sar-DBM})]^{2+}$. Detection of this side product suggests that the acidic work up employed does not lead to complete extrusion of Mg^{2+} from the sarcophagine chelator. Steps were not taken to improve the conversion of $[\text{Mg}(\text{sar-DBM})]^{2+}$ to sar-DBM in this reaction, since enough sar-DBM had been isolated to enable full characterisation and subsequent bioconjugation reactions. The ^1H NMR spectrum of $[\text{Mg}(\text{sar-DBM})]^{2+}$ (figure 64, top) showed more signals than expected in the sarcophagine region (3.5-2.7 ppm). It is likely that slow extrusion of Mg^{2+} from $[\text{Mg}(\text{sar-DBM})]^{2+}$ occurs over time in the NMR tube to give a mixture of $[\text{Mg}(\text{sar-DBM})]^{2+}$ and sar-DBM. COSY (figure 64) was used to aid in structural assignment of $[\text{Mg}(\text{sar-DBM})]^{2+}$.

A second side product was eluted from the HPLC column with a retention time of 26.4 min (figure 63, orange arrow), lyophilised to give a white powder, and then characterised by ^1H NMR (figure 65, top), COSY (figure 65, bottom), and high-resolution mass spectrometry (figure 66). The compound was identified as sar-DBM₂ (4.5 mg, 0.6 %, **22**, figure 65). As with $[\text{Mg}(\text{sar-DBM})]^{2+}$, this compound was found to be a mixture of the Mg^{2+} complex and the metal-free ligand as shown by

the sarcophagine region where signals corresponding to both $[\text{Mg}(\text{sar-DBM}_2)]^{2+}$ and sar-DBM_2 are present. This mixture is observed in the high-resolution mass spectrum of sar-DBM_2 (figure 66a) where both species are present: sar-DBM_2 observed $m/z = 1017.08$, calculated $m/z = 1017.08$; $[\text{Mg}(\text{sar-DBM}_2)]^{2+}$ observed $m/z = 520.03$, calculated $m/z = 520.03$. Expanded views of these peaks (figure 66b,c) show isotopic peak distributions indicative of a species containing four bromine atoms.

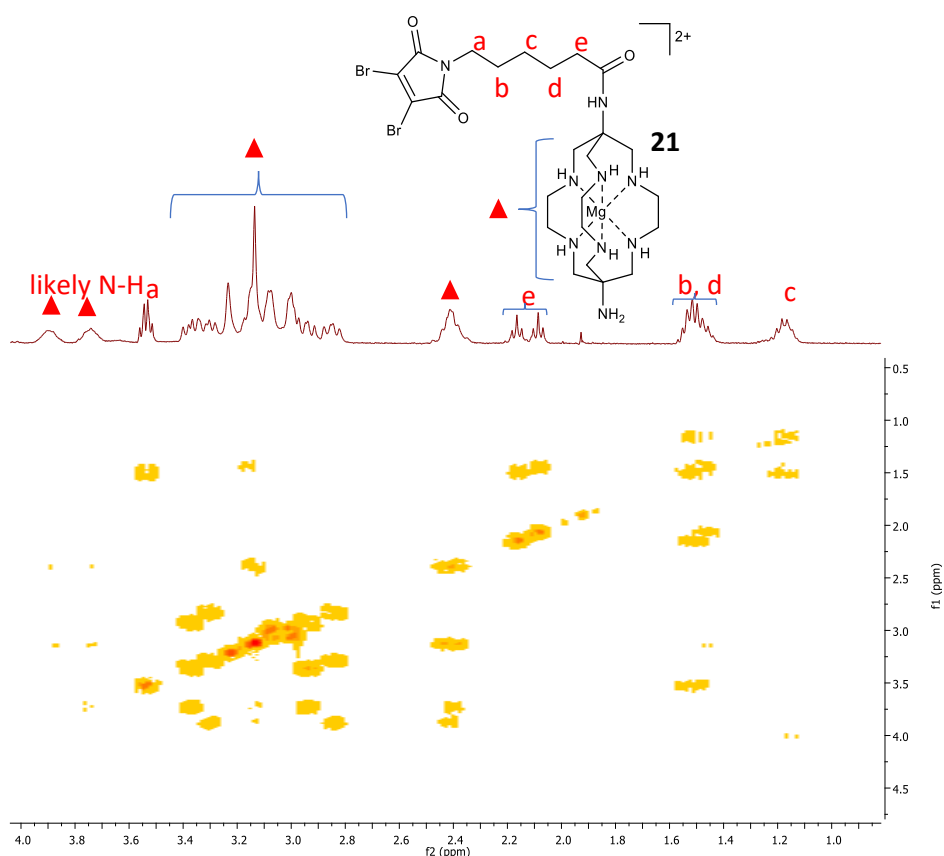


Figure 64 - ^1H NMR spectrum (top, D_2O , 400 MHz) and COSY (bottom) of $[\text{Mg}(\text{sar-DBM})]^{2+}$ (**21**), which is present as a mixture of the Mg^{2+} complex and the metal free sar-DBM species. The full ^1H NMR spectrum of $[\text{Mg}(\text{sar-DBM})]^{2+}$ is included in the appendix (see figure 119).

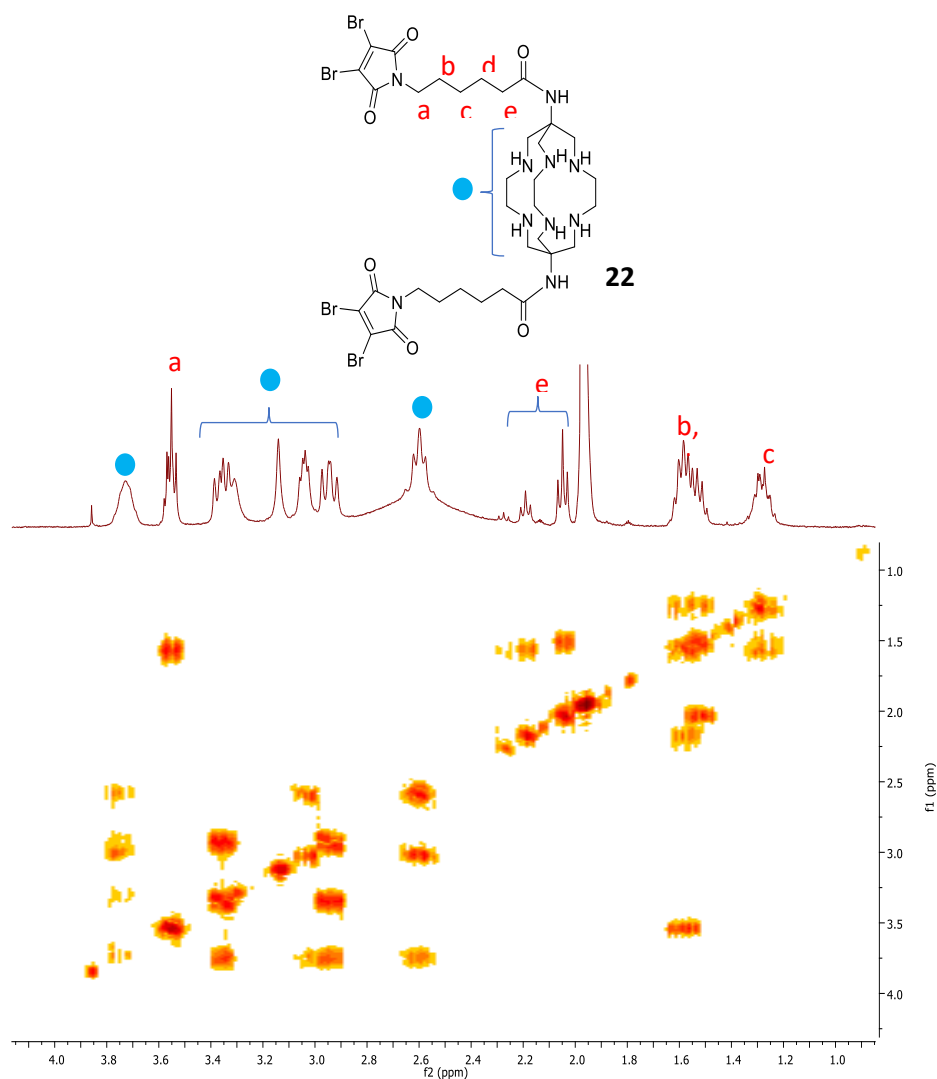


Figure 65 - Structure, ¹H NMR spectrum (top, CD₃CN, 400 MHz), and COSY (bottom) of sar-DBM₂ (22), which is present as a mixture of the Mg²⁺ complex and the metal free sar-DBM₂ species (CD₃CN, 400 MHz). Integrals have not been given here, but the full ¹H NMR spectrum of sar-DBM₂ is given in the appendix (see figure 120).

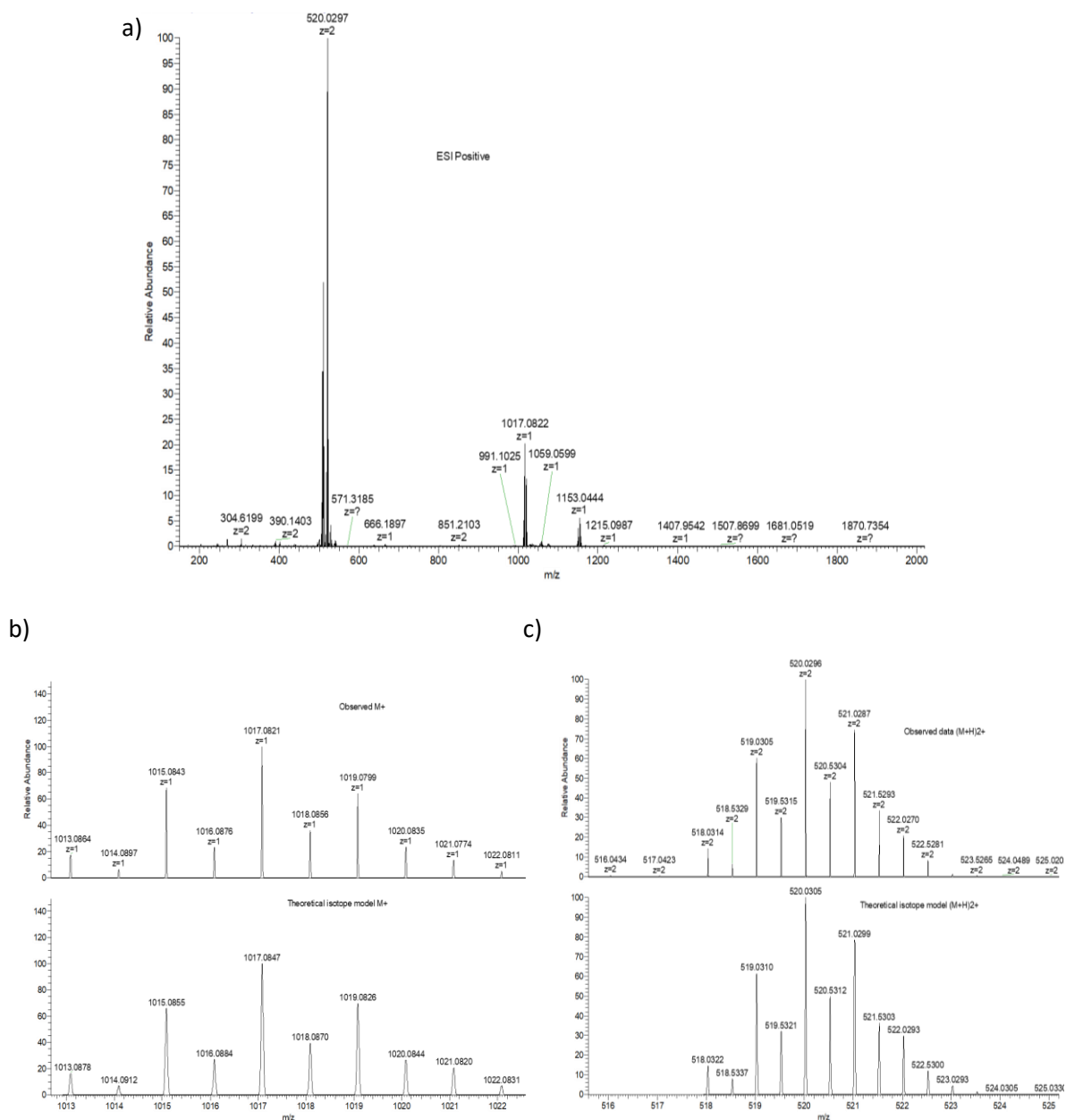
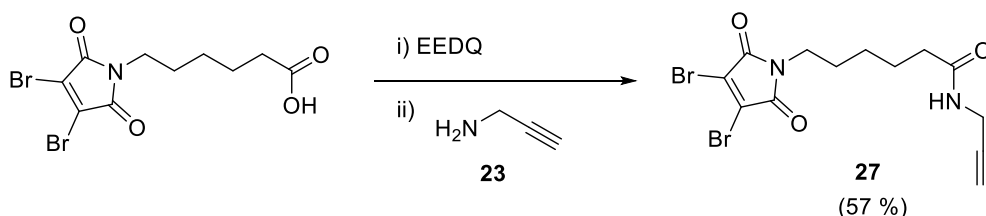


Figure 66 - Mass spectrum for sar-DBM₂, a) full mass spectrum, b) expanded view of the region corresponding to sar-DBM₂ observed (top) and calculated (bottom), c) expanded view of the region corresponding to [Mg(sar-DBM₂)]²⁺ observed (top) and calculated (bottom).

The chromatograms in figures 59-63 all contain a peak at 26.8 min corresponding to sar-DBM₂, although the size of this peak varied greatly with the reaction conditions used. The size of this peak increased with the inclusion of DIPEA (figure 60, red), when 3 eq. of 3,4-dibromomaleimide-N-hexanoic acid and EEDQ were used (figure 8, green), when the temperature of the reaction was increased to 40 °C (figure 62, red), and when the reaction duration was increased to 3 h (figure 63,

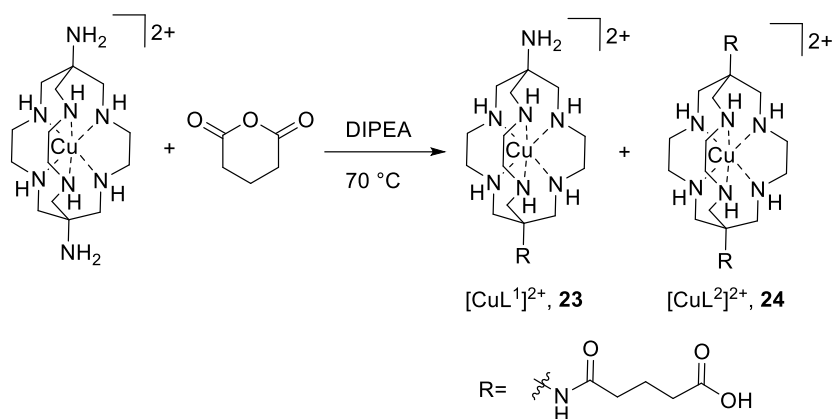
green). However, using optimised conditions (see above) the yield of sar-DBM₂ was low (0.6 %) relative to the desired product sar-DBM (8 %).

Whilst significant yield improvements were made during optimisation between the [Mg(NH₂)₂sar]²⁺ and 3,4-dibromomaleimide-N-hexanoic acid, the yield of sar-DBM was lower than expected. In prior studies, amide couplings between 3,4-dibromomaleimide-N-hexanoic acid and primary amines such as propargylamine (**23**, scheme 3) typically result in yields of approximately 50 %.⁴ It is likely that the steric encumbrance of the bicyclic rings decreases the reactivity of the primary amines of (NH₂)₂sar relative to those of unhindered primary amines such as those on propargylamine for example. This finding is consistent with early observations where (NH₂)₂sar could not be conjugated efficiently to electrophilic residues (e.g. glutamic acid) on antibodies (see 1.4.2).⁹

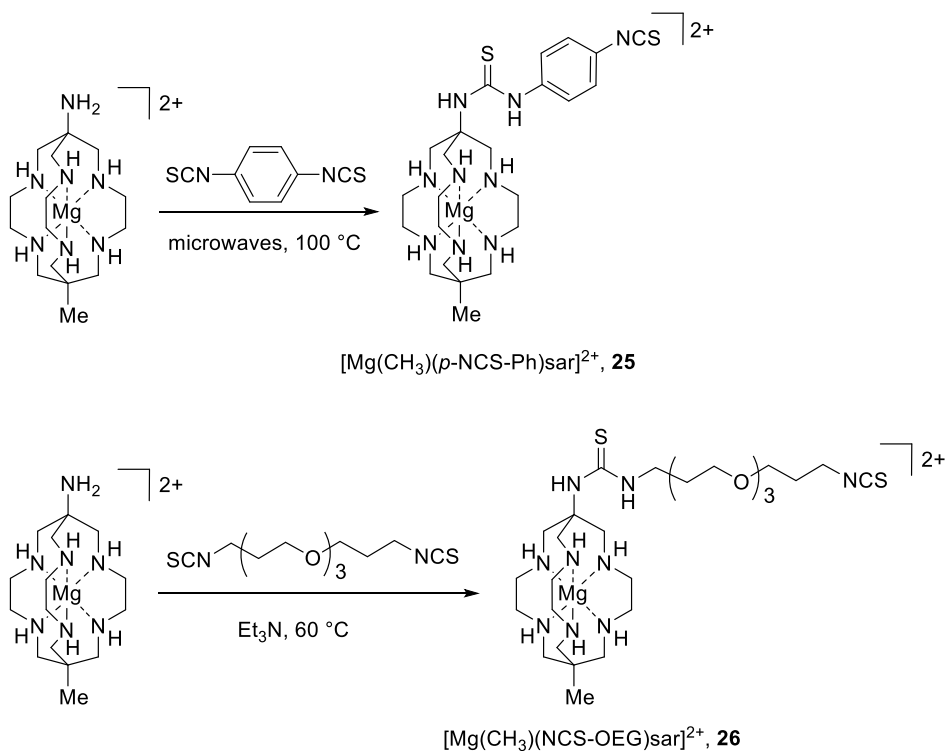


Scheme 3 - Amide coupling between 3,4-dibromomaleimide-N-hexanoic acid and propargylamine (23**).**⁴

As mentioned, EEDQ activates carboxylic acids by generating a reactive anhydride intermediate (**20**, scheme 2) *in situ*. The primary amines of [Mg(NH₂)₂sar]²⁺ then react with the anhydride intermediate forming sar-DBM. In previous studies, [Cu(NH₂)₂sar]²⁺ has been functionalised using glutaric anhydride (see 1.4.2).¹ Cu²⁺ was used to protect the secondary amines of the sarcophagine, preventing them from reacting with the glutaric anhydride. Mono- ([CuL¹]²⁺, **23**, scheme 4) and dialkylated ([CuL²]²⁺, **24**, scheme 4) bifunctional chelators were produced by this reaction both in approximately 30 % yield (estimated chromatographically).¹⁰ These yields are higher than those achieved in the coupling of [Mg(NH₂)₂sar]²⁺ to 3,4-dibromomaleimide-N-hexanoic acid mediated by EEDQ (8 %). The synthesis of [CuL¹]²⁺ and [CuL²]²⁺ was carried out in the presence of the base DIPEA and at 70 °C, whilst the synthesis of sar-DBM was carried out without DIPEA and at ambient temperature.



Scheme 4 - Synthesis of $[\text{CuL}^1]^{2+}$ and $[\text{CuL}^2]^{2+}$.¹



Scheme 5 - Synthesis of $[\text{Mg}(\text{CH}_3)(p\text{-NCS-Ph)sar}]^{2+}$ (**25**) and $[\text{Mg}(\text{CH}_3)(\text{NCS-OEG)sar}]^{2+}$ (**26**).¹¹

A sarcophagine derivative has been coupled to isothiocyanate species *via* the sarcophagine's primary amine (scheme 5).¹¹ Here, Mg^{2+} complexation was used as a secondary amine protection strategy to prevent secondary amine groups from reacting with the isothiocyanate species. $(\text{NH}_2)(\text{CH}_3)\text{sar}$ was used, which possesses only one primary amine, preventing the formation of a species containing two pendant isothiocyanate groups. The coupling reaction between $[\text{Mg}(\text{NH}_2)(\text{CH}_3)\text{sar}]^{2+}$ and 1,4-phenyl-bis(isothiocyanate) was carried out in a microwave reactor with heating to 100 °C, generating $[\text{Mg}(\text{CH}_3)(p\text{-NCS-Ph)sar}]^{2+}$ (**25**, scheme 5) in 45 % yield. Similarly, the coupling reaction between

$[\text{Mg}(\text{NH}_2)(\text{CH}_3)\text{sar}]^{2+}$ and 1,17-dithio-6,9,12-trioxa-2,16-diazaheptadeca-1,16-diene was carried out at 60 °C with the inclusion of triethylamine, generating $[\text{Mg}(\text{CH}_3)(\text{NCS-OEG})\text{sar}]^{2+}$ (**26**, scheme 5) in 39 % yield.

Collectively the literature suggests that elevated reaction temperatures and/or the inclusion of base are required to achieve good yields in sarcophagine coupling reactions to amine reactive species. However, the optimisation study conducted above has shown that increased temperatures and the inclusion of base negatively impact upon the coupling reaction between $[\text{Mg}(\text{NH}_2)_2\text{sar}]^{2+}$ and 3,4-dibromomaleimide-N-hexanoic acid mediated by EEDQ. The likely two limiting factors here are the low stability of the dibromomaleimide group in the presence of base, and the formation of the dialkylated sar-DBM₂ species under these forcing conditions. Although the low yielding synthesis of sar-DBM is a limitation of this work, bioconjugations to antibodies typically require only very small amounts of sar-DBM (usually micrograms), and sufficient amounts of sar-DBM were isolated for this purpose

2.4 Synthesis of sar-DBM-trastuzumab

The conjugation of sar-DBM to an IgG antibody was assessed. Trastuzumab was chosen as a model IgG for two reasons: i) the behaviour and biodistribution of trastuzumab is well-understood since it is widely used for the treatment of HER2 positive breast cancer; ii) the antibody lacks any solvent-accessible free cysteine residues, which otherwise could compete with reduced disulfides (at the antibody hinge region) for sar-dbm. The bioconjugate formed in this reaction is hydrolysed to give a dithiomaleamic acid (DTM), therefore the bioconjugate will be referred to as sar-DTM-trastuzumab.

2.4.1 Conjugation of sar-DBM to trastuzumab monitored by SDS-PAGE

Trastuzumab was received in physiological saline solution (0.9%) and was buffer exchanged into borate buffered saline (BBS, pH 8.5). To decrease the concentration of trace metal ion contaminants, 5 mM EDTA was added to the BBS solution, and then it was treated with chelex resin. This serves two purposes: firstly, the bifunctional chelator may complex trace metal ions decreasing the radiolabelling efficiency of the bioconjugate; secondly, metal ions mediate the reoxidation of reduced disulfide bonds, which can lead to reduced conjugation efficiency. Conjugation between dibromomaleimides and antibodies has been shown to take place efficiently in BBS at pH 8.5. Additionally, at this pH, rapid dibromomaleimide

conjugation is followed by maleimide hydrolysis to yield stable thiomaleamic acid derivatives.⁴

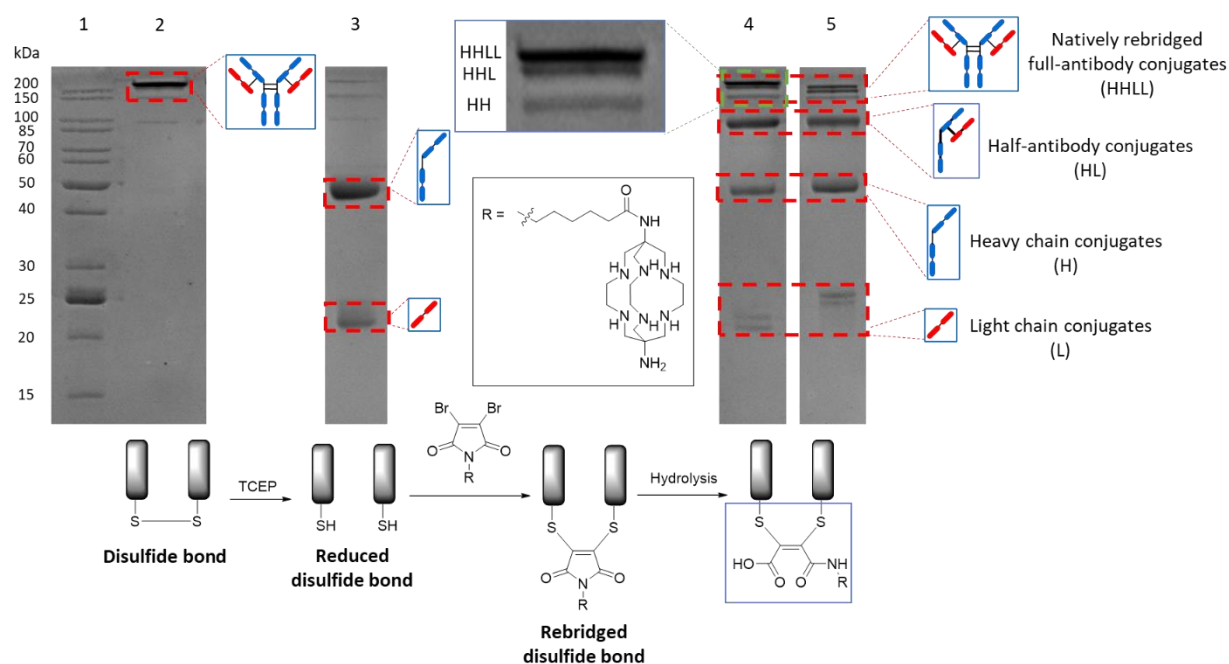


Figure 67 - SDS-PAGE was used to track the progression of a typical conjugation reaction between sar-DBM and trastuzumab. Lane 1 - Molecular weight ladder, lane 2 - trastuzumab, lane 3 - reduced trastuzumab, lane 4 - sar-DTM-trastuzumab, lane 5 - sar-DTM-trastuzumab + DTT.

The progression of dibromomaleimide conjugations can be effectively monitored using sodium dodecyl sulphate–polyacrylamide gel electrophoresis (SDS-PAGE). This analytical technique allows proteins to be separated from a mixture based on their molecular weights. During bioconjugation samples of unmodified trastuzumab (figure 67, lane 2), reduced trastuzumab (figure 67, lane 3), and sar-DTM-trastuzumab (figure 67, lanes 4 and 5) were analysed by SDS-PAGE (figure 67). A molecular weight ladder (figure 67, lane 1) was included, enabling estimation of the molecular weights of analysed proteins/protein fragments. Native unmodified trastuzumab has a high molecular weight (deglycosylated MW 145167 Da) and appears as a single band near the top of the gel (figure 67, lane 2).

First, reduction of trastuzumab was achieved by adding 6 equivalents of tris(2-carboxyethyl)phosphine (TCEP) to the antibody, and incubating the mixture for 2 hours at 37 °C. TCEP was chosen as the reducing agent as it does not react with dibromomaleimide reagents. Reduction can also be achieved using 2-mercaptoethanol, or other thiol based reducing agents. However, using thiol-based

reagents necessitates the removal of excess reducing agent prior to the addition of the dibromomaleimide to prevent competition between the excess reducing agent and the reduced disulfides. Reduction of antibody *interchain* disulfide bonds results in cleavage of the covalent bonds between heavy and light chains. Complete reduction of antibody disulfide groups was evidenced by the presence of just two protein bands (figure 67, lane 2): one for the heavy chain (~50 kDa) and another for the light chain (~20 kDa). Complete reduction is important for dibromomaleimide conjugations since oxidised, bridged disulfide bonds do not react with dibromomaleimides, resulting in lower amounts of cargo attached to antibodies. Under physiological conditions, reduced antibody chains remain associated with one another due to non-covalent interactions (e.g. Van-der Waals forces and hydrogen bonding). However, the denaturing conditions of SDS-PAGE disrupt proteins' non-covalent interactions, allowing separation of non-covalently bound antibody fragments from one another.

When sar-DBM was added to reduced trastuzumab, sar-DTM-trastuzumab conjugates were formed. Four major classes of antibody bioconjugate fragments were formed (HHLL, HL, H, L), along with the two minor antibody fragment products (HHL, HH) (figure 67, lane 4). At the top of the lane a band corresponding to full-antibody conjugate (HHLL) was visible. Half-antibody conjugate fragments (HL) were also generated from the reaction between sar-DBM and reduced trastuzumab (figure 67, lane 4). Lower intensity bands corresponding to heavy chain (H) and light chain (L) species were also present in the sar-DTM-trastuzumab conjugate (figure 67, lane 4). Two other minor fragment products were formed in the conjugation between sar-DBM and trastuzumab, corresponding to a species with two heavy chains and one light chain (HHL) and a species with two heavy chains (HH). These minor products were observed by SDS-PAGE as low intensity bands between the half- and full-antibody bands (figure 67, lane 4, expanded view). Similar to the case of the reduced antibody, under non-denaturing conditions, these antibody fragments are likely to remain associated to one another due to non-covalent interactions.

To assess whether maleimide hydrolysis had taken place, reducing conditions were also used (figure 67, lane 5). Dithiothreitol (DTT) was added to sar-DTM-trastuzumab prior to denaturing during SDS-PAGE sample preparation (reducing conditions). If the conjugate has not undergone hydrolysis, thiol exchange takes

place leading to the presence of significant amounts of heavy and light chain fragments, similar to that observed in the reduced trastuzumab lane (figure 67, lane 3). Comparison of “non-reducing” (figure 67, lane 4) and “reducing” (figure 67, lane 5) lanes revealed that hydrolysis had taken place. Full- and half-antibody bands were present in both lanes and there were minimal differences in the intensity of the bands associated with heavy and light chain species.

SDS-PAGE showed that a significant amount of HL conjugate – the half-antibody fragment - was present in the sample of sar-DTM-trastuzumab (figure 67, lane 4). The formation of HL conjugates is in competition with the formation of full-antibody conjugates (figure 70, figure 73). HL conjugates possess one *interchain* disulfide between the heavy chain and the light chain and can also contain one *intrachain* disulfide on the heavy chain. Whilst the *intrachain* disulfide bond is not structurally required to form HL fragments, its presence precludes the formation of HHLL conjugates by preventing *interchain* disulfide bond formation between heavy chains.

Ideally dibromomaleimides reform disulfide bonds between pairs of reduced thiols (a, figure 68), and so the presence of heavy and light chain fragments indicates sub-optimal conjugation. Protein bands corresponding to heavy chain and light chain species can be produced for two reasons: i) the reduced thiols of the heavy and light chains do not react with sar-DBM to give conjugates; or ii) the reduced thiols of heavy and light chains do react with sar-DBM, but no *interchain* disulfide rebridging takes place (b, figure 68). The minor products HHL and HH are also formed by a combination of these two pathways.

The desired conjugation product is the natively rebridged full-antibody conjugate. There are two main reasons for this:

i) Natively rebridged antibody conjugates are homogeneous and consistently possess a drug to antibody ratio (DAR) of 4 (despite the attachment of a chelator rather than a drug molecule the term “DAR” is used here for DBM-conjugates).⁴ Homogeneous conjugates are desired since they display improved bioactivity *in vivo* compared to heterogeneous conjugates (see 1.4.4).¹²

ii) Full-antibody conjugates most closely mimic unmodified native antibodies, possessing high thermal stability and near-native antibody Fc profiles (FCγR binding or ADCC activity, see 1.5.2).¹³

Whilst a significant proportion of the sar-DBM-trastuzumab analysed was present as the full-antibody conjugate (figure 67, lane 4), the sample was heterogeneous containing other fragments including HHL, HH, HL, H, and L conjugates. This mixture indicates a sub-optimal conjugation has taken place reaction between sar-DBM and trastuzumab.

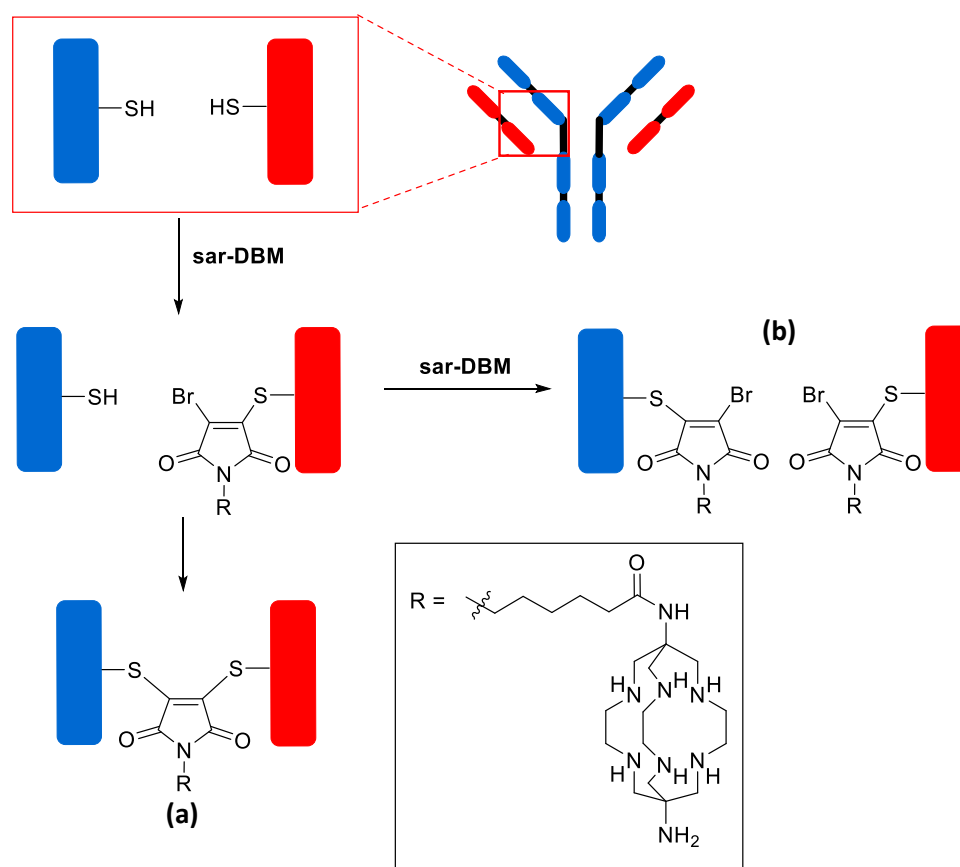


Figure 68 - The conjugation reaction between sar-DBM and trastuzumab to give desired rebridged species (a) and undesired non-rebridged conjugates (b).

2.4.2 The effect of varying hydrolysis periods on the bioconjugation reaction between sar-DBM and trastuzumab

The impact of varying the post-conjugation hydrolysis period for the conjugation of sar-DBM to trastuzumab was assessed (figure 69). 8 eq. of sar-DBM were added to reduced trastuzumab and incubated at 37 °C for 5 min, 24 h, or 48 h. A sample of bioconjugate was taken at each hydrolysis time point, mixed with loading buffer

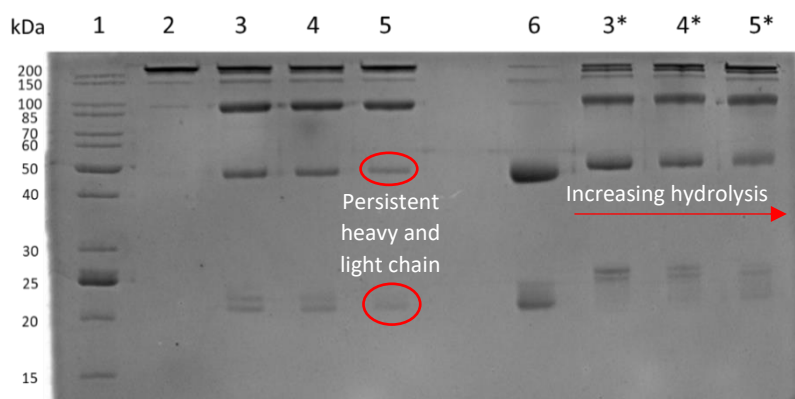


Figure 69 - The conjugation reaction between reduced trastuzumab and 8 eq. sar-DBM was monitored over time by SDS-PAGE. Lane 1 - molecular weight ladder, lane 2 - trastuzumab, lane 3 - 5 min post-conjugation, lane 4 - 24 h post-conjugation, lane 5 - 48 h post-conjugation, lane 6 - reduced trastuzumab, lanes 3*-5* - as in lanes 3-5 + DTT.

and denatured at 65 °C. The samples of sar-DBM-trastuzumab from each post-conjugation hydrolysis time point were compared by SDS-PAGE under non-reducing and reducing conditions (figure 69). After five minutes incubation with sar-DBM, a large proportion of reduced disulfides had been rebridged as evidenced by the appearance of full- and half-antibody conjugates (figure 69, lane 3). Under reducing conditions (figure 69, lane 3*), a significant proportion of the full- and half-conjugates remained. However, hydrolysis at this time point was incomplete as shown by an increase in the intensity of the bands associated with heavy and light chain fragments under reducing conditions relative to non-reducing conditions (figure 69, lane 3). As the duration of the post-conjugation hydrolysis period was increased from 5 min to 24 h and then to 48 h, the proportion of hydrolysed sar-DBM-trastuzumab increased. This was evidenced by a closer match between lanes 4 and 4*, 5 and 5* as compared to lane 3 and 3* (figure 69). It was also noted that under non-reducing conditions, the intensity of the bands associated with heavy and light chain decreased from 5 min to 48 h (figure 69, lanes 3 to 5). This is likely due to gradual reoxidation of unmodified reduced thiols in solution over time, rather than more efficient dibromomaleimide conjugation at these time points. Comparing lanes 5 and 5* (figure 69), minimal changes were observed indicating that hydrolysis is nearing completion after 48 h. Therefore, in subsequent bioconjugation reactions of sar-DBM to trastuzumab, the conjugation reaction was left at 37 °C for 48 h to promote complete hydrolysis. Whilst these conditions

promote complete conjugate hydrolysis, small amounts of undesired heavy and light chain species were still observed (figure 69, lane 5).

2.4.3 The effect of varying the number of sar-DBM equivalents on the bioconjugation reaction between sar-DBM and trastuzumab

The number of equivalents of dibromomaleimide added in antibody conjugation reactions has a significant impact on the heterogeneity of the bioconjugate formed (figure 70). The addition of too few equivalents of DBM results in 'under-conjugation' with unmodified reduced thiols remaining post-conjugation (which can potentially oxidise to reform disulfide bonds). Too many equivalents of DBM can result in 'over-conjugation'. To assess the influence of the number of equivalents of sar-DBM, conjugation to trastuzumab was undertaken using 8, 16 or 24 eq. of sar-DBM. Bioconjugates were left to hydrolyse at 37 °C for 48 h and then analysed by SDS-PAGE under non-reducing and reducing conditions (figure 71).

When the amount of sar-DBM added was increased from 8 eq. to 16 eq. and then 24 eq. there was no observed decrease in the intensity of the bands associated with heavy and light chain species. Under all three different reaction conditions, efficient dithiol rebridging took place generating mostly full- and half-antibody conjugates. Interestingly, no evidence of over-conjugation was observed when 16 or 24 eq. of sar-DBM were used as evidenced by no change in the intensity of the bands associated with heavy and light chain species (figure 71, lanes 4 and 5). Bioconjugates were also analysed under reducing conditions (figure 71, lanes 3*-5*). There was a negligible increase in the amount of heavy and light chain formed upon treatment with DTT (figure 71, lanes 3*-5*) relative to when non-reducing conditions were used (figure 71, lanes 3-5), indicating complete hydrolysis to afford conjugates that are stable towards excess thiol. Following conjugation under optimised conditions (8 eq. sar-DBM, 48 h hydrolysis period, 37 °C), sar-DBM-trastuzumab was isolated from excess reagents using a combination of size exclusion methods including separation on a PD10 size exclusion column, and spin filtration through a 50 kDa MWCO spin filter.

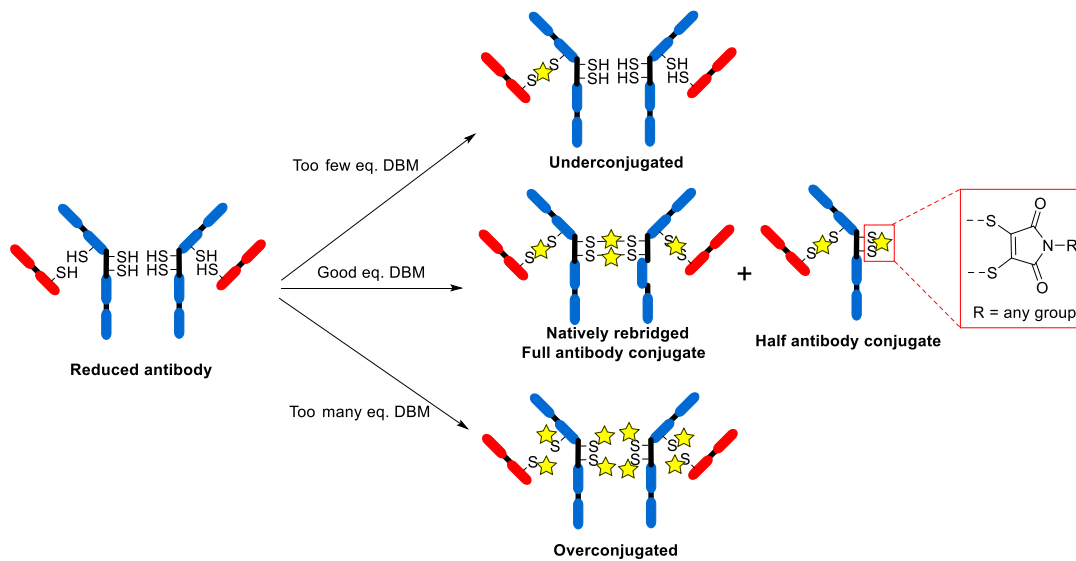


Figure 70 - The number of equivalents of DBM can lead to under-conjugation or over-conjugation. Note that full-antibody conjugate formation is in competition with half-antibody conjugate formation *via* intrachain disulfide bond formation. Here an illustrative dibromomaleimide is used where R = any group.

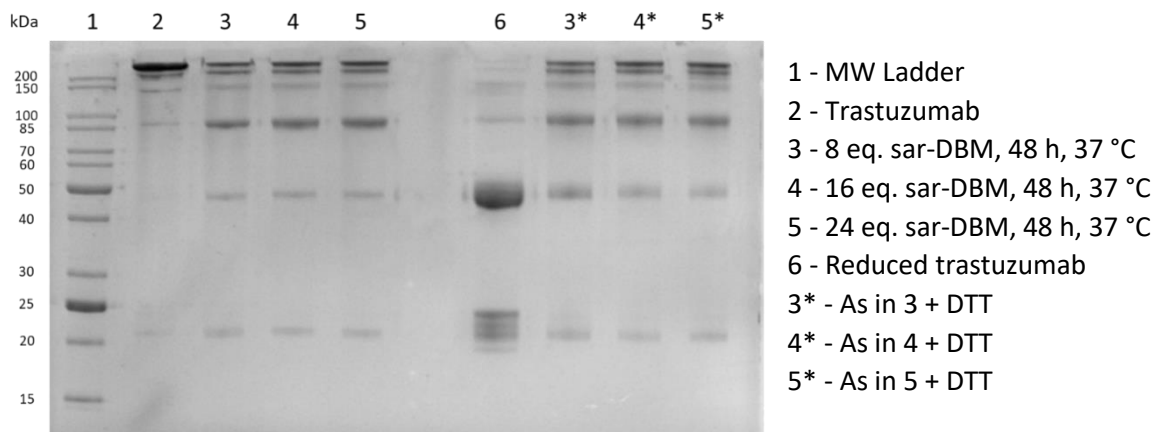


Figure 71 - The conjugation reaction between reduced trastuzumab and varying equivalents of sar-DBM was monitored by SDS-PAGE.

2.4.4 Mass spectrometry of sar-DTM-trastuzumab

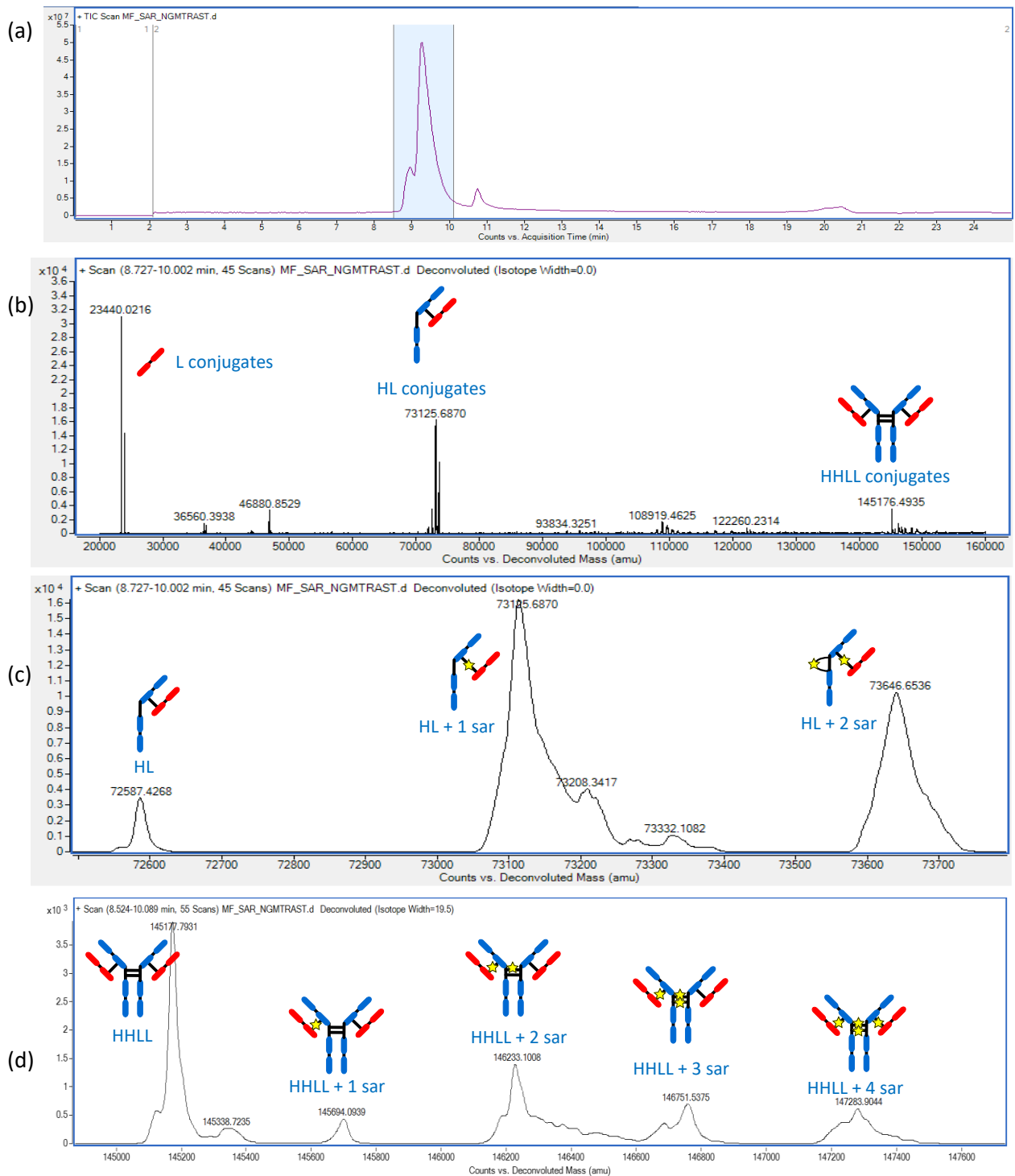


Figure 72 - SE-HPLC separation of sar-DTM-trastuzumab (highlighted region) from other sample components. High resolution ESI deconvoluted mass spectrum of sar-DTM-trastuzumab: (b) full spectrum, (c) expanded view of the region associated with half-antibody conjugates, and (d) expanded view of the region associated with full-antibody conjugates (see table 3 for assignments).

Table 3: ESI-MS data for trastuzumab and sar-DTM-trastuzumab

Antibody species	Counts vs Deconvoluted Mass (amu)	
	Observed	Calculated
trastuzumab		
HHLL	145176	145167
HL	72587	72584
H	-	49150
L	23440	23440
sar-DTM-trastuzumab		
L + 1 sar	23970	23980
HL + 1 sar	73126	73116
HL + 2 sar	73646	73639
HHLL + 1 sar	145694 (weak)	145709
HHLL + 2 sar	146233	146232
HHLL + 3 sar	146751	146755
HHLL + 4 sar	147283	147278

Mass spectrometry was used to better understand the homogeneity and speciation of the sar-DTM-trastuzumab conjugate (figure 72, table 3). Prior to MS analysis PNGase F was used to deglycosylate the sample. Monoclonal antibodies are subjected to N-glycosylation during production (see 1.3.1), leading to between 3-5 abundant glycoforms in most cases.¹⁴ Unless the glycans are of interest to the study, they are usually removed from the antibody during sample preparation for mass spectrometry analysis. Deglycosylation results in a simplification of the mass spectral signals.

After deglycosylation, the sample contained a mixture of deglycosylated immunoconjugate (the analyte of interest) and PNGase F. Separation of these components was achieved using SE-HPLC (figure 72a) prior to mass spectrometry analysis. Figure 72b shows mass spectra obtained for sar-DTM-trastuzumab - this data is summarised in table . A range of sar-DTM-trastuzumab fragments were detected, including light chain, half-antibody, and full-antibody conjugates. Unmodified light chain, half-antibody and full-antibody were also detected. Signals corresponding to sar-DTM-trastuzumab conjugates (figure 72) were broader than those corresponding to previously characterised DBM conjugates.^{13,15} This behaviour for sar-DTM-trastuzumab has previously been attributed to trace metal

ion complexation, which leads to a range of species that are distinguishable by mass spectrometry leading to broader signals.¹⁶

MS analysis (figure 72, table 3) showed that the light chain conjugate contained just one sarcophagine moiety as expected due to the presence of a single thiol attachment point on the light chain. Ideally this light chain conjugate would only be a transient intermediate, undergoing a second Michael addition with a heavy chain thiol resulting in disulfide rebridging (a, figure 68). Observation of light chain conjugate indicates incomplete, non-native thiol rebridging between sar-DBM and trastuzumab. As discussed, it is possible that before the second Michael addition takes place (rebridging), another molecule of sar-DBM reacts with the thiol on the adjacent heavy chain, preventing the formation of a rebridged disulfide (b, figure 68). Alternatively, after the first Michael addition, the intermediate species undergoes hydrolysis, preventing the second Michael addition. This behaviour has been previously observed for dibromomaleimide conjugation to a Gbr2 adapter protein at pH 8 (see 4.2.1, figure 112b).²⁰ Unmodified light chain was also detected in the mass spectrum for sar-DTM-trastuzumab, indicating incomplete conjugation between light chain thiols and sar-DBM.

The expanded view mass spectrum shown in figure 72c reveals the presence of two signals corresponding to half-antibody conjugates. Conjugation leads to the species containing two sarcophagine moieties (HL + 2 sar, figure 73), likely consisting of one *interchain* rebridged disulfide between the heavy and light chains, and one *intrachain* disulfide on the heavy chain. Incomplete conjugation also generated the half-antibody conjugate containing just one sarcophagine moiety (HL + 1 sar). In this species, sar-DBM either rebridges an *interchain* disulfide bond between the heavy and light chains, or it forms an *intrachain* disulfide bridge on the heavy chain thiols (figure 20). In the case of *intrachain* disulfide bridge formation on the heavy chain, a further step is required to reform the disulfide bond between heavy and light chains by reoxidation to generate a half-antibody conjugate (figure 20).

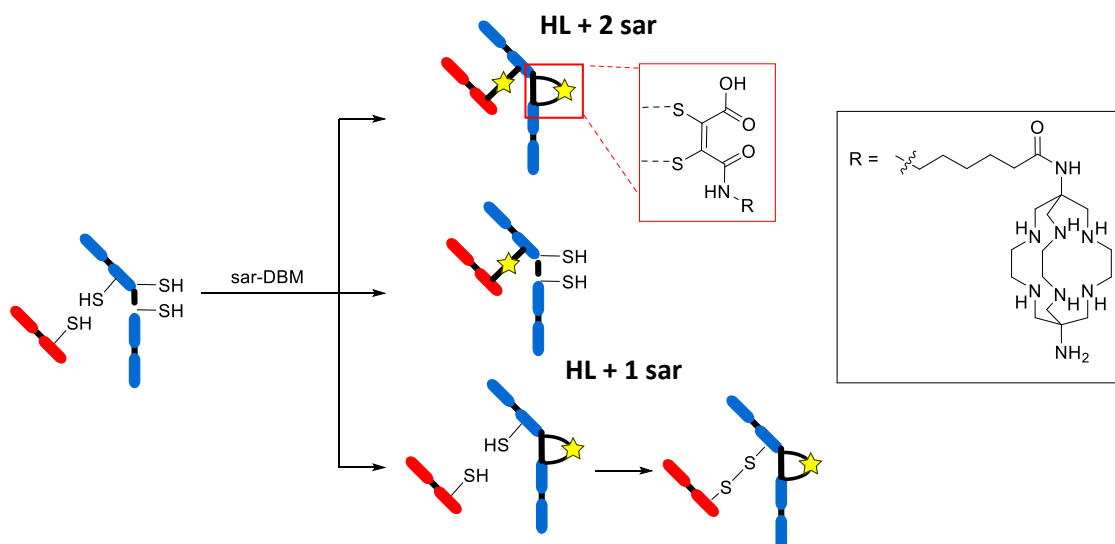


Figure 73 - Formation and disulfide structure for HL + 1 sar, and HL + 2 sar.

Figure 72d shows an expanded view of the mass spectrum containing signals corresponding to full-antibody conjugates. Multiple conjugates were detected including full antibody conjugate bearing one (HHLL + 1 sar), two (HHLL + 2 sar), three (HHLL + 3 sar), and four (HHLL + 4 sar) sarcophagine moieties. HHLL + 4 sar is the desired full-antibody conjugate resulting from native disulfide rebridging. Full-antibody conjugates with DAR<4 can be formed because of incomplete conjugation, followed by reoxidation of unmodified thiols to reform disulfide bonds. Native unmodified trastuzumab was also detected despite complete reduction of the antibody prior to adding sar-DBM. This species was generated by complete, and native reoxidation of all reduced disulfide bonds present within the antibody.

2.4.5 Comparison of sar-DTM-trastuzumab with reported alkyne-DTM-trastuzumab conjugates (**27**-trastuzumab)

As mentioned above, the dibromomaleimide derivative containing an alkyne group (alkyne-DBM, **27**, scheme 3, figure 74) has been previously studied and examples of SDS-PAGE data and mass spectrometry data exist for the conjugate (alkyne-DTM-trastuzumab). Comparing these data with SDS-PAGE and mass spectrometry data obtained for sar-DTM-trastuzumab allows for comparison of the relative reactivity, and overall conjugation efficiency generated by each dibromomaleimide derivative. Importantly the conjugation reaction between alkyne-DBM and trastuzumab was carried out under the same conditions as the conjugation reaction between sar-

DBM and trastuzumab (BBS, pH 8.5, 6 eq. TCEP 2 h at 37 °C, and 8 eq. of DBM reagent).

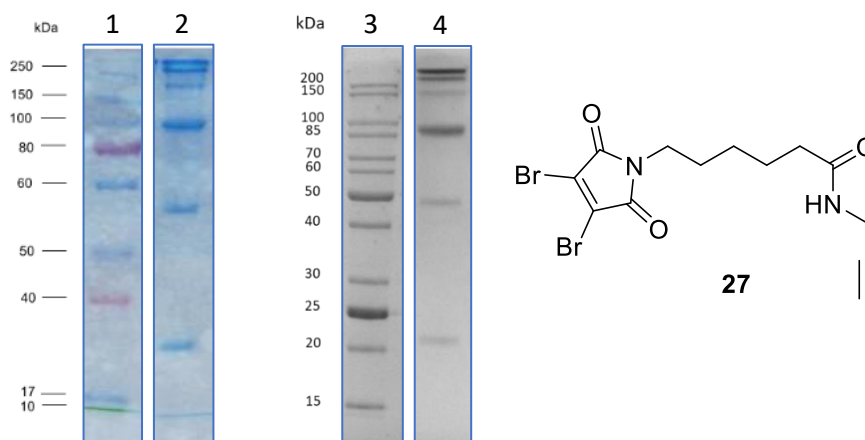


Figure 74 - Comparison of SDS-PAGE data obtained for alkyne-DTM-trastuzumab⁶ and sar-DTM-trastuzumab. Lane 1 - molecular weight ladder for lane 2, lane 2 - alkyne-DTM-trastuzumab, lane 3 - molecular weight ladder for lane 4, lane 4 - sar-DTM-trastuzumab. The structure of alkyne-DBM (27) is also given.

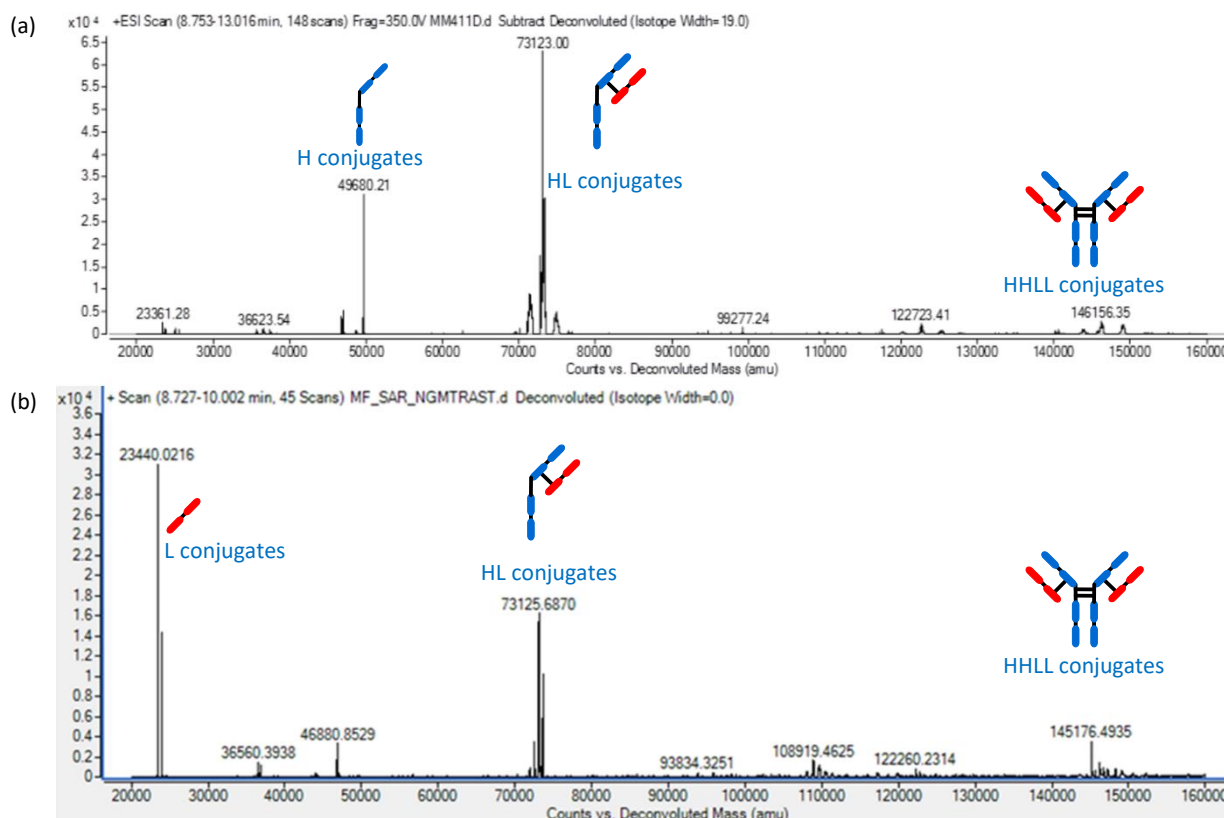


Figure 75 - A comparison of the mass spectra obtained for (a) 27-trastuzumab,⁶ and (b) sar-DTM-trastuzumab.

Figure 74 compares SDS-PAGE data obtained for alkyne-DTM-trastuzumab and sar-DTM-trastuzumab.⁶ Comparing lanes 2 and 4 (figure 74), the conjugates are similar

in terms of the relative intensities of the protein bands corresponding to each antibody fragment. Figure 75 compares the mass spectrum for sar-DTM-trastuzumab with the mass spectrum of alkyne-DTM-trastuzumab from the literature.⁶ This comparison shows that both conjugates contain a mixture of antibody fragment products including HHLL and HL conjugates. The mass spectrum of alkyne-DTM-trastuzumab (figure 75a) shows a heavy chain conjugate bearing two alkyne moieties (49680.21 amu). In contrast, the mass spectrum of sar-DTM-trastuzumab (figure 22b) shows no evidence of heavy chain conjugates. Note that the peak at 46880.85 amu is below the mass of an unmodified heavy chain (49150 amu). There is little evidence of light chain conjugates in the mass spectrum of alkyne-DTM-trastuzumab (figure 75a). However, light chain species are apparent in the mass spectrum of sar-DTM-trastuzumab (figure 75b). As previously discussed, the mass spectra obtained for sar-DTM-trastuzumab (figure 72) shows the presence of unmodified antibody fragments indicative of incomplete conjugation when sar-DBM is added to reduced trastuzumab. The mass spectrum for alkyne-DTM-trastuzumab (figure 75a) contains almost no evidence of unmodified trastuzumab fragments, which suggests a near-complete conjugation reaction took place between alkyne-DBM and trastuzumab.

Collectively SDS-PAGE and mass spectrometry show that incomplete conjugation has taken place between sar-DBM and trastuzumab to give a mixture of antibody fragments with varying DARs.

2.5 ⁶⁴Cu radiolabelling of sar-DTM-trastuzumab

To determine whether sar-DTM-trastuzumab could be radiolabelled, the conjugate was added to a solution containing ⁶⁴Cu²⁺. Mild radiolabelling conditions were used (pH 7, at ambient temperature) since the immunoconjugate is susceptible to denaturing under highly acidic/alkaline conditions (pH < 5.5 or pH > 8.5) and at elevated temperatures (> ~40 °C) (see 1.3.1). Sarcophagines typically display good radiolabelling characteristics with ⁶⁴Cu²⁺ under these mild conditions.

First, the impact of bioconjugate concentration on the radiochemical yield was assessed for the radiolabelling of sar-DTM-trastuzumab with ⁶⁴Cu²⁺. Samples with a range of sar-DTM-trastuzumab concentrations (1 nM - 100 μM) were radiolabelled with ⁶⁴Cu²⁺. Radiochemical yields (figure 76a) were determined using instant thin layer chromatography (ITLC) with radio-detection. Citrate buffer (0.1 M, pH 5.5)

was used as the mobile phase. Development of ITLC strips using this eluent causes protein-bound radioactivity to remain at the base line ($R_f < 0.5$), and non-protein-bound radioactivity to move towards the solvent front ($R_f > 0.5$). It is important to note that colloidal ^{64}Cu also has an $R_f < 0.5$, and so can lead to overestimation of radiochemical yields when using ITLC. Aliquots of the $^{64}\text{Cu}^{2+}$ stock solution were taken periodically and analysed by ITLC where it was found that $>99\%$ of ^{64}Cu radioactivity had an $R_f > 0.5$ suggesting minimal colloid formation. Beyond 5 min incubation time, radiochemical yields did not change indicating complete radiolabelling at this time-point demonstrating the well-documented ability of sarcophagines to rapidly form complexes with Cu^{2+} under mild conditions.⁹ Radiochemical yields increased as the concentration of sar-DTM-trastuzumab was increased. Near quantitative ($>99.5\%$) radiochemical yields were obtained at a bioconjugate concentrations of $10\ \mu\text{M}$ and $100\ \mu\text{M}$. A lower radiochemical yield of 77.2% was achieved at a bioconjugate concentration of $1\ \mu\text{M}$. Below this concentration, the radiochemical yields were considerably lower - 16.2% at $100\ \text{nM}$, 1.9% at $10\ \text{nM}$, and 1.1% at $1\ \text{nM}$.

Radiolabelling was also assessed by SE-HPLC (figure 76b). Phosphate buffered saline (PBS) with added EDTA ($5\ \text{mM}$) was used as the mobile phase. ^{64}Cu -sar-DTM-trastuzumab had a retention time of $7.75\ \text{min}$ (figure 76b, black trace) consistent with the retention time of unmodified trastuzumab (figure 76b, purple trace). A control experiment was performed where $^{64}\text{Cu}^{2+}$ was added to trastuzumab and allowed to react for $5\ \text{min}$. SE-HPLC (figure 76b, blue trace) revealed that only a negligible amount ($< 1\%$) of ^{64}Cu was bound to the native antibody. In this control experiment, the majority of the ^{64}Cu was eluted with a retention time of $11.58\ \text{min}$ corresponding to $[\text{}^{64}\text{Cu}(\text{EDTA})]^{2-}$ (figure 76b, green trace). In contrast, when $^{64}\text{Cu}^{2+}$ was added to sar-DTM-trastuzumab, near-quantitative ($>98\%$) radiochemical yields were achieved at a specific activity of $43.6\ \text{MBq}\ \text{mg}^{-1}$, corresponding to a molar activity of $6.33\ \text{GBq}\ \mu\text{mol}^{-1}$.

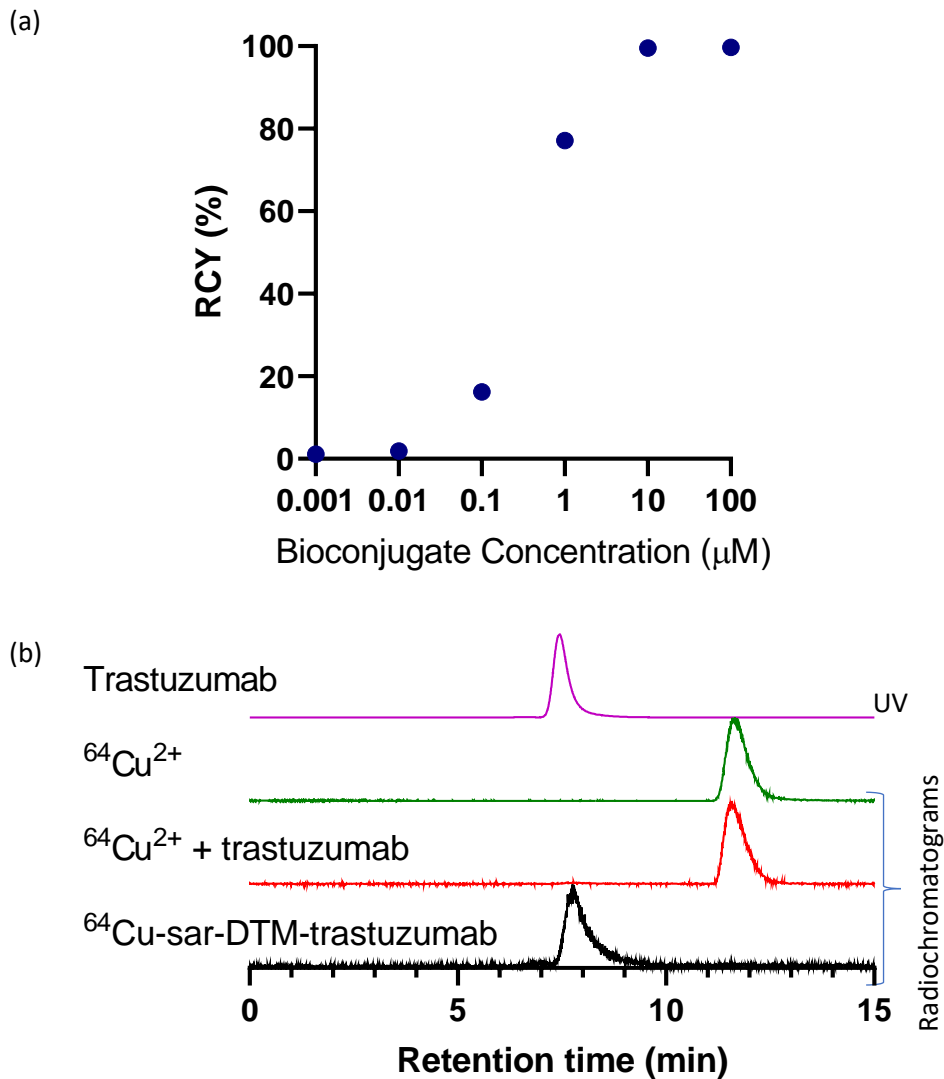


Figure 76 - a) Radiochemical yields for the reaction of $^{64}\text{Cu}^{2+}$ with sar-DTM-trastuzumab at different concentrations (100 μM , 10 μM , 1 μM , 100 nM, 10 nM, and 1 nM) of immunoconjugate at ambient temperature for 5 min. b) SE-HPLC radiochromatograms: UV trace (280 nm) for trastuzumab (purple); radiochromatograms for $^{64}\text{Cu}^{2+}$ (green), $^{64}\text{Cu}^{2+}$ + trastuzumab (red), and ^{64}Cu -sar-DTM-trastuzumab (black).

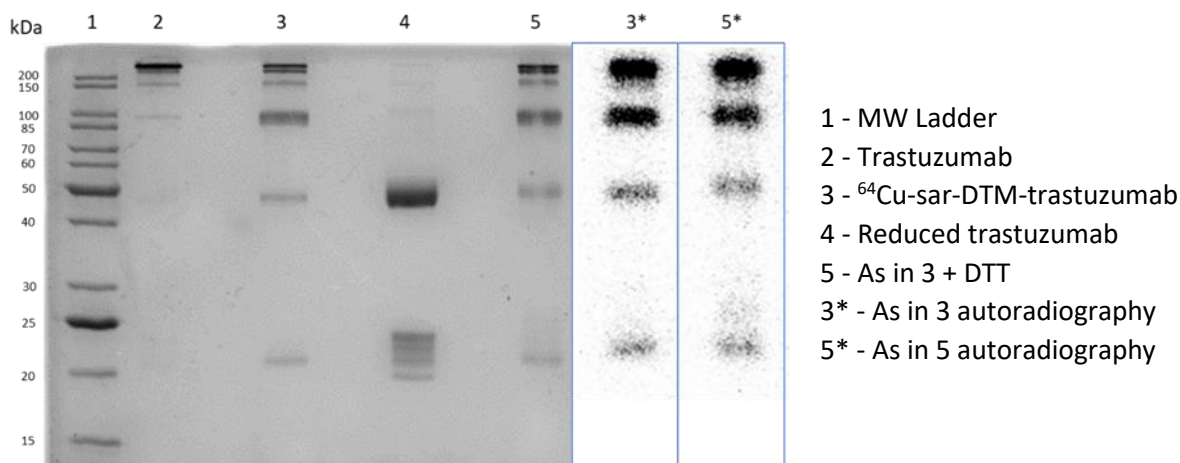


Figure 77 - SDS-PAGE bright light image (left) and autoradiography image (right) of ^{64}Cu -sar-DTM-trastuzumab.

The maximum specific activity achieved for ^{64}Cu -sar-DTM-trastuzumab is lower than specific activities observed for other ^{64}Cu -sar-antibody conjugates in the literature. A carboxylic acid bearing sarcophagine (L_1 , scheme 4) has been conjugated to the antibody rituximab *via* the amines of lysine side chains where an average loading of 0.5 ± 0.1 chelators per antibody was achieved.¹⁷ This bioconjugate was then radiolabelled with $^{64}\text{Cu}^{2+}$ to a specific activity of approximately 353 MBq/mg. In another study, $[\text{Mg}(\text{CH}_3)(p\text{-NCS-Ph})\text{sar}]^{2+}$ (scheme 5) was conjugated to trastuzumab *via* amines on lysine residues achieving an average loading of 1.3 ± 0.3 chelators per antibody.¹¹ After removing Mg^{2+} , this conjugate was radiolabelled with $^{64}\text{Cu}^{2+}$ to a specific activity of 5.4 GBq/mg.

^{64}Cu -sar-DTM-trastuzumab was analysed by SDS-PAGE (figure 77) to determine the relative distribution of ^{64}Cu radioactivity among the antibody fragments within the sample. The gel was imaged using bright light imaging, and then a phosphor imager was used to obtain autoradiography images. Comparison of these images shows that the radioactivity signal from the radiolabelled immunoconjugate was coincident with the stained protein bands corresponding to “full” and “half” antibody (figure 77, lanes 3, 3*). Quantitative analysis showed that 41.1% of ^{64}Cu signal was associated with full antibody species, 33.4% was associated with half-antibody species, 14.5% was associated with heavy chain fragments, and 10.6% was associated with light chain fragments. ^{64}Cu -sar-DTM-trastuzumab was also analysed by SDS-PAGE under reducing conditions (figure 77, lane 5*). The bioconjugate was stable towards thiol-mediated degradation as shown by the coincident radioactivity signal and stained protein bands (figure 77, lanes 5 and 5*).

2.6 Serum stability of ^{64}Cu -sar-DTM-trastuzumab

As previously discussed (see 1.3.2), the stability of a radiolabelled bioconjugate is crucial. Degradation of radiotracer before it has accumulated at its target can lead to reduced target tissue to non-target tissue contrast, and reduced image quality. Intravenously administered radiotracers are exposed to blood before they accumulate at their target tissues. Since antibodies circulate for 15 – 30 days in the blood, radioimmunoconjugates must be highly stable in this environment.¹⁸ Serum (or plasma) makes up 55% of whole blood by volume and contains a mixture of proteins, peptides and small molecules. Many of these contain one or more reactive thiols, which have the potential to contribute to bioconjugate degradation. Prior to hydrolysis, dithiomaleimide conjugates are susceptible to thiol exchange reactions (see 1.7.2). Thiols such as 2-mercaptoethanol, or glutathione have been purposely added to dithiomaleimide conjugates, leading to thiol exchange resulting in cleavage of thioether bonds to regenerate the unmodified thiol-bearing biomolecule.^{19,20}

It is widely accepted that copper ions bind to albumin and/or transcuprein in the blood.²¹ Albumin possesses a high affinity copper binding site at its N-terminus involving a histidine residue (K_d 10^{-12} – 10^{-17} M),²¹ whilst transcuprein has a higher affinity (K_d 10^{-17} – 10^{-19} M) for copper than albumin and is able to bind two copper ions in its tetrameric form.²² Extracellular superoxide dismutase is also known to bind copper in the blood although this protein is much less abundant (53.6 ± 2.5 ng/ml)²³ than albumin ($33 - 52$ mg/mL)²⁴ or transcuprein (2.73 ± 0.765 mg/mL)²⁵. These high affinity serum proteins directly compete with the chelator for binding to $^{64}\text{Cu}^{2+}$.

To assess the serum stability of ^{64}Cu -sar-DTM-trastuzumab a sample of the bioconjugate was added to human serum to give a final concentration of 0.58 mg of bioconjugate per 1 mL of serum, and incubated at 37 °C. This concentration was chosen to achieve a 1 in 10 dilution of bioconjugate solution in human serum. Aliquots were taken for analysis by SE-HPLC at 0 h, 20 h, and 40 h (figure 78). At these time points, the radiochromatograms showed a single species, corresponding to ^{64}Cu -sar-DTM-trastuzumab with a retention time of 7.75 min. The high serum stability of ^{64}Cu -sar-DTM-trastuzumab is in good agreement with the literature where high stability has been observed for dibromomaleimide-trastuzumab conjugates over 7 days in serum.¹⁵ Additionally, these results confirm the high

serum stability of the ^{64}Cu -sarcophagine radio-complex as previously observed in the literature where very high stability has been observed over 2 days in serum.^{3,17,26}

A control experiment was conducted where $^{64}\text{Cu}^{2+}$ was added to serum and incubated at 37 °C for 20 h and then analysed by SE-HPLC (figure 78, red trace). Two signals with retention times of 8.53 min and 11.58 min were observed. The peak at 8.53 min most likely corresponds to serum protein-bound ^{64}Cu radioactivity, including ^{64}Cu -albumin species. The late eluting peak at 11.58 min has a retention time consistent with non-protein bound ^{64}Cu radioactivity, and is attributed to $[\text{}^{64}\text{Cu}(\text{EDTA})]^{2-}$. Interestingly, these two peaks in the control experiment are poorly resolved, and there is considerable overlap between the peaks. This observation is most likely due to competition for ^{64}Cu binding between serum proteins and EDTA in solution under HPLC conditions.

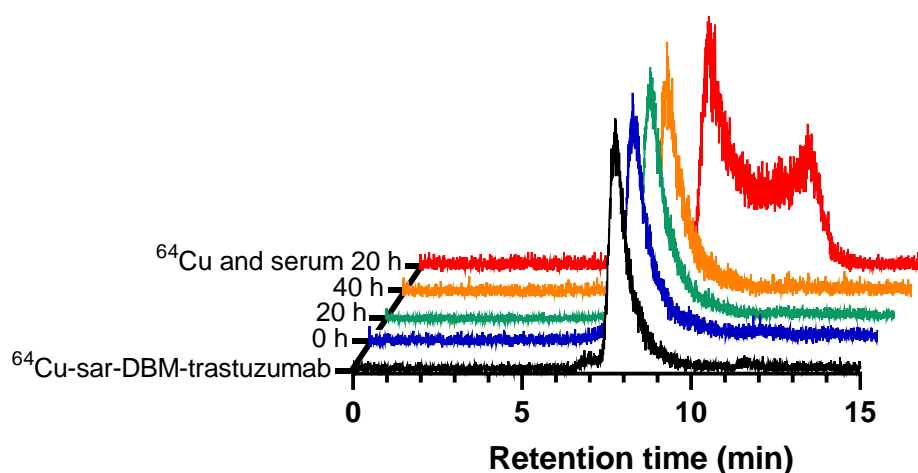


Figure 78 - SE-HPLC chromatograms of ^{64}Cu -sar-DBM-trastuzumab (black) after incubation with human serum for 0 h (blue), 20 h (green), and 40 h (orange). A control experiment was also carried out by incubating $^{64}\text{Cu}^{2+}$ in serum at 37 °C for 20 h (red).

2.7 *In vitro* specificity of ^{64}Cu -sar-DBM-trastuzumab for the HER2 receptor

This *in vitro* study was carried out in collaboration with Dr Truc Pham who assisted in the design and execution of this experiment. Modification of an antibody can result in decreased binding to its target receptor (see 1.4.4). To assess the impact of trastuzumab modification upon the specificity and binding of ^{64}Cu -sar-DBM-trastuzumab to HER2 receptors, a cell uptake study (figure 79a) was conducted using human ovarian cancer cells (SKOV3 cells), which overexpress HER2.²⁷ ^{64}Cu -

sar-DTM-trastuzumab was added to SKOV3 cells and then incubated on ice for 1 h. After incubation the supernatant was removed, cells were washed and harvested, and cell-bound ^{64}Cu radioactivity was quantified by gamma counting. Results showed that 2.14 ± 0.69 % of added radioactivity remained bound to the SKOV3 cells after washing. When unmodified trastuzumab ($2 \mu\text{M}$) was added to the SKOV3 cells, uptake was significantly ($p < 0.05$) decreased (0.44 ± 0.07 %). To further demonstrate that the radioimmunoconjugate had retained its specificity for HER2, ^{64}Cu -sar-DTM-trastuzumab was added to SKOV3 cells (2×10^5 cells) in the presence of increasing concentrations of unmodified trastuzumab. This effectively generates a 'blocking gradient' where the radioimmunoconjugate faces increasing competition with trastuzumab for the HER2 receptor. After incubation the supernatant was removed, cells were washed and harvested, and cell-bound ^{64}Cu radioactivity was quantified by gamma counting. ^{64}Cu -sar-DTM-trastuzumab showed uptake in SKOV3 cells with uptake inhibited by increasing concentrations of unmodified trastuzumab (figure 79b). Previous cell binding studies have used the same concentration range (1-2000 nM) of unmodified trastuzumab to achieve target receptor (HER2) blocking for a radiolabelled trastuzumab bioconjugate. Collectively, the data presented in figure 79 demonstrates that ^{64}Cu -sar-DTM-trastuzumab has specificity for the HER2 receptor. Literature binding studies involving trastuzumab bioconjugates and SKOV-3 cell lines often generate uptake percentages between 80%-90% radioactivity binding.²⁸ The comparably low uptakes seen in this thesis are likely caused by either: i) insufficient number of cells (low receptor concentration), or ii) low specific activity leading to effective blocking of the target receptor by non-radioactive trastuzumab in the administered bioconjugate sample.

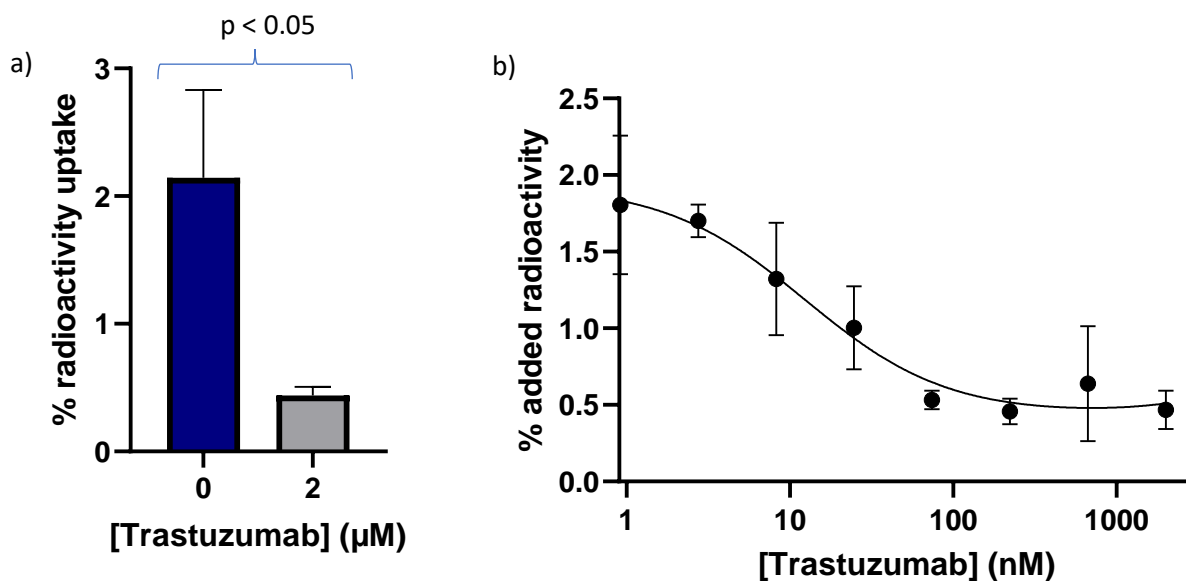


Figure 79 - a) % of radioactivity uptake for ^{64}Cu -sar-DTM-trastuzumab (10 kBq, 1 μg total added compound) in SKOV3 cells (2×10^5 cells) with (2 μM) and without (0 μM) unmodified trastuzumab. The difference in uptake is significant with $p < 0.05$. **b)** Cell binding study of ^{64}Cu -sar-DTM-trastuzumab with SKOV3 cells (2×10^5 cells) in the presence of increasing concentrations of unmodified trastuzumab. Error bars show standard deviation. Binding studies were carried out in experimental triplicate (n=3, n=3, n=2).

2.8 Evaluation of ^{64}Cu -sar-DTM-trastuzumab in healthy mice

This *in vivo* study was carried out collaboratively. Experimental design was carried out with guidance from Dr Jana Kim, Dr Kavitha Sunassee, Dr Truc Pham and George Firth. Animal husbandry, administration of the radioimmunoconjugate, and PET/CT imaging was carried out by Dr Jana Kim and Dr Truc Pham. Dissection for biodistribution was conducted in collaboration with Dr Charlotte Rivas and Dr Truc Pham. Lastly, PET image analysis was conducted in collaboration with Dr Truc Pham.

To demonstrate the *in vivo* stability and biodistribution of ^{64}Cu -sar-DTM-trastuzumab in the absence of diseased tissues, healthy mice were administered the radioimmunoconjugate and assessed over 48 hours. Future work with ^{64}Cu -sar-DTM-trastuzumab or similar radioimmunoconjugates may involve the use of xenograft tumour models (see 4.2.3). Xenograft tumours cannot be grown effectively in immunocompetent mice since non-self-markers (e.g. major histocompatibility complex 1) on the surface of the cancer cells lead to host immune system-mediated cancer cell death, preventing the growth and

development of tumours. Therefore, NOD scid gamma (NSG) mice were chosen for this proof-of-concept study due to their immunodeficiency.

2.8.1 *Ex vivo* biodistribution of ^{64}Cu -sar-DTM-trastuzumab in healthy mice
 ^{64}Cu -sar-DTM-trastuzumab was administered intravenously (*via* tail vein) to mice under anaesthesia. Groups of mice were culled at 2 h, 24 h, and 48 h p.i, dissected, and their organs weighed, and gamma counted. The *ex vivo* biodistribution of ^{64}Cu -sar-DTM-trastuzumab was then evaluated as a percentage of the injected dose per gram of tissue (% ID/g) for each organ harvested (figure 80). Blood was also taken by cardiac puncture, for analysis.

A range of bifunctional chelators have been conjugated to the antibody rituximab and radiolabelled with $^{64}\text{Cu}^{2+}$.¹⁷ Comparing the biodistributions generated by the radioimmunoconjugates showed that less stable radiocomplexes such as ^{64}Cu -DTPA (see 1.3.3) were rapidly cleared from the blood pool, with ^{64}Cu radioactivity accumulating in the liver, before being excreted into the faeces within 48 h. In contrast, radioimmunoconjugates containing more stable ^{64}Cu -radiocomplexes using chelators such as NOTA (see 1.3.3) or sarcophagine displayed prolonged retention in the blood pool over 48 h, with minimal liver uptake and minimal faecal excretion. The biodistribution study for ^{64}Cu -sar-DTM-trastuzumab (figure 80) showed that a significant proportion of ^{64}Cu radioactivity remained in the blood pool over the period studied as is typical for highly stable radioimmunoconjugates. The amount of radioactivity in the blood slowly decreased from 45.6 ± 4.3 %ID/g at 2 h p.i. to 18.7 ± 1.9 %ID/g at 48 h p.i.

Biodistribution data for ^{64}Cu -sar-DTM-trastuzumab (figure 80) showed limited uptake in the liver after 2 h (10.3 ± 1.0 %ID/g) falling to 8.2 ± 0.6 %ID/g after 24h and 6.5 ± 0.5 % after 48 h. This low uptake and gradual clearance of ^{64}Cu radioactivity in the liver highlights the high stability of the $[\text{}^{64}\text{Cu}(\text{sar})]^{2+}$ radiocomplex, in agreement with the literature.¹⁷ Biodistribution data showed that uptake and retention of ^{64}Cu radioactivity occurred in some healthy tissues (figure 80). Notably the skin, uterine horn, and ovaries - healthy tissues known to express HER2 - displayed either increased uptake or persistent retention of ^{64}Cu radioactivity over the course of the study.²⁹⁻³¹ This observation supports the hypothesis that ^{64}Cu -sar-DTM-trastuzumab retains specificity and affinity for HER2. In the skin, uptake increased from 1.0 ± 0.2 % ID/g at 2 h p.i to 4.9 ± 0.7 % ID/g at 24 h p.i. Retention was seen 48 h p.i. where 5.3 ± 0.4 % ID/g was present in the skin.

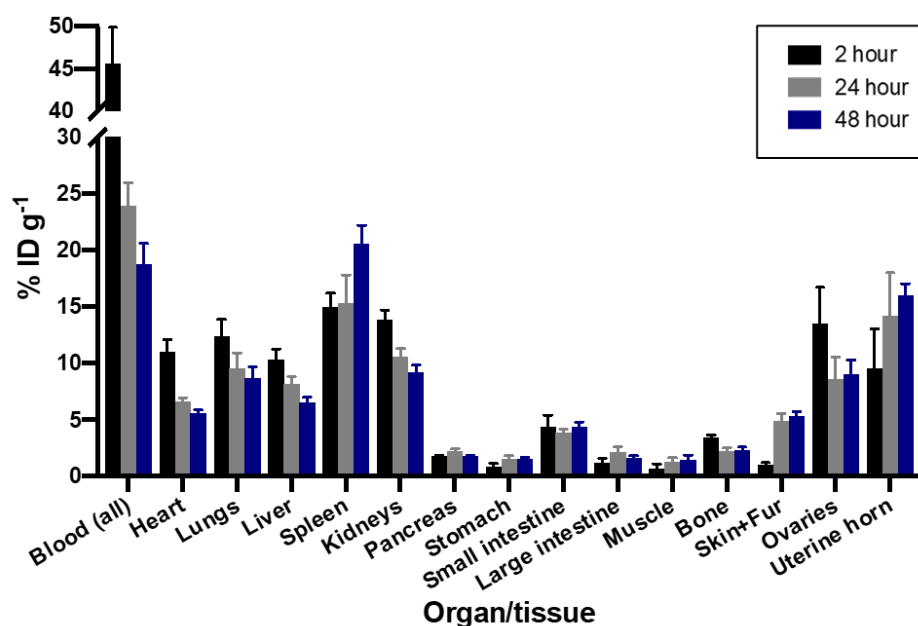


Figure 80 - Ex vivo biodistribution data of ^{64}Cu -sar-DTM-trastuzumab (n=4 mice per time point). Error bars correspond to standard deviation.

2.8.2 PET imaging of ^{64}Cu -sar-DTM-trastuzumab in healthy mice

To support the biodistribution data, two additional healthy female NSG mice were administered ^{64}Cu -sar-DTM-trastuzumab and subjected to PET/CT scanning under anaesthesia at 2 h, 24 h, and 48 h p.i. Maximum intensity projections (MIP) of the PET/CT data (figure 81a) show the same trends observed in the *ex vivo* biodistribution data (figure 80). At 2 h p.i. ^{64}Cu radioactivity was observed in many components of the circulatory system including the heart, carotid arteries, descending aorta, and renal arteries. Rapid uptake in the ovaries (figure 81, white arrows) is also clearly visible at this time-point, highlighting the specificity of ^{64}Cu -sar-DTM-trastuzumab for HER2, which is naturally expressed in the ovaries. In agreement with biodistribution data, the 24 h and 48 h MIPs display diminishing ^{64}Cu radioactivity in the blood pool indicative of slow clearance typical of stable radioimmunoconjugates. The radioactivity in each tissue of interest was calculated as a percentage of the injected dose per cm^3 ($\% \text{ID}/\text{cm}^3$) and displayed in the bar chart in figure 81b. A maximum mean uptake of $26.32 \% \text{ID}/\text{cm}^3$ in the blood was observed at 2 h p.i., decreasing to a mean uptake of $12.03 \% \text{ID}/\text{cm}^3$ at 48 h p.i. HER2 is also naturally expressed in the skin where uptake and retention of ^{64}Cu radioactivity was observed. After 2 h p.i. uptake in the skin was $1.35 \% \text{ID}/\text{g}$; this increased to $3.51 \% \text{ID}/\text{g}$ at 24 h p.i., and remained high at 48 h p.i. where an uptake of $3.62 \% \text{ID}/\text{g}$ was achieved. This observed uptake and retention in skin highlights the specificity and affinity of ^{64}Cu -sar-DTM-trastuzumab for HER2.

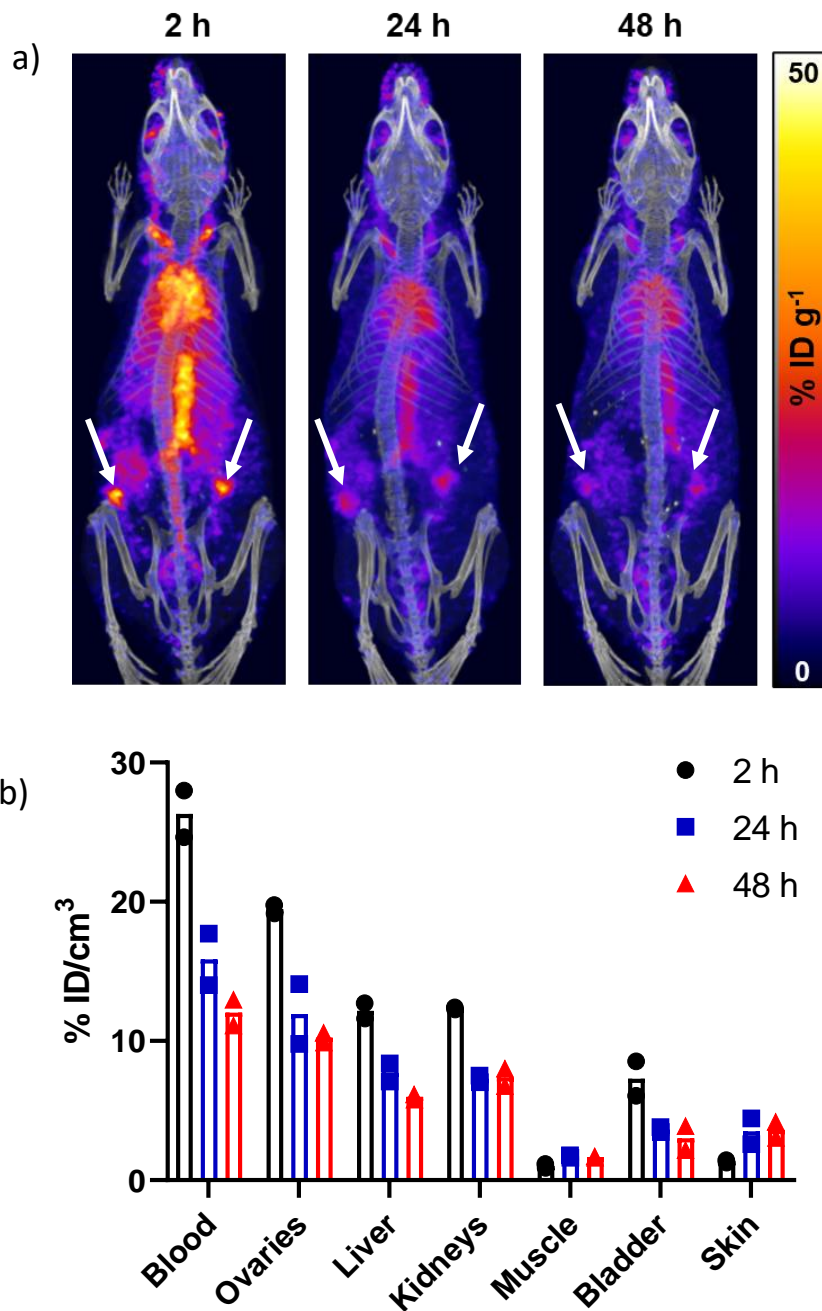


Figure 81 - a) PET/CT maximum intensity projections of a healthy female NOD scid gamma mouse administered ⁶⁴Cu-sar-DTM-trastuzumab, at 2 h, 24 h, and 48 h p.i.. White arrows indicate the ovaries that are positive for HER2. b) Regions of interest were selected using VivoQuant (Invivo), and percentage injected dose per millilitre (% ID/cm³) were calculated for each. Bars show mean values (n=2), individual data points are plotted.

2.8.3 SDS-PAGE analysis of *ex vivo* serum samples from mice administered ^{64}Cu -sar-DTM-trastuzumab

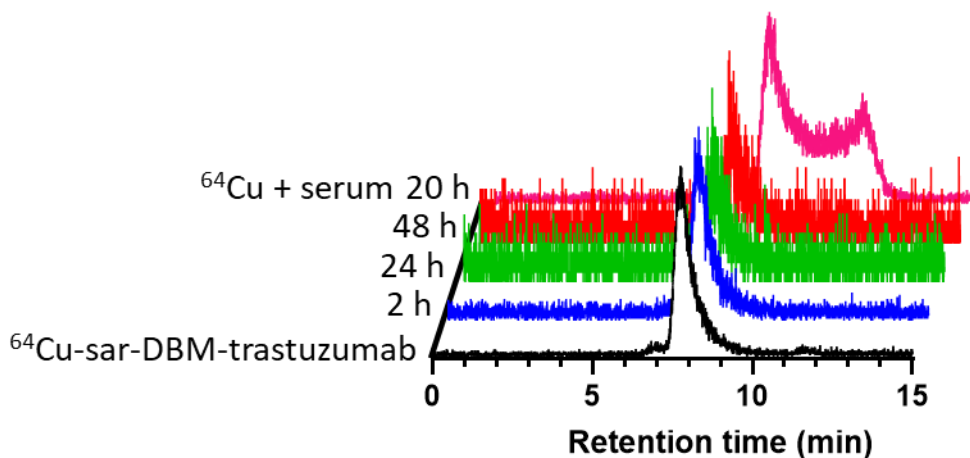


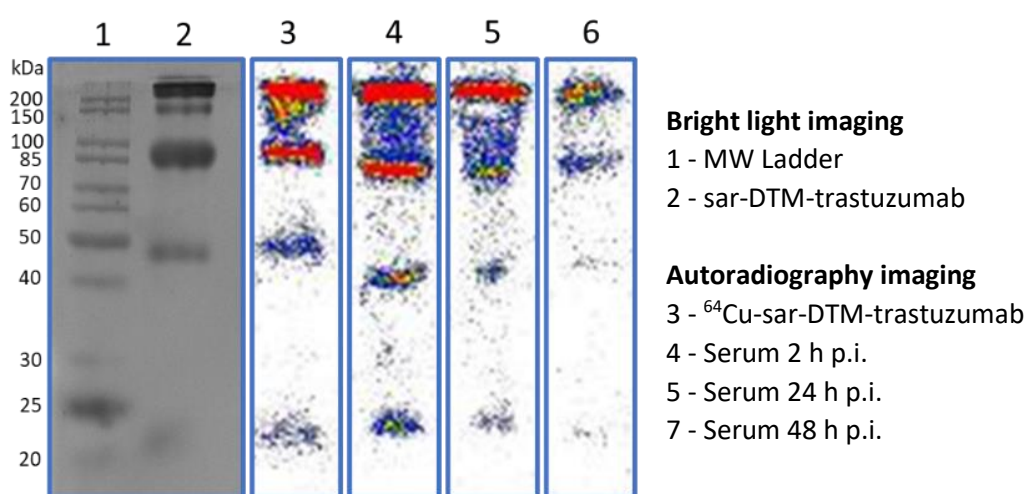
Figure 82 - SE-HPLC analysis of *ex vivo* serum samples showed a single radioactive signal in each chromatogram, with the retention time of each signal corresponding to ^{64}Cu -sar-DTM-trastuzumab (black). Chromatograms obtained using *ex vivo* serum samples did not contain peaks corresponding to serum protein-bound ^{64}Cu radioactivity (pink).

As well as quantifying blood for ^{64}Cu radioactivity, blood serum was also analysed by SE-HPLC: blood was centrifuged to separate serum from other blood components. Serum was then collected and analysed by SE-HPLC (figure 82). The radiochromatograms obtained for each time point only contain one signal with a retention time matching that of ^{64}Cu -sar-DTM-trastuzumab (7.75 min). Importantly, there were no observable species with retention times matching serum proteins (figure 82, pink trace) or $[\text{}^{64}\text{Cu}(\text{EDTA})]^{2-}$ (11.58 min). These results indicate that ^{64}Cu -sar-DTM-trastuzumab has good stability *in vivo* over 48 h.

Serum was also analysed by SDS-PAGE (figure 83) revealing radioactive bands (figure 83, lanes 4-6) that corresponded to denatured fragments of non-radioactive sar-DTM-trastuzumab (figure 83, lane 2) and radioactive ^{64}Cu -sar-DTM-trastuzumab (figure 83, lane 3). The majority of ^{64}Cu radioactivity remains associated with full- and half-antibody conjugates highlighting the stability of the rebridged disulfide bonds *in vivo*. Note that for the serum samples some of the bands appear to have migrated further through the gel than in the lane corresponding to ^{64}Cu -sar-DTM-trastuzumab. Rather than transmetallation or thiol exchange processes, this observation is due to “overloading” of the gel with

protein. To ensure adequate radioactivity was present in each lane for detection by autoradiography, a large amount of undiluted serum (~10 uL) was loaded onto lanes 4-6 (figure 83). Overloading in this manner can lead to altered protein mobility within the gel matrix and “smearing” of protein bands. Importantly, SDS-PAGE analysis of *ex vivo* mouse serum did not show protein bands with molecular weights corresponding to albumin conjugates (albumin MW=66.5 kDa), indicating the high stability of ⁶⁴Cu-sar-DTM-trastuzumab *in vivo* for at least 48 h.

Figure 83 - SDS-PAGE of *ex vivo* serum samples (bright light and autoradiography imaging) shows radioactive bands corresponding to ⁶⁴Cu-sar-DTM-trastuzumab.



2.9 Chapter 2 summary

Sar-DBM was synthesised following an optimisation process, which increased yields from 0.8 % using initial conditions, to a final 8 % using optimised conditions. Sar-DBM was fully characterised by ¹H NMR, ¹³C NMR, and high resolution ESI mass spectrometry, and analytical HPLC was used to confirm high chemical purity. [Mg(sar-DBM)]²⁺ and sar-DBM₂ were also isolated as minor products of the reaction and were characterised by ¹H NMR, ¹³C NMR, and mass spectrometry. Compared to literature syntheses involving EEDQ mediated coupling reactions between 3,4-dibromomaleimide-N-hexanoic acid and other amines such as propargylamine, yields were low when [Mg(NH₂)₂sar]²⁺ was used as the amine. This was attributed to steric encumbrance of the bicyclic rings. Additionally, yields were low in comparison to coupling reactions between the primary amines of other sarcophagine derivatives and amine reactive species.

Sar-DBM was conjugated to reduced trastuzumab to give sar-DTM-trastuzumab. Optimisation studies showed that using 8 eq. of sar-DBM with a post-conjugation

hydrolysis duration of 48 h promoted efficient conjugation. SDS-PAGE analysis demonstrated that reduced disulfide bonds had been efficiently rebridged to give immunoconjugates whose structure closely resembles that of unmodified native trastuzumab. A range of sar-DTM-trastuzumab fragments were observed by mass spectrometry, with variable chelator loading indicative of incomplete conjugation.

Sar-DTM-trastuzumab was then radiolabelled with $^{64}\text{Cu}^{2+}$ achieving near quantitative radiochemical yields (>99.5 %) under mild conditions to give a specific activity of 43.6 MBq/mg. ^{64}Cu -sar-DTM-trastuzumab was observed to be stable in human serum at 37 °C for 40 hours with evidence of bioconjugate degradation or transchelation of ^{64}Cu -radioactivity to serum proteins.

^{64}Cu -sar-DTM-trastuzumab was incubated with SKOV3 cells (HER2 +ve) where cell uptake decreased as the concentration of unmodified trastuzumab was increased, indicative of specific binding of ^{64}Cu -sar-DTM-trastuzumab to HER2.

Lastly, the biodistribution and stability of ^{64}Cu -sar-DTM-trastuzumab were assessed in healthy mice over 48 h. *Ex vivo* biodistribution data showed that ^{64}Cu -sar-DTM-trastuzumab cleared from the blood slowly over 48 h in agreement with the expected pharmacokinetic behaviour for a stable IgG radioimmunoconjugate. Limited uptake was observed in the liver indicating the high stability of the [$^{64}\text{Cu}(\text{sar})$] $^{2+}$ radiocomplex. SE-HPLC of *ex vivo* serum samples also showed high radioimmunoconjugate stability: ^{64}Cu -radioactivity remained associated with the bioconjugate over 48 h with no evidence of degradation or transchelation to serum proteins. *Ex vivo* biodistribution studies showed uptake and retention of ^{64}Cu -sar-DTM-trastuzumab in healthy tissues that naturally express HER2 such as the ovaries, uterine horn, and the skin. *In vivo* PET imaging studies showed similar results with slow blood clearance observed for ^{64}Cu -sar-DTM-trastuzumab over 48 h, and uptake observed in the ovaries and skin. These results suggest that ^{64}Cu -sar-DTM-trastuzumab retained specificity for the HER2 receptor.

2.10 Chapter 2 experimental

Materials: Chemicals and reagents were obtained from Sigma-Aldrich (Dorset, UK) unless otherwise specified. The highest available purity (lowest metal ion-containing) chemicals were used. 18.2 M Ω water was used to prepare all solutions. PD-10 size exclusion columns were purchased from GE Healthcare UK Ltd.

(Buckinghamshire, UK). Trastuzumab was obtained as the biosimilar Herzuma in solution (21 mg/mL) from the Pharmacy Department at Guy's and St. Thomas' NHS Trust, London. Fresh human serum was obtained from a healthy volunteer. Preparative high-performance liquid chromatography (HPLC) purification was carried out using an Agilent PrepStar LC system with in-line UV. NMR spectra were acquired on either a Bruker 400 MHz spectrometer, or a Bruker 700 MHz (Bruker UK Limited, Coventry, UK). NMR spectra were referenced to residual solvent signals, or in the case where deuterium oxide was the solvent in ^{13}C NMR spectra, a trifluoroacetic acid reference was used. Analytical reverse phase HPLC was carried out using an Agilent 1260 Infinity II equipped with an Eclipse XDB-C18 column (4.6 \times 150 mm, 5 μm) with a 1 mL min^{-1} flow rate and UV spectroscopic detection at 220 nm, 254 nm, and 330 nm, and a gradient mobile phase with a flow rate of 1 mL/min. (Gradient: A = 0.1 % FA in water, B = 0.1 % FA in acetonitrile. 0-2 min 5 % B in A, 2-11 min 5 % \rightarrow 95 % B in A, 12-12.10 min 95 % \rightarrow 5 % B in A, 12.10-15 min 5 % B in A.) Instant thin layer chromatography strips (ITLC-SG) were obtained from Varian Medical Systems UK, Ltd. (Crawley, UK), and ITLC strips were visualised using a Lab Logic B-MS-1000 plate reader with a B-FC-2000P detector equipped with a B-FC-3600 photomultiplier. Analytical size exclusion radioHPLC traces were acquired using an Agilent 1200 Series HPLC system with an in-line radioactivity detector (Ray Test Gabi with a Ray Test Na-I 1x1" Std. detector). A BioSepTM SEC-s2000 LC Column (5 μm , 145 \AA , 300 \times 7.8 mm) was used with a mobile phase of PBS and sodium ethylenediamine tetraacetate (2 mM) at a flow rate of 1 mL/min.

[Mg(NH₂)₂sar](OTf)₂: (NH₂)₂sar (prepared from CoCl₂ according to the literature,³²⁻³⁴ 100 mg, 318 μmol) and Mg(OTf)₂ (103 mg, 318 μmol) were added to acetonitrile (5 mL). The mixture was heated to reflux for 30 min, then allowed to cool to room temperature. The resulting solution was then evaporated to dryness to yield a white solid. [Mg(NH₂)₂sar](OTf)₂: 176 mg, 277 μmol , 87 %. ^1H NMR (400 MHz, D₂O) δ 3.61 (m, 6H), 3.15 (m, 12H), 2.68 (m, 6H), 2.42 (m, 6H).

sar-DBM: [Mg(NH₂)₂sar](CF₃SO₃)₂ (250 mg, 393 μmol , 1 eq.) was dried *in vacuo*; separately 3,4-dibromo-maleimide-N-hexanoic acid⁶ (446 mg, 1.214 mmol, 3 eq.) and EEDQ (296 mg, 1.197 mmol, 3 eq) were also dried *in vacuo*. 3,4-dibromo-maleimide-N-hexanoic acid and EEDQ were added to dry acetonitrile (20 mL) and stirred for 1 hour at ambient temperature. [Mg(NH₂)₂sar](CF₃SO₃)₂ was added and the reaction was stirred for 3 hours at ambient temperature. Glacial acetic acid

(12.5 mL) was then added and the solution evaporated to dryness. Water (10 mL) was added to the dry residue, and the supernatant was separated from insoluble material. The supernatant was lyophilised to give a white powder, containing the desired product. The crude product was purified by preparative reverse phase HPLC (Agilent PrepHT XDB-C18) using mobile phase A (water with 0.1 % TFA) and mobile phase B (acetonitrile with 0.1 % TFA) with an eluting gradient (10 mL/min, 0-5 min 0 % B in A, 5-10 min 0 % → 20 % B in A, 10-40 min 20 % → 60 % B in A). The desired product sar-DBM was eluted with a retention time of 21.8 min, and was then lyophilised to give an off-white powder (20.7 mg, 8 % yield). ¹H NMR (700 MHz, D₂O) δ 3.50 (s, 3H), 3.45 (t, J = 8.2 Hz, 2H), 3.15 (s, 12H), 3.00 (s, 12H), 2.28 (s, 3H), 2.11 (t, J = 8.2 Hz, 2H), 1.43 (m, 4H), 1.12 (m, 2H). ¹³C NMR (176 MHz, D₂O) δ 178.55, 166.45, 129.33, 55.91, 54.92, 50.83, 50.45, 47.86, 46.14, 39.47, 35.94, 27.44, 25.55, 24.34. High resolution ESI-MS +ve mode, [C₂₄H₄₄Br₂N₉O₃]⁺ observed m/z = 666.19, calculated m/z = 666.19. Analytical HPLC retention time, 5.92 min. Analytical reverse phase HPLC was carried out using an Agilent 1260 Infinity II equipped with an Eclipse XDB-C18 column (4.6 × 150 mm, 5 μm) with a 1 mL/min flow rate and UV spectroscopic detection at 220 nm, 254 nm, and 330 nm, and a gradient mobile phase with a flow rate of 1 mL/min. Gradient: A = 0.1% FA in water, B = 0.1 % FA in acetonitrile. 0-2 min 5 % B in A, 2-11 min 5 %→95 % B in A, 12-12.10 min 95 %→5 % B in A, 12.10-15 min 5 % B in A.

[Mg(sar-DBM)]²⁺: Same method as sar-DBM. Upon HPLC purification, [Mg(sar-DBM)]²⁺ was eluted at 20.8 min, and then lyophilised to give a white powder (9.5 mg, 1.9 %). ¹H NMR shows species is present as a mixture of Mg²⁺ complex and free chelator therefore no integrals given for the cage protons: ¹H NMR (400 MHz, D₂O) δ 3.90 (m, cage), 2.74 (m, cage), 3.54 (dd, 2H), 3.40-2.82 (m, cage), 2.41 (m, cage), 2.13 (dt, 2H), 1.51 (m, 4H), 1.18 (m, 2H). Low resolution ESI-MS +ve mode (C₂₄H₄₃Br₂MgN₉O₃²⁺): calculated m/z = 344.5, observed m/z 344.5.

sar-DBM₂: Same method as sar-DBM. Upon HPLC purification, sar-DBM₂ was eluted with a retention time of 26.4 min, and then lyophilised to give a white powder (4.5 mg, 0.6 %). ¹H NMR shows species is present as a mixture of Mg²⁺ complex and free chelator therefore no integrals given for the cage protons: ¹H NMR (400 MHz, CD₃CN) δ 3.70 (m, cage), 3.52 (t, 4H), 3.36-3.28 (m, cage), 3.11 (s, cage), 3.03-3.00 (m, cage), 2.94-2.89 (m, cage), 2.62-2.52 (m, cage), 2.02 (t, 4H), 1.60-1.45 (m, 8H),

1.28-1.19 (m, 4H). High resolution ESI-MS +ve mode ($C_{34}H_{53}Br_4N_{10}O_6^+$): calculated $m/z = 1017.08$, observed $m/z = 1017.08$.

sar-DTM-trastuzumab: Trastuzumab (5 mg) was dissolved in aqueous borate buffered saline (BBS, 1.5 mL) solution (50 mM sodium borate, 50 mM NaCl, and 5 mM ethylenediaminetetraacetic acid (EDTA), pH 8.5) to give an antibody concentration of 23 μ M. To this antibody solution was added tris(2-carboxyethyl)phosphine solution (TCEP, 10 mM in BBS, 21 μ L, 6 eq.) and warmed at 37 °C for 2 h. Then sar-DBM (10 mM in water, 28 μ L, 8 eq.) was added to the reduced antibody solution where a colour change from a colourless to pale yellow solution was observed. This solution was then warmed at 37 °C for 48 h. The bioconjugate was loaded onto a PD-10 column (preconditioned with aqueous ammonium acetate (0.2 M) solution) and eluted with aqueous ammonium acetate (0.2 M) in 0.5 mL fractions. Fraction protein content was assessed using a NanoDrop™ 2000 spectrophotometer. Fractions 6 and 7 were combined, and further purified and buffer exchanged into aqueous ammonium acetate (0.1 M) by six cycles of spin filtration (4000 rcf, 15 min) through a Vivaspin (50 kDa MWCO). The bioconjugate sar-DTM-trastuzumab (3.62 mg) was recovered in 200 μ L solution at a concentration of 125 μ M

SDS-PAGE analysis of sar-DTM-trastuzumab: A sample of immunoconjugate (3 μ L) was diluted with water (10 μ L), followed by addition of SDS-PAGE loading buffer (2 μ L). This solution was mixed thoroughly and then heated to 65 °C for 5 min to denature the protein. The sample was then loaded onto the gel (12 % acrylamide with 4% stacking gel), along with a molecular weight marker, a sample of trastuzumab (prepared in the same way), and a sample of reduced trastuzumab (also prepared in the same way). The stability of the bioconjugates in the presence of a large excess of thiol was also assessed by preparing samples in the same fashion as described above, with the addition inclusion of dithiothreitol (DTT) (10 mM in water, 1 μ L, \geq 100 eq.) prior to denaturing. Separation of protein components was achieved by applying a constant voltage to the gels (35 mA, 35 min) in SDS running buffer. Gels were stained with Coomassie blue, destained, and then bright light imaged (Invitrogen, iBright FL1000 , Thermo Fisher Scientific).

ESI-MS analysis of sar-DTM-trastuzumab: Sar-DTM-trastuzumab was analysed using an Agilent 6510 QTOF LC-MS system (Agilent, UK). Agilent 1200 HPLC system

equipped with an Agilent PLRP-S, 1000A, 8 μ M, 150 mm x 2.1 mm column. sar-DTM-trastuzumab was buffer exchanged to ammonium acetate (0.2 M, pH 6.9) using a Vivaspin (50 kDa MWCO) to a final concentration of 6.5 μ M. To 100 μ L of this bioconjugate solution was added PNGase F (1.0 μ L, New England Biolabs) at 37 °C for 16 h. Then the sample was diluted to 1.8 μ M with ammonium acetate buffer (0.2 M, pH 6.9) and 10 μ L were injected on the column using mobile phase A (water with 0.1% formic acid) and B (acetonitrile with 0.1% formic acid) with an eluting gradient (as shown in table 4) at a flow rate of 300 μ L/min. The oven temperature was maintained at 60 °C. Agilent 6510 QTOF mass spectrometer was operated in a positive polarity mode, coupled with an ESI ion source. The ion source parameters were set up with a VCap of 3500V, a gas temperature at 350 °C, a dry gas flow rate at 10 L/min and a nebulizer of 30 psig. Mass spectrum time of flight (ToF) was acquired under conditions of a fragmentor at 350 V, a skimmer at 65 V and an acquisition rate at 0.5 spectra/s in a profile mode, within a scan range between 700 and 5000 m/z. The data was then analysed by deconvoluting to a zero-charge mass spectrum using a maximum entropy deconvolution algorithm.

Table 4. LC-MS mobile phase A/ B gradient elution

Time (min)	Solvent A (%)	Solvent B (%)
0.0	85	15
1.0	85	15
1.50	68	32
2.0	68	32
7.0	50	50
9.0	5	95
10.0	5	95
12.0	85	15
15.0	85	15

$^{64}\text{Cu}^{2+}$ production and purification: Production and purification of $^{64}\text{Cu}^{2+}$ were performed by Dr Zilin Yu. A concave high purity gold target was electroplated with ^{64}Ni (95.6 % isotopically enriched), rinsed with water and then dried. This target was then irradiated with protons on a CTI RDS 112 cyclotron (11 MeV, 1 cm beam

diameter) with a beam current of 30 μA , for 8 h to induce the $^{64}\text{Ni}(p,n)^{64}\text{Cu}$ reaction. HCl (9 M, 150 μL) was added to the irradiated surface and then evaporated at 95 $^{\circ}\text{C}$. This was repeated three times and then HCl (9 M, 300 μL) was added to the irradiated surface and loaded onto an anion exchange column (AG[®] 1-X8 Anion Exchange Resin, pre-rinsed with water and HCl (6 M)). This step was repeated three times to give a total of 900 μL added to the column. The column was then eluted sequentially under gravity with 6 M HCl (5 mL) to remove excess ^{64}Ni ; followed by 4 M HCl (5 mL), to remove any radio-cobalt impurities; 0.1 M HCl (10 mL) was used to elute $^{64}\text{Cu}^{2+}$. Twenty fractions (1 mL each) were collected in total. Fractions 14 and 15 contained most of the ^{64}Cu radioactivity produced, with a radionuclidic purity greater than 99.9 %.

^{64}Cu -sar-DTM-trastuzumab: An aliquot from fraction 15 containing $^{64}\text{Cu}^{2+}$ (56.5 MBq, 448 μL) was dried under a stream of N_2 at 100 $^{\circ}\text{C}$, and then redissolved in aqueous ammonium acetate solution (0.1 M, 339 μL). A sample of $^{64}\text{Cu}^{2+}$ from this solution (5 MBq, 30 μL) was then added to an aqueous solution of sar-DTM-trastuzumab (100 μg , in 9.4 μL of 0.1 M ammonium acetate). The sample was agitated and left at ambient temperature for 5 min. Radiochemical yields were determined using ITLC-SG strips spotted with 1 μL of radiolabelling mixture, which were developed in a mobile phase of 0.1 M citrate buffer (pH 5.5). For ^{64}Cu -sar-DTM-trastuzumab: $R_f < 0.1$; for unreacted $^{64}\text{Cu}^{2+}$: $R_f > 0.9$. Size exclusion HPLC was also used to assess radiochemical yield. Analytical size exclusion radio HPLC traces were acquired using an Agilent 1200 Series HPLC system with an in-line radioactivity detector (Ray Test Gabi with a Ray Test Na-I 1x1" Std. detector). A BioSep[™] SEC-s2000 LC Column (5 μm , 145 Å , 300 x 7.8 mm) was used with a mobile phase of PBS and sodium ethylenediamine tetraacetate (5 mM) at a flow rate of 1 mL/min. ^{64}Cu -sar-DTM-trastuzumab had a retention time of 7.75 min, and unreacted $^{64}\text{Cu}^{2+}$ eluted at 11.58 min. Near quantitative radiochemical yields (>98 %) were achieved at a specific activity of 43.6 MBq/mg, corresponding to a molar activity of 6.33 GBq/ μmol .

Sar-DTM-trastuzumab was also labelled at varying bioconjugate concentrations. An aliquot from fraction 15 containing $^{64}\text{Cu}^{2+}$ (1 MBq) was dried under a stream of N_2 at 100 $^{\circ}\text{C}$, and then redissolved in aqueous ammonium acetate solution (0.1 M, 20 μL) to give a 50 kBq μL^{-1} solution (pH 7). Sar-DTM-trastuzumab was diluted to 125 μM in ammonium acetate (0.1 M). To 8 μL of this bioconjugate solution was added

2 μL (100 kBq) of $^{64}\text{Cu}^{2+}$ in ammonium acetate (0.1 M), agitated and then left at room temperature for 5 min (this dilution gives a 100 μM solution). ITLC was used to assess radiochemical yield as described above. This process was repeated at bioconjugate concentrations of 10 μM , 1 μM , 100 nM, 10 nM, and 1 nM.

Serum stability of ^{64}Cu -sar-DTM-trastuzumab: An aliquot of ^{64}Cu -sar-DTM-trastuzumab (0.2 - 1.0 MBq) was added to human serum in a ratio of one part radiolabelled solution to four parts serum (by volume), and incubated at 37 °C. Aliquots were taken for analysis by size exclusion HPLC at 0 h, 20 h, and 40 h. 0.58 mg bioconjugate/mL of serum.

SKOV3 binding study of ^{64}Cu -sar-DTM-trastuzumab: SKOV3 cells were grown in T150 flasks in culture medium. Cells were aspirated and washed with PBS, then treated with trypsin to detach the cells from the flask and then washed again with PBS. The cells were resuspended in HBSS with 0.2 % BSA to give 2×10^5 cells per tube in 250 μL . Trastuzumab solution (500 μL , 2 μM – 0 μM , in HBSS with 0.2 % BSA) was added to each tube, followed by ^{64}Cu -sar-DTM -trastuzumab (250 μL , 1 μg , 10 kBq, in HBSS with 0.2 % BSA). Tubes were incubated on ice for 1 hr. The cells were washed by centrifuging at 500 rcf for 3 min, aspirating the supernatant, and resuspending in ice cold PBS (1 mL), centrifuging once more at 500 rcf for 3 min, and aspirating the supernatant. The radioactivity associated with cell pellets was counted using a Wallac 1282 Compugamma Universal Gamma Counter. Non-linear regression analysis was performed using a one site total binding fit model (Graphpad Prism 8).

Biodistribution of ^{64}Cu -sar-DTM-trastuzumab in healthy female NSG mice: All *in vivo* studies were carried out in accordance with national and local regulations under UK Home Office project and personal licences. The biodistribution of ^{64}Cu -sar-DTM-trastuzumab was assessed in twelve 9-week-old NOD scid gamma (NSG) mice, which were purchased from Charles River UK and left to acclimatise for five days before use with *ad libitum* access to water and diet (PicoLab Rodent Diet 20, LabDiet, St Louis, Missouri). Mice were housed in cages of 6 equipped with Lignocel soft wood pellets, environmental enrichment, and maintained at a temperature of 20 °C to 24 °C and 45% to 65 % humidity. For injection, mice were anaesthetised by inhalation of a 3% isoflurane-oxygen mixture and placed on a nose cone for maintenance with a 1.5-2.5 % isoflurane-oxygen mixture. The mice were injected

intravenously (tail vein) with ~1.5 MBq (150 µg, 150 µL in 0.9 % saline) of ⁶⁴Cu-sar-DTM-trastuzumab. Mice were housed individually in grid floor cages after injection. Biodistribution mice were placed in three groups (n=4), which were culled under anaesthesia at 2 h, 24 h, or 48 hours post injection by cervical dislocation, followed by tail nick to ensure cessation of circulation. Organs were harvested, washed in PBS, dried briefly, and then placed in gamma counter tubes for weighing and radioactivity counting. The radioactivity associated with each tube was counted using a Wallac 1282 Compugamma Universal Gamma Counter. This data was processed to calculate the % injected dose per gram (% ID/g).

PET/CT imaging study of ⁶⁴Cu-sar-DTM-trastuzumab in healthy female NSG mice:

An *in vivo* PET imaging study was carried out on two 9-week-old NSG mice, which were purchased from Charles River UK and left to acclimatise for five days before use with *ad libitum* access to water and diet. PET images were acquired in a nanoScan® *in vivo* pre-clinical PET/CT imager (Mediso, Hungary). The mice were anaesthetised by inhalation of a 3 % isoflurane-oxygen mixture and placed on a nose cone for maintenance with a 1.5-2.5 % isoflurane-oxygen mixture. These mice were then injected intravenously (*via* tail vein) with ⁶⁴Cu-sar-dtm-trastuzumab ~2.5 MBq (250 µg, 140 µL in 0.9 % saline). PET acquisition was started at 1h post-injection (60 min scan) and scans were repeated at 23 h (60 min scan), and 46 h (120 min scan) post injection. The scanner bed was maintained at 37 °C, and respiration monitoring was conducted throughout the scan. Scans were acquired at 1:5 coincidence mode and 5-ns coincidence time window. Images were reconstructed using Tera-Tomo 3D reconstruction (Mediso) with 4 iterations, 6 subsets, 1–3 coincidence mode, voxel sized 0.4 mm (isotropic), energy window 400–600 keV with attenuation and decay correction.

SDS-PAGE of *ex vivo* serum samples: For each of the mice used for biodistribution, upon confirmation of death, ~200 µL of blood was harvested from each mouse by cardiac puncture. One drop was placed aside for the biodistribution study whilst the rest was placed in a vet tube with gentle agitation and set aside for 1 hour. Vet tubes were centrifugated at 4000 rcf for 12 minutes. The serum was aspirated and analysed by size exclusion HPLC and SDS-PAGE as previously described.

2.11 Chapter 2 references

- 1 M. T. Ma, J. A. Karas, J. M. White, D. Scanlon and P. S. Donnelly, A new

- bifunctional chelator for copper radiopharmaceuticals: A cage amine ligand with a carboxylate functional group for conjugation to peptides, *Chem. Commun.*, 2009, 3237–3239.
- 2 M. S. Cooper, M. T. Ma, K. Sunassee, K. P. Shaw, J. D. Williams, R. L. Paul, P. S. Donnelly and P. J. Blower, Comparison of ⁶⁴Cu-Complexing Bifunctional Chelators for Radioimmunoconjugation: Labeling Efficiency, Specific Activity, and in Vitro / in Vivo Stability, *Bioconjug. Chem.*, 2012, **23**, 1029–1039.
 - 3 M. T. Ma, M. S. Cooper, R. L. Paul, K. P. Shaw, J. A. Karas, D. Scanlon, J. M. White, P. J. Blower and P. S. Donnelly, Macrobicyclic Cage Amine Ligands for Copper Radiopharmaceuticals: A Single Bivalent Cage Amine Containing Two Lys 3 -bombesin Targeting Peptides, *Inorg. Chem.*, 2011, **50**, 6701–6710.
 - 4 M. Morais, J. P. M. Nunes, K. Karu, N. Forte, I. Benni, M. E. B. Smith, S. Caddick, V. Chudasama and J. R. Baker, Optimisation of the dibromomaleimide (DBM) platform for native antibody conjugation by accelerated post-conjugation hydrolysis, *Org. Biomol. Chem.*, 2017, **15**, 2947–2952.
 - 5 C. Bahou, D. A. Richards, A. Maruani, E. A. Love, F. Javaid, S. Caddick, J. R. Baker and V. Chudasama, Highly homogeneous antibody modification through optimisation of the synthesis and conjugation of functionalised dibromopyridazinediones, *Org. Biomol. Chem.*, 2018, **16**, 1359–1366.
 - 6 M. Morais, J. P. M. Nunes, K. Karu, N. Forte, I. Benni, M. E. B. Smith, S. Caddick, V. Chudasama and J. R. Baker, Supplementary Information - Optimisation of the dibromomaleimide (DBM) platform for native antibody conjugation by accelerated post-conjugation hydrolysis, *Org. Biomol. Chem.*, 2017, **15**, S1-63.
 - 7 C. Ge, S. Huvelle, C. B. Baltus, L. Juen, N. Joubert, A. Desgranges and C. Martin, Impact of Maleimide Disubstitution on Chemical and Biological Characteristics of HER2 Antibody – Drug Conjugates, , DOI:10.1021/acsomega.9b03510.
 - 8 M. Morais, N. Forte, V. Chudasama and J. R. Baker, in *Methods in*

- Molecular Biology*, eds. S. Massa and N. Devoogdt, 2019, vol. 2033, pp. 15–24.
- 9 N. M. Di Bartolo, A. M. Sargeson, T. M. Donlevy and S. V. Smith, Synthesis of a new cage ligand, SarAr, and its complexation with selected transition metal ions for potential use in radioimaging†, *J. Chem. Soc. Dalt. Trans.*, 2001, 2303–2309.
- 10 M. T. Ma, The University of Melbourne, 2010.
- 11 B. M. Paterson, G. Buncic, L. E. McInnes, P. Roselt, C. Cullinane, D. S. Binns, C. M. Jeffery, R. I. Price, R. J. Hicks and P. S. Donnelly, Bifunctional Cu-64-labelled macrobicyclic cage amine isothiocyanates for immuno-positron emission tomography, *Dalt. Trans.*, 2015, **44**, 4901–4909.
- 12 P. Adumeau, K. E. Carnazza, C. Brand, S. D. Carlin, T. Reiner, B. J. Agnew, J. S. Lewis and B. M. Zeglis, A pretargeted approach for the multimodal PET/NIRF imaging of colorectal cancer, *Theranostics*, 2016, **6**, 2267–2277.
- 13 C. Bahou, E. A. Love, S. Leonard, R. J. Spears, A. Maruani, K. Armour, J. R. Baker and V. Chudasama, Disulfide Modified IgG1: An Investigation of Biophysical Profile and Clinically Relevant Fc Interactions, *Bioconjug. Chem.*, 2019, **30**, 1048–1054.
- 14 S. Rosati, Y. Yang, A. Barendregt and A. J. R. Heck, Detailed mass analysis of structural heterogeneity in monoclonal antibodies using native mass spectrometry, *Nat. Protoc.*, 2014, **9**, 967–976.
- 15 J. P. M. Nunes, M. Morais, V. Vassileva, E. Robinson, V. S. Rajkumar, M. E. B. Smith, R. B. Pedley, S. Caddick, J. R. Baker and V. Chudasama, Functional native disulfide bridging enables delivery of a potent, stable and targeted antibody–drug conjugate (ADC), *Chem. Commun.*, 2015, **51**, 10624–10627.
- 16 C. Imberti, S. Y. A. Terry, C. Cullinane, F. Clarke, G. H. Cornish, N. K. Ramakrishnan, P. Roselt, A. P. Cope, R. J. Hicks, P. J. Blower and M. T. Ma, Enhancing PET Signal at Target Tissue in Vivo: Dendritic and Multimeric Tris(hydroxypyridinone) Conjugates for Molecular Imaging of $\alpha v\beta 3$ Integrin Expression with Gallium-68, *Bioconjug. Chem.*, 2017, **28**, 481–495.
- 17 M. S. Cooper, M. T. Ma, K. Sunassee, K. P. Shaw, J. D. Williams, R. L. Paul, P.

- S. Donnelly and P. J. Blower, Comparison of ⁶⁴Cu-Complexing Bifunctional Chelators for Radioimmunoconjugation: Labeling Efficiency, Specific Activity, and in Vitro / in Vivo Stability, *Bioconjug. Chem.*, 2012, **23**, 1029–1039.
- 18 S. Mankarious, M. Lee, S. Fischer, K. H. Pyun, H. D. Ochs, V. A. Oxelius and R. J. Wedgwood, The half-lives of IgG subclasses and specific antibodies in patients with primary immunodeficiency who are receiving intravenously administered immunoglobulin., *J. Lab. Clin. Med.*, 1988, **112**, 634–40.
- 19 M. E. B. Smith, F. F. Schumacher, C. P. Ryan, L. M. Tedaldi, D. Papaioannou, G. Waksman, S. Caddick and J. R. Baker, Protein modification, bioconjugation, and disulfide bridging using bromomaleimides, *J. Am. Chem. Soc.*, 2010, **132**, 1960–1965.
- 20 C. P. Ryan, M. E. B. Smith, F. F. Schumacher, D. Grohmann, D. Papaioannou, G. Waksman, F. Werner, J. R. Baker and S. Caddick, Tunable reagents for multi-functional bioconjugation: reversible or permanent chemical modification of proteins and peptides by control of maleimide hydrolysis, *Chem. Commun.*, 2011, **47**, 5452.
- 21 M. C. Linder, Ceruloplasmin and other copper binding components of blood plasma and their functions: An update, *Metallomics*, 2016, **8**, 887–905.
- 22 N. Liu, L. S. Lo, S. H. Askary, L. Jones, T. Z. Kidane, T. T. M. Nguyen, J. Goforth, Y.-H. Chu, E. Vivas, M. Tsai, T. Westbrook and M. C. Linder, Transcuprein is a macroglobulin regulated by copper and iron availability, *J. Nutr. Biochem.*, 2007, **18**, 597–608.
- 23 A. Strom, K. Kaul, J. Brüggemann, I. Ziegler, I. Rokitta, S. Püttgen, J. Szendroedi, K. Müssig, M. Roden and D. Ziegler, Lower serum extracellular superoxide dismutase levels are associated with polyneuropathy in recent-onset diabetes, *Exp. Mol. Med.*, 2017, **49**, e394–e394.
- 24 J. D. Hoppe, P. C. Scriba and H. Klüter, *Human Albumin*, Karger, Freiburg, 2009, vol. 36.
- 25 S. Yoshino, K. Fujimoto, T. Takada, S. Kawamura, J. Ogawa, Y. Kamata, Y.

- Kodera and M. Shichiri, Molecular form and concentration of serum α 2-macroglobulin in diabetes, *Sci. Rep.*, 2019, **9**, 1–10.
- 26 B. M. Paterson and P. S. Donnelly, *Macrocyclic Bifunctional Chelators and Conjugation Strategies for Copper-64 Radiopharmaceuticals*, Elsevier Inc., 1st edn., 2016, vol. 68.
- 27 A. Magnifico, L. Albano, S. Campaner, D. Delia, F. Castiglioni, P. Gasparini, G. Sozzi, E. Fontanella, S. Menard and E. Tagliabue, Tumor-initiating cells of HER2-positive carcinoma cell lines express the highest oncoprotein levels and are sensitive to trastuzumab, *Clin. Cancer Res.*, 2009, **15**, 2010–2021.
- 28 S. K. Sharma, J. M. Glaser, K. J. Edwards, E. Khozeimeh Sarbisheh, A. K. Salih, J. S. Lewis and E. W. Price, A Systematic Evaluation of Antibody Modification and ^{89}Zr -Radiolabeling for Optimized Immuno-PET, *Bioconjug. Chem.*, 2021, **32**, 1177–1191.
- 29 G. Krähn, U. Leiter, P. Kaskel, M. Udart, J. Utikal, G. Bezold and R. U. Peter, Coexpression patterns of EGFR, HER2, HER3 and HER4 in non-melanoma skin cancer, *Eur. J. Cancer*, 2001, **37**, 251–259.
- 30 M. F. Press, C. Cordon-Cardo and D. J. Slamon, Expression of the HER-2/neu proto-oncogene in normal human adult and fetal tissues., *Oncogene*, 1990, **5**, 953–62.
- 31 J. P. Holland, E. Caldas-Lopes, V. Divilov, V. A. Longo, T. Taldone, D. Zatorska, G. Chiosis and J. S. Lewis, Measuring the pharmacodynamic effects of a novel Hsp90 inhibitor on HER2/ neu expression in mice using ^{89}Zr -DFO-trastuzumab, *PLoS One*, , DOI:10.1371/journal.pone.0008859.
- 32 R. J. Geue, A. M. Sargeson, T. W. Hambley, M. R. Snow and J. M. Harrowfield, Metal Ion Encapsulation: Cobalt Cages Derived from Polyamines, Formaldehyde, and Nitromethane, *J. Am. Chem. Soc.*, 1984, **106**, 5478–5488.
- 33 R. A. Krause and E. A. Megargle, Student Synthesis of Tris(ethylenediarnine)cobalt(III) chloride, *J. Chem. Educ.*, 1976, **53**, 6268.
- 34 I. J. Clark, I. I. Creaser, R. J. Geue, K. S. Hagen, G. A. Lawrance, P. A. Lay, A. M. Sargeson and F. R. Wilne, The synthesis and structure of encapsulating

ligands: Properties of bicyclic hexamines, *Aust. J. Chem.*, 1994, **47**, 143–179.

3 Comparison of a dibromomaleimide-based bifunctional chelator to a commercially available maleimide-based bifunctional chelator

3.1 Chapter 3 introduction

In the previous chapter ^{64}Cu -sar-DTM-trastuzumab was prepared and assessed *in vivo* up to 48 h post injection. Immunoconjugates bearing DFO have been radiolabelled extensively with the longer-lived radionuclide ^{89}Zr ($t_{1/2}$ 3.3 d) enabling imaging at more distant time points post-injection (see 1.5). In this chapter a DFO-functionalised dibromomaleimide (DFO-DBM) was developed and used to produce a ^{89}Zr -radioimmunoconjugate. The commercially available bifunctional chelator DFO-maleimide (DFO-mal) (see 1.5.2) was also used to produce a ^{89}Zr -radioimmunoconjugate, enabling comparison with DFO-DBM.

3.2 Chapter 3 aims

The overall aim of this chapter was to compare the performance of a dibromomaleimide-based bifunctional chelator with a commercially available maleimide-based bifunctional chelator.

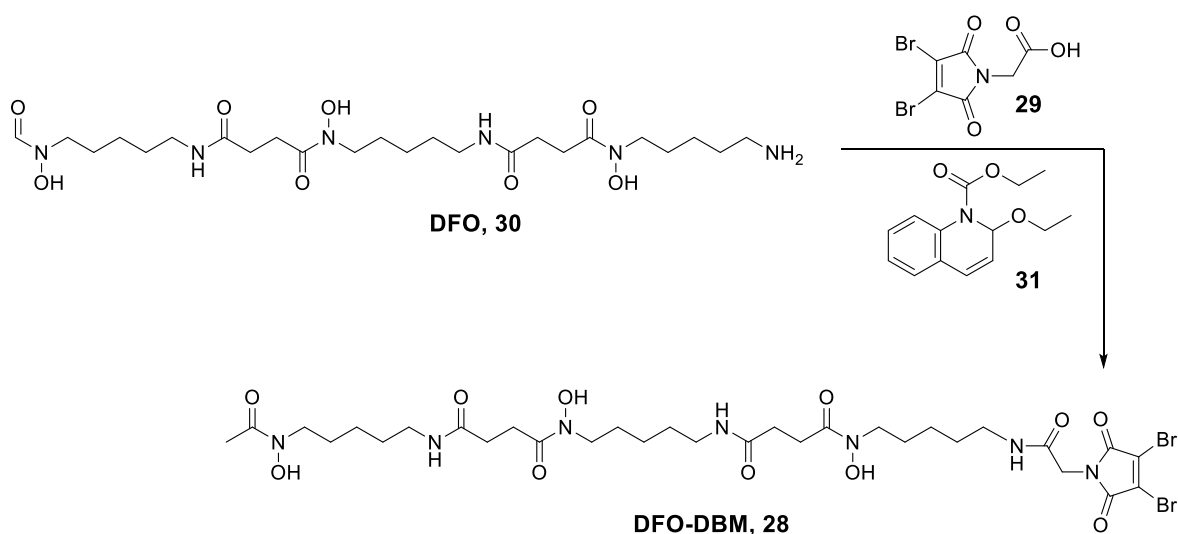
To achieve this aim, this chapter describes:

1. The synthesis of a new dibromomaleimide-based bifunctional chelator (DFO-DBM) based on the chelator desferrioxamine (DFO).
2. The conjugation of DFO-DBM and DFO-mal to trastuzumab to give DFO-DTM-trastuzumab and DFO-mal-trastuzumab
3. The ^{89}Zr -radiolabelling of DFO-DTM-trastuzumab and DFO-mal-trastuzumab
4. The stabilities of ^{89}Zr -DFO-DTM-trastuzumab and ^{89}Zr -DFO-mal-trastuzumab in both glutathione solution and human serum
5. *In vitro* assessment of target receptor specificity and immunoreactive fractions for ^{89}Zr -DFO-DTM-trastuzumab and ^{89}Zr -DFO-mal-trastuzumab
6. The use of bioorthogonal 'click' chemistry to produce DFO-conjugates

3.3 Synthesis of DFO-DBM (28)

Synthesis of DFO-DBM (**28**, scheme 6) was achieved *via* an amide coupling reaction between 3,4-dibromomaleimide-N-acetic acid (**29**, scheme 6, synthesised according to the literature, see appendix figures 121 and 122 for ^1H and ^{13}C NMR characterisation respectively)³ and DFO (**30**, scheme 6). This reaction was mediated

by the coupling reagent EEDQ (**31**, scheme 6). As previously mentioned (see 2.3.3), EEDQ is commonly used in the literature to mediate amide couplings between amines and dibromomaleimides bearing carboxylic acids.¹⁻³ 3,4-dibromomaleimide-N-acetic acid and EEDQ were dissolved in dimethylsulfoxide (DMSO), and then DFO was added, and stirred for 3 h to give DFO-DBM (**28**, scheme 6). The reaction was acidified with a trifluoroacetic acid (TFA) to quench unreacted EEDQ and prevent dibromomaleimide hydrolysis. Components of the reaction mixture were then separated using preparative C18 reverse phase HPLC, to give DFO-DBM in 22 % yield.



Scheme 6 - Synthesis of DFO-DBM (28**)**

The analytical C18 reverse-phase HPLC chromatogram of DFO-DBM (figure 84) shows a major peak with a retention time of 7.95 min. The ¹H NMR spectrum (figure 85) of DFO-DBM contains 12 signals corresponding to 12 proton environments. Some ethyl and pentyl protons in the DFO motif have similar chemical shifts resulting in coincident resonances at 400 MHz (figure 85, environments b-f, g, h, k). Signals corresponding to protons in environments j and l are also observed (in DMSO-d₆). A singlet is observed at 4.08 ppm (figure 85, environment a) corresponding to the methylene protons of the linker between the dibromomaleimide and the DFO chelator. Lastly, the terminal methyl group of the DFO chelator is seen as a singlet resonance at 1.96 ppm (figure 85, environment i). Structural assignments of the protons for DFO-DBM were made with the aid of COSY NMR data (appendix, figure 123).

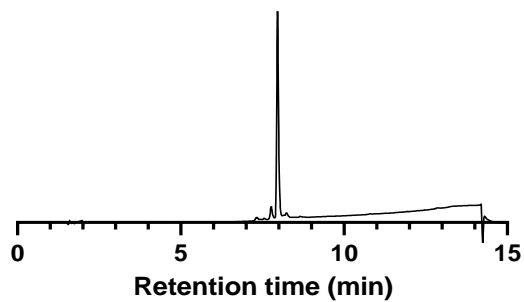


Figure 84 - Analytical C18 reverse-phase HPLC chromatogram with UV detection at λ_{254} of DFO-DBM with a retention time of 7.95 min. For details see 2.10.

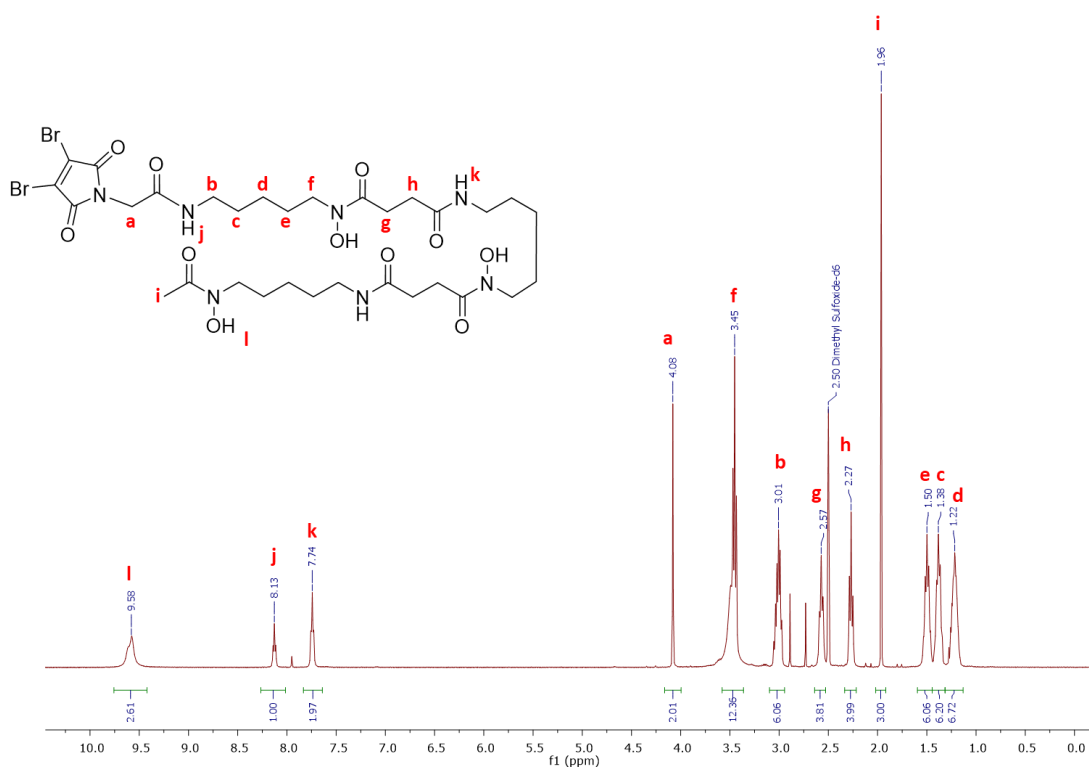


Figure 85. ^1H NMR spectrum for DFO-DBM (D6-DMSO, 400 MHz). The similar chemical environment of the atoms along the DFO pentyl and ethyl chains resulted in coincident resonances at 400 MHz.

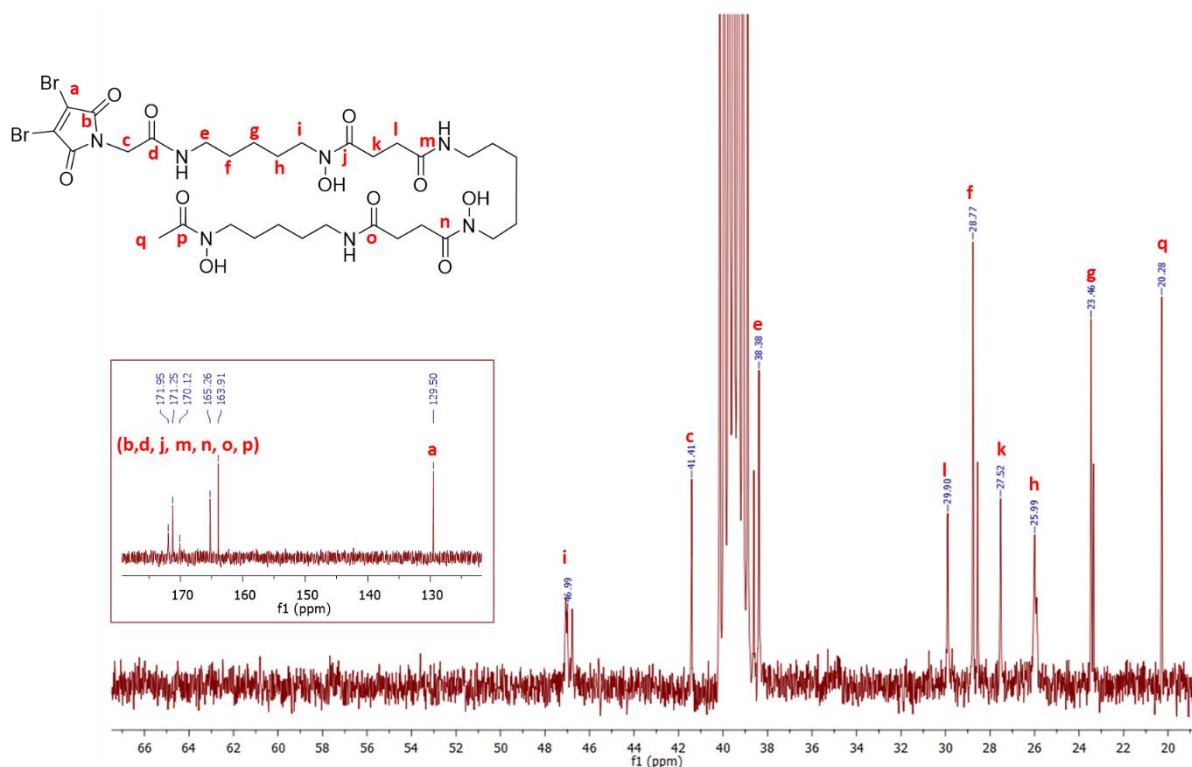


Figure 86. ^{13}C NMR spectrum for DFO-DBM (DMSO- d_6 , 100 MHz). The similar chemical environment of the atoms along the DFO pentyl and ethyl chains resulted in often coincident, or nearly coincident resonances at 100 MHz.

The ^{13}C NMR spectrum of DFO-DBM (figure 86) shows that the atoms along the DFO pentyl and ethyl chains are in similar chemical environments resulting in coincident, or nearly coincident resonances for many of these signals at 100 MHz. For example, whilst DFO-DBM possesses 7 carbonyl carbons (figure 86, environments b, d, j, m, n, o, p), only five signals are seen in the ^{13}C NMR spectrum in the region associated with carbonyl carbons (171.95–163.91 ppm). The vinylic carbons (figure 86, environment a) of the dibromomaleimide group resonate at 129.50 ppm. Structural assignments of the carbon atoms for DFO-DBM were made with the aid of HSQC NMR data (appendix, figure 124). Dibromomaleimides containing a methylene linker are known to hydrolyse rapidly (within an hour) in pH 8.5 BBS at ambient temperatures.¹ The presence of only one vinylic carbon signal in the ^{13}C NMR spectrum indicates that the dibromomaleimide is sufficiently stable in DMSO. The carbon atom of the methylene linker between the dibromomaleimide and DFO motif resonates at 41.41 ppm.

Lastly, mass spectrometry was used to characterise DFO-DBM (figure 87a) where an $[\text{M}+\text{H}]^+$ peak at $m/z = 856.1894$ was observed in good agreement with the

calculated $[M+H]^+$ $m/z = 856.1912$. The peak corresponding to $[M+Na]^+$ was also observed at $m/z = 878.1716$, in good agreement with the calculated $m/z = 878.1735$. As previously mentioned (see 2.3.3), bromine has two stable isotopes ^{79}Br and ^{81}Br with 51% and 49% abundance respectively. Therefore, compounds containing bromine atoms give rise to characteristic isotope patterns in a mass spectrum. An expanded view of the $[MH]^+$ peak (figure 87b) shows the characteristic isotope fingerprint pattern for a species containing two bromine atoms, in good agreement with the calculated isotope pattern.

134617 #5-20 RT: 0.07-0.24 AV: 8 NL: 1.39E6
T: FTMS {1,1} + p ESI Full ms [100.00-1000.00]

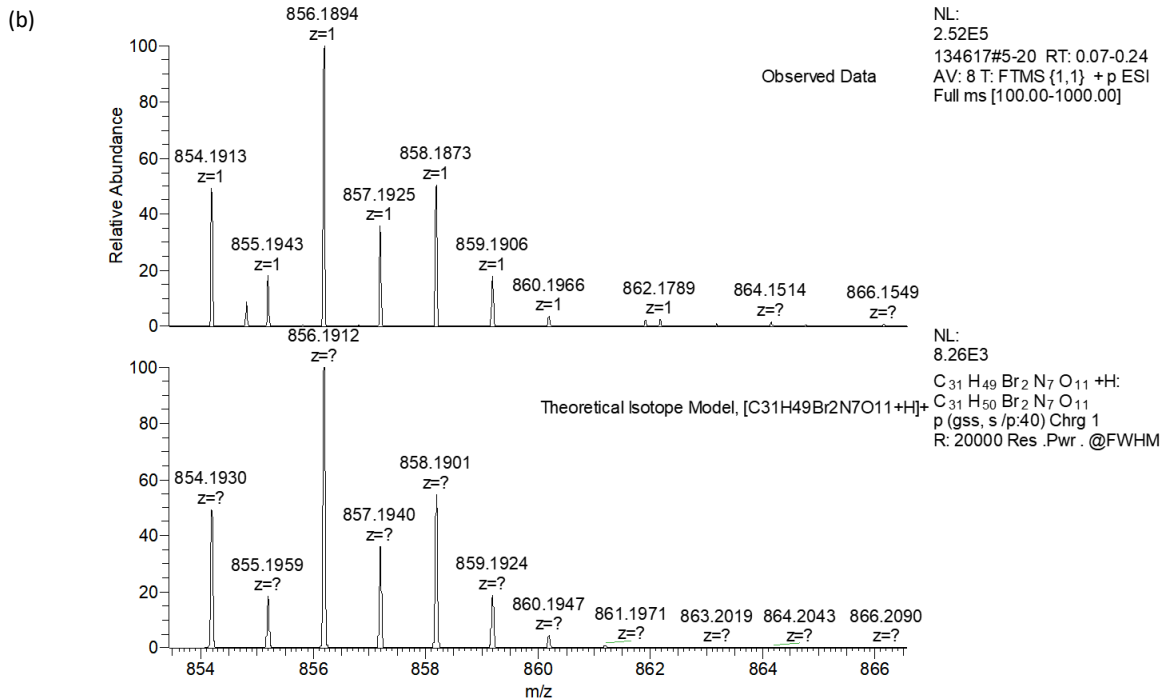
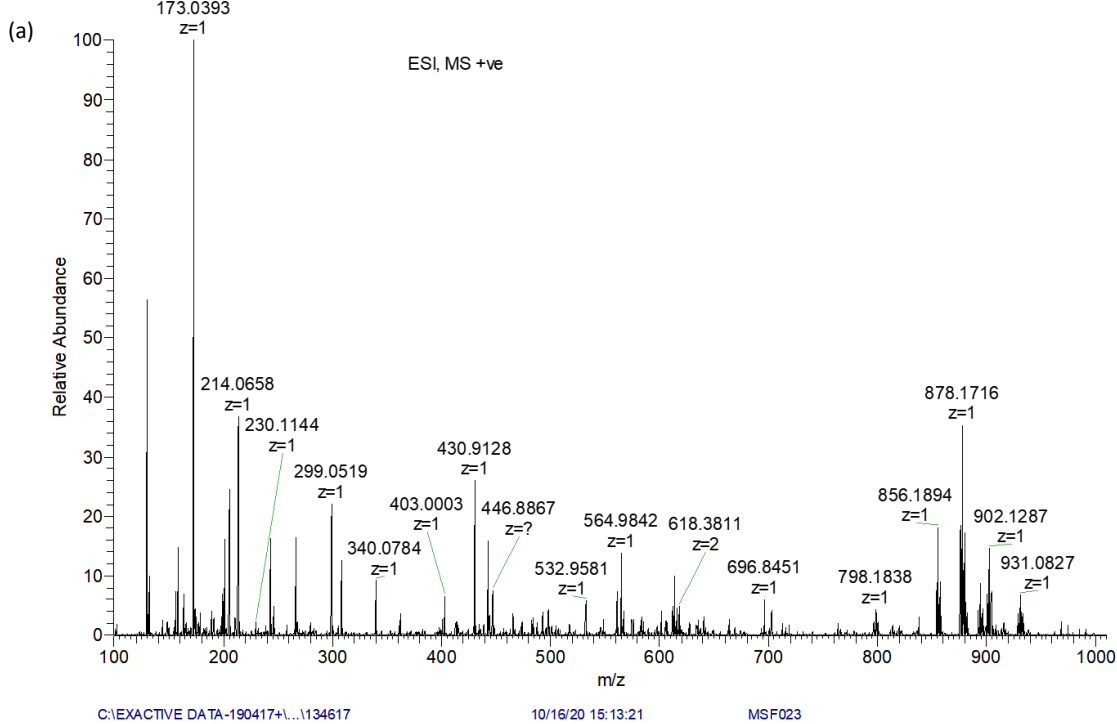
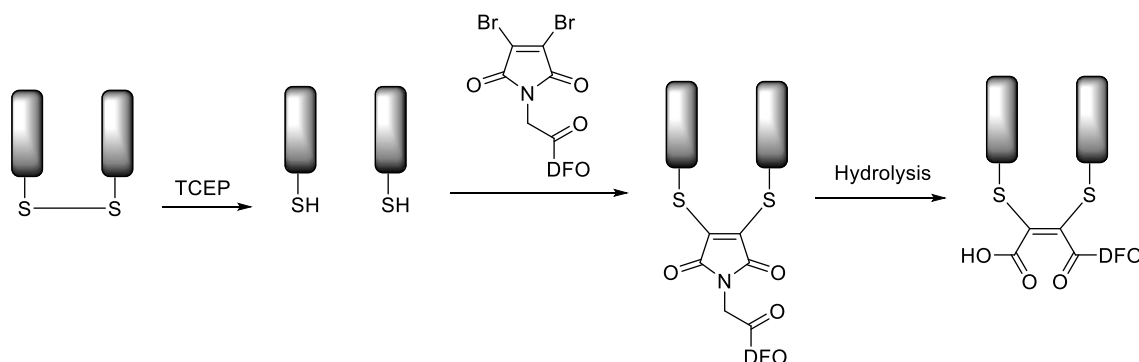


Figure 87 - High-resolution ESI-mass spectrum for DFO-DBM: (a) full mass spectrum; (b) expanded view of the [MH]⁺ signal showing (top) observed data and (bottom) calculated isotope pattern.

3.4 Synthesis and characterisation of DFO-DBM-trastuzumab

The conjugation reaction between DFO-DBM and trastuzumab was attempted using the same method as discussed previously for the bioconjugation reaction between sar-DBM and trastuzumab (see 2.4) and SDS-PAGE was used to monitor the progression of the conjugation reaction.



Scheme 7 - The reaction between DFO-DBM and reduced disulfides, with subsequent hydrolysis to give a dithiomaleamic acid conjugate.

Scheme 7 shows the reaction between DFO-DBM and a reduced disulfide, with subsequent hydrolysis to give a dithiomaleamic acid conjugate. Compared to sar-DBM, DFO-DBM contains a shorter alkyl linker between the chelator and the dibromomaleimide. It has been shown that the proximity of the amide bond to the dithiomaleimide group impacts the rate of hydrolysis (see 1.7.2). Dithiomaleimide conjugates bearing shorter, less electronically insulative linkers undergo hydrolysis more quickly than those with longer, more electronically insulative linkers.¹ To optimise the conjugation and subsequent hydrolysis reaction between DFO-DBM and trastuzumab, three post-conjugation hydrolysis periods were trialled and the resulting bioconjugates were assessed by SDS-PAGE under non-reducing and reducing conditions (figure 88).

Trastuzumab was reduced with 6 eq. of TCEP, and complete reduction was evidenced by the presence of two protein bands (figure 88, lane 6). The addition of DFO-DBM to the reduced antibody mixture results in conjugation. The desired product is the full-antibody conjugate bearing four DFO-DBM moieties. “Half-antibody” conjugate formation is in competition with formation of this desired product and is often produced in dibromomaleimide conjugations. As previously discussed (see 2.4.1), half-antibody conjugates form as a result of intrachain disulfide bridging between two thiol groups on one heavy chain.

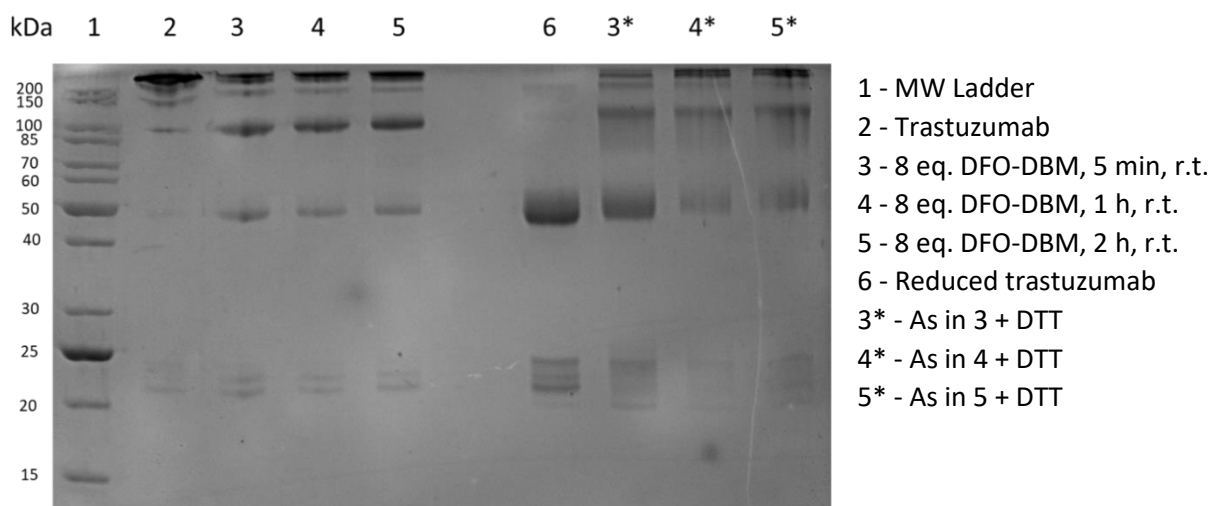


Figure 88 - The conjugation reaction between reduced trastuzumab and DFO-DBM was monitored over time by SDS-PAGE (lanes 3-5). Conjugation products were also analysed using reducing SDS-PAGE conditions (lanes 3*-5*).

8 eq. of DFO-DBM were added to reduced trastuzumab and incubated at ambient temperature, with samples analysed by SDS-PAGE at 5 min, 1 h, or 2 h under non-reducing (figure 88, lanes 3-5) and reducing (figure 88, lanes 3*-5*) conditions. After 5 min incubation with DFO-DBM, a large proportion of reduced disulfides were rebridged as evidenced by the appearance of full- and half-antibody conjugates (figure 88, lane 3). Whilst a significant proportion of the full- and half-conjugates remained under reducing conditions (figure 88, lane 3*), hydrolysis was incomplete as evidenced by increased intensity of the bands associated with heavy and light chain fragments relative to those observed under non-reducing conditions (figure 88, lane 3). As the duration of the post-conjugation hydrolysis period increased from 5 min to 1 h, and then to 2 h, the proportion of DFO-DBM-trastuzumab that had been hydrolysed increased: as the hydrolysis period duration increased fewer changes were observed when comparing reducing and non-reducing conditions indicating that hydrolysis was nearing completion after 2 h. Therefore, in subsequent bioconjugation reactions of DFO-DBM to trastuzumab, the conjugation reaction was left at ambient temperature for 2 h to promote complete hydrolysis. Whilst these conditions promoted complete conjugate hydrolysis, small amounts of undesired heavy and light chain species were still observed (figure 88, lane 5).

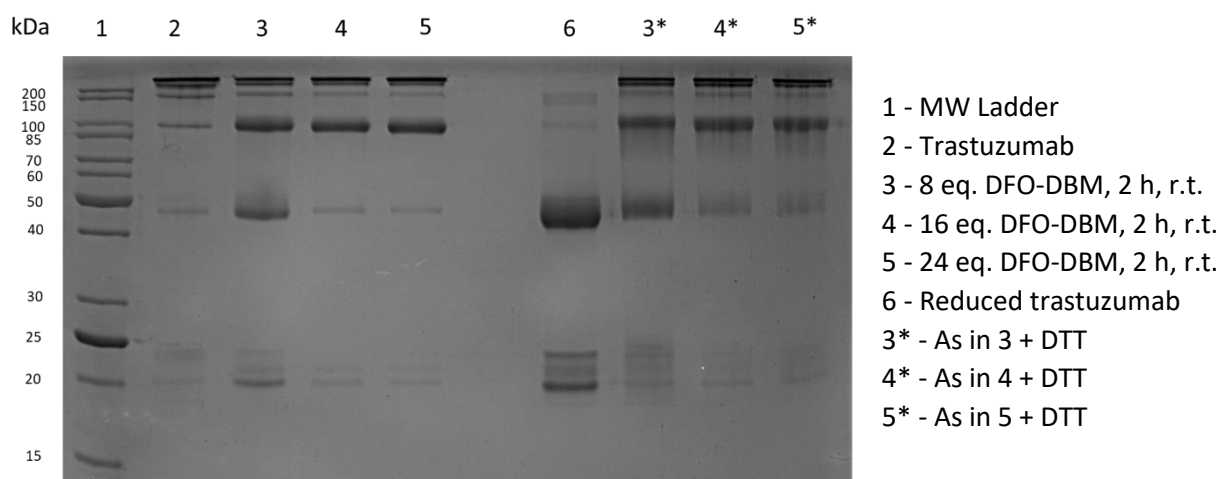


Figure 89 - The conjugation reaction between reduced trastuzumab and varying equivalents of DFO-DBM was monitored by SDS-PAGE (lanes 3-5). Conjugation products were also analysed using reducing SDS-PAGE conditions (lanes 3*-5*).

To assess the influence of the number of equivalents of DFO-DBM used, conjugation to trastuzumab was undertaken using 8, 16 or 24 eq. of DFO-DBM (figure 89). Improved conjugation efficiency was observed when >8 eq. of DFO-DBM was used. When 16 eq. or 24 eq. of DFO-DBM were used (figure 89, lanes 4 and 5), a decrease in intensity was observed for the bands associated with heavy chain and light chain fragments compared to when 8 eq. of DFO-DBM were used (figure 89, lane 3). Regardless of the number of equivalents of DFO-DBM used, complete hydrolysis was observed after 2 h, as indicated by negligible heavy and light chain reformation under reducing conditions (figure 89, lanes 3*-5*). No difference in the relative intensity of bands was observed between the conjugation reaction when 16 eq. or 24 eq. of DFO-DBM were used. Therefore 16 eq. of DFO-DBM were used in future conjugation reactions with trastuzumab.

Size exclusion methods including PD10 columns and spin filtration through a 50 kDa MWCO spin filter were used to isolate DFO-DTM-trastuzumab from excess reagents. After deglycosylation (see 1.3.1, 2.4.4), the bioconjugate was analysed by high resolution mass spectrometry (figure 90, table 5). Half-and full-antibody DFO-DTM-trastuzumab conjugates were detected (Figure 90a, Table 5), as well as unmodified light chain, and unmodified full-antibody.

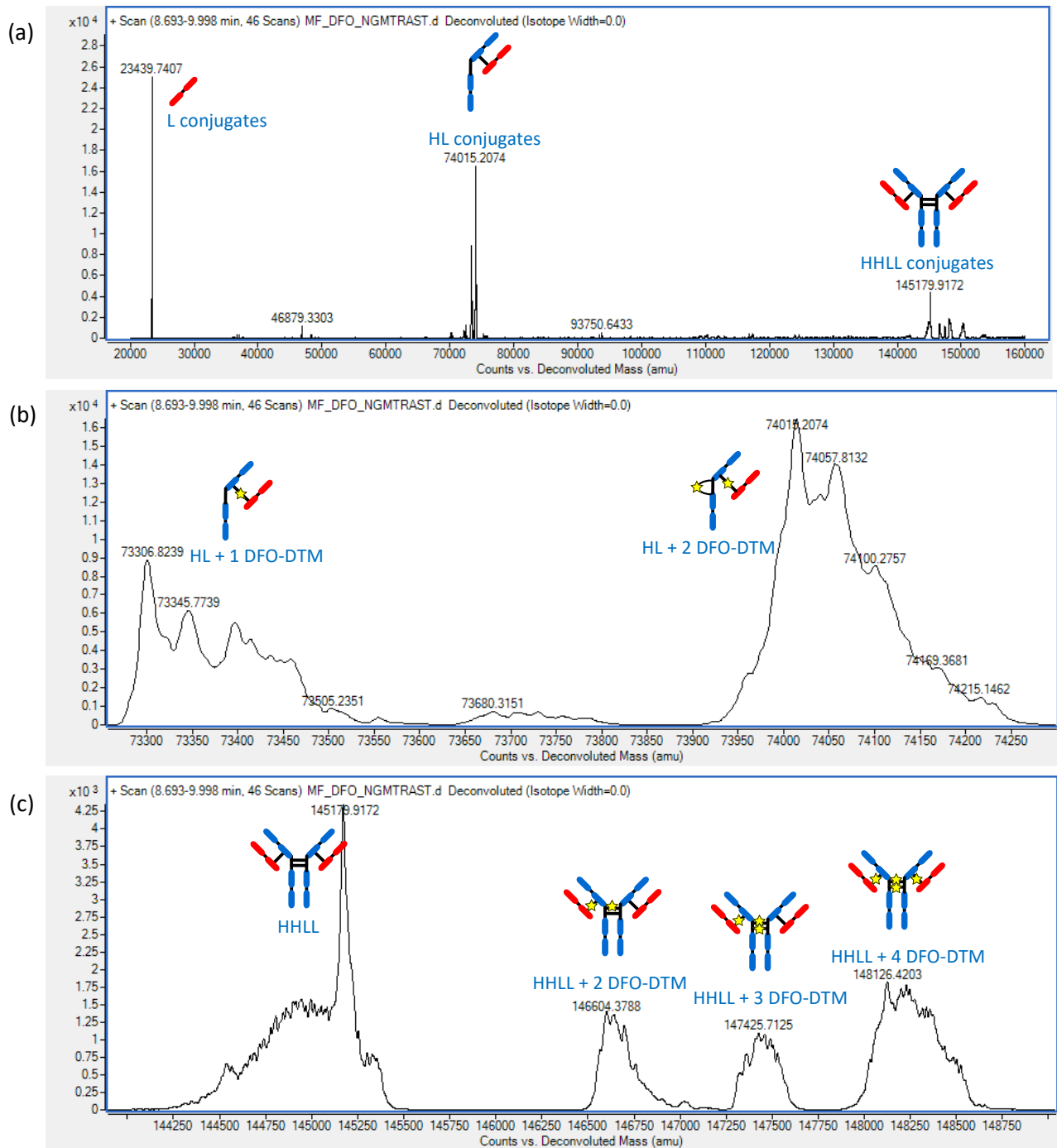


Figure 90 - High resolution ESI deconvoluted mass spectrum of DFO-DTM-trastuzumab: (a) full spectrum, (b) expanded view of the region associated with half-antibody conjugates, and (c) expanded view of the region associated with full-antibody conjugates (see table 5 for assignments).

Table 5 - ESI-MS data for DFO-DTM-trastuzumab

Antibody species	Counts vs Deconvoluted Mass (amu)	
	Observed	Calculated
trastuzumab		
HHLL	145180	145167
HL	-	72584
H	-	49150
L	23440	23440
DFO-DTM-trastuzumab		
HL + 1 DFO-DTM	73307	73305
HL + 2 DFO-DTM	74015	74017
HHLL + 2 DFO-DTM	146604	146610
HHLL + 3 DFO-DTM	147324	147322
HHLL + 4 DFO-DTM	148032	148034

The expanded mass spectrum view of the region associated with half-antibody conjugates (figure 90b) showed the presence of two conjugate species. These corresponded to half-antibody conjugates bearing one DFO-DTM moiety (HL + 1 DFO-DTM) and two DFO-DTM moieties (HL + 2 DFO-DTM). The expanded mass spectrum view of the region associated with full-antibody conjugates (figure 90c) showed the presence of three conjugate species. These corresponded to full-antibody bearing two DFO-DTM moieties (HHLL + 2 DFO-DTM), three DFO-DTM moieties (HHLL + 3 DFO-DTM), or four DFO-DTM moieties (HHLL + 4 DFO-DTM). Generally, mass spectrum signals for DFO-DTM-trastuzumab were broader than those typically observed for DBM conjugates described in previous works.^{4,5} This behaviour was also seen in the mass spectrum for sar-DTM-trastuzumab (see 2.4.4) and has been attributed to trace metal ion complexation, which leads to a range of species that are distinguishable by mass spectrometry leading to broader signals.⁶

Previous studies have shown that dibromomaleimide conjugates can display variable loading though the major product often has a DAR of 4. For example, alkyne-DBM (**32**, 2-(3,4-dibromo-2,5-dioxo-2,5-dihydro-1H-pyrrol-1-yl)-N-(prop-2-yn-1-yl)acetamide, figure 91) was conjugated to trastuzumab, and analysed by mass spectrometry.⁷ Results showed two major peaks corresponding to HHLL + 4

alkyne-DTM, and HL + 2 alkyne-DTM both with DAR of 4. However, minor peaks were also observed in the mass spectrum corresponding to variably conjugated half- and full-antibody conjugates with DAR less than or greater than 4, though these peaks were much less intense. When larger and more complex molecules are appended to dibromomaleimides, the resulting conjugates often display more variable loading. For example, doxorubicin-DBM (**33**, figure 91) was conjugated to trastuzumab and analysed by mass spectrometry.⁷ Expanded views of the mass spectrum regions corresponding to and half- and full-antibody conjugates demonstrated that a mixture of species was present. For the half-antibody region, the most intense peak corresponded to the half-antibody conjugate bearing two doxorubicin moieties. A smaller, less intense peak was also visible in this region corresponding to the half-antibody conjugate bearing just one doxorubicin moiety. For the full-antibody region, the most intense peak corresponded to the full-antibody conjugate bearing four doxorubicin moieties. Less intense peaks were also visible corresponding to unmodified trastuzumab, and full-antibody conjugates bearing two or three doxorubicin moieties. The authors describe the possibility of payload loss occurring *via* acid catalysed maleamic acid cyclisation to give maleic anhydride-rebridged disulfide bonds (**34**, scheme 8).⁸ This process was accelerated for the doxorubicin conjugate by the high temperatures used during LCMS analysis (60 °C, 0.1 % formic acid). Interestingly, these anhydride species are relatively stable towards hydrolysis, meaning that maleic acid conjugates (**35**, scheme 8) are not formed under the same acidic conditions and elevated temperatures. Importantly, the mass spectrum for DFO-DTM-trastuzumab (figure 90) contained no evidence to support maleic anhydride formation as a route to DFO payload loss from the conjugate meaning that incomplete conjugation was likely to be the main formation route for conjugates with DAR<4.

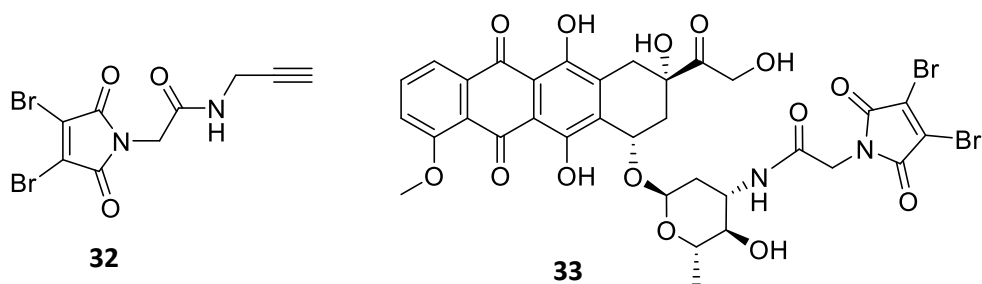
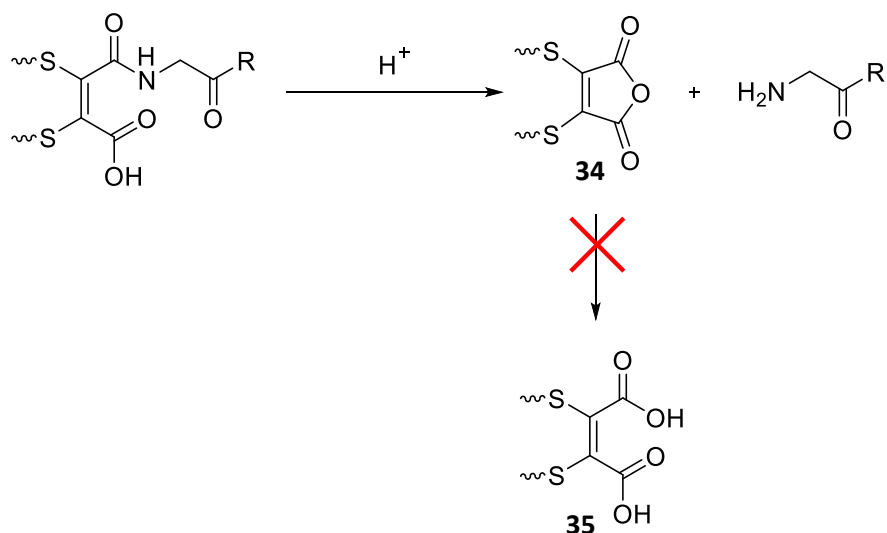


Figure 91 - Structures for alkyne-DBM (32), and doxorubicin-DBM (33).

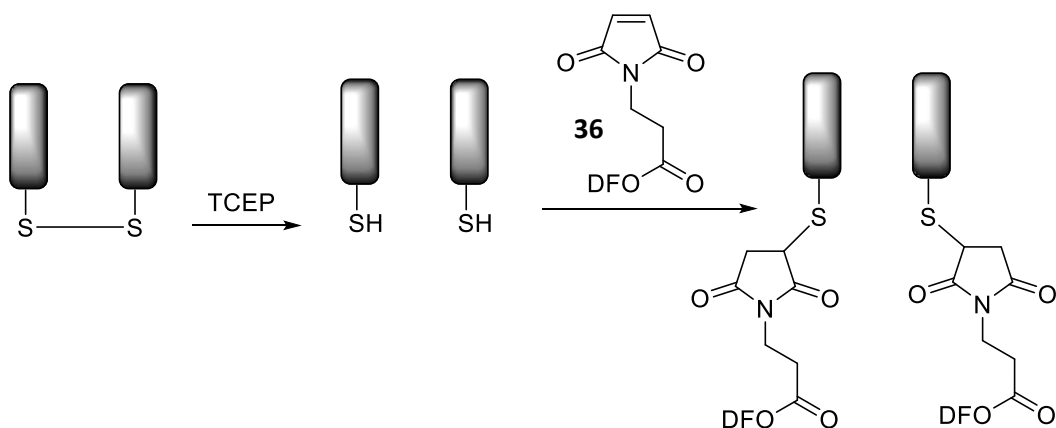


Scheme 8 - Cyclisation of a dithiomaleamic acid to give a maleic anhydride (34). Under the same conditions this maleic anhydride does not ring open to give the dithiomaleic-acid (35).

3.5 Synthesis and characterisation of DFO-mal-trastuzumab

The stability of ^{89}Zr -DFO-DTM-trastuzumab was assessed alongside ^{89}Zr -DFO-mal-trastuzumab, produced from DFO-maleimide (DFO-mal, **36**, scheme 9) - a commercially available bifunctional chelator.

When DFO-mal was added to reduced trastuzumab, a conjugation reaction took place (*via* Michael addition) between reduced thiols and DFO-mal in a 1:1 ratio (scheme 9). Note that this method does not result in disulfide rebridging, in contrast to conjugations with dibromomaleimides. 16 eq. of DFO-mal were used for two reasons: i) to mimic the number of equivalents of DFO-DBM that were added in the synthesis of DFO-DTM-trastuzumab; ii) to promote complete conjugation between



Scheme 9 - The conjugation reaction between reduced dithiols and DFO-mal (36).

DFO-mal and all eight reduced thiols of the antibody. The conjugation reaction between DFO-mal and trastuzumab was monitored using SDS-PAGE (figure 92). Complete disulfide reduction was evidenced by the presence of just two protein bands (figure 92, lane 3): one for the heavy chain (~50 kDa) and another for the light chain (~20 kDa). Addition of DFO-mal had minimal impact on the intensity of the bands associated with heavy and light chains and did not generate significant amounts of higher molecular weight species such as half- and full-antibody conjugates, consistent each hinge region cysteine group reacting with a single equivalent of DFO-mal.

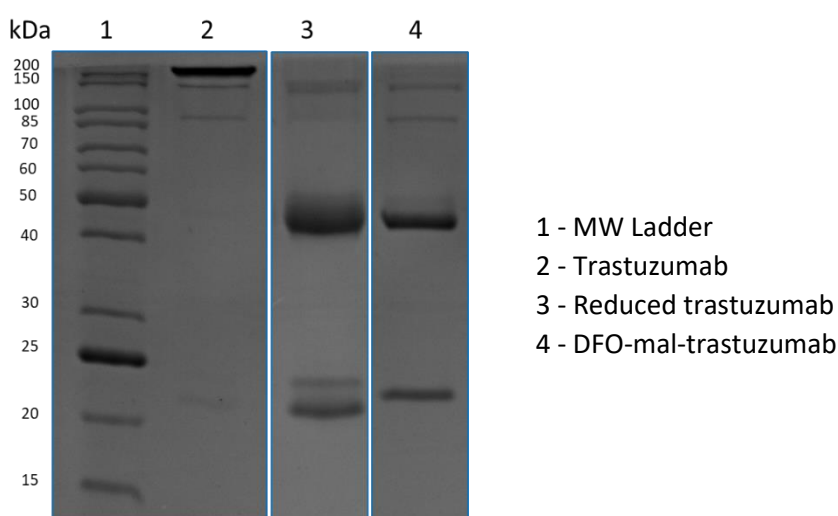


Figure 92 - The conjugation reaction between DFO-mal and trastuzumab was monitored using SDS-PAGE.

DFO-mal-trastuzumab was then analysed using high resolution mass spectrometry (figure 93, table 5). The mass spectrum for DFO-mal-trastuzumab (figure 93a) shows two major peaks corresponding to heavy and light chain conjugates. The expanded view of the region of the mass spectrum region associated with light chain conjugates (figure 93b) shows multiple peaks. The signal at 24152 amu corresponds to a light chain bearing one DFO-mal moiety (L + 1 DFO-mal), in good agreement with the calculated value (24151 amu). The other peaks within this cluster likely appear as a result of adduct formation. For example, the most intense peak corresponds to a species with a mass of 24196 amu. This difference in mass could be due to adduct formation with two sodium ions (each with 22 amu) resulting in an increase of 44 amu. Similarly, the expanded view of the region of the mass spectrum region associated with heavy chain conjugates (figure 93c) shows a complex peak. The peak with the lowest mass corresponds to a heavy chain

conjugate bearing three DFO-mal moieties (H + 3 DFO-mal). This is the greatest number of DFO-mal moieties that can be conjugated to a heavy chain fragment *via* Michael addition to reduced interchain disulfides. The observed value of 51289 amu is in good agreement with the calculated value of 51280 amu. Overall mass spectroscopy suggests that complete conjugation has occurred between DFO-mal and reduced trastuzumab to generate a species with 8 DFO-mal moieties per trastuzumab – one DFO chelator for every reduced thiol group.

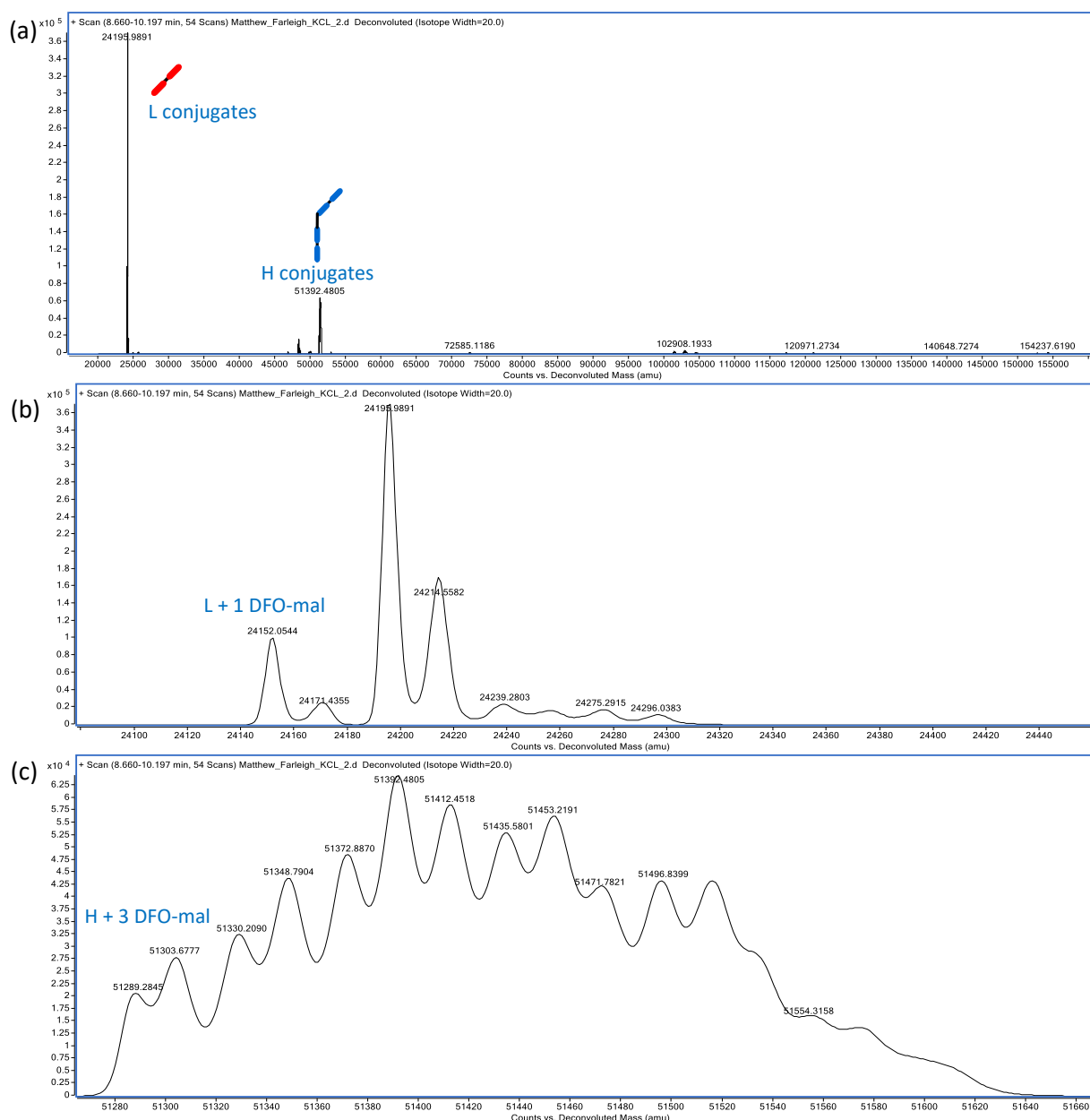


Figure 93 - High resolution ESI deconvoluted mass spectrum of DFO-mal-trastuzumab: (a) full spectrum, (b) expanded view of the region associated with light chain conjugates, and (c) expanded view of the region associated with heavy chain conjugates (see table 5 for assignments).

Table 5 - ESI-MS data for DFO-mal-trastuzumab

Counts vs Deconvoluted Mass (amu)		
Antibody species	Observed	Calculated
trastuzumab		
HLL	-	145167
H	-	49150
L	-	23440
DFO-mal-trastuzumab		
L + 1 DFO-mal	24152	24151
H + 3 DFO-mal	51289	51280

3.6 Comparing the bioconjugations DFO-DBM and DFO-maleimide with trastuzumab

Since DFO-DBM and DFO-mal were both conjugated to trastuzumab *via* reduced disulfide bond thiols, reduction was carried out using the same method for each bifunctional chelator. Likewise, the number of equivalents of each bifunctional chelator added was the same as previously mentioned. However, the durations of the conjugation reactions were different: the maleimide reaction with trastuzumab was complete within 30 min, whereas the DBM conjugation reaction was left for 2 h to ensure complete hydrolysis. The conjugates were isolated and purified in the same way (size-exclusion), and recovery was similar for DFO-DTM-trastuzumab and DFO-mal-trastuzumab with 47 % and 49 % antibody recovery efficiency respectively. During the conjugation reaction, regardless of which bifunctional chelator was used, approximately half of the initial amount of antibody was lost. Purification by PD10 size exclusion column was not observed to significantly decrease the amount of conjugate present. Instead, the majority of the product was likely lost during spin filtration. In the future this limitation could be overcome by using dialysis techniques, though less concentrated final products are typically obtained using these methods.

SDS-PAGE is a useful technique for monitoring the progression of dibromomaleimide-based conjugation reactions where the reduction and subsequent rebridging of interchain disulfides can be monitored. In contrast, since maleimides cannot rebridge reduced disulfide bonds, the number and position of

protein bands are unchanged post-reduction. Comparing the SDS-PAGE gels obtained for DFO-DTM-trastuzumab (figure 89, lane 4) and DFO-mal-trastuzumab (figure 92, lane 4), the former more closely resembled unmodified trastuzumab. In short, the interchain covalent bond structure in DFO-DTM-trastuzumab resembled unmodified trastuzumab more closely than DFO-mal-trastuzumab. As previously mentioned (see 1.5.2), antibody conjugates that lack covalent bonds between interchain protein domains typically display decreased thermal stability and compromised Fc profiles (FCγR binding or ADCC activity).⁴ In this respect, it is likely that DFO-DTM-trastuzumab (containing interchain disulfide bonds) possesses advantages over DFO-mal-trastuzumab (lacking interchain disulfide bonds).

3.7 Radiolabelling DFO-DTM-trastuzumab and DFO-mal-trastuzumab with $^{89}\text{Zr}^{4+}$

DFO-DTM-trastuzumab and DFO-mal-trastuzumab were radiolabelled in a solution (HEPES, 0.2 M) containing $^{89}\text{Zr}^{4+}$. PBS and HEPES are both commonly used buffer solutions in radiolabelling reactions with $^{89}\text{Zr}^{4+}$.^{9,10} ^{89}Zr is typically received in its oxalate form (typically in 1.0 M oxalic acid) and must be neutralised prior to dissolution in the final buffer solution. Studies typically rely upon initial treatment of the ^{89}Zr stock solution with solutions of Na_2CO_3 , then adding this neutralised solution to the final buffer solution. Instead, to prepare the ^{89}Zr radiolabelling solution, a Sep-Pak Light Plus QMA cartridge-based method was used, simplifying this process.¹¹ An aqueous solution containing $^{89}\text{Zr}(\text{oxinate})_4$ was loaded onto the Sep-Pak Light Plus QMA cartridge and washed with water to remove the oxalic acid, then eluted with HCl (1 M) to give $^{89}\text{ZrCl}_4$ in HCl solution. Drying of this solution under a stream of N_2 gas, followed by reconstitution in HEPES (0.2 M) yielded the final radiolabelling solution at pH 7. This solution was then used to radiolabel DFO-DTM-trastuzumab and DFO-mal-trastuzumab with $^{89}\text{Zr}^{4+}$. Typically, the conjugates were dissolved in ammonium acetate solution (0.1 M) to a concentration of 50 μM . 5 μL of the $^{89}\text{Zr}^{4+}$ radiolabelling solution was then added to 10 μL of the conjugate solution. Radiolabelling was allowed to proceed for 10 min, at ambient temperature and ITLC was used to determine radiochemical yields. Various concentrations of bioconjugate were assessed (3 nM - 33.3 μM , figure 94a) and the $^{89}\text{Zr}^{4+}$ stock solution was analysed periodically by ITLC showing minimal colloid formation over time.

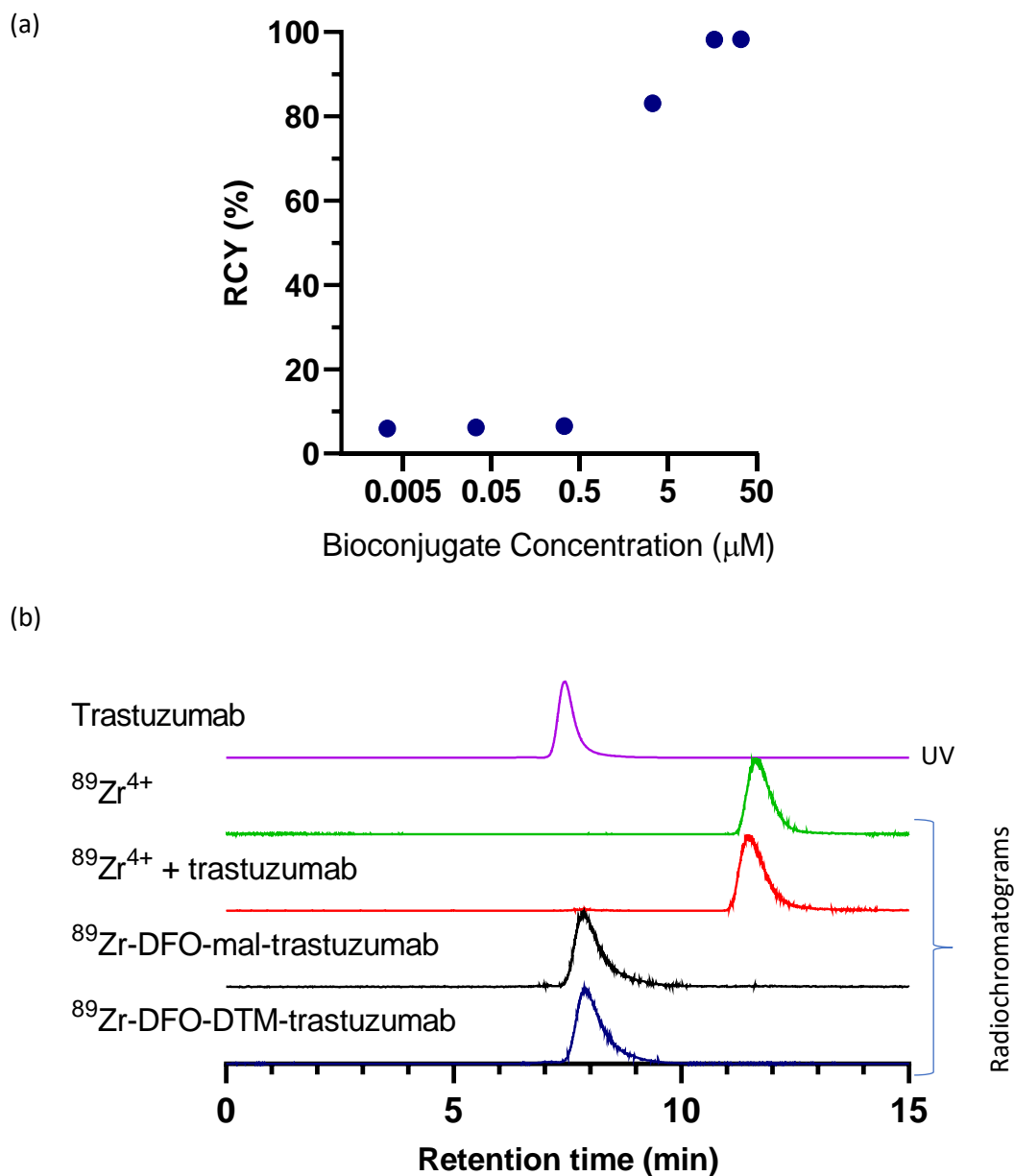


Figure 94 - a) Radiochemical yields for the reaction of $^{89}\text{Zr}^{4+}$ with DFO-DTM-trastuzumab at different concentrations (33.3 μM , 16.7 μM , 3.3 μM , 333.3 nM, 33.3 nM, and 3.3 nM) of immunoconjugate at ambient temperature for 10 min. b) SE-HPLC: UV trace (280 nm) for trastuzumab (purple); radiochromatograms for $^{89}\text{Zr}^{4+}$ (green), $^{89}\text{Zr}^{4+}$ + trastuzumab (red), ^{89}Zr -DFO-mal-trastuzumab (black), and ^{89}Zr -DFO-DTM-trastuzumab (blue).

Radiochemical yields increased as the concentration and amounts of DFO-DTM-trastuzumab was increased. Near quantitative (>98 %) radiochemical yields were obtained at bioconjugate concentrations of 16.7 μM and 33.3 μM . A lower

radiochemical yield of 83.1 % was achieved at a bioconjugate concentration of 3.3 μM . Below this concentration, radiochemical yields were less than 7%.

SE-HPLC was also used to analyse the products of these radiolabelling reactions, using previously discussed methods (figure 94b, see 2.10). ^{89}Zr -DFO-DTM-trastuzumab had a retention time of 7.75 min closely matching the retention time observed for unmodified trastuzumab (figure 94b, purple trace). Non-protein-bound $^{89}\text{Zr}^{4+}$ was eluted at 11.58 min most likely as [$^{89}\text{Zr}(\text{EDTA})$] (figure 94b, green trace). $^{89}\text{Zr}^{4+}$ was added to trastuzumab and allowed to react for 10 min to assess the extent of non-specific binding of $^{89}\text{Zr}^{4+}$ to unmodified trastuzumab. SE-HPLC (figure 94b, red trace) showed only a small amount (<2 %) of ^{89}Zr was bound to the native antibody. In contrast, near-quantitative (>99 %) radiochemical yields were achieved when $^{89}\text{Zr}^{4+}$ was added to DFO-DTM-trastuzumab with a maximum specific activity of 5 MBq/mg. These results demonstrate that conjugation of DFO-DBM to trastuzumab facilitates radiolabelling with $^{89}\text{Zr}^{4+}$.

DFO-mal-trastuzumab was radiolabelled under the same conditions as DFO-DTM-trastuzumab. Radiochemical yields were assessed using ITLC, showing that ^{89}Zr -DFO-DTM-trastuzumab was formed in near quantitative (>98 %) radiochemical yield at a bioconjugate concentration of 33.3 μM . ^{89}Zr -DFO-mal-trastuzumab was also analysed by SE-HPLC (figure 94b, black trace) where radiochemical yields were in agreement with ITLC (>98 %). Additionally, the retention time of DFO-mal-trastuzumab matched the retention time observed for unmodified trastuzumab.

A maximum specific activity of 40 MBq/mg was achieved for ^{89}Zr -DFO-mal-trastuzumab; higher than the maximum specific activity achieved for ^{89}Zr -DFO-DTM-trastuzumab described above (5 MBq/mg). Additionally, near quantitative radiolabelling was achievable at lower bioconjugate concentrations for DFO-mal-trastuzumab than with DFO-DTM-trastuzumab. ^{89}Zr -DFO-mal-trastuzumab likely has a higher DAR than ^{89}Zr -DFO-DTM-trastuzumab due to reduced thiols reacting in a 1:1 ratio with DFO-maleimide: mass spectrometry suggests a DAR close to 8 for DFO-mal-trastuzumab (see 3.5).

Prior studies have reported significantly higher specific activities for ^{89}Zr -radiolabelled antibody conjugates. N-(S-acetyl)thioacetyl-DFO (DFO-SATA, see 1.5.2) was conjugated to the monoclonal antibody 323/A3 (anti-EpCAM, see 1.3.3).¹² ^{89}Zr was received as $^{89}\text{Zr}(\text{oxalate})_4$ and oxalic acid was removed by

sublimation under vacuum before 100 μ L of solution containing the bioconjugate (0.1 M ammonium acetate) was added and left for 1 h at ambient temperature. ITLC analysis of the radiolabelling mixture indicated >90 % radiochemical yield. The radioimmunoconjugate was then separated from excess unreacted $^{89}\text{Zr}^{4+}$ by size exclusion chromatography (Sephadex G-25) to give a specific activity of 185 MBq/mg.

More recently, TFP-DFO (see 1.5.2) has been used to produce a DFO-trastuzumab conjugate, containing 6.8 ± 0.8 accessible chelators per trastuzumab.¹³ ^{89}Zr was received in 1 M oxalic acid as $^{89}\text{Zr}(\text{oxalate})_4$, and neutralised by the addition of 1 M Na_2CO_3 . DFO-trastuzumab was added (0.25 mg, 50 μ L, 0.9 % saline), mixed gently, and incubated at ambient temperature for 1-2 h. ITLC analysis of the radiolabelling indicated radiochemical yields of 78 ± 4 % were achieved after 1 h. The bioconjugate was separated from unreacted $^{89}\text{Zr}^{4+}$ by size exclusion chromatography (Sephadex G-25M) achieving a specific activity of 104.3 ± 2.1 MBq/mg with 99 % radiochemical purity.

In another study, DFO-NCS (see 1.5.2) was conjugated to daratumumab (anti-CD38) by incubation in sodium carbonate solution (pH 9, 0.1 M) at 37 °C for 1 h. The bioconjugate was then added to a solution containing neutralised $^{89}\text{Zr}(\text{oxalate})_4$ and incubated at 37 °C for 1 h. As above, it was necessary to remove excess unreacted $^{89}\text{Zr}^{4+}$ from the radioimmunoconjugate, this time using a 40 kDa MWCO Zeba spin column. A specific activity of 370 MBq/mg was achieved.¹⁴

The specific activities achieved for ^{89}Zr -DFO-DTM-trastuzumab and ^{89}Zr -DFO-mal-trastuzumab could be improved by adding a greater amount of ^{89}Zr to achieve non-quantitative radiochemical yields followed by removal of unreacted $^{89}\text{Zr}^{4+}$ by size exclusion chromatography as discussed above. Further work is required to fully understand and improve upon the low specific activities generated for ^{89}Zr -DFO-DTM-trastuzumab and DFO-mal-trastuzumab. There are three major hypotheses that could explain the low specific activities obtained:

i) The number of radiometallic ions that can be attached to a bioconjugate is proportional to the number of chelators attached to the bioconjugate. For DFO-DTM-trastuzumab and DFO-mal-trastuzumab, mass spectrometry analysis (see 3.4 and 3.5) showed that approximately 4 and 8 DFO moieties are attached to the bioconjugates respectively. This should be sufficient to achieve higher specific

activities. Many site-specific conjugates in the literature have lower DAR but still achieve high specific activities. For example, DFO-maleimide has been site-specifically conjugated to heavy chain 'free' thiol residues in an engineered trastuzumab antibody.¹⁵ Mass spectrometry results suggest that this conjugate had a DAR of 2, with one DFO-mal moiety appended to each heavy chain. The resulting conjugate was radiolabelled with $^{89}\text{Zr}^{4+}$ achieving a specific activity of 107.3 ± 18.5 MBq/mg.

ii) To coordinate $^{89}\text{Zr}^{4+}$, the DFO chelator must be accessible by the solvent. It is possible that conjugation of DFO-DBM to interchain disulfides places the chelator in a position that is not readily accessible by the solvent, thereby limiting the efficiency of the radiolabelling reaction. In contrast, the conjugation of DFO-maleimide to a single reduced thiol may position the DFO chelator in a more optimal position leading to improved radiolabelling characteristics.

iii) Lastly, the presence of trace metal ion contaminants can greatly reduce radiochemical yields by competing with $^{89}\text{Zr}^{4+}$ for the DFO chelator. EDTA and chelex resin were used to reduce the possibility of trace metal ion contamination. However, it is possible that during bioconjugation, purification, or radiolabelling trace metal ions were unwittingly introduced to the bioconjugate resulting in sub-optimal radiolabelling and low specific activities.

The synthesis and radiolabelling of ^{89}Zr -DFO-mal-trastuzumab can be compared with prior studies involving this radioimmunoconjugate. One study conjugated DFO-maleimide to trastuzumab, followed by radiolabelling with $^{89}\text{Zr}^{4+}$ to produce ^{89}Zr -DFO-mal-trastuzumab with a specific activity of 91 MBq/mg.¹⁶ This study used a 10 eq. of TCEP with incubation at 37 °C for 30 min to achieve antibody reduction. In contrast, we used 6 eq. of TCEP with incubation at 37 °C for 2 h to achieve antibody reduction. Additionally, the study used 20 eq. of DFO-maleimide, whereas we used 16 eq. Despite these differences, mass spectrometry showed similar results to those discussed above for DFO-mal-trastuzumab indicating a DAR close to 8. This suggests that there were minimal structural differences between DFO-mal-trastuzumab generated in previous studies and the work discussed here. Therefore, differences in the specific activities generated for ^{89}Zr -DFO-mal-trastuzumab in the literature and the results discussed here are likely caused by radiochemical challenges such as trace metal ion contamination.

The relative distribution of ^{89}Zr -radioactivity present in different ^{89}Zr -DFO-DTM-trastuzumab antibody fragments was analysed by SDS-PAGE (figure 95) as described previously (see 2.5). Radioactive bands as visualised by autoradiography were coincident with protein bands visualised by bright light imaging. Quantitative analysis showed that 54.4 % of ^{89}Zr signal was associated with full-antibody conjugates, whilst 34.9 % of ^{89}Zr signal was associated with half-antibody. Of the remaining ^{89}Zr signal, 7.7 % was associated with heavy chain conjugates and 3.0 % was associated with light chain conjugates. These results are suggestive of efficient disulfide rebridging, with the majority of ^{89}Zr radioactivity associated with half- and full-antibody conjugates.

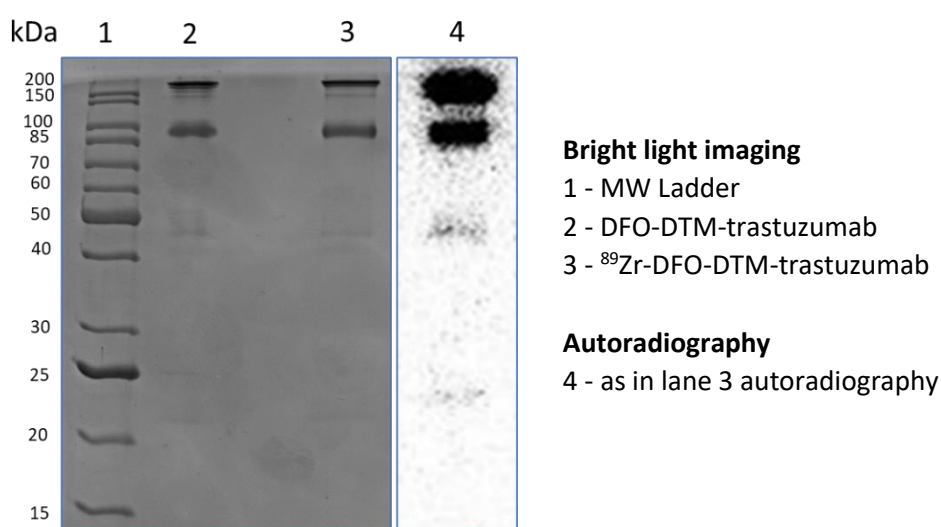


Figure 95 - SDS-PAGE bright light image (left) and autoradiography image (right) of ^{89}Zr -DFO-DTM-trastuzumab. The radioactivity signal from the radiolabelled immunoconjugate was coincident with the stained protein bands corresponding to full- and half-antibody.

Similarly, SDS-PAGE analysis of ^{89}Zr -DFO-mal-trastuzumab (figure 96) showed that the radioactivity signal (autoradiography) from the radiolabelled immunoconjugate was coincident with the stained protein bands (figure 96, lanes 3 and 4). Quantitative analysis showed that 63.4 % of ^{89}Zr signal was associated with the heavy chain and 25.3 % was associated with the light chain. The ratio of between the ^{89}Zr signal associated with the heavy chain and the light chain approximates 2.5:1. This value is significant as this also corresponds to the number of DFO-mal moieties on the heavy chain (up to 3 DFO-mal) and light chain (1 DFO-mal) as determined previously by mass spectrometry (figure 93, table 5). The remaining

^{89}Zr radioactivity was associated with full- (6.6 %), and half-antibody (4.7 %) conjugates.

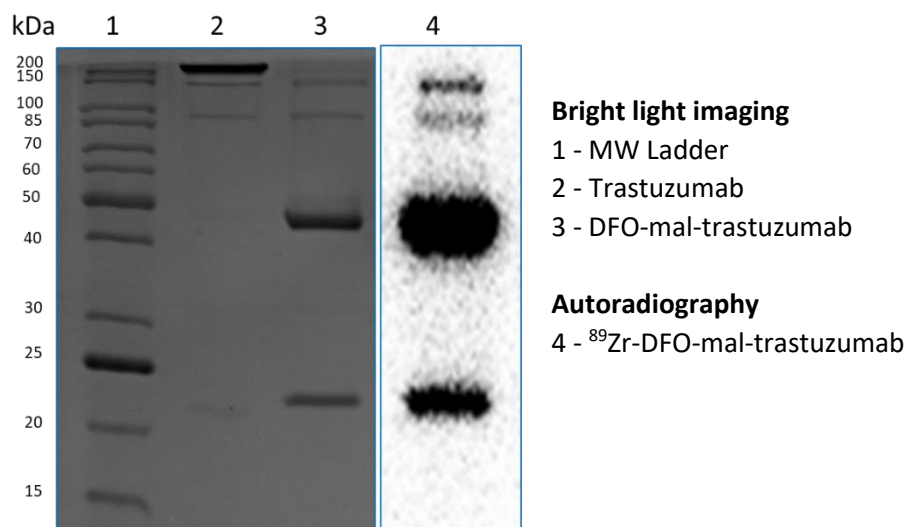


Figure 96 - SDS-PAGE bright light image (left) and autoradiography image (right) of ^{89}Zr -DFO-mal-trastuzumab. The radioactivity signal from the radiolabelled immunoconjugate was coincident with the stained protein bands corresponding to heavy and light chain species.

3.8 Stability of ^{89}Zr -DFO-DTM-trastuzumab and ^{89}Zr -DFO-mal-trastuzumab in glutathione solution and human serum over 8 days

The retro-Michael instability of maleimide conjugates (see 1.6.2) is a well-established route to payload loss.¹⁷⁻¹⁹ Retro-Michael mediated degradation generates maleimide species, which can form conjugates with other thiol species in solution. Whilst hydrolysis of maleimide conjugates renders them stable towards this degradation, this process is slow relative to payload loss. NMR studies have shown that under near physiological conditions (0.2 M PBS, pH 7.4, 37 °C, with 10 % D_2O) significant payload loss was observed from maleimide-thiol (4-mercaptophenylacetic acid, N-acetyl-L-cysteine, 3-mercaptopropionic acid) conjugates over 5 days when one molar equivalent of glutathione was added.²⁰ In contrast, dithiomaleamic acid conjugates are mechanistically unsusceptible to retro-Michael mediated payload loss (see 1.7). However, prior to hydrolysis dithiomaleimide conjugates can undergo thiol exchange resulting in loss of payload. Therefore, dibromomaleimide conjugates are subjected to post-conjugation hydrolysis prior to use, generating maleamic acid derivatives that are stable towards thiol exchange.

The relative stabilities of ^{89}Zr -DFO-mal-trastuzumab and ^{89}Zr -DFO-DTM-trastuzumab were compared by incubating the immunoconjugates in glutathione solution at 37 °C for 8 days. Both immunoconjugates were radiolabelled with $^{89}\text{Zr}^{4+}$ to a specific activity of 2.5 MBq/mg. Biologically, most cells have a cytosolic glutathione concentration of between 1-2 mM, though concentrations can be as high as 10 mM in the cytosol of certain cells such as hepatocytes.²¹ Therefore, 10 mM glutathione concentration was used in this study to represent the most forcing biologically relevant conditions. Aliquots were taken for analysis by SE-HPLC (figure 97) after 0 d, 1 d, 4 d, and 8 d. This glutathione stability study was conducted at both pH 5.5 and pH 7.0.

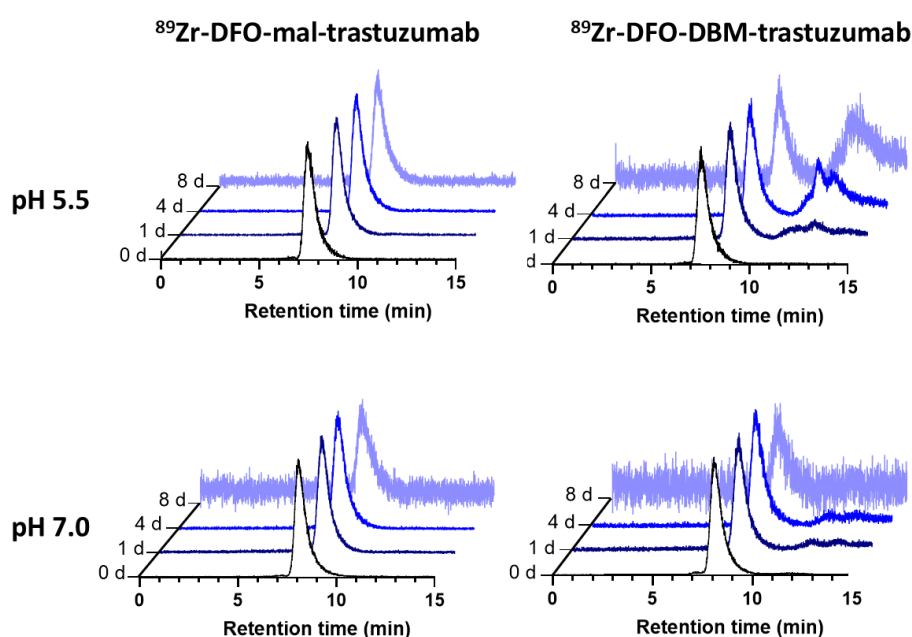


Figure 97 - SE-HPLC radiochromatograms obtained for the stability study of ^{89}Zr -DFO-mal-trastuzumab and ^{89}Zr -DFO-DTM-trastuzumab in 10 mM glutathione solution over 8 d at 37 °C, either at pH 5.5 or pH 7.0.

SE-HPLC radiochromatograms for the glutathione stability of ^{89}Zr -DFO-mal-trastuzumab (figure 97, left) show the presence of a single peak, corresponding to ^{89}Zr -DFO-mal-trastuzumab (7.75 min), at each time point assessed, and at both pH values assessed. These results indicate high stability for this radioimmunoconjugate over 8 days under the conditions tested. In contrast, SE-HPLC radiochromatograms for the glutathione stability of ^{89}Zr -DFO-DTM-trastuzumab (figure 97, right) showed that after 1 d incubation in glutathione solution at 37 °C, in addition to ^{89}Zr -DFO-DTM-trastuzumab, new signals were present with retention times consistent with non-protein-bound ^{89}Zr radioactivity (>11.5 min). This observation was consistent

with loss of ^{89}Zr radioactivity from ^{89}Zr -DFO-DTM-trastuzumab. At pH 5.5, these late-eluting peaks comprised 27 % of total ^{89}Zr radioactivity after 1 d, increasing to 55 % and 63 % at 4 d and 8 d respectively. At pH 7 non-protein-bound radioactivity comprised 15 % of total ^{89}Zr radioactivity after 1 d, increasing to 18 % after 4 d. At pH 7, poor signal to noise ratio at the 8-day time-point prevented accurate quantification of radioactive species. The observation that ^{89}Zr radioactivity is lost from the bioconjugate more quickly at pH 5.5 compared to pH 7 suggested that this process was pH dependent.

Exposure of dithiomaleic acid conjugates to low pH has previously been used as a method to release the *N*-functionalised payload. At pH 4.5 in a mixture of methanol and water, complete payload cleavage has been observed from an *N*-functionalised DBM derivative after just 72 h.⁸ Prior studies have evaluated the degree of payload loss from trastuzumab-DTM-AlexaFluor conjugates containing either a methylene linker (as in DFO-DTM-trastuzumab) or a phenyl linker (see 1.7.2).¹ This experiment was conducted in citrate-phosphate buffer solution at pH 5.5 and pH 7.4 over 24 h or 10 d respectively. At pH 5.5 no loss of payload was detected for the conjugate with the methylene linker over 24 h. Conversely, 4 % of the phenyl-maleamic acid conjugate payload was lost after 24 h at pH 5.5. Both conjugates were stable at pH 7.4 with no payload loss detected up to 10 d.

To evaluate the effect of glutathione presence upon the stability of ^{89}Zr -DFO-DTM-trastuzumab and ^{89}Zr -DFO-mal-trastuzumab at pH 7, the radioimmunoconjugates were incubated in HEPES (0.2 M) for 8 d at 37 °C, *without* glutathione. SE-HPLC of the resulting solution (figure 98) showed a single peak in each radiochromatogram with retention times corresponding to the radioimmunoconjugates, suggesting good stability for both immunoconjugates over 8 d in HEPES. As previously mentioned, ^{89}Zr -DFO-DTM-trastuzumab was unstable at pH 7 in HEPES when 10 mM glutathione was present, with ≥ 18 % of the ^{89}Zr signal lost from the conjugate over 8 d. These results suggest that at pH 7, the presence of glutathione results in loss of ^{89}Zr from ^{89}Zr -DFO-DTM-trastuzumab. These results are unprecedented since prior studies have demonstrated the high stability of DTM conjugates in the presence of glutathione near neutral pH.

There are three potential explanations for the observed instability of ^{89}Zr -DFO-DTM-trastuzumab in glutathione solution:

i) Glutathione competes with DFO for $^{89}\text{Zr}^{4+}$, resulting in transchelation of $^{89}\text{Zr}^{4+}$ from DFO to glutathione, forming a ^{89}Zr -glutathione species. This is unlikely since the ^{89}Zr -DFO complex is present in ^{89}Zr -DFO-mal-trastuzumab and ^{89}Zr -DFO-DTM-trastuzumab, yet instability is only observed for the latter. An additional carboxylate is present in ^{89}Zr -DFO-DTM-trastuzumab, which could contribute to this decreased stability *via* interaction with the Zr^{4+} coordination sphere. However, this hypothesis seems unlikely since chelators with higher denticity than DFO (>6 donor atoms) often show comparable or even superior complex stability with Zr^{4+} compared to DFO (see 1.5.1).

ii) Glutathione-mediated thiol exchange leads to loss of payload generating an ^{89}Zr -DFO-DBM-glutathione conjugate. This is also unlikely, since prior to radiolabelling and incubation in glutathione solution, hydrolysis of the dithiomaleimide species was carried out to give dithiomaleamic acid conjugates, which are not susceptible to thiol exchange. Hydrolysis and resulting thiol stability were confirmed by SDS-PAGE by the addition of 100 eq. of DTT (figures 88 and 89).

iii) At pH 5.5, payload loss may have occurred *via* dithiomaleic acid cyclisation to give a maleic anhydride (scheme 8). This reaction results in the loss of the *N*-functionalised payload.⁸ However, as previously mentioned, the instability observed for ^{89}Zr -DFO-DTM-trastuzumab at pH 7 in the presence of 10 mM glutathione is unprecedented in the literature. Additional work is necessary to confirm the validity of these observations and elucidate the method for payload loss.

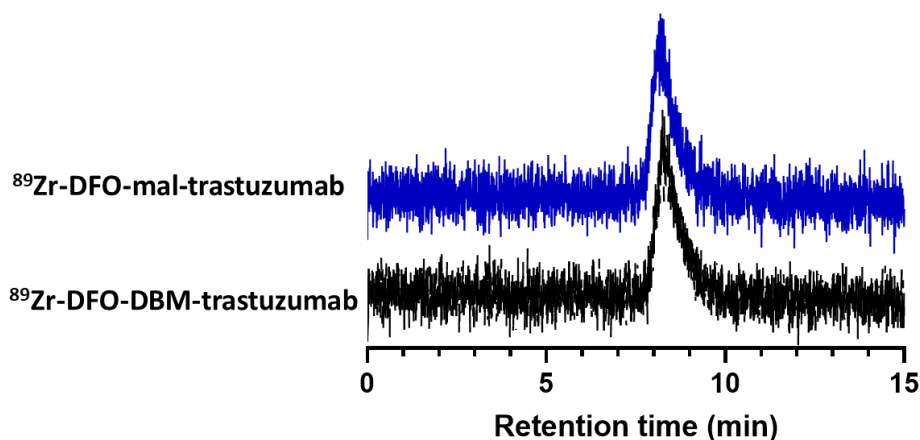


Figure 98 - SE-HPLC radiochromatograms of ^{89}Zr -DFO-mal-trastuzumab and ^{89}Zr -DFO-DTM-trastuzumab after incubation in HEPES solution for 8 d at 37 °C.

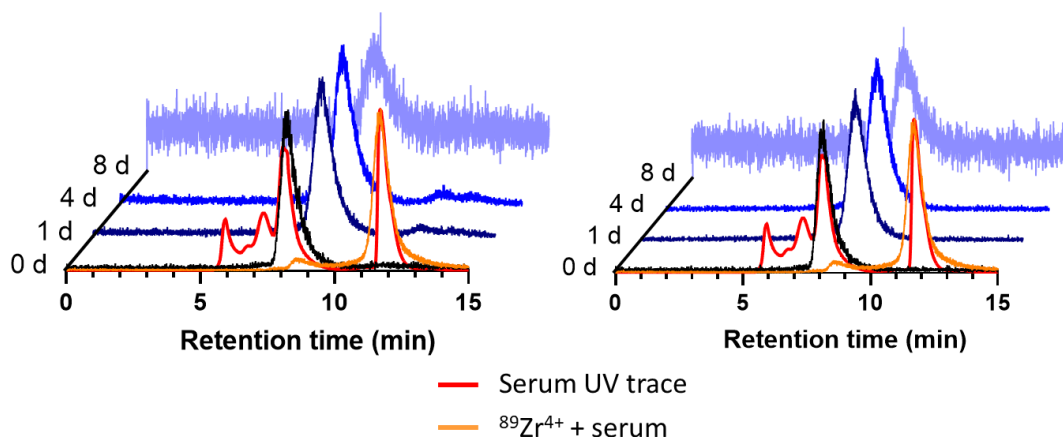
^{89}Zr -DFO-DTM-trastuzumab ^{89}Zr -DFO-mal-trastuzumab

Figure 99 - SE-HPLC radiochromatograms obtained for the stability study of ^{89}Zr -DFO-DTM-trastuzumab and ^{89}Zr -DFO-mal-trastuzumab in human serum over 8 d at 37 °C. Also shown is the UV trace obtained for human serum at 254 nm.

The stabilities of ^{89}Zr -DFO-mal-trastuzumab and ^{89}Zr -DFO-DTM-trastuzumab were also assessed in human serum over 8 d at 37 °C. The immunoconjugates were radiolabelled to a specific activity of 2.5 MBq/mg, and then diluted to a concentration of 0.66 mg of bioconjugate per 1 mL of human serum. Aliquots were taken for analysis by SE-HPLC at 0 d, 1 d, 4 d, and 8 d. SE-HPLC radiochromatograms (figure 99) showed that for ^{89}Zr -DFO-mal-trastuzumab a single peak was observed at each timepoint with retention times corresponding to the radioimmunoconjugate (7.75 min). Importantly, there were no peaks corresponding to activity bound to serum proteins (figure 99, red trace, orange trace). Signals from the radio-detector are recorded with a 30 second delay relative to the UV detector, due to the configuration of these different detectors in series. Therefore, the apparently coincident radio and UV peaks eluting at c. 8 min are in fact eluted approximately 30 seconds apart. Collectively these results indicate that ^{89}Zr -DFO-mal-trastuzumab had good stability in human serum over 8 d at 37 °C. In contrast, instability was observed for ^{89}Zr -DFO-DTM-trastuzumab where after 1 d incubation in serum a new signal was present corresponding to 2 % of total radioactivity, with a retention time >11.5 min, consistent with non-protein-bound radioactivity. Since the mobile phase contained 5 mM EDTA, it is possible that $^{89}\text{Zr}^{4+}$ first binds to serum proteins and is then chelated to give an EDTA bound ^{89}Zr species. As the incubation time in human serum increased, this non-protein-bound radioactivity signal increased to 3 % after 4 days, and 5 % after 8 days. This

observation indicates a gradual loss of ^{89}Zr radioactivity from ^{89}Zr -DFO-DTM-trastuzumab in human serum. However, at each time point evaluated, the majority of ^{89}Zr radioactivity remained associated with the peak corresponding to ^{89}Zr -DFO-DTM-trastuzumab, indicating good overall stability for this species in human serum where >95 % of total ^{89}Zr -radioactivity remained associated with ^{89}Zr -DFO-DTM-trastuzumab over 8 d at 37 °C.

The small degree of instability observed for ^{89}Zr -DFO-DTM-trastuzumab in human serum was unexpected, as was the observed high stability of ^{89}Zr -DFO-mal-trastuzumab. In a previous study a dibromomaleimide bearing the fluorophore Alexa Fluor 448 was attached to trastuzumab.²² The resulting conjugate was incubated in human serum at 37 °C for 7 d, and showed high stability, with no transfer of the fluorophore to serum albumin observed over the 7 d incubation experiment, and no “unconjugated” fluorophore was detected. The study also assessed a maleimide analogue of this fluorescent conjugate and found that it was unstable: significant transfer of the fluorophore to serum albumin was observed by SE-HPLC after only 4 d. The instability of ^{89}Zr -DFO-mal-trastuzumab in human serum has been observed in a prior study where ^{89}Zr -DFO-mal-trastuzumab was incubated in human serum for one week at 37 °C, and the stability of the conjugate was assessed using ITLC (mobile phase 50 mM EDTA, pH 5.0).²³ After one week, just 63 ± 12 % of the radioimmunoconjugate remained intact. The cause for the difference in stability observed for ^{89}Zr -DFO-mal-trastuzumab in prior studies compared to the results discussed here are unclear. It is possible that different ratios of bioconjugate-to-serum, and differences in the methods used to analyse stabilities contribute to these contradictory results.

Samples of ^{89}Zr -DFO-DTM-trastuzumab and ^{89}Zr -DFO-mal-trastuzumab from the stability experiments were also analysed by SDS-PAGE (figure 100). Lanes containing bioconjugate samples from serum stability studies used significantly less radioactivity due to restrictions on the maximum amount of undiluted serum that can be loaded onto the SDS-PAGE gel - this led to reduced intensity of bands in lanes 6 and 7 compared to lanes 2-5 (figure 100).

After 8 d at 37 °C in HEPES, ^{89}Zr signal remained associated with half- and full-antibody fragments for ^{89}Zr -DFO-DTM-trastuzumab indicating high stability (figure 100, lane 2). ^{89}Zr -DFO-mal-trastuzumab also showed high stability in HEPES after 8

d at 37 °C, with ^{89}Zr signal associated with the heavy and light chains (figure 100, lane 3). Instability was observed for ^{89}Zr -DFO-DTM-trastuzumab in 10 mM glutathione at pH 7 after incubation for 8 d at 37 °C: lane 4 contains a low intensity band (7 % of total radioactivity signal in lane) corresponding to low-molecular weight, non-protein bound ^{89}Zr -radioactivity (figure 100, lane 4) indicative of ^{89}Zr loss from the immunoconjugate. In contrast, ^{89}Zr -DFO-mal-trastuzumab showed high stability under these conditions after 8 d: no ^{89}Zr signal is observed in the region associated with non-protein bound radioactivity. ^{89}Zr -DFO-DTM-trastuzumab displayed high stability in human serum after 8 d at 37 °C, where the majority of ^{89}Zr signal corresponded to half- and full-antibody conjugates (figure 100, lane 6), with no ^{89}Zr signal observed in the region associated with serum albumin. Similarly, for ^{89}Zr -DFO-mal-trastuzumab, the majority of ^{89}Zr signal corresponded to heavy and light chains (figure 100, lane 7). These SDS-PAGE results are in agreement with SE-HPLC data for these stability experiments, which also evidence some release of ^{89}Zr from DFO-DTM-trastuzumab in the presence of GSH.

The bright light images of ^{89}Zr -DFO-DTM-trastuzumab after 8 d at 37 °C in HEPES (figure 100, lane 2) and GSH (figure 100, lane 4) were compared, with no increase in the intensity of heavy or light chains observed. This suggests that GSH-mediated cleavage of rebridged disulfides is not responsible for loss of ^{89}Zr from ^{89}Zr -DFO-DTM-trastuzumab.

Interestingly, the bright light images obtained for ^{89}Zr -DFO-mal-trastuzumab samples showed significant amounts of HH, and HHL conjugates (figure 100, lanes 3 and 5). SDS-PAGE analysis of the conjugate immediately after conjugation shows the presence of almost exclusively heavy and light chain (figure 92). Since maleimides are not capable of rebridging disulfides bonds, the reformation of HH and HHL fragments must be due to gradual reoxidation of reduced (and unreacted) thiols over 8 d at 37 °C. Since pairs of unmodified thiols are required to reform disulfide bonds, reoxidation to give HH and HHL fragments indicates incomplete conjugation - at least a proportion of ^{89}Zr -DFO-mal-trastuzumab contains < 8 DFO moieties.

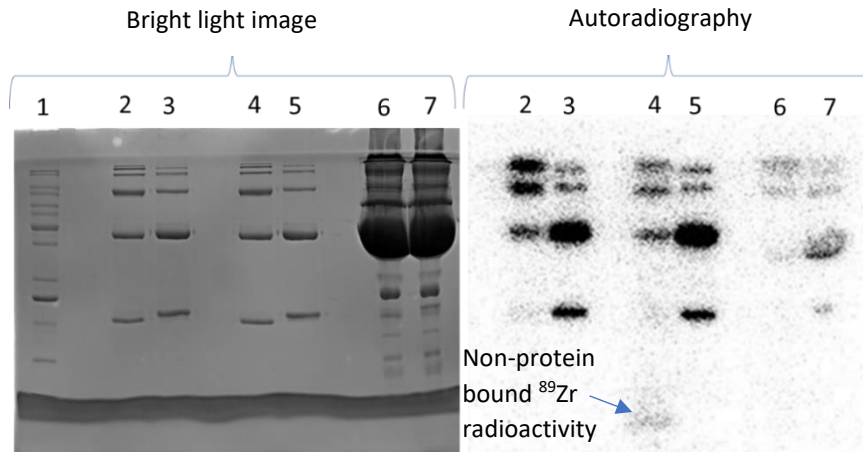


Figure 100 - SDS-PAGE gels for the stability of ^{89}Zr -DFO-mal-trastuzumab and ^{89}Zr -DFO-DTM-trastuzumab in HEPES, glutathione (GSH, pH 7), and human serum after 8 d at 37 °C. Lane 1 - MW Ladder, lane 2 - ^{89}Zr -DFO-DTM-trastuzumab in HEPES, lane 3 - ^{89}Zr -DFO-mal-trastuzumab in HEPES, lane 4 - ^{89}Zr -DFO-DTM-trastuzumab in GSH, lane 5 - ^{89}Zr -DFO-mal-trastuzumab in GSH, lane 6 - ^{89}Zr -DFO-DTM-trastuzumab in serum, lane 7 - ^{89}Zr -DFO-mal-trastuzumab in serum.

3.9 Specificity of ^{89}Zr -DFO-DTM-trastuzumab and ^{89}Zr -DFO-mal-trastuzumab for HER2

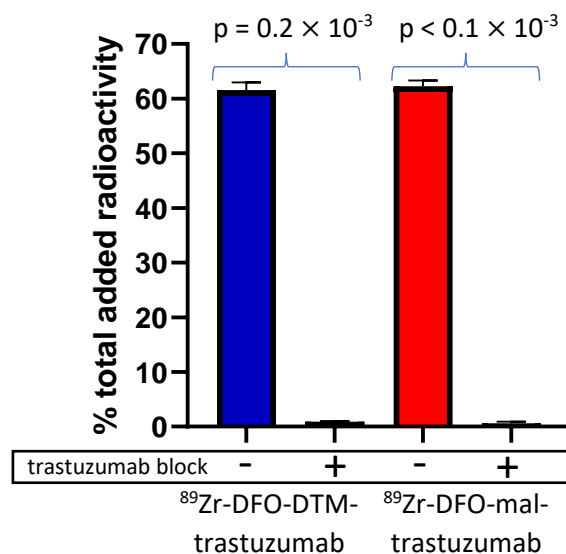


Figure 101 – Uptake of ^{89}Zr -DFO-DTM-trastuzumab (2 kBq, 0.4 μg total added compound) and ^{89}Zr -DFO-DTM-trastuzumab (2 kBq, 0.4 μg total added compound) in SKOV3 cells (2 million), with (+) and without (-) unmodified trastuzumab (15 μg) to block HER2 receptors. Bars show mean values (n=3, technical repeats) and error bars show standard deviation.

In vitro studies were carried out in collaboration with Chris Davis who provided SKOV3 cells and assisted with the design and execution of the studies. The first experiment aimed to assess and compare the specificity of ^{89}Zr -DFO-DTM-trastuzumab and ^{89}Zr -DFO-mal-trastuzumab for HER2. DFO-DTM-trastuzumab and DFO-mal-trastuzumab were radiolabelled with $^{89}\text{Zr}^{4+}$ to a specific activity of 5 MBq/mg. This specific activity was chosen since it was the highest specific activity achieved for DFO-DTM-trastuzumab, and the same was used for DFO-mal-trastuzumab to enable comparison between the radioimmunoconjugates. The radioimmunoconjugates (2 kBq, 0.4 μg) were then added to SKOV3 cells (300 μL , 2 million cells) and left to incubate for 1 h at 4 $^{\circ}\text{C}$. After incubation the supernatant was removed, cells were washed and harvested, and cell-bound ^{89}Zr radioactivity was quantified by gamma counting (figure 101). This process was repeated but with the addition of excess unmodified trastuzumab (15 μg) to block HER2 binding sites. ^{89}Zr -DFO-DTM-trastuzumab demonstrated uptake in SKOV3 cells with 61.6 ± 1.4 % of total added radioactivity bound to the cells. When unmodified trastuzumab was added, cell binding was inhibited and just 0.9 ± 0.1 % of total added radioactivity was bound to the SKOV3 cells. This difference was statistically significant ($p=0.2 \times 10^{-3}$). Similarly, ^{89}Zr -DFO-mal-trastuzumab demonstrated uptake in SKOV3 cells with 60.5 ± 1.0 % of total added radioactivity bound to the cells. When unmodified trastuzumab was added, cell binding was inhibited and just 0.6 ± 0.3 % of total added radioactivity was bound to the SKOV3 cells ($p<0.1 \times 10^{-3}$). Collectively these data show that ^{89}Zr -DFO-DTM-trastuzumab and ^{89}Zr -DFO-mal-trastuzumab retained specificity for the HER2 receptor with no statistically significant difference in uptake between the two radioimmunoconjugates.

3.10 Evaluation of immunoreactive fraction for ^{89}Zr -DFO-DTM-trastuzumab and ^{89}Zr -DFO-mal-trastuzumab

As previously discussed, (see 1.3.1 and 1.5.2) antibody modification can negatively impact a conjugate's biological activity compared to the native unmodified antibody. The fraction of radioimmunoconjugate that retains affinity for its target receptor post-modification is described as the immunoreactive fraction. This metric can be used to quantitatively assess the impact of antibody modification upon target receptor affinity. The immunoreactive fraction for a conjugate can be evaluated using a method developed by Lindmo and co-workers.²⁴ This method involves determining radioimmunoconjugate cell uptake over a range of increasing

cell concentrations effectively providing an increasing concentration of the target receptor per measurement. As the concentration of target receptor increases, the proportion of cell-bound radioimmunoconjugate is expected to increase until all bioconjugate with retained target receptor affinity has bound to the cell surface receptor and then “plateaus”. The plateau typically occurs at less than 100 % cell uptake, as a proportion of the immunoconjugate will no longer have affinity for the target receptor. To accurately calculate the immunoreactive fraction, an infinitely high concentration of cells would be required to ensure a plateau has been reached. This scenario can be approximated by plotting the reciprocal of cell uptake against the reciprocal of the cell concentration to give a straight line. The y-intercept of this straight line is equivalent to the reciprocal of the immunoreactive fraction. Immunoreactive fractions are usually expressed as a decimal where 0.00 refers to a sample with no affinity for the target receptor, and 1.00 refers to a sample where all antibody conjugates possess affinity for the target receptor.

⁸⁹Zr-DFO-DTM-trastuzumab and ⁸⁹Zr-DFO-mal-trastuzumab were each (2 kBq, 0.4 µg) added to varying concentrations of SKOV3 cells and incubated for 1 h at 4 °C followed by washing, and gamma-counting of cells to quantify cell-bound ⁸⁹Zr radioactivity. This process was repeated with the addition unmodified trastuzumab (15 µg) where cell-bound ⁸⁹Zr radioactivity represented non-specific binding to SKOV3. Cell bound radioactivity was calculated as a % of total added radioactivity and plotted against the SKOV3 cell concentration (figure 102). A one site - total binding model was used to generate a non-linear fit for the data generated by each radioimmunoconjugate. For all cell concentrations non-specific binding was negligible (<1 %) for both radioimmunoconjugates. The reciprocal of cell uptake was plotted against the reciprocal of the cell concentration to give a straight line (figure 103). The reciprocal of the y-intercept was calculated to give the immunoreactive fraction for each radioimmunoconjugate. The immunoreactive fraction for ⁸⁹Zr-DFO-DTM-trastuzumab was calculated to be 0.46, whilst the immunoreactive fraction for ⁸⁹Zr-DFO-mal-trastuzumab was calculated to be 0.49. These results indicate that the two radioimmunoconjugates possessed similar immunoreactive fractions. These immunoreactive fractions are lower than that generally seen in the literature. For example, a ⁸⁹Zr-DFO-trastuzumab conjugate bearing 6.8 ± 0.8 chelators per antibody (conjugated *via* a DFO-TFP-ester, see 1.5.2,

figure 31) had an immunoreactive fraction of 0.87 although a different HER2 cell line (BT-474) was used in this instance.¹³

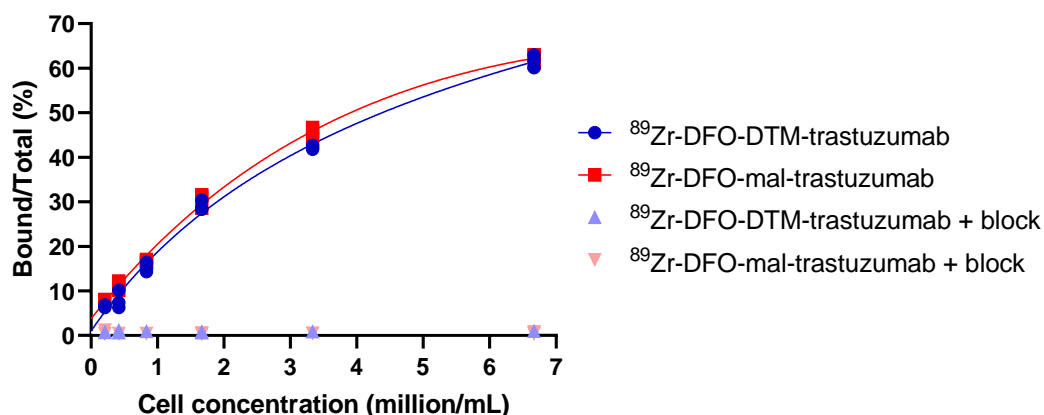


Figure 102 - Bound/total radioactivity (% of total added radioactivity that is bound to the SKOV3 cells) versus SKOV3 cell concentration. For each radioimmunoconjugate, data was gathered in technical triplicate at each cell concentration and all data points are shown.

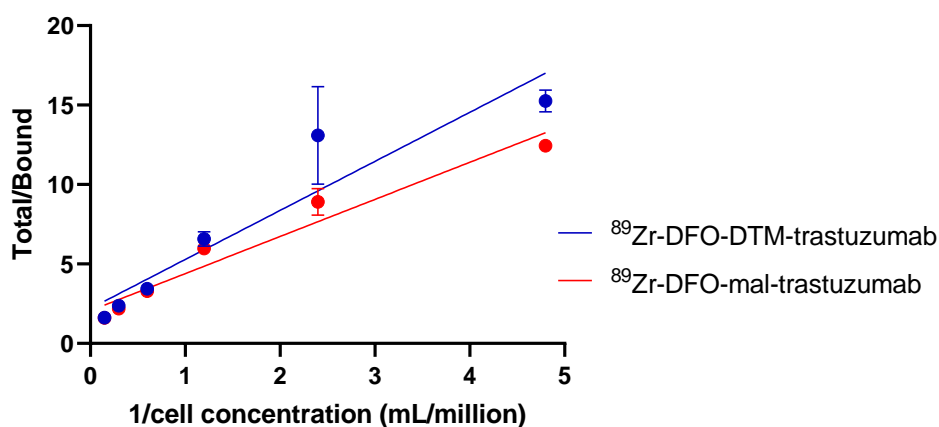


Figure 103 - Total/Bound radioactivity (the total amount of added radioactivity divided by the amount of radioactivity bound to SKOV3 cells) versus 1/cell concentration, used to calculate the immunoreactive fraction of ⁸⁹Zr-DFO-DTM-trastuzumab (blue) and ⁸⁹Zr-DFO-mal-trastuzumab (red) in SKOV3 cells by extrapolation to infinite antigen excess (1/y-intercept). Mean values (n=3, technical triplicate) are shown with error bars representing standard deviation. Straight lines show linear regression for each data set.

Compromised target receptor affinity and reduced immunoreactivity can be caused by the attachment of excessive chelators to the antibody. This has been observed for stochastic conjugates, where chelators can be conjugated to residues involved in antigen binding interfering with receptor binding (see 1.4.4).²⁵ This behaviour

was exemplified in an optimisation study where varying equivalents of DFO-NCS (see 1.5.2) were conjugated to trastuzumab to give antibody conjugates bearing varying numbers (1.4 - 10.9) of chelators. After radiolabelling with $^{89}\text{Zr}^{4+}$, the radiochemical yield, specific activity and immunoreactive fraction (against SKOV3 cells) were calculated for each variably loaded conjugate. The number of chelators per antibody had little impact on both the radiochemical yield (>95%) and the specific activity. However, as the number of chelators per antibody increased, the immunoreactive fraction was shown to decrease. When 1.4 ± 0.5 chelators were present per antibody, an immunoreactive fraction of 0.93 was calculated, falling to 0.82 when 10.9 ± 0.7 chelators were present per antibody. The former conjugate was also observed to have superior performance *in vivo* compared to the latter. Radioimmunoconjugates were administered to female nude mice bearing subcutaneous SKOV3 tumours. *Ex vivo* biodistribution studies were carried out 120 h post-injection where it was found that the conjugate bearing 1.4 ± 0.5 chelators produced superior tumour uptake (38.7 ± 3.8 %ID/g) compared to the conjugate bearing 10.9 ± 0.7 chelators, which generated 16.2 ± 3.2 %ID/g tumour uptake. At the same time point, pronounced liver uptake (27.6 ± 4.1 %ID/g) was observed for the conjugate bearing 10.9 ± 0.7 chelators compared to the conjugate bearing 1.4 ± 0.5 chelators (6.3 ± 1.8 %ID/g). These results demonstrate that excessive conjugation can negatively impact bioconjugate behaviour *in vivo*.

In the same study the bioconjugate's immunoreactive fraction was also determined using a calibration-free concentration assay (CFCA).²⁵ This method involves assessment of a bioconjugate's affinity for its target receptor using a chip-based system, which creates a high antigen excess facilitating quantitative binding. Histidine-tagged recombinant HER2 was added to a sensor chip preconditioned with Ni^{2+} ions. The histidine tag bound to the Ni^{2+} coated flow cell of the sensor chip effectively immobilising the HER2 receptor. The bioconjugate was then added and allowed to bind to immobilised HER2 receptors. Unbound bioconjugate was then washed away before cleaving the bioconjugate-receptor complex from the sensor chip surface by the addition of EDTA solution. This bioconjugate-receptor complex solution was then analysed by surface plasmon resonance to calculate the proportion of bioconjugate that retained affinity for the target receptor - the immunoreactive fraction. This analysis showed that for the conjugate bearing the highest number of chelators the immunoreactive fraction was approximately 0.64

compared with 0.82 as determined by the Lindmo assay method discussed above. In contrast there was better agreement between the methods for the conjugates bearing the lowest number of chelators where immunoreactive fractions of 0.93 were determined by both methods. The CFCA based method is considered to be more accurate than the Lindmo assay, and is also more predictive of *in vivo* behaviour.^{25,26} Additionally, the CFCA method does not require the use of radioactive bioconjugate simplifying immunoreactive fraction determination.

The immunoreactive fraction of a ⁸⁹Zr-DFO-mal-mAb conjugate has been evaluated previously.²³ DFO-maleimide was conjugated to huA33 (anti-A33, colorectal cancer) *via* reaction with reduced interchain disulfides. The resulting conjugate (DFO-mal-huA33) was radiolabelled with ⁸⁹Zr⁴⁺ and a saturation binding assay was performed using SW1222 human colorectal cancer cells that express A33. An immunoreactive fraction of 0.92 ± 0.06 was determined for ⁸⁹Zr-DFO-mal-huA33.

Prior studies typically use high specific activity radioimmunoconjugates enabling the use of small amounts of antibody. For example, the last study discussed used just 2 ng (207.2 ± 14.8 kBq, 103.6 ± 7.4 MBq/mg) of radioimmunoconjugate added to 20 million cells in 100 µL. In comparison, our studies required the addition of 400 ng (2 kBq, 5 MBq/mg) of radioimmunoconjugate to enable detection. Using this low specific activity, it is likely that the radioimmunoconjugate is in significant competition with non-radioactive conjugate for binding to HER2 receptors at the cell concentrations used. Whilst the mathematical extrapolation approach used in the Lindmo assay should mitigate this competitive effect, a data set of sufficient quality (approaching plateau) is required to yield accurate results. Therefore, it is suggested that the immunoreactive fractions generated in this work for ⁸⁹Zr-DFO-DTM-trastuzumab (0.46) and ⁸⁹Zr-DFO-mal-trastuzumab (0.49) are lower than the true immunoreactive fraction.

Higher specific activities, a greater number of cells, or both would be required to improve the accuracy of the extrapolation approach used in the Lindmo assay. Higher cell numbers become impractical since pellet formation is difficult to avoid at high cell concentrations, though increasing the volume could enable the use of a greater number of cells whilst avoiding pellet formation. Alternatively, as mentioned, if the specific activity were increased to match what is often used in the literature (approximately 100 - 200 MBq/mg), the assay would likely generate more

accurate immunoreactive fractions. Additionally, a calibration free concentration assay could be used to achieve more accurate determination of immunoreactive fractions as described above.

Since the same specific activity and number of cells were used when assessing the immunoreactive fractions for ^{89}Zr -DFO-DTM-trastuzumab and ^{89}Zr -DFO-mal-trastuzumab, the two values can be compared relative to one another; the two radioimmunoconjugates have similar immunoreactive fractions suggesting that the DBM conjugation has had no worse impact on immunoreactivity than existing maleimide technology.

3.11 Bioorthogonal DFO conjugation strategy using SPAAC

The following studies were carried out in collaboration with Yanbo Zhao (UCL) who performed the conjugation reactions and carried out LCMS analysis of the conjugates. The dibromomaleimide reagent (DBM-BCN, **37**, figure 104) was synthesised by Nafiska Forte (UCL).

Previous site-specific DFO-antibody conjugations have been achieved enzymatically, or by using bioorthogonal click reactions (see 1.5.2) such as the inverse electron demand Diels-Alder reaction (IEDDA), and the strain promoted azide-alkyne cycloaddition (SPAAC).^{9,27,28} These site-specific conjugates are more homogeneous than their stochastically conjugated analogues, and are less susceptible to overconjugation so typically display high target receptor affinity. These prior studies have used engineered antibodies bearing azide groups or have relied upon substantial chemical modifications to facilitate conjugation. The use of these modified antibodies precludes accurate determination of native unmodified antibody pharmacokinetics and biodistribution *in vivo*.

In comparison, disulfide-based conjugation methodologies minimally impact biomolecule structure. Bioorthogonal click chemistry has been combined with these disulfide-rebridging technologies to generate site-specific conjugates that more closely resemble native unmodified antibodies and proteins. Functionalised dibromopyridazinediones have been used to attach orthogonal 'clickable' handles including alkyne and strained alkyne groups to Fab fragments *via* reduced disulfide rebridging (see 1.7.2).²⁹ Similarly, a dibromomaleimide bearing bicyclo[6.1.0]nonyne (DBM-BCN, **37**, figure 104) has been conjugated to trastuzumab, enabling attachment of an azide-functionalised drug molecule *via*

SPAAC (figure 104).³⁰ The high efficiency of 'click' chemistry conjugation techniques means that the final bioconjugate possesses similar homogeneity and DAR loading to the initial BCN-conjugate after disulfide rebridging. The initial conjugation reaction using DBM-BCN is the same regardless of the azide species' identity improving the repeatability of the conjugation reaction. This is a distinct advantage of this method compared to conjugations involving direct attachment of the payload to the dibromomaleimide.

Building upon this work, the bioorthogonal attachment of a DFO-azide species to DBM-BCN protein conjugates was investigated. First DFO-azide (**38**, figure 105) was synthesised *via* an amide coupling between DFO and azido-PEG4-NHS-ester (**39**, figure 105). Yields were relatively low (19 %), which is attributed to hydrolysis of the NHS-ester caused by the presence of water in the DMSO solvent. In the future anhydrous DMSO could be used to increase the yields of this reaction. Characterisation was achieved by ¹H NMR (figure 106), high resolution mass spectrometry (figure 107), and infrared spectrometry (see appendix, figure 125) where a peak was observed at 2100 cm⁻¹, the characteristic stretching frequency for an azide group.

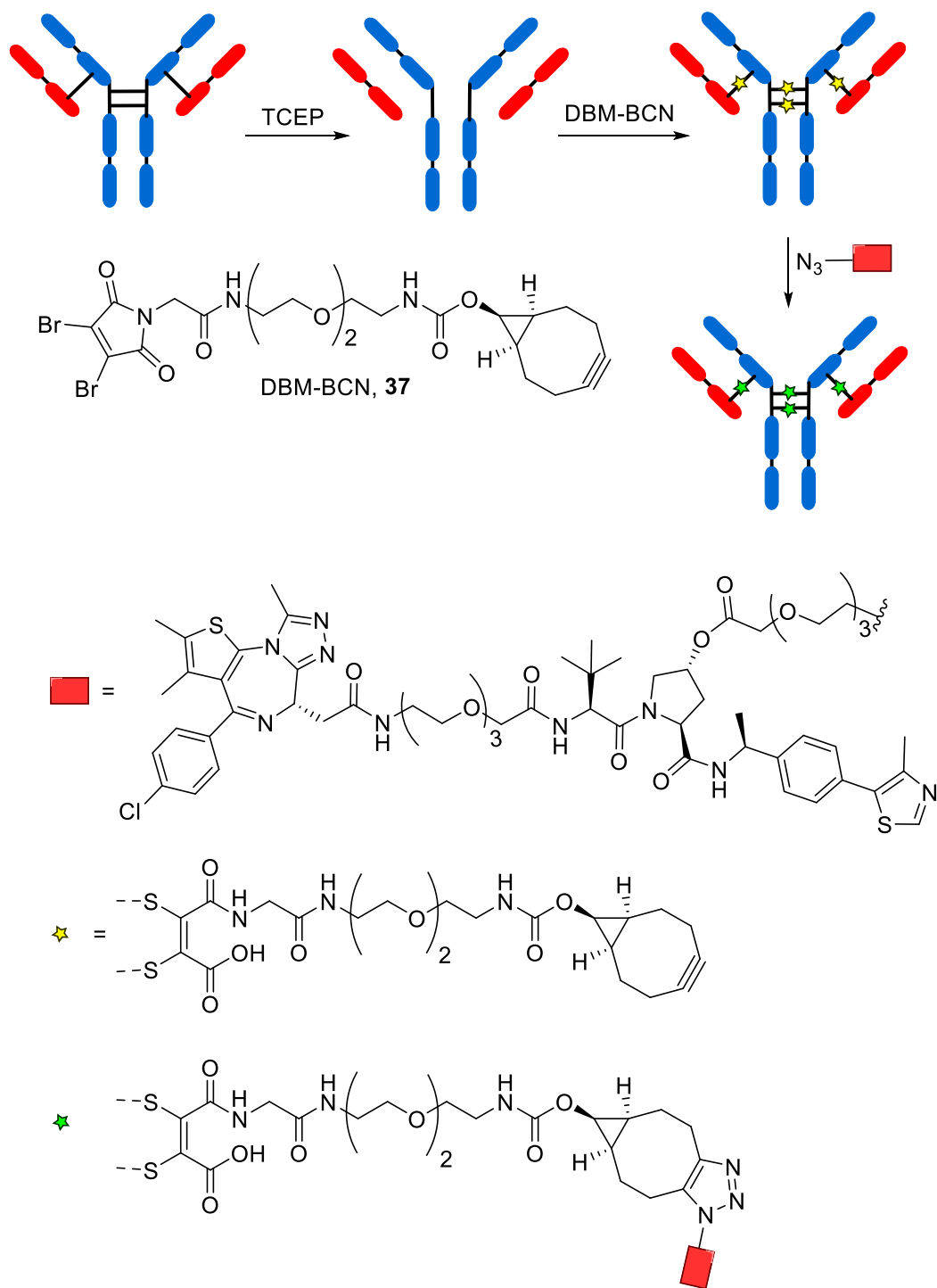


Figure 104 - Initial conjugation of DBM-BCN (37) to reduced antibody disulfides followed by attachment of an azide-functionalised drug molecule *via* SPAAC.³⁰

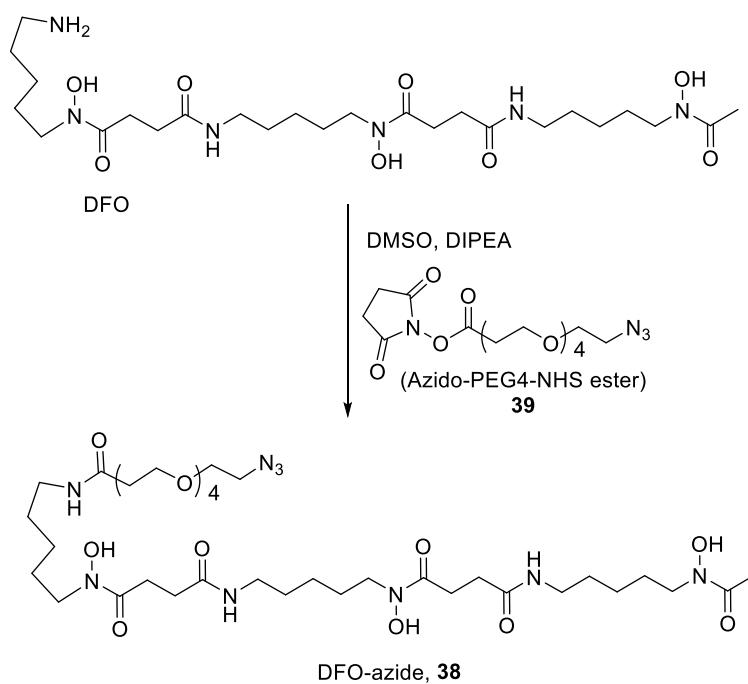
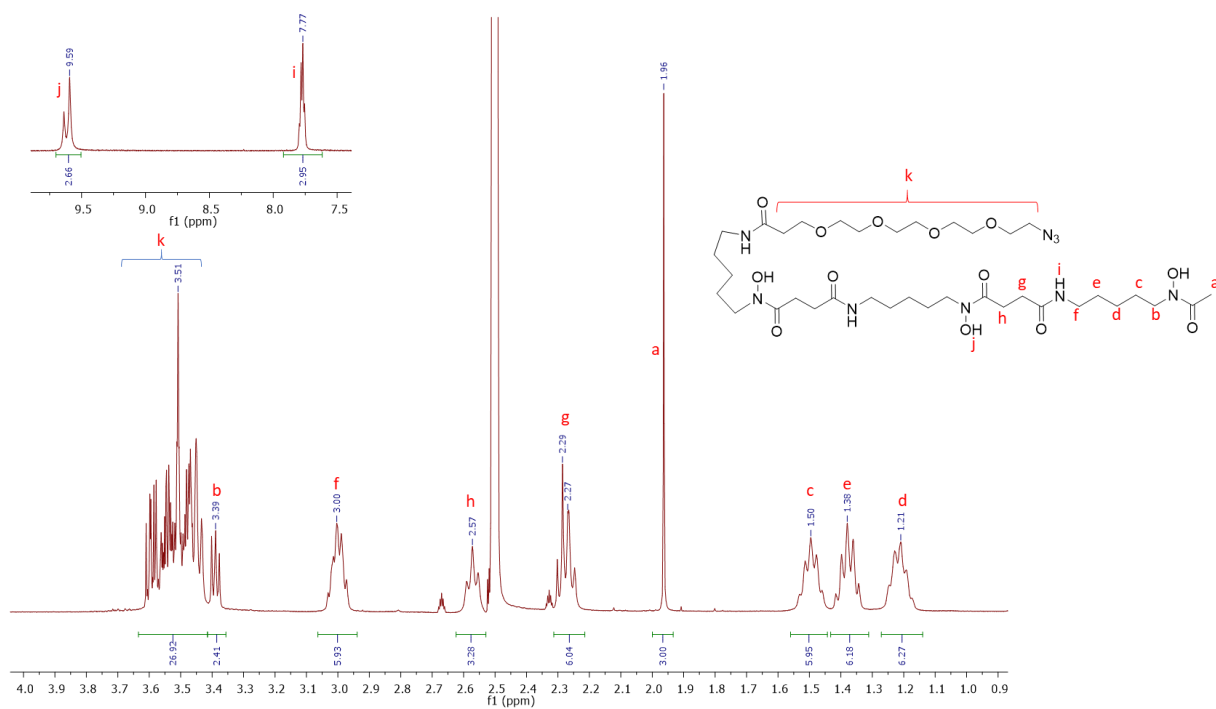


Figure 105 - Synthesis of DFO-azide (39) via amide coupling between DFO and azido-PEG4-NHS ester (38).



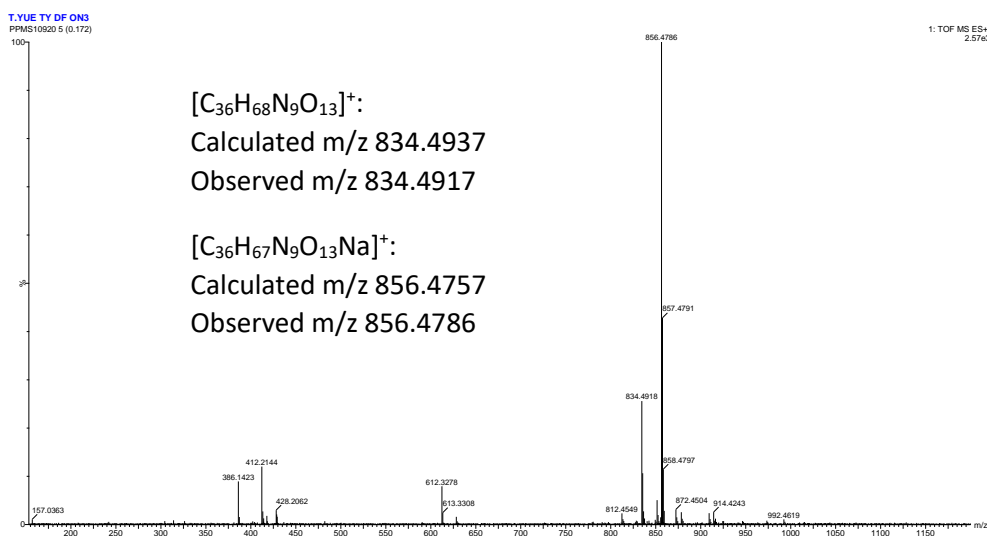


Figure 107 - High resolution mass spectrum for DFO-azide, ESI +ve mode.

Separately DBM-BCN³⁰ was conjugated to a trastuzumab Fab fragment, and also to native unmodified trastuzumab (figure 108). This work was undertaken by Yanbo Zhao (UCL). Disulfide reductions and DBM-BCN conjugations were both carried out in BBS buffer (pH 8.5). For the Fab fragment just one interchain disulfide bond was present meaning that 3 eq. of TCEP were used for the reduction, compared to the full antibody, which has four interchain disulfides, where 8 eq. of TCEP were used. Similarly, 6 eq. of DBM-BCN were added to the reduced Fab, whilst 15 eq. were used for the reduced antibody to ensure complete conjugation. Both conjugates were incubated for 1 h at ambient temperature and then excess reagents were removed by spin filtration (10 kDa MWCO). Conjugates were incubated overnight in BBS (pH 8.5, 37 °C) to ensure dithiomaleimide hydrolysis to give Fab-DTM-BCN and trastuzumab-DTM-BCN. The conjugates were then buffer exchanged into phosphate buffered saline (pH 7) and 10 eq. of DFO-azide was added to Fab-DTM-BCN, and 20 eq. of DFO-azide was added to trastuzumab-DTM-BCN. Conjugation *via* SPAAC took place overnight at 37 °C to give the final conjugates: Fab-DTM-BCN-DFO and trastuzumab-DTM-BCN-DFO (figure 25).

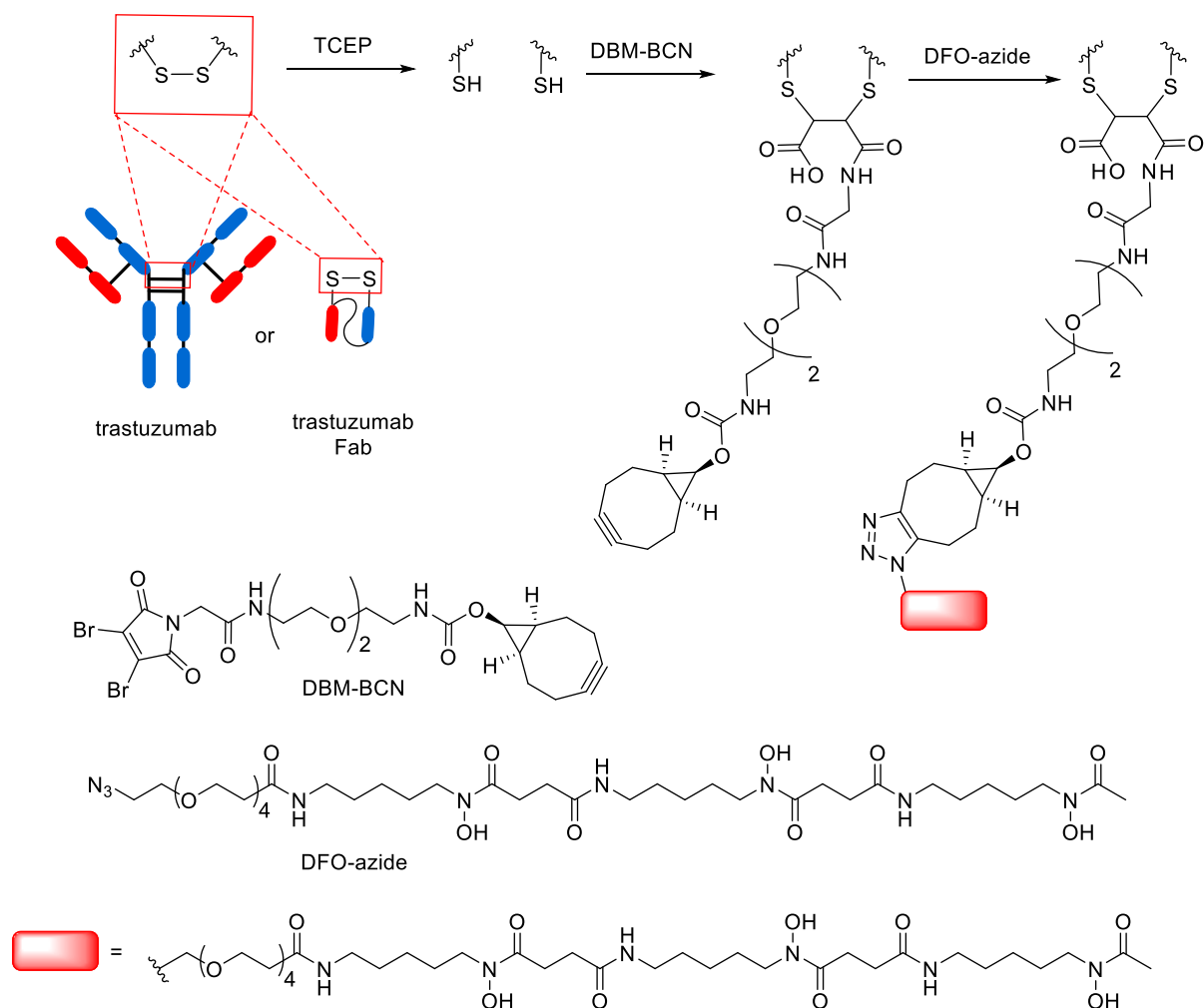


Figure 108 - Synthesis of Fab-DTM-BCN-DFO and trastuzumab-DTM-BCN-DFO.

LCMS analysis showed that the Fab-DFO conjugate was highly homogeneous with a DAR of 1 (figure 109a). No unmodified Fab or Fab-DTM-BCN was detected indicating the high efficiency of both the initial dibromomaleimide conjugation and the subsequent SPAAC reaction. LCMS analysis of the trastuzumab conjugate showed a major peak corresponding to the half-antibody conjugate bearing two DFO moieties (figure 109b,c). As discussed previously (see 2.4.1) this species is considered to have a DAR of 4 since pairs of half-antibody conjugate remain non-covalently associated in solution despite disulfide cleavage between the heavy chains. Full-antibody conjugate bearing four DFO-moieties was also observed (figure 109d), with no evidence of unmodified trastuzumab or trastuzumab-DTM-BCN. Overall, the conjugates generated using this two-step methodology appear to be more homogeneous than those generated using DFO-DBM where a wider range of DFO-loading was observed including the presence of unmodified trastuzumab

and trastuzumab fragments (see 3.4). These results suggest that for DFO-DBM, the direct attachment of the DFO to the dibromomaleimide impacted the bioconjugation negatively, possibly due to the increased steric bulk of the DFFO chelator relative to the BCN group.

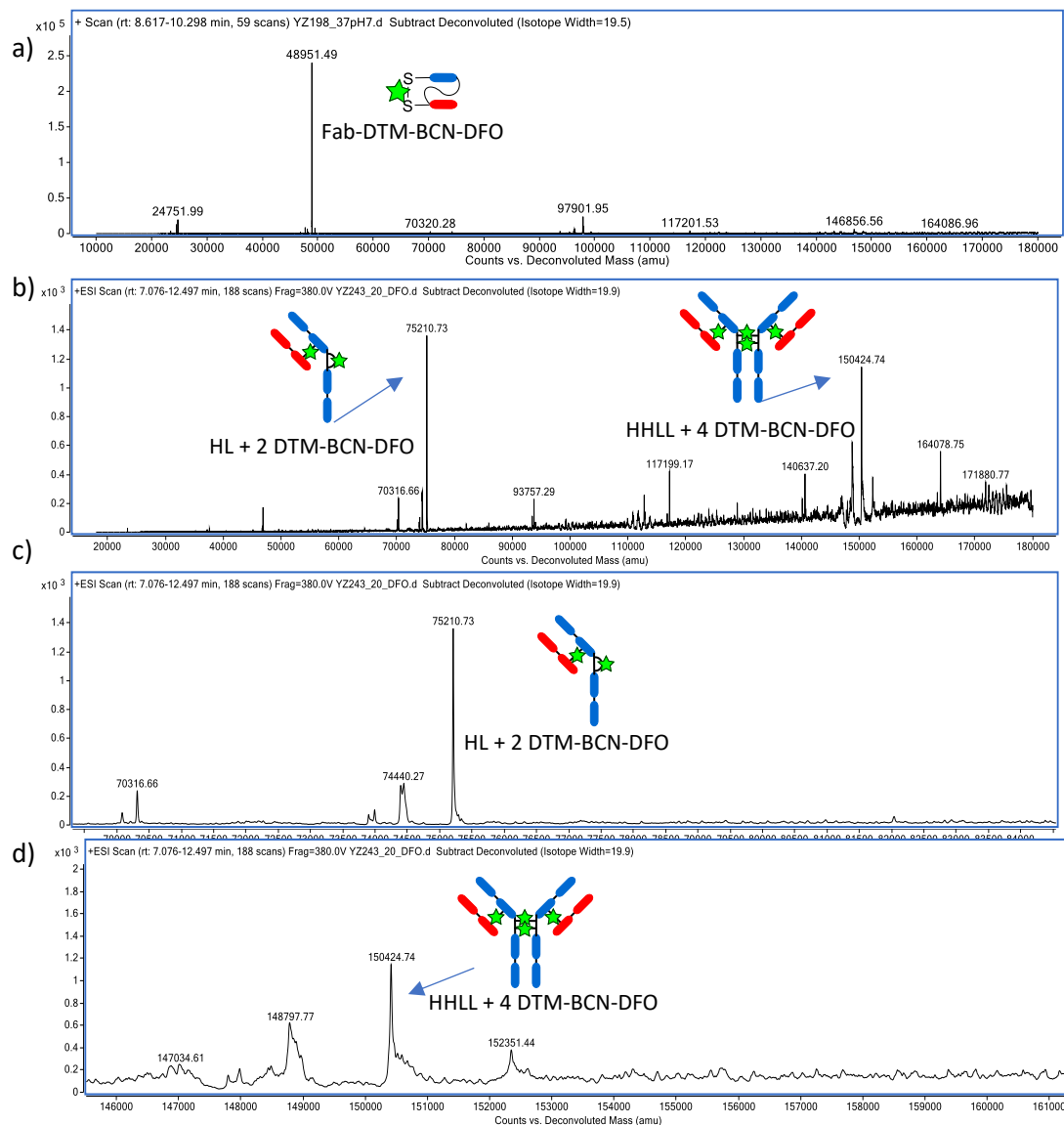


Figure 109 - High resolution ESI deconvoluted mass spectrum of: a) full spectrum Fab-DTM-BCN-DFO; (b) full spectrum trastuzumab-DTM-BCN-DFO, (c) expanded view of the mass spectrum for trastuzumab-DTM-BCN-DFO in the region associated with half-antibody conjugates, and (d) expanded view of the mass spectrum for trastuzumab-DTM-BCN-DFO in the region associated with full-antibody conjugates (see table 6 for assignments).

Table 6 - ESI-MS data for trastuzumab-DTM-BCN-DFO and Fab-DTM-BCN-DFO.

Identity	Counts vs Deconvoluted Mass (amu)	
	Observed	Calculated
trastuzumab		
HHLL	-	145167
HL	-	72584
trastuzumab-DTM-BCN-DFO		
HL + 2 DTM-BCN-DFO	75210	75215
HHLL + 4 DTM-BCN-DFO	150425	150429
Fab	-	47755
Fab-DTM-BCN-DFO	48951	48948

The use of click chemistry has yielded better quality DFO-trastuzumab conjugates. However, the real benefit of this methodology lies in its potential application. SPAAC is a highly robust conjugation method that requires very little optimization when using different BCN species. Likewise, the DBM-BCN platform is simple, and can generate homogeneous bioconjugates bearing BCN groups. Currently, other researchers wishing to use this conjugation method must synthesise their own dibromomaleimide reagents (DBM-BCN). In contrast many chelator-azide species are commercially available. In the future, DBM-BCN may be commercially available. This technology has the potential to facilitate simple, reliable, and site-specific conjugation reactions between chelators bearing azide groups and biomolecules such as antibodies containing solvent accessible disulfide bonds.

3.12 Chapter 3 summary

A new dibromomaleimide-based bifunctional chelator (DFO-DBM) has been synthesised *via* the coupling reaction between DFO and 3,4-dibromomaleimide-*N*-acetic acid mediated by EEDQ. This protocol was informed by experience from the synthesis of sar-DBM from the previous chapter highlighting the synthetic flexibility of these dibromomaleimide reagents.

DFO-DBM was conjugated to reduced trastuzumab alongside the commercially available bifunctional chelator DFO-maleimide. SDS-PAGE analysis showed that DFO-DBM effectively rebridged reduced interchain disulfide bonds forming mostly half-antibody and full antibody conjugates. In contrast the maleimide conjugate,

which reacts with thiols in a 1:1 ratio resulted in the formation of heavy chain and light chain conjugates. Mass spectrometry results were largely in agreement with SDS-PAGE where for DFO-DTM-trastuzumab, half- and full-antibody conjugates were visible, though variable loading (DAR<4) was apparent, indicative of incomplete conjugation. For DFO-mal-trastuzumab the major peaks observed by mass spectrometry corresponded to light chain bearing one maleimide moiety, and heavy chain bearing three maleimide moieties indicative of complete conjugation.

DFO-DTM-trastuzumab and DFO-mal-trastuzumab were labelled with ^{89}Zr where near quantitative (>98 %) radiolabelling was observed for both species. However, lower specific activities were achieved for ^{89}Zr -DFO-DTM-trastuzumab (5 MBq/mg) compared to ^{89}Zr -DFO-mal-trastuzumab (40 MBq/mg). For ^{89}Zr -DFO-DTM-trastuzumab the majority of ^{89}Zr radioactivity was associated with full- and half-antibody conjugates, whilst for ^{89}Zr -DFO-mal-trastuzumab the majority of ^{89}Zr -signal was associated with heavy and light chain conjugates.

The stabilities of ^{89}Zr -DFO-DTM-trastuzumab and ^{89}Zr -DFO-mal-trastuzumab were compared in glutathione solution (10 mM) at pH 5.5 and pH 7 over 8 days. ^{89}Zr -DFO-mal-trastuzumab was stable at pH 5.5 and pH 7 with no bioconjugate degradation or transchelation to glutathione observed over the study. In contrast ^{89}Zr -DFO-DTM-trastuzumab demonstrated instability at pH 5.5 where 63 % of ^{89}Zr signal was lost from ^{89}Zr -DFO-DTM-trastuzumab over 8 d. Instability was also observed at pH 7 where ≥ 18 % of ^{89}Zr -radioactivity was lost from the conjugate over 8 d. At pH 5.5, acid mediated dithiomaleic anhydride formation is the most likely route to this observed instability in the presence of glutathione and has been observed for dithiomaleamic acid conjugates in prior studies. Instability at pH 7 in the presence of glutathione is unprecedented in the literature and requires further assessment to understand the mechanism of this instability. The stabilities of ^{89}Zr -DFO-DTM-trastuzumab and ^{89}Zr -DFO-mal-trastuzumab were also assessed in human serum over 8 days where both conjugates displayed high stability with minimal transfer of ^{89}Zr radioactivity to serum proteins.

Next the HER2 target receptor specificity was assessed for ^{89}Zr -DFO-DTM-trastuzumab and ^{89}Zr -DFO-mal-trastuzumab in SKOV3 cells (HER2 +ve). The conjugates displayed similar, and high specificity for the HER2 receptor with cell binding blocked by the addition of excess unmodified trastuzumab. Studies showed

that ^{89}Zr -DFO-DTM-trastuzumab and ^{89}Zr -DFO-mal-trastuzumab had similar immunoreactive fractions of 0.46 and 0.49 respectively. These values were lower than those reported in the literature for similar conjugates including other examples of ^{89}Zr -DFO-mal-trastuzumab, although these differences were attributed to low specific activities.

Lastly, a two-step method was investigated to conjugate DFO to a trastuzumab Fab fragment and to native trastuzumab. This involved initial conjugation to DBM-BCN *via* reduced disulfide bonds followed by a bioorthogonal 'click' reaction with DFO-azide to yield the final conjugates. LCMS showed that this two-step method generated conjugates that were more homogeneous than those produced using DFO-DBM.

3.13 Chapter 3 experimental

DFO-DBM: 3,4-Dibromo-maleimide-1-acetic acid⁷ (100 mg, 321 μmol) and EEDQ (279 mg, 1.13 mmol) were dissolved in dimethylsulfoxide (DMSO) (4 mL) with stirring. Desferrioxamine (DFO) mesylate (627 mg, 963 μmol) was added, and the reaction was stirred for 3 h. The reaction was then quenched by the addition of TFA (40 μL). The crude product was purified by preparative reverse phase HPLC (Agilent PrepHT XDB-C18) using mobile phase A (water with 0.1 % TFA) and mobile phase B (acetonitrile with 0.1 % TFA) with an eluting gradient (10 mL min^{-1} , 0-10 min 5 % B in A, 10-60 min 5 % \rightarrow 35 % B in A). The product was eluted with a retention time of 43.5 min, and was then lyophilised to give a white powder (61.2 mg, 22 % yield). ^1H NMR (400 MHz, DMSO) δ 9.57 (s, 3H), 8.13 (t, J = 5.5 Hz, 1H), 7.74 (t, J = 5.2 Hz, 2H), 4.08 (s, 2H), 3.45 (t, J = 7.0 Hz, 6H), 3.07 – 2.96 (m, 6H), 2.57 (t, J = 7.1 Hz, 4H), 2.27 (t, J = 7.3 Hz, 4H), 1.96 (s, 3H), 1.55 – 1.45 (m, 6H), 1.43 – 1.32 (m, 6H), 1.28 – 1.16 (m, 6H). ^{13}C NMR (101 MHz, DMSO) δ 171.95, 171.25, 170.12, 165.26, 163.91, 129.50, 47.07, 41.41, 39.52, 38.38, 29.90, 28.77, 27.52, 25.99, 23.46, 20.28. High-resolution ESI-MS +ve mode, $[\text{C}_{31}\text{H}_{50}\text{Br}_2\text{N}_7\text{O}_{11}]^+$ m/z = 856.1912 (observed), m/z = 856.1915 (calculated). Analytical HPLC retention time, 7.95 min (see 2.10 for analytical HPLC methods).

DFO-DBM-trastuzumab: Trastuzumab (5 mg) was dissolved in borate buffered saline (BBS, 1.5 mL) solution (50 mM sodium borate, 50 mM NaCl, and 5 mM ethylenediaminetetraacetic acid (EDTA), pH 8.5) to give an antibody concentration of 23 μM . To this antibody solution was added tris(2-carboxyethyl)phosphine

solution (TCEP, 10 mM in BBS, 21 μ L, 6 eq.) and warmed at 37 $^{\circ}$ C for 2 h. Then DFO-DBM (10 mM in DMF, 28 μ L, 8 eq.) was added to the reduced antibody solution where a colour change from a colourless to pale yellow solution was observed. This solution was then left for two hours at room temperature. The bioconjugate was loaded onto a PD-10 column (pre-conditioned with aqueous ammonium acetate (0.2 M) solution) and eluted with ammonium acetate (0.2 M) in 0.5 mL fractions. Fraction protein content was assessed using a NanoDrop 2000 spectrophotometer. Fractions 6 and 7 were combined, and further purified and buffer exchanged into aqueous ammonium acetate (0.1 M) by six cycles of spin filtration (4000 rcf, 15 min) through a Vivaspin (50 kDa MWCO). DFO-DTM-trastuzumab (2.36 mg) was recovered in 200 μ L at a concentration of 81 μ M.

DFO-mal-trastuzumab: Trastuzumab (4.1 mg) was dissolved in BBS as prepared above to give an antibody concentration of 23 μ M. TCEP (18 μ L, 10 mM, 6 eq.) was added and the solution was warmed at 37 $^{\circ}$ C for 2 h. Then DFO-maleimide (46 μ L, 10 mM, in DMSO, 16 eq.) was added and incubated at ambient temperature for 30 min. The mixture was loaded onto a PD-10 column (pre-conditioned as above) and eluted with ammonium acetate (0.2 M) in 0.5 mL fractions. Fraction protein content was assessed using a Nanodrop 2000 spectrophotometer. Fractions 5-7 were combined and purified by spin filtration as above to recover DFO-mal-trastuzumab (2.01 mg) in 335 μ L at a concentration of 42 μ M.

SDS-PAGE: SDS-PAGE analysis of DFO-DTM-trastuzumab and DFO-mal-trastuzumab was carried out using the same method as discussed previously (see 2.10)

ESI-MS: Mass spectrometry analysis of DFO-DTM-trastuzumab and DFO-mal-trastuzumab was carried out using the same method as discussed previously (see 2.10)

Preparation of $^{89}\text{Zr}^{+4}$ in HEPES buffer: This method was adapted from the literature.¹¹ No-carrier-added $^{89}\text{Zr}(\text{ox})_4$ (ox = oxalate) (radionuclidic purity >99.9%) produced at the BV Cyclotron, Amsterdam, was purchased from Perkin Elmer. A SEP-Pak light QMA cartridge was preconditioned with EtOH (5 mL), saline (0.9 %, 10 mL), and water (10 mL). $^{89}\text{Zr}(\text{ox})_4$ was diluted with water to a total volume of 250 μ L and then loaded onto the preconditioned purification cartridge. The cartridge was washed with water (10 mL) to remove oxalic acid. To elute $^{89}\text{Zr}^{4+}$, a solution of aqueous HCl (0.5 mL, 1 M) was used: the first 150 μ L was discarded, and the

remaining 350 μL contained $^{89}\text{Zr}^{4+}$, which was then dried under a stream of N_2 at 100 $^\circ\text{C}$. A further 500 μL of water were added, agitated to dissolve solids, and then dried once more under a stream of N_2 at 100 $^\circ\text{C}$. Aqueous HEPES buffer (0.2 M, pH 7) was then added to give $^{89}\text{Zr}^{4+}$ in HEPES buffer.

^{89}Zr -radiolabelling of DFO-DBM-trastuzumab and DFO-mal-trastuzumab Either DFO-DTM-trastuzumab or DFO-mal-trastuzumab was diluted to a concentration of 50 μM in ammonium acetate (0.1 M, pH 7). To 10 μL of this solution was added 5 μL of $^{89}\text{Zr}^{4+}$ (100 kBq) in HEPES (0.2 M) to give a 33.3 μM solution of bioconjugate. This was agitated and left at room temperature for 10 min. Radiochemical yields were determined using ITLC-SG strips spotted with 1 μL of radiolabelling mixture, which were developed in a mobile phase of 0.1 M citrate buffer (pH 5.5). For ^{89}Zr -DFO-DTM-trastuzumab and ^{89}Zr -DFO-mal-trastuzumab: $R_f < 0.1$; for unreacted $^{89}\text{Zr}^{4+}$: $R_f > 0.9$. Size exclusion HPLC was also used to assess radiochemical yields.

Serum stability of ^{89}Zr -DFO-DBM-trastuzumab and ^{89}Zr -DFO-mal-trastuzumab: Immunoconjugates were radiolabelled with $^{89}\text{Zr}^{4+}$ to a specific activity of 2.5 MBq/mg in HEPES solution (0.2 M, pH 7). One-part radioimmunoconjugate solution (0.2-1.0 MBq) was added to ten-parts human serum (by volume), to give a concentration of 0.66 mg of bioconjugate per 1 mL of human serum and incubated at 37 $^\circ\text{C}$. Aliquots were taken for analysis by SE-HPLC at 5 min, 1 d, 4 d, and 8 d.

Glutathione stability of ^{89}Zr -DFO-DBM-trastuzumab and ^{89}Zr -DFO-mal-trastuzumab: Immunoconjugates were radiolabelled with $^{89}\text{Zr}^{4+}$ to a specific activity of 2.5 MBq/mg in HEPES (0.2 M, pH 7). Separately, HEPES solution (0.2 M) was degassed using an N_2 stream for 30 min. This degassed solution was then used to make up a GSH solution (20 mM). Radioimmunoconjugate solution (0.2-1.0 MBq) was then added to an equal volume of the GSH solution to give a 10 mM final concentration of GSH in 0.2 M HEPES at pH 7. These samples were incubated at 37 $^\circ\text{C}$ and aliquots were taken for analysis by size exclusion HPLC at 5 min, 1 d, 4 d, and 8 d. The experiment was repeated at pH 5.5 by dissolving the GSH in degassed H_2O instead of HEPES solution.

HEPES stability of ^{89}Zr -DFO-DBM-trastuzumab and ^{89}Zr -DFO-mal-trastuzumab: Immunoconjugates were radiolabelled with $^{89}\text{Zr}^{4+}$ to a specific activity of 2.5 MBq/mg in HEPES (0.2 M, pH 7). Radioimmunoconjugate (1 MBq) was added to an

equal volume of HEPES (0.2 M) and incubated for 8 d at 37 °C, and then analysed by SE-HPLC.

Evaluation of immunoreactive fraction for ^{89}Zr -DFO-DBM-trastuzumab and ^{89}Zr -DFO-mal-trastuzumab: This method was adapted from the paper by Lindmo and co-workers.²⁴ SKOV3 cells were grown in T175 flasks in culture medium. Cells were aspirated and washed with PBS, then treated with trypsin to detach the cells from the flask. The cells were washed twice using PBS with 0.1 % BSA and made up to a concentration of 10 million cells/mL in PBS with 0.1 % BSA. Immunoconjugates were radiolabelled with $^{89}\text{Zr}^{4+}$ to a specific activity of 5 MBq/mg in HEPES (0.2 M, pH 7), and diluted in PBS with 0.1 % BSA to give a 13.3 kBq/mL solution. Cells were resuspended and pipetted (600 μL) in triplicate into eppendorf tubes. Five serial 1:2 dilutions were performed using PBS with 0.1 % BSA to give cell concentrations of 10, 5, 2.5, 1.25, 0.63, 0.31 million cells/mL. Radioimmunoconjugate solution was then added (2 kBq, 150 μL) to each of these samples to give a total volume of 450 μL , with final cell concentrations of 6.66, 3.33, 1.66, 0.83, 0.42, 0.20 million cells/mL. These samples were then placed on ice and left on ice for 1 hour on a shaker (500 rpm). Cells were washed three times by centrifuge protocol using PBS with 0.1 % BSA. The radioactivity associated with the resulting pellets were counted using a gamma counter. Competitive inhibition (blocking) studies were conducted using the same procedure but with the addition of unmodified trastuzumab (15 μg , 1.2 μL) to the cell suspension before the addition of radioimmunoconjugate. Immunoreactive fractions were determined by linear regression analysis of a plot of total/bound radioactivity versus 1/cell concentration and calculated as 1/y-intercept.

DFO-azide: DFO mesylate (50 mg, 89 μmol , 1 eq.) was dissolved in DMSO (1 mL) and DIPEA (9.8 mg, 13.3 μL , 1 eq.) was added. Then azido-PEG4-NHS ester (34 mg, 1.1 eq.) was added and stirred for 15 min, then TFA (11.7 μL , 2 eq.) was added to quench the reaction. The product was purified by preparative reverse phase (C18) HPLC using a mobile phase of water with 0.1 % TFA (solvent A), and acetonitrile with 0.1 % TFA (solvent B) with the following method: 0 \rightarrow 3 min, 4 mL/min, 5 % B in A; 3 \rightarrow 5 min, 10 mL/min, 5% B in A; 5 \rightarrow 65 min, 10 mL/min, 5% \rightarrow 95% B in A; 65 \rightarrow 70 min, 10 mL/min, 95% \rightarrow 5% B in A. The product eluted at 24.8 min, and lyophilised to give a white powder (14.1 mg, 17 μmol , 19%). ^1H NMR (400 MHz, DMSO) δ 9.62 (3H), 7.78 (3H), 3.63 – 3.42 (m, 28H), 3.39 (t, 2H), 3.05 – 2.94 (m, 6H), 2.57 (t, 4H),

2.27 (q, 6H), 1.96 (s, 3H), 1.57 – 1.44 (m, 6H), 1.43 – 1.31 (m, 6H), 1.28 – 1.14 (m, 6H). High-resolution ESI-MS +ve mode: $[C_{36}H_{68}N_9O_{13}]^+$ $m/z = 834.4917$ (observed), $m/z = 834.4937$ (calculated). Infrared spectroscopy (2100 cm^{-1} , N_3).

DBM-BCN: Synthesis of DBM-BCN was performed by Nafsika Forte (UCL) according to the literature.³⁰

Fab-DTM-BCN-DFO: This conjugation was carried out by Yanbo Zhao. To trastuzumab Fab (100 μL , 12 nmol, 120 μM) in BBS buffer (pH 8.5) was added TCEP (3.6 μL , 0.036 μmol , 10mM solution in water, 3 eq). After 1.5 h at 37 $^\circ\text{C}$, DBM-BCN (7.2 μL , 0.072 μmol , 10 mM solution in anhydrous DMF, 6 eq) was added in the conjugation and the mixture was incubated for 1h at 22 $^\circ\text{C}$. The excess reagents were then removed *via* ultrafiltration (10 kDa MWCO) into BBS buffer (pH 8.5). The concentration was determined by UV/Vis absorbance and adjusted to 20.0 μM . The solution was incubated for 18 h at 37 $^\circ\text{C}$ and then buffer exchanged into PBS (pH 7). To Fab-DTM-BCN (50 μL , 5 nmol, 100 μM) in PBS (pH 7) was added DFO-azide (5 μL , 0.050 μmol , 10 mM solution in DMF, 10 eq) and the mixture was incubated for 18h at 37 $^\circ\text{C}$. Excess reagent was then removed *via* ultrafiltration (10 kDa MWCO) into EDTA solution (40 mM phosphate, 20 mM NaCl, 6 mM EDTA, pH 7.0). Mass spectrometry was carried out using the same method discussed previously (see 2.10).

Trastuzumab-DBM-BCN-DFO: This conjugation reaction was carried out by Yanbo Zhao. To trastuzumab (100 μL , 23 nmol, 23 μM) in BBS buffer (pH 8.5) was added TCEP (1.84 μL , 18.4 nmol, 10mM solution in water, 8 eq). After 2 h at 37 $^\circ\text{C}$, DBM-BCN (3.45 μL , 34.5 nmol, 10 mM solution in anhydrous DMF, 15 eq) was added in the conjugation and the mixture was incubated for 1h at 22 $^\circ\text{C}$. The excess reagents were then removed *via* ultrafiltration (10 kDa MWCO) into BBS buffer (pH 8.5). The concentration was determined by UV/Vis absorbance and adjusted to 20.0 μM . The solution was incubated for 18 h at 37 $^\circ\text{C}$ and then buffer exchanged into PBS (pH 7). To trastuzumab-DTM-BCN (100 μL , 2 nmol, 20 μM) in PBS (pH 7.0) was added DFO-azide (4 μL , 40 nmol, 10 mM solution in DMF, 20 eq) and the resulting mixture was incubated for 18 h at 37 $^\circ\text{C}$. Excess reagent was then removed *via* ultrafiltration (10 kDa MWCO) into EDTA solution as above. Mass spectrometry was carried out using the same method discussed previously (see 2.10).

3.14 Chapter 3 references

- 1 M. Morais, J. P. M. Nunes, K. Karu, N. Forte, I. Benni, M. E. B. Smith, S. Caddick, V. Chudasama and J. R. Baker, Optimisation of the dibromomaleimide (DBM) platform for native antibody conjugation by accelerated post-conjugation hydrolysis, *Org. Biomol. Chem.*, 2017, **15**, 2947–2952.
- 2 C. Ge, S. Huvelle, C. B. Baltus, L. Juen, N. Joubert, A. Desgranges and C. Martin, Impact of Maleimide Disubstitution on Chemical and Biological Characteristics of HER2 Antibody – Drug Conjugates, , DOI:10.1021/acsomega.9b03510.
- 3 M. Morais, N. Forte, V. Chudasama and J. R. Baker, in *Methods in Molecular Biology*, eds. S. Massa and N. Devoogdt, 2019, vol. 2033, pp. 15–24.
- 4 C. Bahou, E. A. Love, S. Leonard, R. J. Spears, A. Maruani, K. Armour, J. R. Baker and V. Chudasama, Disulfide Modified IgG1: An Investigation of Biophysical Profile and Clinically Relevant Fc Interactions, *Bioconjug. Chem.*, 2019, **30**, 1048–1054.
- 5 J. P. M. Nunes, M. Morais, V. Vassileva, E. Robinson, V. S. Rajkumar, M. E. B. Smith, R. B. Pedley, S. Caddick, J. R. Baker and V. Chudasama, Functional native disulfide bridging enables delivery of a potent, stable and targeted antibody–drug conjugate (ADC), *Chem. Commun.*, 2015, **51**, 10624–10627.
- 6 C. Imberti, S. Y. A. Terry, C. Cullinane, F. Clarke, G. H. Cornish, N. K. Ramakrishnan, P. Roselt, A. P. Cope, R. J. Hicks, P. J. Blower and M. T. Ma, Enhancing PET Signal at Target Tissue in Vivo: Dendritic and Multimeric Tris(hydroxypyridinone) Conjugates for Molecular Imaging of $\alpha\beta 3$ Integrin Expression with Gallium-68, *Bioconjug. Chem.*, 2017, **28**, 481–495.
- 7 M. Morais, J. P. M. Nunes, K. Karu, N. Forte, I. Benni, M. E. B. Smith, S. Caddick, V. Chudasama and J. R. Baker, Supplementary Information - Optimisation of the dibromomaleimide (DBM) platform for native antibody conjugation by accelerated post-conjugation hydrolysis, *Org. Biomol. Chem.*, 2017, **15**, S1-63.
- 8 L. Castañeda, A. Maruani, F. F. Schumacher, E. Miranda, V. Chudasama, K.

- A. Chester, J. R. Baker, M. E. B. Smith and S. Caddick, Acid-cleavable thiomaleamic acid linker for homogeneous antibody-drug conjugation, *Chem. Commun.*, 2013, **49**, 8187–8189.
- 9 B. M. Zeglis, C. B. Davis, R. Aggeler, H. C. Kang, A. Chen, B. J. Agnew and J. S. Lewis, Enzyme-Mediated Methodology for the Site-Specific Radiolabeling of Antibodies Based on Catalyst-Free Click Chemistry, *Bioconjug. Chem.*, 2013, **24**, 1057–1067.
- 10 B. M. Zeglis and J. S. Lewis, The Bioconjugation and Radiosynthesis of ⁸⁹Zr-DFO-labeled Antibodies, *J. Vis. Exp.*, , DOI:10.3791/52521.
- 11 F. Man, A. A. Khan, A. Carrascal-Miniño, P. J. Blower and R. T.M. de Rosales, A kit formulation for the preparation of [⁸⁹Zr]Zr(oxinate)₄ for PET cell tracking: White blood cell labelling and comparison with [¹¹¹In]In(oxinate)₃, *Nucl. Med. Biol.*, 2020, **90–91**, 31–40.
- 12 W. E. Meijs, H. J. Haisma, R. P. Klok, F. B. van Gog, E. Kievit, H. M. Pinedo and J. D. M. Herscheid, Zirconium-labeled monoclonal antibodies and their distribution in tumor-bearing nude mice., *J. Nucl. Med.*, 1997, **38**, 112–8.
- 13 J. P. Holland, E. Caldas-Lopes, V. Divilov, V. A. Longo, T. Taldone, D. Zatorska, G. Chiosis and J. S. Lewis, Measuring the pharmacodynamic effects of a novel Hsp90 inhibitor on HER2/ neu expression in mice using ⁸⁹Zr-DFO-trastuzumab, *PLoS One*, , DOI:10.1371/journal.pone.0008859.
- 14 A. Ghai, D. Maji, N. Cho, C. Chanswangphuwana, M. Rettig, D. Shen, J. DiPersio, W. Akers, F. Dehdashti, S. Achilefu, R. Vij and M. Shokeen, Preclinical Development of CD38-Targeted [⁸⁹Zr]Zr-DFO-Daratumumab for Imaging Multiple Myeloma, *J. Nucl. Med.*, 2018, **59**, 216–222.
- 15 J. N. Tinianow, H. S. Gill, A. Ogasawara, J. E. Flores, A. N. Vanderbilt, E. Luis, R. Vandlen, M. Darwish, J. R. Junutula, S. P. Williams and J. Marik, Site-specifically ⁸⁹Zr-labeled monoclonal antibodies for ImmunoPET, *Nucl. Med. Biol.*, 2010, **37**, 289–297.
- 16 M. T. Ma, L. K. Meszaros, B. M. Paterson, D. J. Berry, M. S. Cooper, Y. Ma, R. C. Hider and P. J. Blower, Tripodal tris(hydroxypyridinone) ligands for immunoconjugate PET imaging with ⁸⁹Zr⁴⁺ : comparison with

- desferrioxamine-B, *Dalt. Trans.*, 2015, **44**, 4884–4900.
- 17 P. A. Szijj, C. Bahou and V. Chudasama, Minireview: Addressing the retro-Michael instability of maleimide bioconjugates, *Drug Discov. Today Technol.*, 2018, **30**, 27–34.
- 18 S. C. Alley, D. R. Benjamin, S. C. Jeffrey, N. M. Okeley, D. L. Meyer, R. J. Sanderson and P. D. Senter, Contribution of linker stability to the activities of anticancer immunoconjugates, *Bioconjug. Chem.*, 2008, **19**, 759–765.
- 19 L. N. Tumey, M. Charati, T. He, E. Sousa, D. Ma, X. Han, T. Clark, J. Casavant, F. Loganzo, F. Barletta, J. Lucas and E. I. Graziani, Mild method for succinimide hydrolysis on ADCs: Impact on ADC potency, stability, exposure, and efficacy, *Bioconjug. Chem.*, 2014, **25**, 1871–1880.
- 20 A. D. Baldwin and K. L. Kiick, Tunable Degradation of Maleimide–Thiol Adducts in Reducing Environments, *Bioconjug. Chem.*, 2011, **22**, 1946–1953.
- 21 H. J. Forman, H. Zhang and A. Rinna, Glutathione: Overview of its protective roles, measurement, and biosynthesis, *Mol. Aspects Med.*, 2009, **30**, 1–12.
- 22 J. P. M. Nunes, M. Morais, V. Vassileva, E. Robinson, V. S. Rajkumar, M. E. B. Smith, R. B. Pedley, S. Caddick, J. R. Baker and V. Chudasama, Functional native disulfide bridging enables delivery of a potent, stable and targeted antibody–drug conjugate (ADC), *Chem. Commun.*, 2015, **51**, 10624–10627.
- 23 P. Adumeau, M. Davydova and B. M. Zeglis, Thiol-Reactive Bifunctional Chelators for the Creation of Site-Selectively Modified Radioimmunoconjugates with Improved Stability, *Bioconjug. Chem.*, 2018, **29**, 1364–1372.
- 24 T. Lindmo, E. Boven, F. Cuttitta, J. Fedorko and P. A. Bunn, Determination of the immunoreactive function of radiolabeled monoclonal antibodies by linear extrapolation to binding at infinite antigen excess, *J. Immunol. Methods*, 1984, **72**, 77–89.
- 25 S. K. Sharma, J. M. Glaser, K. J. Edwards, E. Khozeimeh Sarbisheh, A. K. Salih, J. S. Lewis and E. W. Price, A Systematic Evaluation of Antibody

- Modification and ⁸⁹Zr-Radiolabeling for Optimized Immuno-PET, *Bioconjug. Chem.*, 2021, **32**, 1177–1191.
- 26 E. Pol, H. Roos, F. Markey, F. Elwinger, A. Shaw and R. Karlsson, Evaluation of calibration-free concentration analysis provided by Biacore™ systems, *Anal. Biochem.*, 2016, **510**, 88–97.
- 27 B. M. Zeglis, C. B. Davis, D. Abdel-Atti, S. D. Carlin, A. Chen, R. Aggeler, B. J. Agnew and J. S. Lewis, Chemoenzymatic Strategy for the Synthesis of Site-Specifically Labeled Immunoconjugates for Multimodal PET and Optical Imaging, *Bioconjug. Chem.*, 2014, **25**, 2123–2128.
- 28 S. H. Ahn, B. A. Vaughn, W. A. Solis, M. L. Lupper, T. J. Hallam and E. Boros, Site-Specific ⁸⁹Zr- And ¹¹¹In-Radiolabeling and in Vivo Evaluation of Glycan-free Antibodies by Azide-Alkyne Cycloaddition with a Non-natural Amino Acid, *Bioconjug. Chem.*, 2020, **31**, 1177–1187.
- 29 A. Maruani, M. E. B. Smith, E. Miranda, K. A. Chester, V. Chudasama and S. Caddick, A plug-and-play approach to antibody-based therapeutics via a chemoselective dual click strategy, *Nat. Commun.*, 2015, **6**, 2–10.
- 30 M. Maneiro, N. Forte, M. M. Shchepinova, C. S. Kounde, V. Chudasama, J. R. Baker and E. W. Tate, Antibody–PROTAC Conjugates Enable HER2-Dependent Targeted Protein Degradation of BRD4, *ACS Chem. Biol.*, 2020, **15**, 1306–1312.

4 Conclusions and future work

4.1 Conclusions

4.1.1 Summary

New bifunctional chelators have been prepared based on state-of-the-art sarcophagine and DFO chelators for binding the long-lived PET radionuclides ^{64}Cu and ^{89}Zr respectively. These dibromomaleimide-derivatives add uniquely to the existing reported sarcophagine and DFO compounds available for attachment to targeted biomolecules bringing together the simplicity of non-site-specific conjugation methods, with the increased control afforded by site-specific conjugation methods.

4.1.2 Comparison of sar-DBM and DFO-DBM

Fast conjugation reactions are preferred since they are more practical. For DFO-DTM-trastuzumab, post-conjugation hydrolysis was complete within 2 h at ambient temperature, whereas sar-DTM-trastuzumab required 48 h at 37 °C to hydrolyse the dithiomaleimide conjugate. These differences likely arise from the use of different linker lengths between the dibromomaleimide group and the chelator. DFO-DBM contains a methyl linker whereas sar-DBM contains a pentyl linker. As discussed in 1.7.2, the greater the electron withdrawal from the maleimide ring system, the faster the rate of hydrolysis. Electron withdrawal through the sigma or pi electronic systems leads to more partial positivity at the carbonyl carbons making them better electrophiles thus leading to a faster rate of hydrolysis. Therefore, longer alkyl linkers, which are more electronically insulative, lead to a slower rate of DBM / DTM hydrolysis.

DFO-DBM produced higher quality bioconjugates than sar-DBM. Bright light imaging of SDS-PAGE gels (figure 110) showed that DFO-DTM-trastuzumab comprised largely of half- and full-antibody conjugates with minimal undesired light chain and heavy chain conjugates detected by LCMS. In contrast, for sar-DTM-trastuzumab, whilst bright light images of SDS-PAGE gels showed that half- and full-antibody conjugates were formed in the conjugation reaction, a wider range of conjugates were detected by LCMS including light chain conjugates.

Differences in reactivity towards reduced thiols may be responsible for the observed differences in antibody fragment conjugate distribution for sar-DTM-trastuzumab and DFO-DTM-trastuzumab. In the literature, the reaction between dibromomaleimides and reduced thiols is considered to be fast.¹ Stopped-flow

kinetic analysis has been used to assess the rate of reaction between reduced somatostatin and dibromomaleimide.² This reaction was complete within 5-10 min to give a somatostatin conjugate. It is possible that DFO-DBM and sar-DBM possess different reactivities towards reduced thiols, leading to different antibody fragment conjugate distributions.

Another explanation is that differences in the rate of post-conjugation hydrolysis could be responsible for these differences in bioconjugate quality. Accelerated post-conjugation hydrolysis has previously been shown to improve bioconjugate homogeneity.³ In the future, a sarcophagine-dibromomaleimide incorporating a methyl linker could be synthesised leading to faster post-conjugation hydrolysis to generate a more homogeneous sarcophagine bioconjugate.

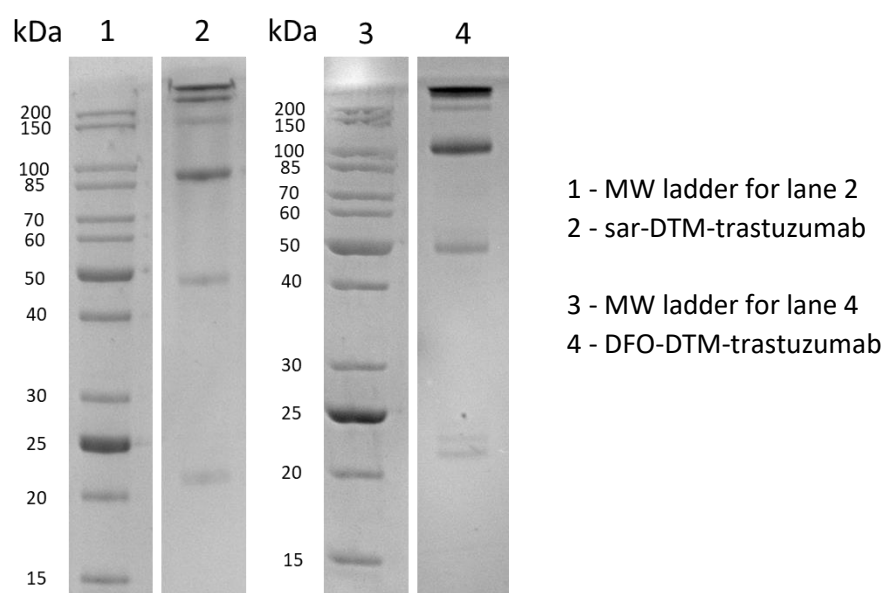


Figure 110 - Comparison of bright light images obtained for SDS-PAGE lanes containing sar-DTM-trastuzumab and DFO-DTM-trastuzumab.

Sar-DTM-trastuzumab and DFO-DTM-trastuzumab were radiolabelled with ⁶⁴Cu and ⁸⁹Zr respectively, achieving near-quantitative radiochemical yields, rapidly (within 10 min) and under mild conditions (ambient temperature, and pH 7). Quantification of SDS-PAGE autoradiographs obtained for ⁶⁴Cu-sar-DTM-trastuzumab and ⁸⁹Zr-DFO-DTM-trastuzumab showed that the distribution of radioactivity among antibody fragments differed for ⁶⁴Cu-sar-DTM-trastuzumab and ⁸⁹Zr-DFO-DTM-trastuzumab (table 6), consistent with SDS-PAGE bright light images (figure 110) and LCMS data of the non-radiolabelled immunoconjugates. A greater proportion of radioactivity signal was associated with full- and half-

antibody conjugates for ^{89}Zr -DFO-DTM-trastuzumab than for ^{64}Cu -sar-DTM-trastuzumab.

Table 6- Comparing the distribution of radioactivity in antibody conjugate fragments for ^{64}Cu -sar-DTM-trastuzumab and ^{89}Zr -DFO-DTM-trastuzumab. (see figures 77, 95)

Species	^{64}Cu -sar-DTM-trastuzumab	^{89}Zr -DFO-DTM-trastuzumab
HLL	41.1%	54.4%
HL	33.4%	34.9%
H	14.5%	7.7%
L	10.6%	3.0%

To demonstrate a proof of concept for dibromomaleimide-based bifunctional chelators, ^{64}Cu -sar-DTM-trastuzumab stability was investigated in human serum where no degradation or radiometal transchelation to serum proteins was observed over 40 h. ^{64}Cu -sar-DTM-trastuzumab was then evaluated *in vivo* where high stability was observed in healthy mice over 48 h. Uptake and retention of ^{64}Cu -sar-DTM-trastuzumab was observed in healthy tissues that naturally express HER2.

In contrast, a comparative study was carried out using ^{89}Zr -DFO-DTM-trastuzumab and a DFO-maleimide derivative ^{89}Zr -DFO-mal-trastuzumab. Radioimmunoconjugate stability was compared in glutathione solution (10 mM) at both pH 5.5 and pH 7, and in human serum. ^{89}Zr -DFO-mal-trastuzumab was more stable than ^{89}Zr -DFO-DTM-trastuzumab over 8 d under all conditions tested. Acid catalysed maleic anhydride formation was the most likely route to payload loss from ^{89}Zr -DFO-DTM-trastuzumab at pH 5.5. The instability observed for ^{89}Zr -DFO-DTM-trastuzumab at pH 7 in 10 mM glutathione was unprecedented, and further work is required to elucidate the mechanism of payload loss from the bioconjugate.

Prior studies have repeatedly observed the instability of maleimide conjugates in the presence of thiols, including glutathione.⁴ This instability arises because retro-Michael reactions result in loss of the maleimide from the conjugate. This enables competing thiols to react with the regenerated maleimide, yielding an undesired new conjugate. Initial maleimide cleavage (via a retro-Michael pathway) occurs at and above pH 7. For example, degradation of maleimide-thiol conjugates has been

observed in the presence of 10 mM glutathione at pH 7.4.⁴ The high stability observed for ⁸⁹Zr-DFO-mal-trastuzumab in glutathione solution at both pH 5.5 and pH 7 was therefore unexpected.

At pH 5.5 loss of maleimide *via* retro-Michael processes is likely to be slow, which could explain the observed stability of ⁸⁹Zr-DFO-mal-trastuzumab at pH 5.5. In theory, ⁸⁹Zr-DFO-mal-trastuzumab should have been unstable at pH 7. Glutathione is only able to react with cleaved maleimides in its reduced form. It is possible that over the course of the stability study, the glutathione slowly oxidised rendering it unreactive towards the cleaved maleimide.

The conjugates produced by sar-DBM and DFO-DBM were relatively heterogeneous compared to those produced by existing site-specific conjugation technologies in the literature. LCMS showed the presence of light chain conjugates for sar-DTM-trastuzumab, indicative of suboptimal disulfide rebridging. Furthermore, LCMS showed that for both bifunctional chelators, half- and full-antibody conjugates possessed variable chelator to antibody ratios indicative of underconjugation.

Prior studies have consistently generated more homogeneous chelator to antibody ratios to give mostly natively rebridged bioconjugates. For example, DFO has been site-specifically conjugated to the heavy chain glutamic acid residues on a mutant CE7 antibody using a bacterial transglutaminase (see 1.5.2). This reaction resulted in quantitative conjugation to give a completely homogeneous DFO-CE7 conjugate as shown by mass spectrometry where each heavy chain was modified with exactly two DFO units.

Homogeneous antibody conjugates have also been generated using a combination of enzyme mediated conjugation and click chemistry (see 1.4.4, 1.5.2). First, enzymatic reactions are used to attach bioorthogonal click chemistry groups (e.g. azide, transcyclooctene) to the biomolecule, followed by the addition of a chelator bearing the corresponding bioorthogonal group (e.g. cyclooctyne, tetrazine). Coupling then takes place *via* click reactions such as the strain promoted azide alkyne coupling (SPAAC) or the inverse electron demand Diels-Alder (IEDDA) reaction. This approach has been used to produce both sarcophagine- and DFO-based radioimmunoconjugates.^{5,6}

Cell free protein synthesis has also been used to produce antibodies bearing the non-natural amino acid *p*-azidomethylphenylalanine. Incorporation of this azide bearing residue into the antibody's structure enabled attachment of a DFO-cyclooctyne derivative *via* SPAAC.⁷

4.1.3 Advantages of dibromomaleimide-based BFCs compared to existing site-specific conjugation methods

Compared to existing site-specific conjugation technologies the main advantage of dibromomaleimide-based BFCs is the ability to use native unmodified antibodies. The bacterial transglutaminase-mediated conjugation discussed above required genetic engineering of the CE7 antibody to replace asparagine-297 with glutamic acid. This limits the applicability of this technology since many researchers lack the facilities to produce genetically modified antibodies. Similarly, insertion of *p*-azidomethylphenylalanine into the primary structure of trastuzumab required the use of cell free protein synthesis, a molecular biology technique that is outside the scope of most bioconjugate chemists.

Non-site-specific conjugations such as the reaction between lysine residues and isothiocyanate-based bifunctional chelators can be applied to a range of antibodies without the need for optimisation. Existing, well-tested non-site-specific antibody conjugation protocols are available, which detail the antibody concentration, reaction conditions and number of equivalents of bifunctional chelator required to prepare a bioconjugate.⁸ These simple protocols use readily available reagents and can be undertaken by inexperienced scientists (e.g. undergraduate students). In contrast, many site-specific conjugation methods require significant optimisation when using different antibodies. For example, attachment of DFO directly to trastuzumab using bacterial transglutaminase would likely require genetic engineering of surrounding residues to ensure efficient conjugation between N297 and DFO. Optimisation processes such as these are time consuming, labour intensive, and expensive, limiting the wide application of these methodologies. Dibromomaleimide conjugations do not require the use of modified antibodies, simplifying application of this conjugation methodology to a range of native unmodified antibodies without the need for significant optimisation prior to conjugation.

Site-specific conjugation to antibodies *via* modification of glycan residues also enables the use of native antibodies. However, this conjugation method inherently

alters the heavy chain glycan structure, which has been shown to alter antibody biodistribution and pharmacokinetics *in vivo*.⁹ Ideally, radiotracers should mimic the biodistribution and pharmacokinetic behaviour of their native unmodified analogues. Dibromomaleimide conjugations do not result in alteration of heavy chain glycan structure, and so are more likely to demonstrate native antibody pharmacokinetic behaviour.

As a result of complexity of site-specific conjugations, these methods are used less frequently than non-site-specific conjugation methods. Isothiocyanate-based bifunctional chelators are commonly used to achieve conjugation to amines on lysine side chains and the N-terminus of proteins such as antibodies.¹⁰⁻¹² The conjugation reaction is simple and can be performed using native unmodified antibodies. A typical isothiocyanate conjugation protocol has been described previously for the synthesis of DFO-antibody conjugates using DFO-NCS.⁸ The antibody was dissolved in either phosphate buffered saline (pH 7.4) or 0.5 M HEPES buffer (pH 7.4), and then adjusted to pH 8.8-9.0 by the addition of small aliquots (10 μ L) of 0.1 M Na₂CO₃ solution. DFO-NCS was then dissolved in anhydrous DMSO to give a concentration between 5-10 mM. Then between 3-4 molar equivalents of the DFO-NCS solution were added to the antibody solution and incubated for 1 h at 37 °C. The resulting immunoconjugate was then purified using a size exclusion column with a 0.5 M HEPES (pH 7.4) eluent.

The overall steps for a dibromomaleimide-based bioconjugation are similar to those described above for isothiocyanate derivatives. The two key differences are the inclusion of an antibody reduction step, and a longer incubation period to ensure dithiomaleimide hydrolysis. These steps do not require special equipment, or particular expertise and could be conducted by bioconjugate chemists familiar with isothiocyanate conjugations. Bioconjugate chemists routinely use maleimide derivatives of chelators to radiolabel proteins, and are adept at performing simple chemical disulfide reduction steps (addition of a reducing reagent to an antibody solution) that are required for maleimide conjugations.¹³⁻¹⁵ The inclusion of an extended incubation period to promote hydrolysis when using dibromomaleimide reagents is a passive step, which does not require any additional labour from the bioconjugate chemist. Therefore, dibromomaleimide-based conjugations, which enable site-specificity, are simple, and can be conducted by researchers who currently use non-site-specific conjugation reactions.

4.1.4 Bioorthogonal conjugation reactions involving dibromomaleimide

Conjugation reactions involving click chemistry are increasingly used to attach cargo or imaging tags to proteins, as orthogonal click reactions are simple, fast and efficient. The protein must be modified prior to conjugation to incorporate a 'clickable' group such as an azide. As mentioned above this has been achieved site-specifically using cell free protein synthesis to incorporate *p*-azidomethylphenylalanine into aglycosylated trastuzumab.⁷ In another study, enzyme mediated reactions, SPAAC, and IEDDA were used sequentially to achieve conjugation of a ⁶⁴Cu-labelled sarcophagine derivative to an antibody (see 1.4.4).^{6,16} First heavy chain glycans were modified using enzyme mediated reactions to append azide groups. Then a transcyclooctene group was attached using a cyclooctyne derivative that reacted with the azide group *via* SPAAC. Lastly, a ⁶⁴Cu-labelled tetrazine functionalised sarcophagine derivative was added, reacting with the transcyclooctene group *via* the IEDDA reaction. Whilst SPAAC and IEDDA are reliable and simple, initial attachment of the azide group often relies upon non-trivial protein synthesis or enzyme mediated reactions.

Azide groups have been attached to antibodies using simpler non-site-specific conjugation methods. For example, a transcyclooctene derivative bearing an isothiocyanate group has been conjugated to huA33 (anti-colorectal carcinoma) *via* reaction with amines on lysine residues. This enabled attachment of a ⁶⁴Cu-labelled tetrazine functionalised sarcophagine derivative *via* the IEDDA reaction. Of course, in this scenario, the final conjugate will be heterogeneous relative to the site-specific conjugation methods described above.

In this thesis, dibromomaleimides were used to facilitate the initial attachment of a bicyclononyne to trastuzumab, enabling conjugation with DFO-azide *via* SPAAC to yield DFO-BCN-trastuzumab. This work combines the simplicity and site specificity of the dibromomaleimide conjugation, with the highly selective and quantitative nature of click-chemistry. These conjugates were significantly more homogeneous than those generated using DFO-DBM or sar-DBM. LCMS data suggested that DFO-BCN-trastuzumab was composed mostly of half- and full-antibody conjugates with an overall chelator to antibody ratio of 4, whereas the DTM derivatives displayed undesired variable loading with chelator to antibody ratios of <4.

LCMS analysis suggested that DFO-BCN-trastuzumab was similarly homogeneous compared with previously reported click chemistry conjugates. Furthermore, the

initial attachment of the BCN click handle to the antibody represents a significant improvement over existing state-of-the-art site-specific conjugation methods. Native unmodified antibodies can be used, heavy chain glycan structure remains unchanged, and different antibodies can be used without the need for conjugation optimisation. Importantly, this conjugation method increases the accessibility of site-specific conjugates for bioconjugate chemists currently using non-site-specific conjugation methods. This approach to site-specific conjugation is highly flexible since it can be applied to conjugate virtually any protein containing a solvent accessible disulfide bond to any azide-containing species, including chelators, fluorophores, drug molecules, and more. Many of these azide-derivatives are commercially available or can be readily synthesised.

4.2 Future work

4.2.1 Improving DBM-conjugate homogeneity

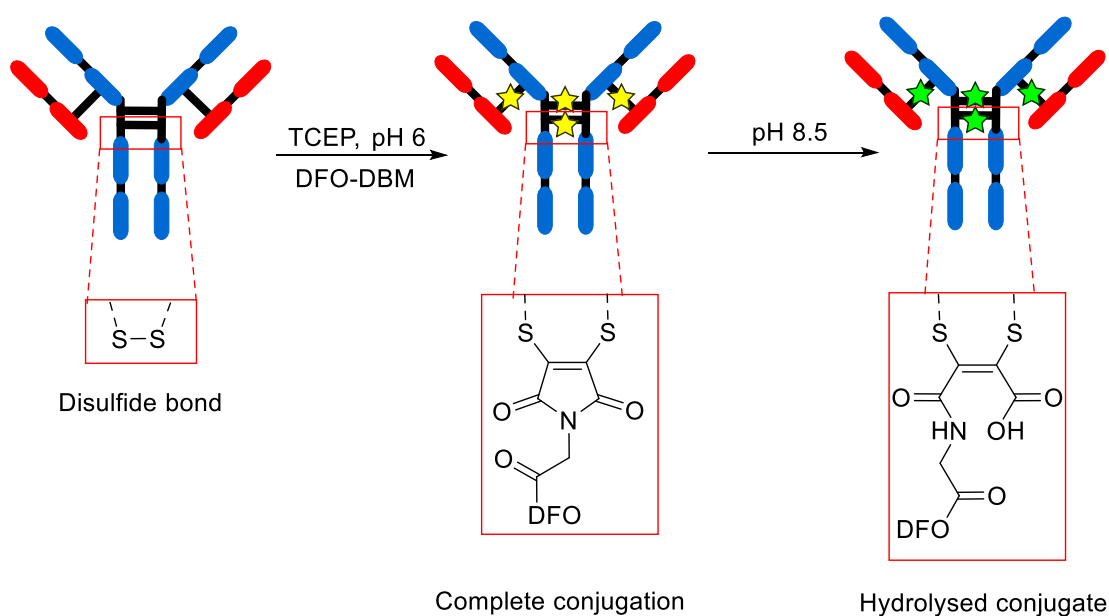


Figure 111 - DFO-DBM conjugation to trastuzumab using two different pH buffers to limit the effect of dibromomaleimide hydrolysis during conjugation (see 1.7.2).¹⁷

The conjugation reaction between DFO-DBM and trastuzumab could be improved to produce more homogeneous bioconjugates, mostly comprising of full-antibody conjugates. Prior studies with dibromomaleimides have generated highly homogeneous conjugates suggesting that further optimisation of sar-DBM and DFO-DBM conjugations may produce more homogeneous conjugates.^{1,3,18} The conjugation reaction between dibromomaleimides and thiols is in competition with

hydrolysis (see 1.7.2). Since hydrolysis is promoted under alkaline conditions, it may be possible to limit this competing process by using a lower pH (e.g. pH 6) during the initial conjugation reaction. After the initial thiol conjugation has taken place, the conjugate could then be buffer exchanged into a hydrolysis buffer at a higher pH (e.g. pH 8.5) to yield the stable bioconjugate (figure 111).

This strategy has been used previously to enable the sequential attachment of two different thiols to a dibromomaleimide (figure 112).¹⁷ First, one equivalent of Grb2 adapter protein was added to a dibromomaleimide (**40**, figure 112) at pH 6 to give a thiobromomaleimide conjugate (**41**, figure 112). Then one equivalent of a thioglucose sodium salt (**42**, figure 112) was added at pH 6 followed by buffer exchange to pH 8 resulting in hydrolysis yielding the desired conjugate bearing two different thiols (**43**, figure 112). In contrast when the conjugation reaction was carried out at pH 8, the initial conjugation to the Grb2 adapter protein resulted in a mixture of the desired thiobromomaleimide, and an undesired hydrolysed product (**44**, figure 112) in a 7:3 molar ratio.

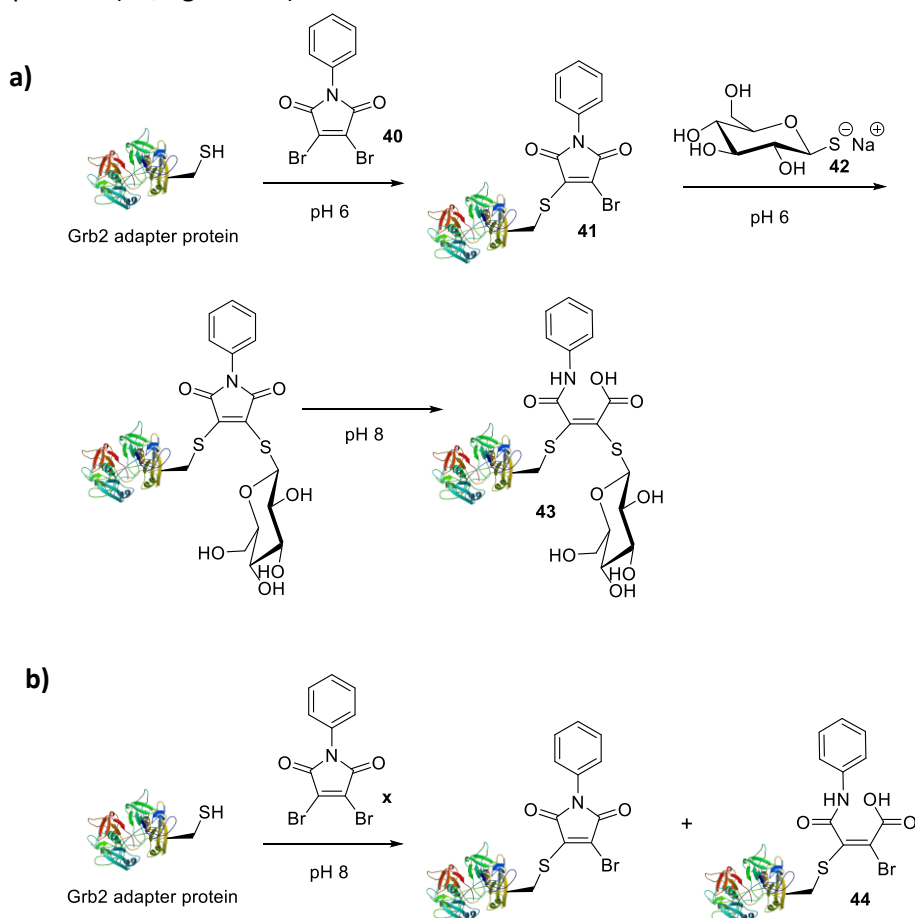


Figure 112 - a) sequential addition of two different thiols to a dibromomaleimide at pH 6 followed by hydrolysis at pH 8 to give the desired conjugate. b) At pH 8 unwanted hydrolysed product is formed.¹⁷

4.2.2 Improving the specific activities of ⁶⁴Cu-sar-DTM-trastuzumab and ⁸⁹Zr-DFO-DTM-trastuzumab

Specific activities in the range of 100-200 MBq/mg are generally desired for *in vitro* and *in vivo* radioimmunoconjugate assessment.¹⁹ This is because at significantly lower specific activities, larger amounts non-radioactive bioconjugate must be administered to achieved the amount of radioactivity required to generate high quality data. Additionally, under these conditions, in the presence of higher concentrations of non-radioactive ligand, adverse pharmacological effects can occur (see 1.3.2). Much lower specific activities were achieved for ⁶⁴Cu-sar-DTM-trastuzumab (43.6 MBq/mg) and ⁸⁹Zr-DFO-DTM-trastuzumab (5 MBq/mg). LCMS data suggested that both ⁶⁴Cu-sar-DTM-trastuzumab (see 2.4.4) and ⁸⁹Zr-DFO-DTM-trastuzumab (see 3.4) possessed <4 chelators per antibody. Ideally, 4 chelators would be present per antibody indicative of complete conjugation. If this were achieved, specific activities would likely improve since there would be a greater number of chelators per antibody available for radiometallic ion complexation. Additionally, ensuring minimal trace ion contamination would significantly improve radiolabelling properties to generate higher specific activities. Lastly, as previously mentioned (see 3.7) more radioactivity could be used during radiolabelling to give non-quantitative radiochemical yields. Removal of excess unreacted radiometallic ions by size exclusion chromatography should yield higher specific activity radioimmunoconjugates.

4.2.3 *In vivo* assessment of ⁸⁹Zr-DFO-DTM-trastuzumab with comparison to ⁸⁹Zr-DFO-mal-trastuzumab and an isothiocyanate analogue.

Future work could include evaluation of ⁸⁹Zr-DFO-DTM-trastuzumab in healthy mice to assess the radioimmunoconjugate's stability and biodistribution up to 1-2 weeks post-injection using *ex vivo* biodistribution studies and PET imaging studies. This builds upon the *in vivo* assessment of ⁶⁴Cu-sar-DTM-trastuzumab, which was only assessed up to 48 h post-injection due to half-life constraints imposed by ⁶⁴Cu ($t_{1/2}$ 12.7 h). ⁸⁹Zr-DFO-DTM-trastuzumab could also be assessed in a disease model using mice bearing xenograft tumours that express HER2 (e.g. SKOV3 ovarian cancer cells). This would enable evaluation of ⁸⁹Zr-DFO-DTM-trastuzumab's tumour targeting properties. In these experiments a blocking study should also be carried

out in the disease model, where ^{89}Zr -DFO-DTM-trastuzumab would be co-administered with a large dose of unmodified trastuzumab (10 mg/kg body weight) to block/decrease HER2-specific uptake of ^{89}Zr -DFO-DTM-trastuzumab. This would enable assessment of the radioimmunoconjugate's specificity for the HER2 receptor.

Similar imaging studies could be performed using ^{89}Zr -DFO-mal-trastuzumab, and ^{89}Zr -DFO-NCS-trastuzumab (made using the commercially available DFO-NCS bifunctional chelator, see 1.5.2). Use of DFO-maleimide conjugate derivatives would enable comparison of ^{89}Zr -DFO-mal-trastuzumab with analogues of the commercially available thiol reactive bifunctional chelator, DFO-maleimide, whilst use of DFO-NCS derivatives would enable comparison with a non-site-specific, stochastic conjugate, where DFO groups are appended to amines of lysine side chains.

4.2.4 ^{89}Zr -radiolabelling of DFO-BCN-trastuzumab, and serum stability of ^{89}Zr -DFO-BCN-trastuzumab

DFO-BCN-trastuzumab has been synthesised using a bioorthogonal conjugation strategy. Future work could examine the ^{89}Zr radiolabelling properties of this bioconjugate and assess the stability of ^{89}Zr -DFO-BCN-trastuzumab in human serum over 1-2 weeks.

This bioorthogonal conjugation strategy has the potential to enable simple click chemistry conjugations to site specifically modified proteins. Of course, this conjugation strategy is not limited to the use of DFO. The addition of any azide-functionalised chelator should enable attachment of a chelator to the BCN-bearing protein *via* SPAAC.

4.2.5 Dibromopyridazinedione-based bifunctional chelators

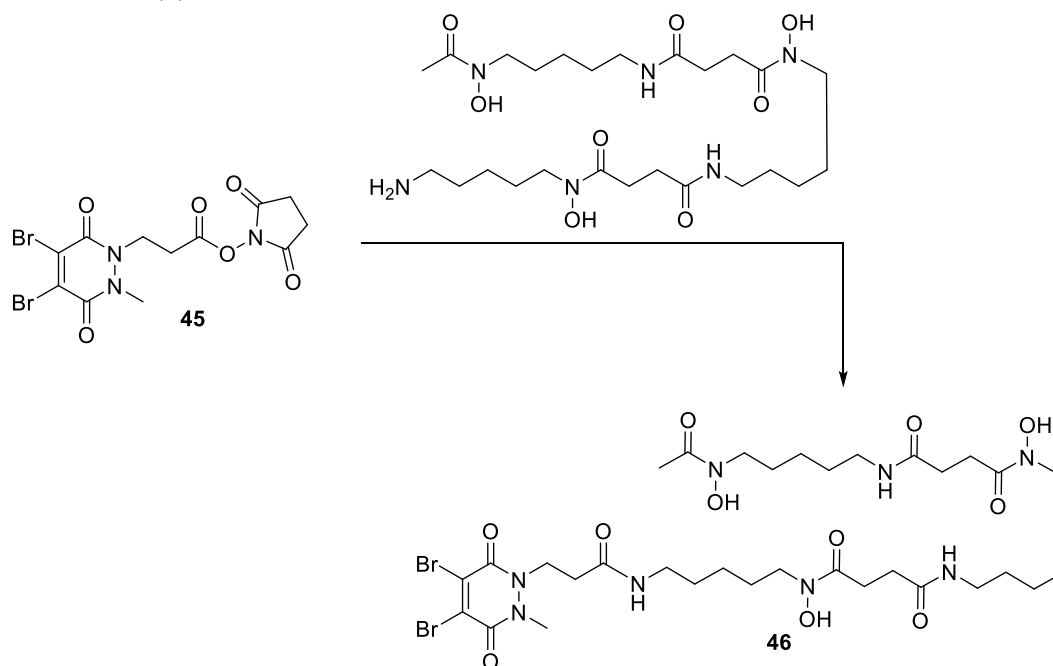


Figure 113 - A proposed synthesis for DFO-dibromopyridazinedione (46) via amide coupling between DFO and dibromopyridazinedione-NHS ester (45).

Dibromopyridazinediones have emerged as a possible replacement for dibromomaleimides (see 1.7.2).^{20–25} Compared to dibromomaleimides, dibromopyridazinediones typically produce more homogeneous bioconjugates comprised of a greater proportion of the desired “natively rebridged” full-antibody conjugate. Additionally, post-conjugation, dibromopyridazinedione conjugates are immediately stable towards thiol-mediated degradation and do not require a hydrolysis step. Lastly, dibromopyridazinedione conjugates are stable towards retro-Michael mediated degradation.

Prior studies have synthesised dibromopyridazinediones functionalised with fluorophores, drug molecules, and strained alkynes.^{20–25} However, this platform has not yet been exploited to produce bifunctional chelators for the site-specific radiolabelling of proteins. Figure 113 shows a proposed synthetic route to a DFO-dibromopyridazinedione bifunctional chelator. Prior studies have used the dibromopyridazinedione-NHS ester (45, figure 113) for the synthesis of functionalised dibromopyridazinediones.²⁴ Addition of DFO (or other chelators) to 45 should generate DFO-dibromopyridazinedione (46, figure 113). Pending successful conjugation, DFO-dibromopyridazinedione could be assessed *in vitro* and *in vivo*.

Lastly, a bioorthogonal approach could be taken to conjugate DFO to a protein using pyridazinedione reagents. Dibromopyridazinedione has previously been functionalised with a strained alkyne and conjugated to trastuzumab.²⁴ Addition of DFO-azide to this conjugate would result in conjugation *via* SPAAC (figure 114). DFO-antibody conjugates generated using this approach could be compared directly with those generated using DFO-dibromopyridazinedione discussed above using SDS-PAGE and LCMS.

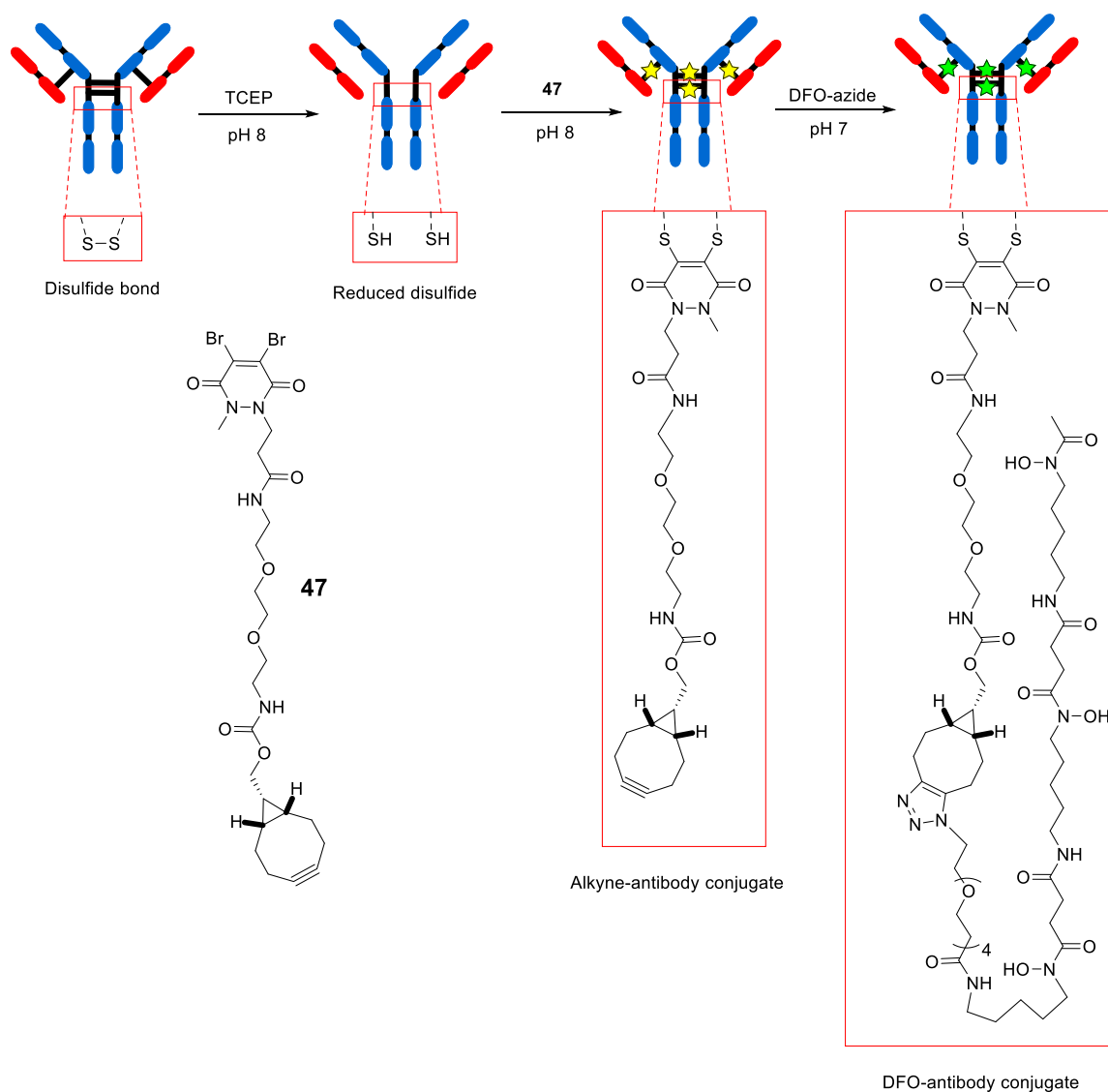


Figure 114 - Bioorthogonal synthesis of a DFO-antibody conjugate using dibromopyridazinedione-alkyne (47) and DFO-azide.

4.2.6 Closing remarks

This thesis demonstrates the use of dibromomaleimides to produce high quality site-specific chelator conjugates. This conjugation method shares both the simplicity of existing non-site-specific conjugations, and the increased control of

state-of-the-art site-specific conjugation methods. There remains significant scope to continue this area of research, and it is hoped that this thesis represents the first steps towards a simple site-specific conjugation method accessible to all bioconjugate chemists.

4.3 Chapter 4 references

- 1 F. F. Schumacher, J. P. M. Nunes, A. Maruani, V. Chudasama, M. E. B. Smith, K. A. Chester, J. R. Baker and S. Caddick, Next generation maleimides enable the controlled assembly of antibody–drug conjugates via native disulfide bond bridging, *Org. Biomol. Chem.*, 2014, **12**, 7261–7269.
- 2 F. F. Schumacher, M. Nobles, C. P. Ryan, M. E. B. Smith, A. Tinker, S. Caddick and J. R. Baker, In Situ Maleimide Bridging of Disulfides and a New Approach to Protein PEGylation, *Bioconjug. Chem.*, 2011, **22**, 132–136.
- 3 M. Morais, J. P. M. Nunes, K. Karu, N. Forte, I. Benni, M. E. B. Smith, S. Caddick, V. Chudasama and J. R. Baker, Optimisation of the dibromomaleimide (DBM) platform for native antibody conjugation by accelerated post-conjugation hydrolysis, *Org. Biomol. Chem.*, 2017, **15**, 2947–2952.
- 4 A. D. Baldwin and K. L. Kiick, Tunable Degradation of Maleimide–Thiol Adducts in Reducing Environments, *Bioconjug. Chem.*, 2011, **22**, 1946–1953.
- 5 B. M. Zeglis, C. B. Davis, R. Aggeler, H. C. Kang, A. Chen, B. J. Agnew and J. S. Lewis, Enzyme-Mediated Methodology for the Site-Specific Radiolabeling of Antibodies Based on Catalyst-Free Click Chemistry, *Bioconjug. Chem.*, 2013, **24**, 1057–1067.
- 6 B. E. Cook, P. Adumeau, R. Membreno, K. E. Carnazza, C. Brand, T. Reiner, B. J. Agnew, J. S. Lewis and B. M. Zeglis, Pretargeted PET Imaging Using a Site-Specifically Labeled Immunoconjugate, *Bioconjug. Chem.*, 2016, **27**, 1789–1795.
- 7 S. H. Ahn, B. A. Vaughn, W. A. Solis, M. L. Lupper, T. J. Hallam and E. Boros,

- Site-Specific ^{89}Zr - And ^{111}In -Radiolabeling and in Vivo Evaluation of Glycan-free Antibodies by Azide-Alkyne Cycloaddition with a Non-natural Amino Acid, *Bioconjug. Chem.*, 2020, **31**, 1177–1187.
- 8 B. M. Zeglis and J. S. Lewis, The Bioconjugation and Radiosynthesis of ^{89}Zr -DFO-labeled Antibodies, *J. Vis. Exp.*, , DOI:10.3791/52521.
- 9 D. Vivier, K. Fung, C. Rodriguez, P. Adumeau, G. A. Ulaner, J. S. Lewis, S. K. Sharma and B. M. Zeglis, The influence of glycans-specific bioconjugation on the Fc γ RI binding and in vivo performance of ^{89}Zr -DFO-Pertuzumab, *Theranostics*, 2020, **10**, 1746–1757.
- 10 S. E. Rudd, P. Roselt, C. Cullinane, R. J. Hicks and P. S. Donnelly, A desferrioxamine B squaramide ester for the incorporation of zirconium-89 into antibodies, *Chem. Commun.*, 2016, **52**, 11889–11892.
- 11 C. Imberti, S. Y. A. Terry, C. Cullinane, F. Clarke, G. H. Cornish, N. K. Ramakrishnan, P. Roselt, A. P. Cope, R. J. Hicks, P. J. Blower and M. T. Ma, Enhancing PET Signal at Target Tissue in Vivo: Dendritic and Multimeric Tris(hydroxypyridinone) Conjugates for Molecular Imaging of $\alpha\text{v}\beta\text{3}$ Integrin Expression with Gallium-68, *Bioconjug. Chem.*, 2017, **28**, 481–495.
- 12 B. M. Paterson, G. Buncic, L. E. McInnes, P. Roselt, C. Cullinane, D. S. Binns, C. M. Jeffery, R. I. Price, R. J. Hicks and P. S. Donnelly, Bifunctional ^{64}Cu -labelled macrobicyclic cage amine isothiocyanates for immuno-positron emission tomography, *Dalt. Trans.*, 2015, **44**, 4901–4909.
- 13 M. T. Ma, L. K. Meszaros, B. M. Paterson, D. J. Berry, M. S. Cooper, Y. Ma, R. C. Hider and P. J. Blower, Tripodal tris(hydroxypyridinone) ligands for immunoconjugate PET imaging with $^{89}\text{Zr}^{4+}$: Comparison with desferrioxamine-B, *Dalt. Trans.*, 2015, **44**, 4884–4900.
- 14 S. Nawaz, G. E. D. Mullen, K. Sunassee, J. Bordoloi, P. J. Blower and J. R. Ballinger, Simple, mild, one-step labelling of proteins with gallium-68 using a tris(hydroxypyridinone) bifunctional chelator: a ^{68}Ga -THP-scFv targeting the prostate-specific membrane antigen, *EJNMMI Res.*, 2017, **7**, 86.
- 15 R. Goldstein, J. Sosabowski, M. Livanos, J. Leyton, K. Vigor, G. Bhavsar, G. Nagy-Davidescu, M. Rashid, E. Miranda, J. Yeung, B. Tolner, A. Plückthun, S.

- Mather, T. Meyer and K. Chester, Development of the designed ankyrin repeat protein (DARPin) G3 for HER2 molecular imaging, *Eur. J. Nucl. Med. Mol. Imaging*, 2015, **42**, 288–301.
- 16 P. Adumeau, K. E. Carnazza, C. Brand, S. D. Carlin, T. Reiner, B. J. Agnew, J. S. Lewis and B. M. Zeglis, A pretargeted approach for the multimodal PET/NIRF imaging of colorectal cancer, *Theranostics*, 2016, **6**, 2267–2277.
- 17 C. P. Ryan, M. E. B. Smith, F. F. Schumacher, D. Grohmann, D. Papaioannou, G. Waksman, F. Werner, J. R. Baker and S. Caddick, Tunable reagents for multi-functional bioconjugation: reversible or permanent chemical modification of proteins and peptides by control of maleimide hydrolysis, *Chem. Commun.*, 2011, **47**, 5452.
- 18 E. A. Hull, M. Livanos, E. Miranda, M. E. B. Smith, K. A. Chester and J. R. Baker, Homogeneous bispecifics by disulfide bridging, *Bioconjug. Chem.*, 2014, **25**, 1395–1401.
- 19 S. K. Sharma, J. M. Glaser, K. J. Edwards, E. Khozeimeh Sarbisheh, A. K. Salih, J. S. Lewis and E. W. Price, A Systematic Evaluation of Antibody Modification and ⁸⁹Zr-Radiolabeling for Optimized Immuno-PET, *Bioconjug. Chem.*, 2021, **32**, 1177–1191.
- 20 L. Castañeda, Z. V. F. Wright, C. Marculescu, T. M. Tran, V. Chudasama, A. Maruani, E. A. Hull, J. P. M. Nunes, R. J. Fitzmaurice, M. E. B. Smith, L. H. Jones, S. Caddick and J. R. Baker, A mild synthesis of N-functionalised bromomaleimides, thiomaleimides and bromopyridazinediones, *Tetrahedron Lett.*, 2013, **54**, 3493–3495.
- 21 M. K. Greene, T. Chen, E. Robinson, N. L. Straubinger, C. Minx, D. K. W. Chan, J. Wang, J. F. Burrows, S. Van Schaeybroeck, J. R. Baker, S. Caddick, D. B. Longley, D. E. Mager, R. M. Straubinger, V. Chudasama and C. J. Scott, Controlled coupling of an ultrapotent auristatin warhead to cetuximab yields a next-generation antibody-drug conjugate for EGFR-targeted therapy of KRAS mutant pancreatic cancer, *Br. J. Cancer*, 2020, **123**, 1502–1512.
- 22 E. Robinson, J. P. M. Nunes, V. Vassileva, A. Maruani, J. C. F. Nogueira, M. E. B. Smith, R. B. Pedley, S. Caddick, J. R. Baker and V. Chudasama,

Pyridazinediones deliver potent, stable, targeted and efficacious antibody–drug conjugates (ADCs) with a controlled loading of 4 drugs per antibody, *RSC Adv.*, 2017, **7**, 9073–9077.

- 23 A. Maruani, P. A. Szijj, C. Bahou, J. C. F. Nogueira, S. Caddick, J. R. Baker and V. Chudasama, A Plug-and-Play Approach for the de Novo Generation of Dually Functionalized Bispecifics, *Bioconjug. Chem.*, 2020, **31**, 520–529.
- 24 C. Bahou, D. A. Richards, A. Maruani, E. A. Love, F. Javaid, S. Caddick, J. R. Baker and V. Chudasama, Highly homogeneous antibody modification through optimisation of the synthesis and conjugation of functionalised dibromopyridazinediones, *Org. Biomol. Chem.*, 2018, **16**, 1359–1366.
- 25 A. Maruani, M. E. B. Smith, E. Miranda, K. A. Chester, V. Chudasama and S. Caddick, A plug-and-play approach to antibody-based therapeutics via a chemoselective dual click strategy, *Nat. Commun.*, 2015, **6**, 2–10.

5 Appendix

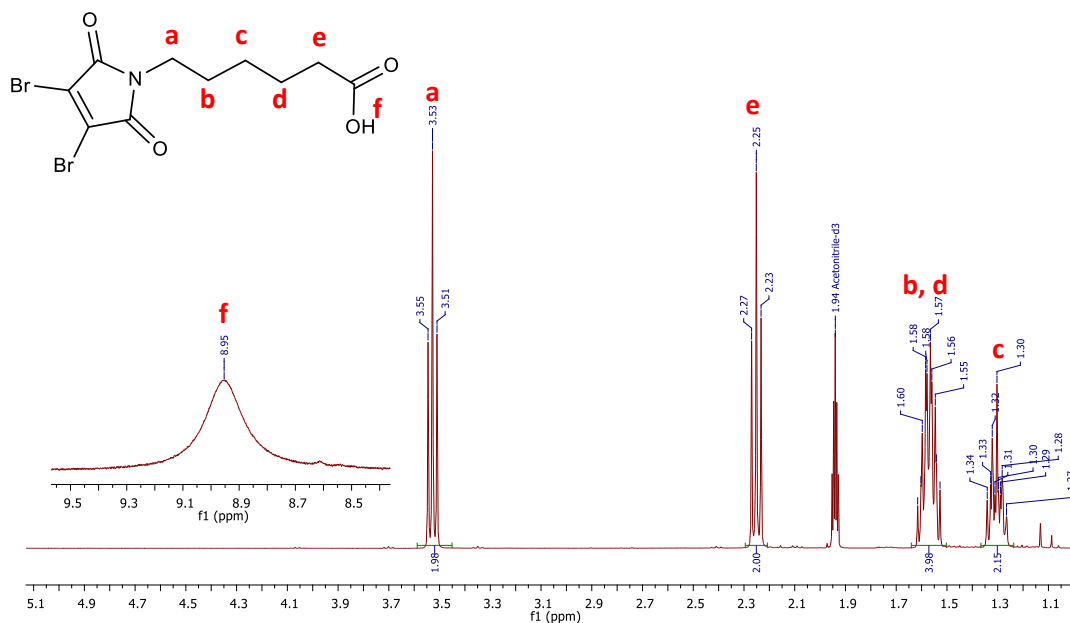


Figure 115 - Assigned structure and ^1H NMR spectrum of 3,4-dibromomaleimide-N-hexanoic acid (CD_3CN , 400 MHz)

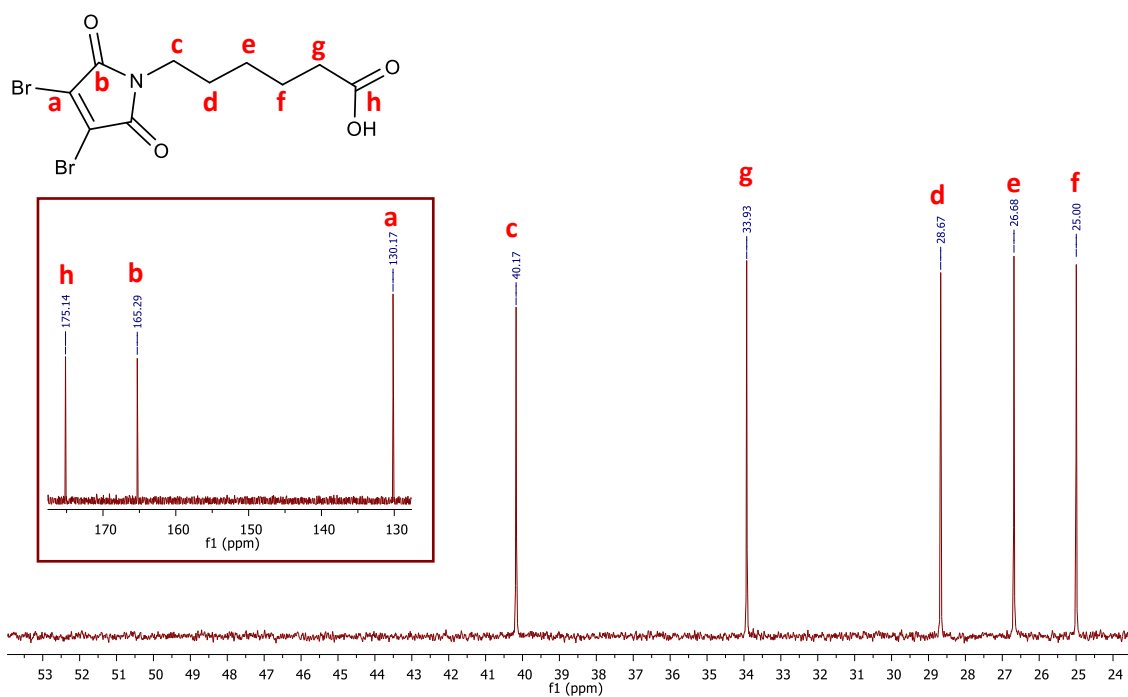


Figure 116 - Assigned structure and ^{13}C NMR spectrum of 3,4-dibromomaleimide-N-hexanoic acid (CD_3CN , 101 MHz)

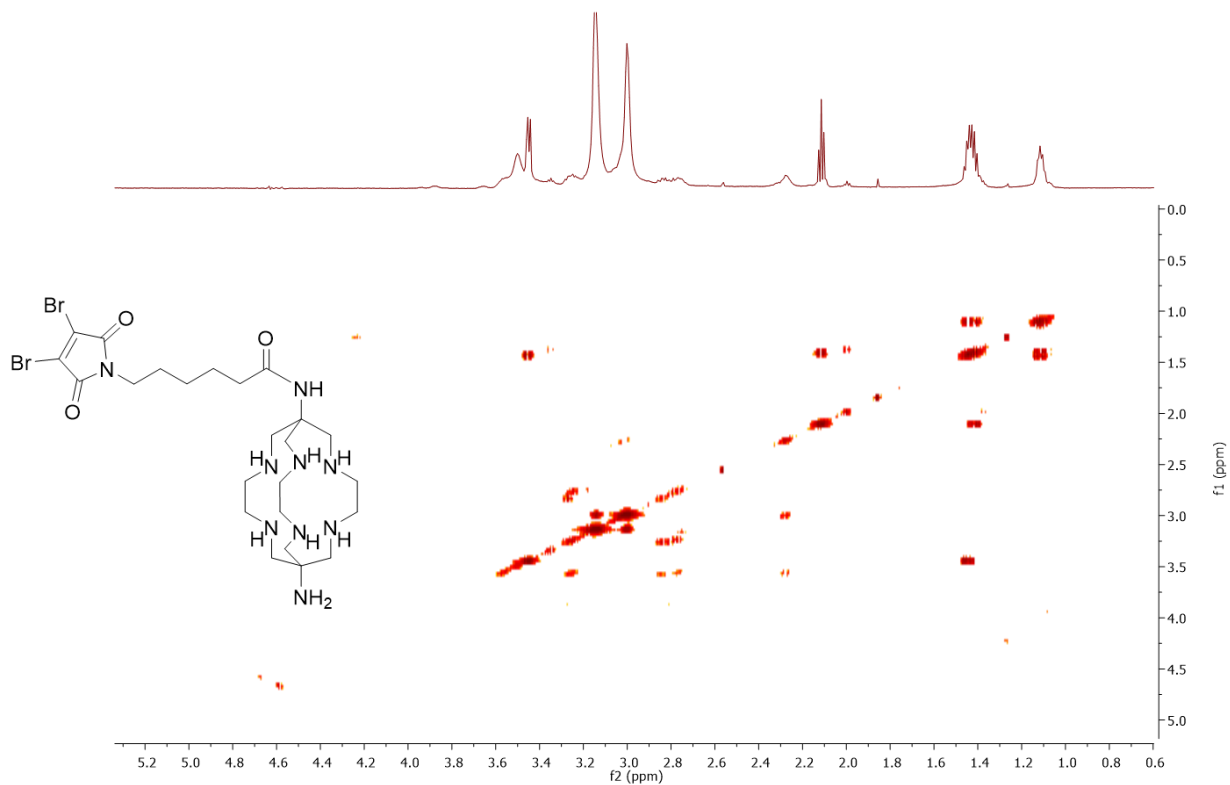


Figure 117 - ^1H - ^1H COSY spectrum for sar-DBM, 700 MHz, D_2O

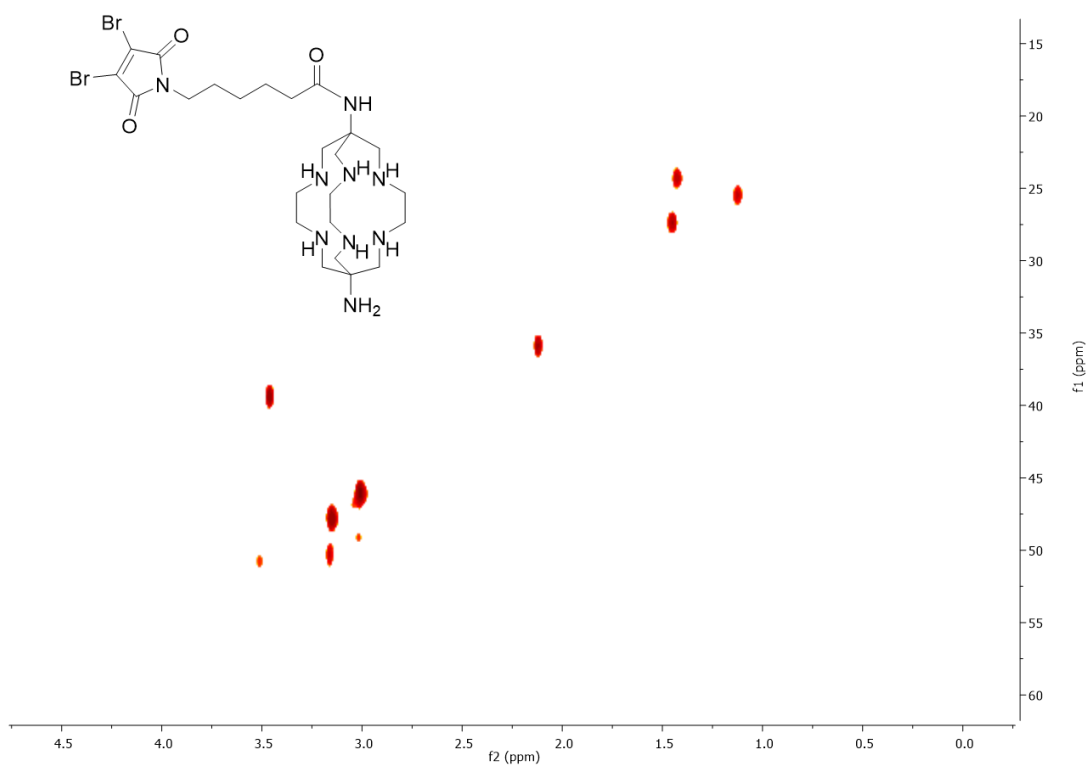


Figure 118 - ^1H - ^{13}C -HSQC NMR spectrum for sar-DBM, 700 MHz, 176 MHz, D_2O

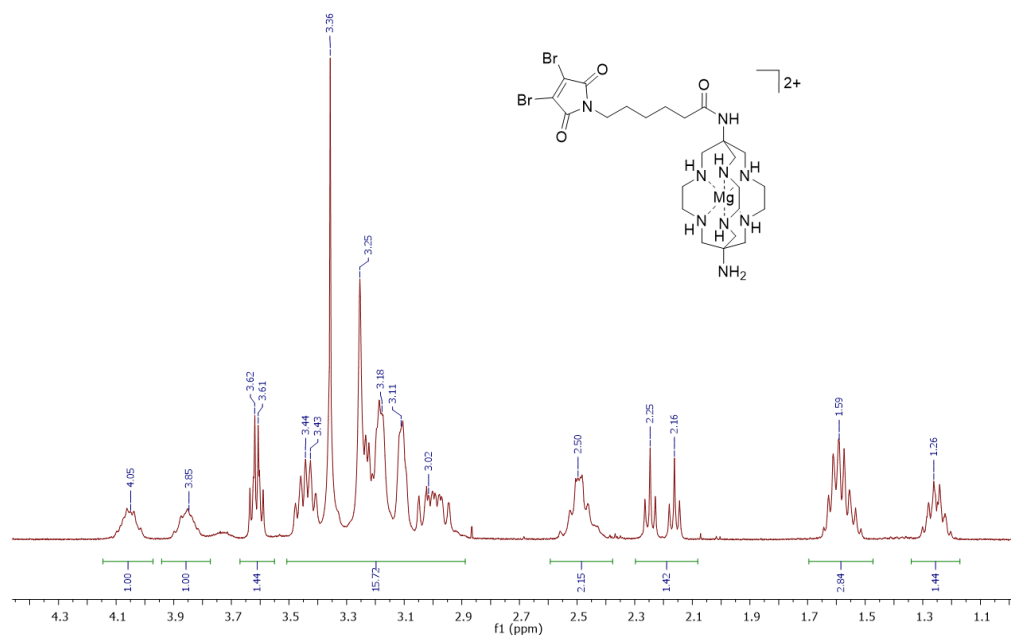


Figure 119 - 1H NMR spectrum for $[Mg(sar-DBM)]^{2+}$, 400 MHz, D_2O

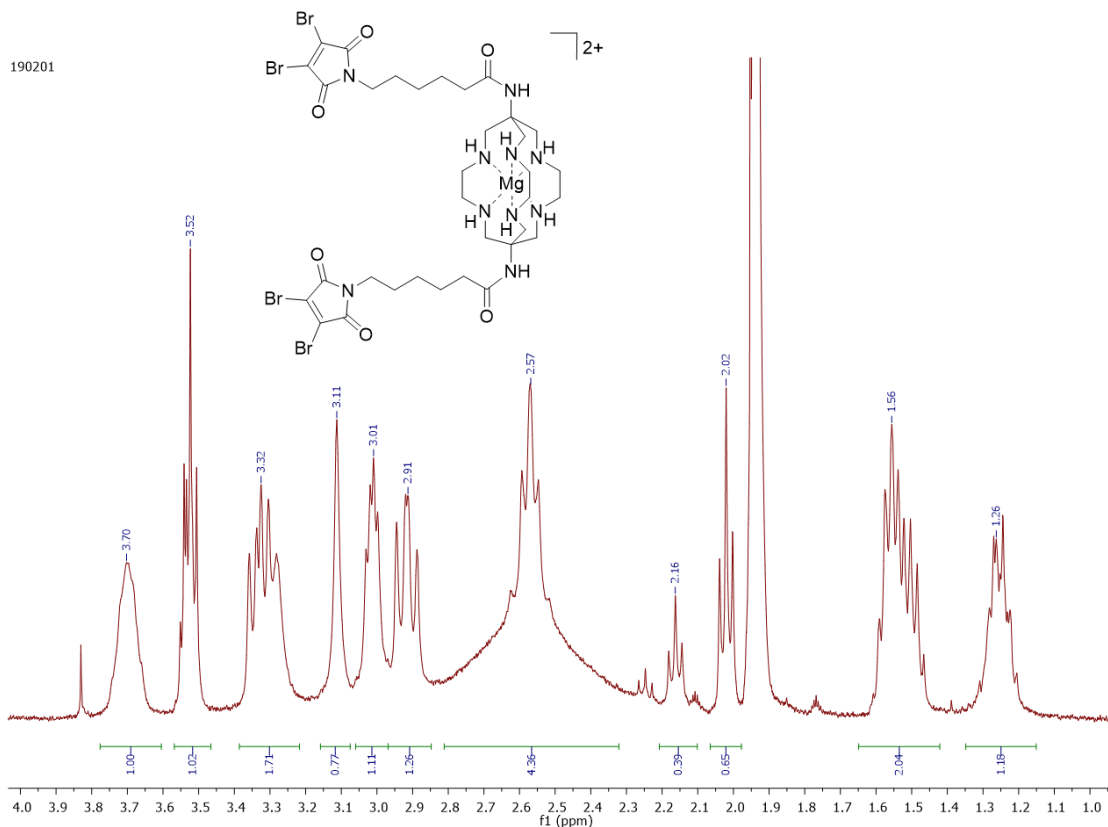


Figure 120 - 1H NMR spectrum for $[Mg(sar-DBM_2)]^{2+}$, 399 MHz, CD_3CN

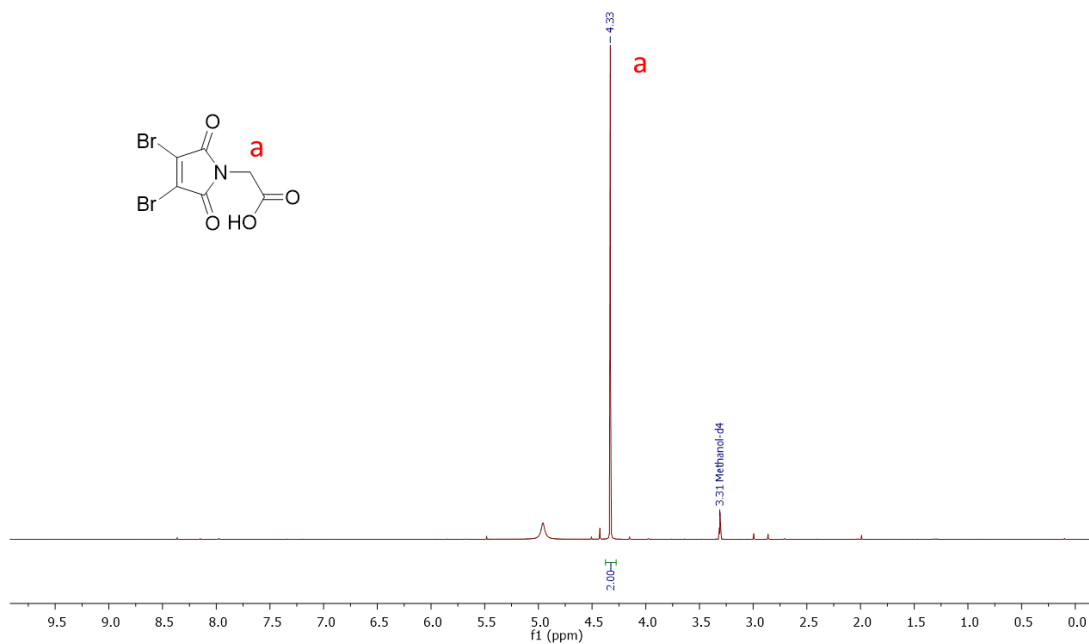


Figure 121 - ^1H NMR spectrum for 3,4-dibromomaleimide-*N*-acetic acid, 400 MHz, MeOD

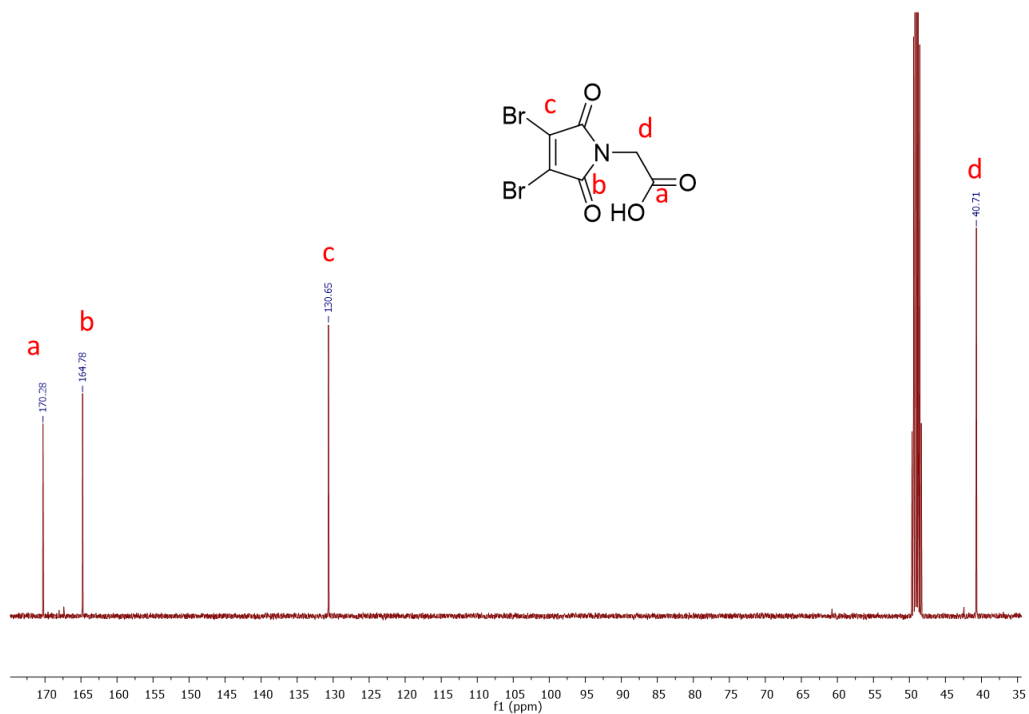


Figure 122 - ^{13}C NMR spectrum for 3,4-dibromomaleimide-*N*-acetic acid, 101 MHz, MeOD

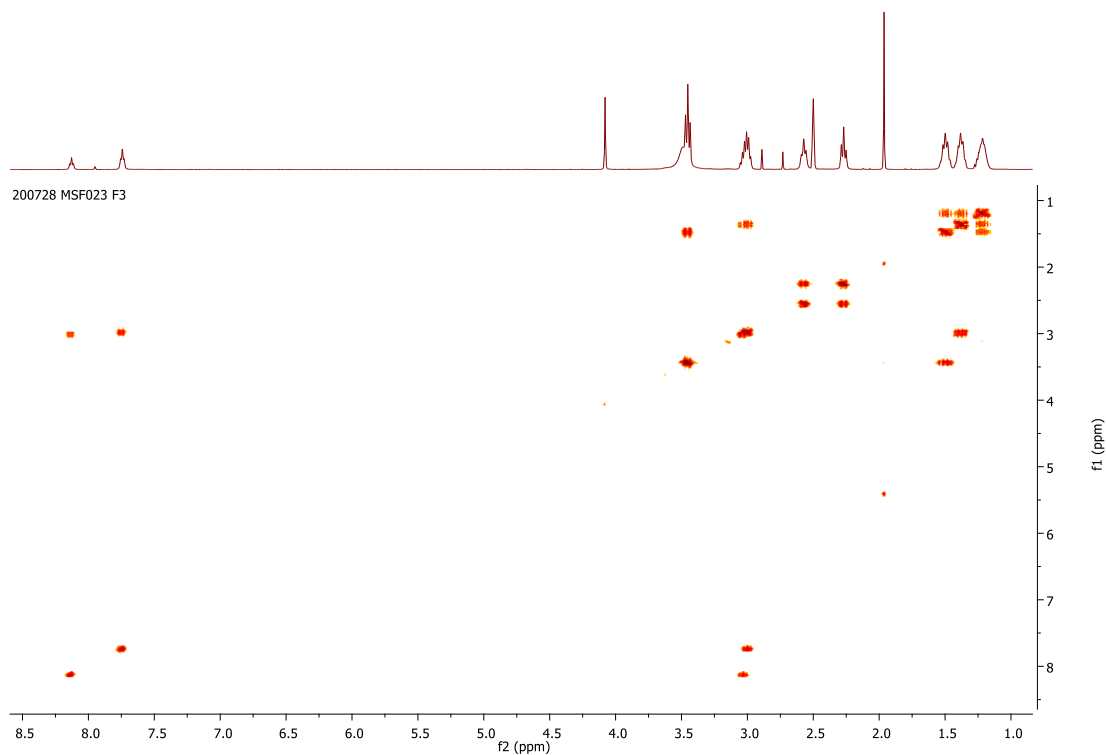


Figure 123 - ^1H - ^1H COSY NMR spectrum for DFO-DBM, 400 MHz, CD_3CN

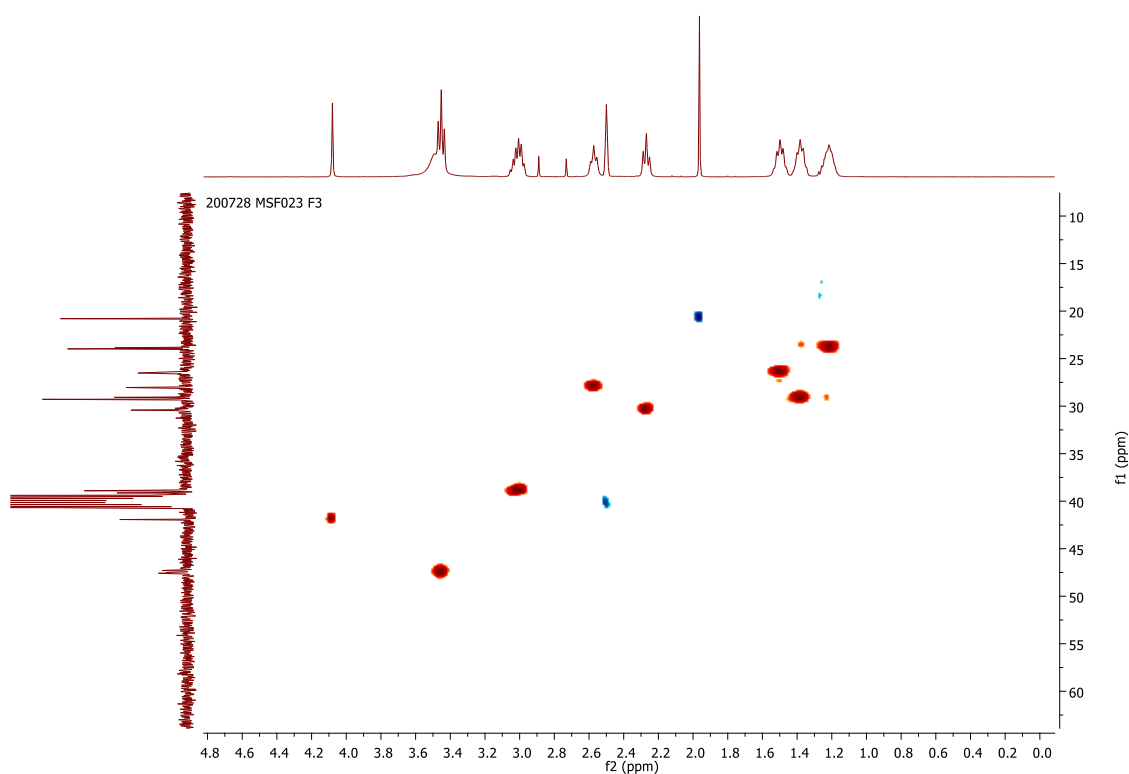


Figure 124 - ^1H - ^{13}C HSQC NMR spectrum for DFO-DBM, 400 MHz, 101 MHz, CD_3CN

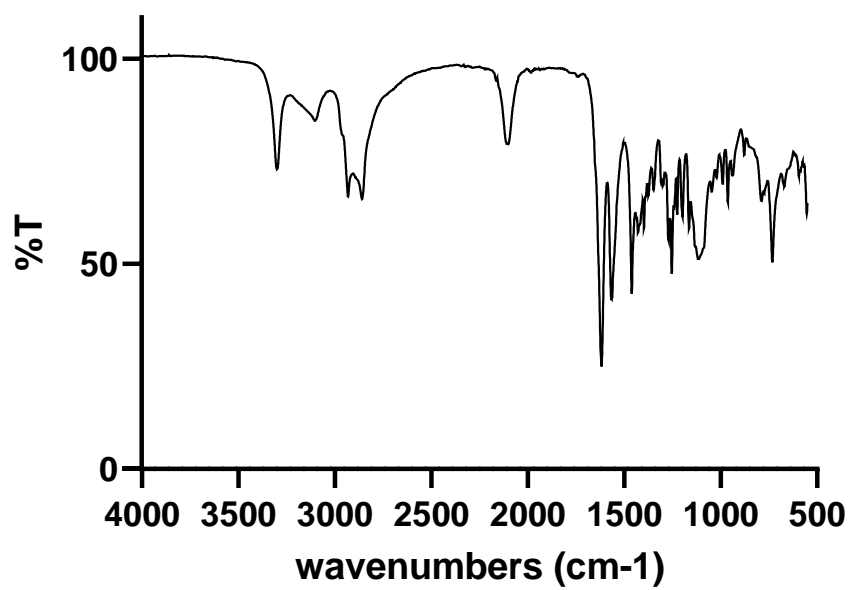


Figure 125 - IR spectrum for DFO-azide